A new critical phase in jammed models : jamming is even cooler than before

Antonio Sclocchi

université
PARIS-SACLAY

A new critical phase in jammed models: jamming is even cooler than before

Thèse de doctorat de l'université Paris-Saclay

École doctorale n° 564 Physique en Île-de-France (EDPIF)
Spécialité de doctorat: Physique
Unité de recherche: Université Paris-Saclay, CNRS, LPTMS, 91405, Orsay, France.
Référent: : Faculté des sciences d'Orsay

Thèse présentée et soutenue à Paris-Saclay, le 17 Décembre 2020, par

Antonio SCLOCCHI

Composition du jury

Giuseppe Foffi Professeur, Université Paris-Saclay Laboratoire de Physique des Solides	Président
Luca Leuzzi Directeur de recherche, Consiglio Nazionale delle Ricerche Institute of Nanotechnology	Rapporteur & Examinateur
Markus Muller Directeur de recherche, Paul Scherrer Institute Condensed Matter Theory Group	Rapporteur & Examinateur
Jean-Louis Barrat Professeur, Université Grenoble-Alpes Laboratory for Interdisciplinary Physics	Examinateur
Andrea Liu Professeure, Hepburn Professor of Physics, University of Pennsylvania Department of Physics and Astronomy	Examinatrice
Matthieu Wyart Professeur, École Polytechnique Fédérale de Lausanne Laboratoire de Physique des Systèmes Complexes	Examinateur

Direction de la thèse

Silvio Franz Professeur, Université Paris-Saclay Laboratoire de Physique Théorique et Modèles Statistiques	Directeur de thèse
Pierfrancesco Urbani Chargé de recherche, CNRS, CEA Saclay Institut de Physique Théorique	Co-Encadrant de thèse

Thèse de doctorat

NNT: 2020UPASP068

Résumé en français

Introduction

Les systèmes désordonnés et vitreux sont l'un des sujets les plus intéressants de la matière condensée et de la physique statistique. Leur paysage énergétique est complexe, caractérisé par de nombreux minima locaux : lorsque la température est suffisamment basse, le système se retrouve piégé dans l'un d'eux. Un phénomène lié à la température zéro est la transition de brouillage ("jamming"). C'est le point où les particules athermiques ayant une interaction répulsive à courte distance, en augmentant leur densité, commencent à sentir la présence les unes des autres. Par exemple, nous pouvons considérer l'empilement de sphères dures dans un volume donné : à une densité critique, les sphères dures sont empilées au maximum avec un réseau de contacts établi entre elles ; cela correspond au point de jamming. Ces dernières années, la physique vitreuse et la transition de jamming ont trouvé un cadre commun dans la solution du modèle des sphères dures dans des dimensions spatiales infinies, correspondant à une théorie du champ moyen. Cela a permis la caractérisation analytique du comportement critique de jamming, qui correspond aux arguments d'échelle de l'espace réel basés sur la stabilité marginale. Une caractéristique remarquable du jamming est sa criticité super-universelle. En fait, les prédictions du champ moyen ont été confirmées par des simulations numériques de sphères à dimensions finies. Plus généralement, le jamming peut être considéré comme le seuil de satisfaction d'un problème de satisfaction de contraintes avec des variables continues (CCSP). Par conséquent, des caractéristiques de jamming ont également été trouvées dans les CCSP comme le perceptron, un modèle introduit comme classificateur binaire dans les réseaux de neurones qui peut être résolu avec des techniques de champ moyen. Dans cette thèse, nous montrons l'émergence de la criticité du jamming dans un nouveau type de phase brouillée ("jammed"). Les contraintes du CCSP peuvent être assouplies, ce qui permet de les enfreindre en payant un coût énergétique. Dans les modèles de sphères, cela correspond à des sphères molles interagissant avec un potentiel mou par paire qui est une fonction croissante du degré de chevauchement entre elles. Nous étudions la phase UNSAT/jammed, tant dans le perceptron que dans les sphères molles à dimension finie, lorsque le potentiel doux est choisi comme étant linéaire. La particularité de ce modèle est que la dérivée première de l'énergie potentielle est constante par parties, avec une discontinuité au point de contact entre les sphères. Ce fait a des conséquences physiques non négligeables : les minima du paysage énergétique sont des points angulaires caractérisés par des contraintes marginalement satisfaites, c'est-à-dire des sphères en contact, même quand le système est profondément dans la phase jammed / UNSAT. Une simple dynamique de type descente de gradient se termine par ces minima singuliers. Nous

découvrons qu'ils sont marginalement stables et critiques, avec un ensemble d'exposants critiques plus nombreux que celui de la transition de jamming. Néanmoins, les valeurs des exposants critiques sont les mêmes que celles de l'universalité du jamming, indépendamment de la dimensionnalité. Elles caractérisent les mécanismes d'excitation/relaxation qui sont non linéaires et analogues à ceux des emballages de sphères marginales. Par conséquent, la phase jammed est auto-organisée critique et marginalement stable. Dans cette phase, la réponse du système aux perturbations est caractérisée par des avalanches sans échelle. La découverte d'une phase critique en dimensions finies est intéressante en soi du point de vue de la physique statistique. En outre, elle offre un nouveau cadre pour étudier les caractéristiques super-universelles du jamming et comprendre ses origines.

Chapitres introductives

Dans le premier chapitre, nous présentons brièvement quelques points principaux de la physique des verres.

En suivant nombreuses revues disponibles [27, 155, 51, 24], nous résumons la phénoménologie des systèmes vitreux et nous introduisons un modèle simple de verres structurels, c'est-à-dire les sphères dures. La théorie des sphères dures a été résolue dans la limite dimensionnelle d infinie (c'est-à-dire dans le champ moyen). Cette solution exacte permet d'étudier les caractéristiques qui ont une nature de champ moyen et obtenir des résultats pour les systèmes à dimensions finies en étendant le petit paramètre $1/d$; cependant, certains effets locaux trouvés dans les modèles de dimension finie ont souvent une origine non perturbative [58, 57]. Le résultat le plus intéressant est la caractérisation du point de jamming des sphères dures.

Dans le scénario de champ moyen, ceci est obtenu par une théorie d'échelle dérivant de la construction de la rupture complète de la symétrie des répliques (fullRSB) [63, 200], développée à l'origine pour les verres de spin (spin glass) [168]. Il est intéressant de noter que les propriétés critiques du jamming sont indépendantes de la dimension spatiale et peuvent être vérifiées dans le point de jamming des emballages de sphères de dimension finie [64].

Au point de brouillage, un réseau de contacts entre les sphères est établi. Le nombre de contacts est égal au nombre de degrés de liberté, saturant ainsi la limite de stabilité de Maxwell [172] pour un système rigide. Cette propriété est appelée *isostaticité* et elle est liée à la stabilité marginale [188] : la suppression d'un seul contact déstabilise le système. Elle déclenche un mouvement collectif des particules qui n'est interrompu que lorsqu'un nouveau contact est formé et que l'isostaticité est rétablie. Cette dynamique critique d'ouverture/fermeture des contacts est contrôlée par deux exposants critiques dans la distribution des forces de contact et des espaces entre les particules. La distribution des courtes distances $\rho(h)$ entre les sphères présente un comportement de loi de puissance $\rho(h) \sim h^{-\gamma}$ pour $h \to 0+$. De même, la distribution des forces de contact présente un pseudo-gap $\rho(f) \sim f^{\theta}$ pour les petites forces $f \to 0^{+}$. Les deux exposants critiques $\gamma \simeq 0,41269...$ et $\theta \simeq 0,42311...$ sont des nombres irrationnels non triviaux calculés dans la théorie de l'échelle du champ moyen. Ils satisfont à la relation de stabilité marginale $\gamma = 1/(2+\theta)$ obtenue par les arguments d'échelle dans l'espace réel [247]. Nous présentons les propriétés des sphères molles athermiques au point de jamming et dans la phase marginalement jammed [158].

Les sphères molles sont obtenues en relâchant les contraintes dures des sphères dures, correspondant à $h_{ij} \geq 0$, $\forall(ij)$, où h_{ij} est la distance par paire entre la sphère i et la sphère j, c'est-à-dire les distances entre leurs centres moins la somme de leurs rayons.

En considérant l'hamiltonien $H = \sum_{(ij)} \nu(h_{ij})$, le potentiel par paire $\nu(h)$ de sphères dures correspond à $\nu(h) = 0$ si $h \geq 0$, $\nu(h) = \infty$ si $h < 0$. Les sphères molles sont obtenues en considérant, par exemple, $\nu(h) = \frac{1}{a}|h|^a\theta(-h)$, avec $a > 1$, qui associe une énergie positive aux sphères qui se chevauchent. Pour une densité élevée, les sphères ne peuvent pas éviter le chevauchement et les configurations d'énergie minimale des systèmes ont $H > 0$: cela correspond à la phase jammed. En diminuant la densité, l'énergie devient plus petite : le régime de très faible énergie correspond au solide marginalement jammed et la limite $H \to 0^+$ correspond à la limite de jamming, où le comportement critique de jamming des sphères dures est récupéré. Les résultats de cette thèse portent sur la phase jammed lorsque l'exposant de potentiel doux est pris pour $a = 1$. Cela correspond au potentiel linéaire et sa dérivée $\nu'(h) = -\theta(-h)$ est discontinue pour $h = 0$, c'est-à-dire lorsque deux sphères sont tangentes.

Dans le chapitre 2, nous présentons le modèle de perceptron en suivant les références [105, 234]. Le modèle est défini par un vecteur $\mathbf{X}$ à dimension N sur l'hypersphère $|\mathbf{X}|^2 = N$ et un ensemble de $M = \alpha N$ vecteurs aléatoires $\boldsymbol{\xi}_\mu$ à dimension N, $\mu = 1, ..., M$, dont les entrées sont des variables aléatoires échantillonnées à partir d'une distribution normale standard. Dans le langage des réseaux de neurones, $\mathbf{X}$ représente les poids neuronaux tandis que $\boldsymbol{\xi}_\mu$ sont les pattern à classer. À chaque vecteur aléatoire $\boldsymbol{\xi}_\mu$ est associé un *gap* $h_\mu = \frac{1}{\sqrt{N}}\boldsymbol{\xi}_\mu \cdot \mathbf{X} - \sigma$, où σ est un paramètre de contrôle fini. Dans la limite thermodynamique $N, M \to \infty$, avec $\alpha \sim O(1)$, le problème de satisfaction des contraintes continues (CCSP) est défini en demandant de trouver $\mathbf{X}$ de sorte que $h_\mu \geq 0$, $\forall\mu$. Si α et σ sont suffisamment petits, ce problème est satisfaisant et la phase correspondante est appelée SAT. Sinon, les contraintes ne peuvent pas être toutes satisfaites simultanément avec un seul $\mathbf{X}$ et le problème est UNSAT. La ligne de transition de satisfaisabilité dans le plan σ-α correspond à la ligne de "jamming", par analogie avec le cas des sphères. Le modèle correspond à un champ moyen et le diagramme de phase peut être trouvé en utilisant la méthode de réplique. Pour $\sigma < 0$, la ligne de transition de jamming est critique et appartient à la même classe d'universalité du jamming des sphères. La phase UNSAT correspond clairement à la phase jammed des sphères molles. Par conséquent, elle peut être étudiée par un potentiel doux $H = \sum_\mu \nu(h_\mu)$, avec $\nu(h) = \frac{1}{a}|h|^a\theta(-h)$. Comme dans le cas des sphères, la phase SAT est à énergie zéro, tandis que les minima de la phase UNSAT ont une énergie positive. Les calculs du chapitre 2 sont effectués pour un potentiel générique $\nu(h)$, donc ils sont utiles aussi pour le cas linéaire $a = 1$ qui fait l'objet du reste des chapitres.
Nous montrons la solution d'échelle des équations fullRSB à la ligne de jamming critique, qui est universelle et indépendante du potentiel doux. À la fin du chapitre, nous récapitulons brièvement la phase UNSAT avec le potentiel harmonique, c'est-à-dire $a = 2$, qui présente quelques caractéristiques communes avec la phase jammed des sphères harmoniques douces de dimensions finies. Le cas harmonique a le même comportement qualitatif que les cas avec d'autres potentiels convexes $a > 1$. La physique change radicalement lorsque $a = 1$ (ou, plus généralement, lorsque $a \leq 1$).

Principaux résultats

Les résultats présentés dans les chapitres 3-4-5-6 sont publiés dans [108]-[107]-[109]-[215].

Dans le chapitre 3, nous étudions la phase UNSAT (jammed) du perceptron avec le

potentiel linéaire. Nous définissons d'abord une version régularisée du modèle ça-veut-dire $H_\epsilon = \sum_\mu \nu_\epsilon(h_\mu)$, avec $\nu_\epsilon(h) = |h|\theta(-h - \frac{\epsilon}{2}) + \frac{(h-\frac{\epsilon}{2})^2}{2\epsilon}\mathbb{I}(-\frac{\epsilon}{2} < h < \frac{\epsilon}{2})$, où $\mathbb{I}$ est la fonction indicatrice. Dans la limite $\epsilon \to 0$, le modèle devient celui d'origine. Cette procédure nous permet d'utiliser des techniques de gradient pour trouver les minima locaux du paysage énergétique.

Nous montrons que dans la phase jammed, où l'énergie est positive, un grand nombre de gaps deviennent marginaux, c'est-à-dire $h_c = 0$ pour $c \in \mathcal{C}$. Nous les appelons *contacts*, ce qui les distingue des *overlaps* pour lesquels $h_o < 0$ pour $o \in \mathcal{O}$. Seuls les overlaps contribuent à l'énergie du système, tandis que les contacts sont cruciaux pour stabiliser les minima du système. Ils fournissent en effet un ensemble de *forces de contact*, f_c pour $c \in \mathcal{C}$, qui sont contenus dans l'intervalle $f_c \in (0, 1)$. Leur présence est nécessaire pour obtenir la stabilité mécanique des minima énergétiques. La cardinalité de l'ensemble des contacts $C = |\mathcal{C}|$ est particulièrement importante. En effet, on définit un *indice d'isostaticité* $c = C/N$ qui est égal à un si les minima du modèle sont isostatiques et $c < 1$ si les minima sont hypostatiques. Nous montrons que dans une partie de la phase UNSAT, le modèle est isostatique, tandis que dans l'autre, il est hypostatique. D'un point de vue théorique, ces deux phases correspondent respectivement à une phase fullRSB et à une phase réplique symétrique (RS). Ceci est contenu dans le fait que le réplicon $\lambda_{replicon}$, c'est-à-dire la plus petite valeur propre de la Hessienne de la théorie de la réplique, satisfait $\lambda_{replicon} \propto 1 - c$. La phase isostatique est marginalement stable. La distribution des petits gaps est caractérisée par le même exposant γ que celui trouvé dans la transition de jamming. Il est intéressant de noter qu'il caractérise également la distribution des petits overlaps, donnant $\rho(h) \sim |h|^{-\gamma}$ pour $h \to 0^{\pm}$. De même, l'exposant θ de la distribution des petites forces au jamming se retrouve dans la distribution des forces de contact. Dans ce cas, en plus des petites forces, l'exposant caractérise également les forces de contact proches de un, c'est-à-dire la limite supérieure du domaine de force $(0, 1)$, ce qui donne $\rho(f) \sim f^\theta$ pour $f \to 0^+$ et $\rho(f) \sim (1 - f)^\theta$ pour $f \to 1^-$. Cette forme de criticité étendue est due à la stabilité marginale et au fait que les mécanismes d'excitation (rupture de contacts) et de relaxation (formation de contacts) sont étendus à la possibilité d'avoir des gaps négatifs $h_\mu < 0$. La stabilité marginale et l'isostaticité du système sont liées à la géométrie sphérique du problème, donnée par $|\mathbf{X}|^2 = N$. Ceci est révélé par le multiplicateur de Lagrange η qui impose cette condition sphérique : dans la phase isostatique $\eta < 0$ et la géométrie effective est non convexe. En raison de la nature du potentiel linéaire, la stabilité (marginale) n'est atteinte que lorsque tous les degrés de liberté sont contraints par un contact. Dans la phase hypostatique, au contraire, $\eta > 0$ et la géométrie du problème est convexe. Cet argument est mis en évidence par l'utilisation d'une Hessienne rééchelonnée défini par le potentiel régularisé.

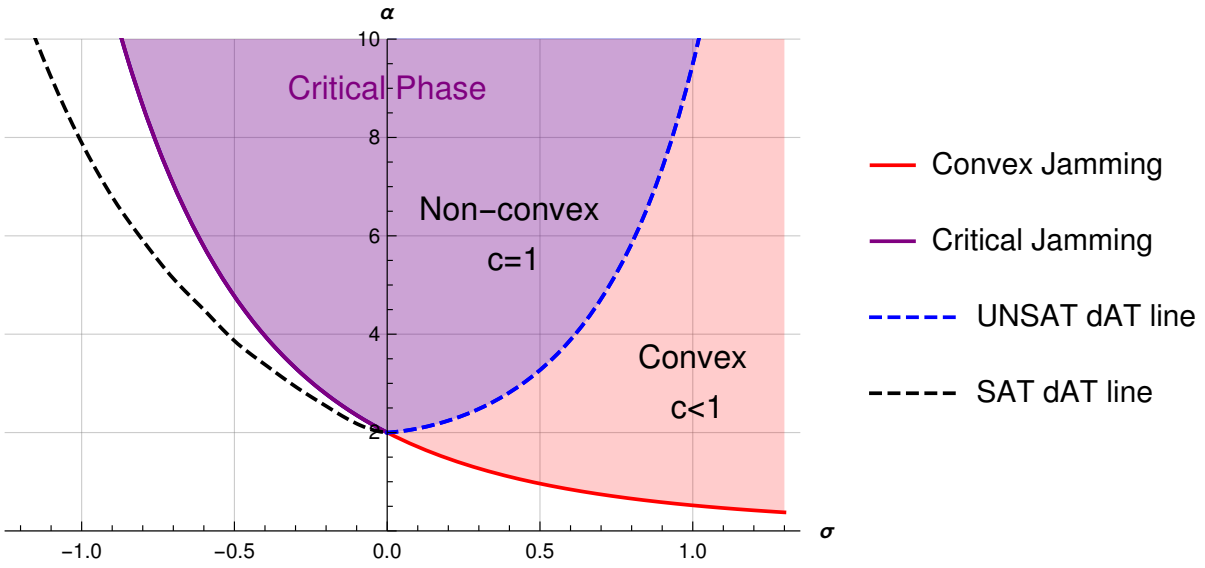

Figure 1: Diagramme de phase du perceptron avec potentiel linéaire. La partie colorée représente la phase jammed. Au-dessus des lignes pointillés, le système est vitreux (fullRSB). La partie violette est la phase isostatique, non convexe et critique. La partie rouge est hypostatique, convexe et non critique.

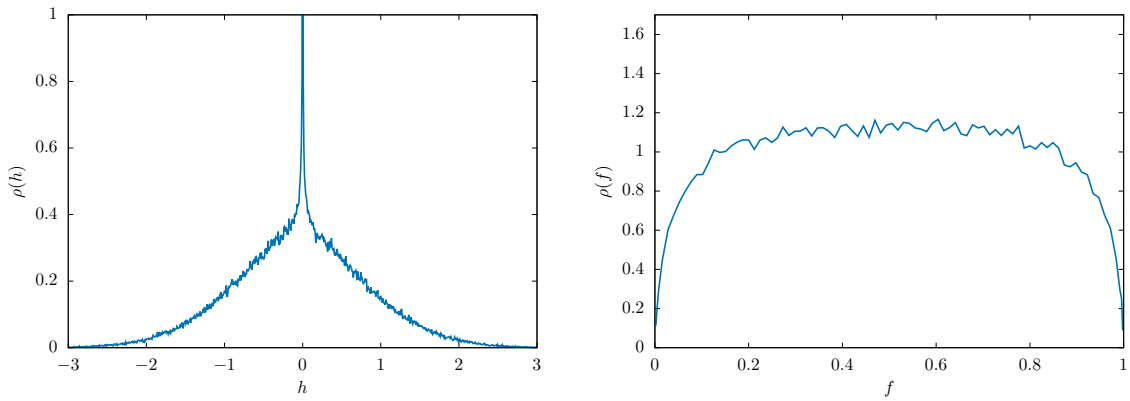

Figure 2: Distributions des gaps (à gauche) et des forces de contact (à droite) dans la phase critique ($\alpha = 2$, $\sigma = 0.4$, energy 1.02). La distribution des gaps a un comportement de loi de puissance pour les petits gaps, $\rho(h) \sim |h|^{-\gamma}$ pour $h \to 0^{\pm}$. La distribution des forces a deux pseudo-gap pour les petites forces et les forces proches de l'unité, $\rho(f) \sim f^{\theta}$ pour $f \to 0^{+}$ et $\rho(f) \sim (1-f)^{\theta}$ pour $f \to 1^{-}$.

La phase isostatique est critique et une théorie d'échelle est élaborée à partir des équations fullRSB. Elle résume les résultats observés dans les simulations numériques et établit le lien avec la classe d'universalité de jamming grâce à une relation contenue dans les équations fullRSB. La phénoménologie exposée dans le chapitre 3 est le fil conducteur pour le reste des chapitres.

Dans le chapitre 4, nous montrons par des simulations numériques que les minima énergétiques de la phase jammed des sphères molles à potentiel linéaire sont critiques de la même manière que dans leur homologue du perceptron. De manière remarquable, ils constituent une phase critique en dimensions deux et trois, ce qui est particulièrement

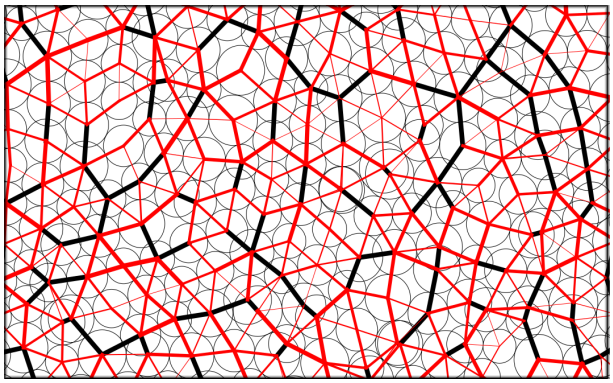

Figure 3: Une configuration stable des sphères dans la phase jammed. Les lignes rouges/noires correspondent aux contacts/chevauchements entre les sphères. Leur épaisseur est proportionnelle à l'intensité de la force correspondante.

intéressant en physique statistique. Nous mesurons les exposants critiques montrant le lien avec la transition de jamming.

De la même manière, la criticité du brouillage dans les basses dimensions est dévoilée en séparant correctement les effets locaux dans les statistiques. Il est intéressant de noter qu'en allant à des densités plus élevées dans la phase jammed avec le potentiel linéaire, les effets locaux disparaissent. Nous caractérisons également les réseaux de sphères qui se touchent et se chevauchent.

Comme dans le cas du perceptron, les overlaps contribuent à l'énergie, tandis que les contacts sont liés à la stabilité du système. Comme lors de la transition de jamming, il s'avère que les fluctuations de la connectivité locale dans le réseau de contacts s'échelonnent plus lentement que la taille du système. C'est la raison pour laquelle, le réseau de contact est "hyperuniforme" et ça montre qu'il existe des corrélations à longue portée. Nous fournissons la définition d'une matrice hessienne rééchelonnée et nous étudions son spectre. Nous montrons la connexion avec le point de jamming et avec le perceptron également dans ce cas.

Dans le chapitre 5, nous définissons un algorithme de compression pour la phase critique UNSAT du perceptron linéaire. Il nous permet d'étudier les avalanches qui caractérisent la réponse du système à une compression infinitésimale, de manière cohérente avec ce qui est attendu dans une phase marginalement stable.

Lorsqu'une configuration isostatique est déstabilisée par une légère augmentation de la pression, certaines forces de contact sortent de leur domaine de définition $(0, 1)$. Le système commence à se déplacer selon les modes doux jusqu'à ce que de nouveaux contacts soient formés et qu'une configuration isostatique (marginalement) stable soit trouvée. Nous développons des arguments d'échelle pour diverses quantités physiques et nous montrons que les statistiques d'avalanche ont un comportement de loi de puissance avec des exposants critiques donnés par la théorie fullRSB [110]. Nous utilisons ce protocole de compression pour étudier numériquement la limite de la pression nulle, c'est-à-dire la limite de jamming, en montrant que le potentiel linéaire a un comportement d'échelle différent des autres potentiels doux convexes.

Contrairement aux cas convexes $a > 1$, la pression a un comportement logarithmique avec la distance de jamming, correspondant à une correction logarithmique au comportement linéaire de l'énergie. Le nombre de overlaps a une tendance de puissance avec un exposant $\nu \sim 0.83$, différent de la valeur 0.5 habituellement obtenue pour les sphères

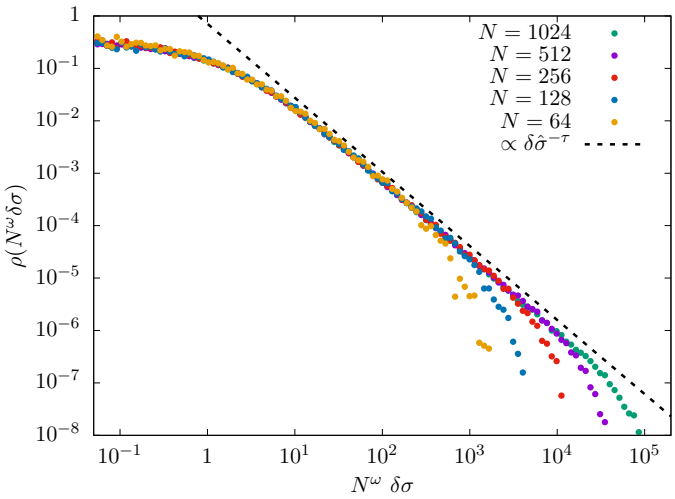

Figure 4: Distribution de la taille des avalanches pour des variations de pression infinitésimales. L'échelle de taille finie est caractérisée par un exposant $\omega \simeq 2.19$ et la distribution de la loi de puissance a un exposant $\tau \simeq 1.41$. Les exposants exacts peuvent être calculés à partir de la théorie.

marginalement jammed indépendamment de la dimensionnalité et du potentiel doux convexe.

Dans le chapitre 6, nous étudions une simple variation du système précédent, qui est un potentiel linéaire par parties. Nous montrons que tous ses points non différentiables donnent lieu à des ensembles d'excitations non linéaires, toujours caractérisées par les mêmes exposants critiques.

La phase jammed du potentiel linéaire avait été étudiée dans les années 1990 [164], mais ses propriétés critiques n'avaient pas été observées. Cette thèse caractérise une nouvelle phase critique dans des modèles de champ moyen et dans les systèmes à dimensions finies. Cela fournit des modèles intéressants de criticité auto-organisée et une nouvelle façon d'étudier l'universalité du jamming.

Acknowledgements

This thesis is the result of the work I have done during the last three years at the Laboratoire de Physique Théorique et Modèles Statistiques (LPTMS), with funding from the Simons Foundation (grants No. 454941, S. Franz). I acknowledge the Institut de Physique Théorique (IPhT) - CNRS, CEA Saclay for frequently hosting me and generously providing computational resources, and the Simons group at ENS Paris where I had the pleasure to spend a part of my time.

I warmly thank the reviewers Luca Leuzzi and Markus Müller and the jury members Jean-Louis Barrat, Giuseppe Foffi, Andrea Liu, Matthieu Wyart for offering their time and good will throughout the process of reviewing my work.

I would like to thank my supervisors, Silvio and Pierfrancesco. They have been invaluable mentors, patiently helping me every time I needed and letting me free to explore every time I had the possibility to. Beyond sharing their deep knowledge of physics, they continuously inspire me with their intellectual curiosity and integrity, with their deep passion for understanding things and solving problems, with their commitment to the beauty of ideas. It has been an honor and a pleasure to be their student: I hope I will have other opportunities in the future to share with them the enthusiasm for scientific progress.
During the first two years of my PhD, I spent a lot of fruitful time with Jacopo, Sungmin and Gianpaolo: I am grateful to them for the good team spirit and for the opportunity to learn many things.
I would like to thank all members of LPTMS, including the PIs, my *parrain* Raoul, my colleagues and particularly Emmanuel, Claudine, Karolina and Zhiqiang who are always kindly available to support us and make the whole system work seamlessly.
I thank the members of the Simons collaboration on Cracking the Glass Problem, from the students to the professors, for having created a thriving community where I have had the opportunity to learn and discuss a lot.
I would like to thank my friends and my "Parisian family" for all the beautiful moments we have shared along these years which have made life definitely more joyful, and for the

aid they provided every time it was needed.
A special thank goes to Marwa, for multiplying the joy and halving the pain, for having shared this journey with me and for being the best possible traveling companion I could ask for.
A special thought goes to my family, in particular to my father, my mother, my sister, my brother and my aunt, for having always supported me and my choices, no matter how dire the circumstances, and for having taught me love, consistency and sacrifice. Without them, nothing would have been possible.

Antonio

Contents

Introduction

Disordered and glassy systems are among the most interesting subjects in condensed matter and statistical physics. Their energy landscape is complex, characterized by many local minima: when the temperature is low enough, the system gets trapped in one of them. A related zero-temperature phenomenon is the jamming transition. This is the point where athermal particles with a repulsive short-range interaction, upon increasing the density, start to feel each other's presence. For example, we can consider the packing of hard spheres in a given volume: at a critical density the hard spheres are maximally packed with a network of contacts established between them; this corresponds to the jamming point.

In recent years, glassy physics and the jamming transition have found a common framework in the solution of the hard sphere model in infinite spatial dimensions, corresponding to a mean-field theory. This has allowed the analytical characterization of the jamming critical behavior, which matches with real-space scaling arguments based on marginal stability.

A remarkable feature of jamming is its super-universal criticality. In fact, the mean-field predictions of critical exponents have been confirmed in numerical simulations of finite dimensional spheres. More generally, jamming can be seen as the satisfiability threshold of a constraint satisfaction problem with continuous variables (CCSP). Consequently, jamming features have been found also in CCSPs like the perceptron, a model introduced as a binary classifier in neural networks that can be solved with mean-field techniques.

In this thesis, we show the emergence of jamming criticality in a new kind of jammed phase. In fact, the constraints of the CCSP can be relaxed, allowing them to be violated by paying an energy cost. In sphere models, this corresponds to soft spheres interacting with a pairwise soft potential being an increasing function of the amount of overlap between them.

We study the UNSAT/jammed phase, both in the perceptron and in finite-dimensional soft spheres, when the soft potential is chosen to be linear. The peculiarity of this model is that the first derivative of the potential energy is piece-wise constant, with a discontinuity at the touching point between spheres. This fact has non-trivial physical consequences: minima of the energy landscape are corner points characterized by marginally satisfied constraints, i.e. touching spheres, even deeply in the jammed/UNSAT phase. A simple gradient-descent-like dynamics ends in these singular minima. We discover that they are marginally stable and critical, with a larger set of critical exponents than the jamming transition. Nevertheless, the values of the critical exponents are the same as those of the jamming universality, independent of dimensionality. They characterize the excitation/relaxation mechanisms which are non-linear and analogous to those of marginal

sphere packings. Therefore, the jammed phase is self-organized critical and marginally stable. In this phase, the response of the system to perturbations is characterized by scale-free avalanches.
Discovering a critical phase in finite dimensions is interesting in itself from the statistical physics point of view. Furthermore, it provides a new setting to investigate the super-universal features of jamming and understand its origins.

Main results

The results presented in this thesis are published in:

- [108] Silvio Franz, Antonio Sclocchi, and Pierfrancesco Urbani. "Critical Jammed Phase of the Linear Perceptron". In: *Phys. Rev. Lett.* 123.11 (2019), p. 115702. doi: 10.1103/PhysRevLett.123.115702.
- [107] Silvio Franz, Antonio Sclocchi, and Pierfrancesco Urbani. "Critical energy landscape of linear soft spheres". In: *SciPost Phys.* 9 (1 2020), p. 12. doi: 10.21468/SciPostPhys.9.1.012. url: https://scipost.org/10.21468/SciPostPhys.9. 1.012.
- [109] Silvio Franz, Antonio Sclocchi, and Pierfrancesco Urbani. "Surfing on minima of isostatic landscapes: avalanches and unjamming transition". In: *Journal of Statistical Mechanics: Theory and Experiment 2021.2* (Feb. 2021), p. 023208. doi: 10.1088/1742-5468/abdc16. url: https://doi.org/10.1088/1742-5468/abdc16.
- [215] Antonio Sclocchi and Pierfrancesco Urbani. "Proliferation of non-linear excitations in the piecewise-linear perceptron". In: *SciPost Phys.* 10 (1 2021), p. 13. doi: 10.21468/SciPostPhys.10.1.013. url: https://scipost.org/10.21468/ SciPostPhys.10.1.013.

In [108], we study the jammed phase of the perceptron with linear potential. We first define a regularized version of the model in order to use gradient-based techniques to find the local minima of the energy landscape. We show that in one section of the jammed phase the minima are isostatic and characterized by the same critical exponents as those of the jamming transition. This is related to the fact that the phase is marginally stable. We also use replica theory to solve the model and we show that the critical jammed phase is described by a full Replica Symmetry Breaking construction (fullRSB). We develop a scaling theory in the critical phase and show that it relates the critical exponents to the jamming universality.
In [107], we show by numerical simulations that the energy minima of the jammed phase of soft spheres with linear potential are critical in the same way as in their perceptron counterpart. Remarkably, they constitute a critical phase in dimensions two and three, which is of particular interest in statistical physics. We measure the critical exponents showing the connection with the jamming transition. We also characterize the networks of touching/overlapping spheres, showing that the contact network is hyperuniform and has system-spanning correlations. We provide the definition of a rescaled Hessian matrix and we study its spectrum. We show the connection with the jamming point also in this case.
In [109], we define a compression algorithm for the critical UNSAT phase of the linear perceptron. It allows us to study the avalanches that characterize the response of the system to an infinitesimal compression, in accordance with what is expected in a marginally

stable phase. We develop scaling arguments for various physical quantities and we show that the avalanche statistics has a power law behavior with critical exponents given by the fullRSB theory. We use this compression protocol to numerically study the limit of zero pressure, i.e. the unjamming limit, showing that the linear potential has different scalings from those provided by the other convex soft potentials.
In [215], we study a simple variation of the previous system, which is a piece-wise linear potential. We show that all its non-differentiable points give rise to sets of non-linear excitations, always characterized by the same critical exponents.

The content of [108]-[107]-[109]-[215] is reproduced in the chapters 3-4-5-6 of this thesis. Additional information is provided with respect to the articles, in particular a detailed analysis of the replica theory, a wider discussion of the singular Hessian and the scaling arguments relating the critical exponents.

Chapter 1

Introduction to glasses and the jamming transition

Glasses, and the adjective "glassy", refer to a whole class of systems characterized by sluggish dynamics in which the degrees of freedom get stuck in a disordered state. They are ubiquitous in the natural world and characterize many different materials, e.g. plastics, molecular glasses, colloidal gels, foams, electron glasses, active glassy matter, spin glasses, granular materials, to name a few. Even if they have a long and well-established history on the experimental point of view, their theoretical understanding has always been challenging and controversial, with no complete microscopic theory from first principles being achieved. In the 1995, P. W. Anderson wrote: "The deepest and most interesting unsolved problem in solid state theory is probably the theory of the nature of glass and the glass transition."[9] Thirteen years later, stating the lack of theoretical consensus, the experimental physicist David A. Weitz joked on the New York Times: "There are more theories of the glass transition than there are theorists who propose them."[53] The reason why amorphous materials are so much more difficult to describe than crystalline solids is that the latter have constituents arranged on perfectly symmetric lattices: this underlying symmetry structure plus small perturbations around it, such as thermal vibrations (i.e. phonons) and defects, made them the prototypical model of solid state theory.[16] Amorphous materials, instead, do not have any structural symmetry and can be qualified as "frozen liquids". The glass transition is not even a proper *bona fide* thermodynamic phase transition and the glass transition temperature T_g is operationally defined as the temperature at which the relaxation time of the system is much larger than the observation time. Therefore, a glassy state is inherently an out-of-equilibrium one since it has larger free-energy than the ground state, and dynamics plays a crucial role in its definition.
The glass transition is a fascinating and intricate subject and a considerable number of reviews have been written about it [11, 118, 123, 78, 12, 228, 145, 84, 32, 86, 156, 144, 51, 27]. This work, however, focuses on the glassy physics at zero temperature where colloids and grains at high density undergo a related transition: the *jamming* transition [158].
The jamming point is a transition to an amorphous solid at high density, happening at the jamming transition density ϕ_J, and it is commonly studied in athermal systems like granular media, emulsions and foams. Increasing density in a colloidal system and getting closer to the jamming transition, many features of the glassy phenomenology can be observed, like an increase of viscosity and a history dependent jamming transition density ϕ_J. Different from molecular glasses, the jamming point is a true critical point characterized by scaling laws and infinite lengthscales, with marginally jammed solids exhibiting an anomalous elastic response due to the presence of soft (zero or low-frequency)

vibrational modes. Due to these analogies, one may be tempted to ask if the glass and jamming transitions are different facets of the same jammed solid phase, which was done by A. J. Liu and S. R. Nagel in 1998 [159] by proposing a unifying *jamming phase diagram*. From the current understanding, we can say that the jamming transition has more peculiar properties than a generic glass transition. In infinite dimensional hard spheres, for example, the jamming transition occurs when the system is already in a marginally stable glassy phase [64].

The focus of this work is the study of the zero temperature jammed phase in two specific models: soft spheres in finite dimensions and their mean-field counterpart, the perceptron. We show that the jammed phase constitutes a new critical phase when we choose the short-range repulsive potential to be a linear function of the properly defined distances (*gaps*). *Critical* means that it is characterized by critical exponents, scaling laws, marginal stability, infinite correlation length and scale free avalanches when slightly perturbed. Both theoretically and by numerical simulations, we show that this critical phase is deeply connected to the jamming point.

In this introductory chapter, we briefly present some highlights of the physics of glasses. Therefore we introduce a simple structural glass model, i.e. hard spheres, whose theory has been solved in the infinite dimensional limit (i.e. mean-field). This exact solution allows the characterization of the jamming point of hard spheres, which presents critical properties that are independent of the space dimensionality and can be verified in the jamming of finite dimensional sphere packings [64]. We present the properties of athermal soft spheres at jamming and in the marginally jammed phase. We conclude the chapter by describing the main physical picture contained in our work about the linear potential and we give an outlook of the organization of the thesis.

1.1 Glasses and the glass transition problem

The glass transition corresponds to the passage of a system from a liquid phase to an amorphous solid. By "liquid" and "solid" in this context we refer to the ability of the system to sustain a shear stress when it is subjected to a shear strain, which gives a quantitative prescription to the intuition that a liquid flows, while a solid does not. This means that at equilibrium, a fluid does not have a shear modulus while a solid does, allowing a harmonic description. This is true at thermodynamic equilibrium. However, considering the dynamical relaxation of a strain by a liquid, this is characterized by a combination of processes with their relaxation time scales. In a supercooled liquid, it happens that the dominant relaxation process becomes slower and slower, at least exponentially for decreasing temperature, until the relaxation time τ_R is much larger than the experimental time scale τ_{exp}: it means that the system "looks" like a solid, since it can sustain a shear stress on the experimental time, but it is an out-of-equilibrium system.
Let's consider a molecular liquid whose temperature T is decreased with a certain cooling rate. If this is "fast enough", it is possible to avoid crystallization at the melting temperature T_m: this is in fact a first order transition that happens by nucleation. Therefore it requires a surface tension (i.e. a positive free energy cost) to be overcome, which gives a time scale τ_N to the process. For $T < T_m$, in the regime $\tau_R << \tau_{exp} << \tau_N$, we have a supercooled liquid whose properties can be seen as a continuation of those of the equilibrium liquid existing for $T > T_m$. The supercooled liquid is actually a metastable state since

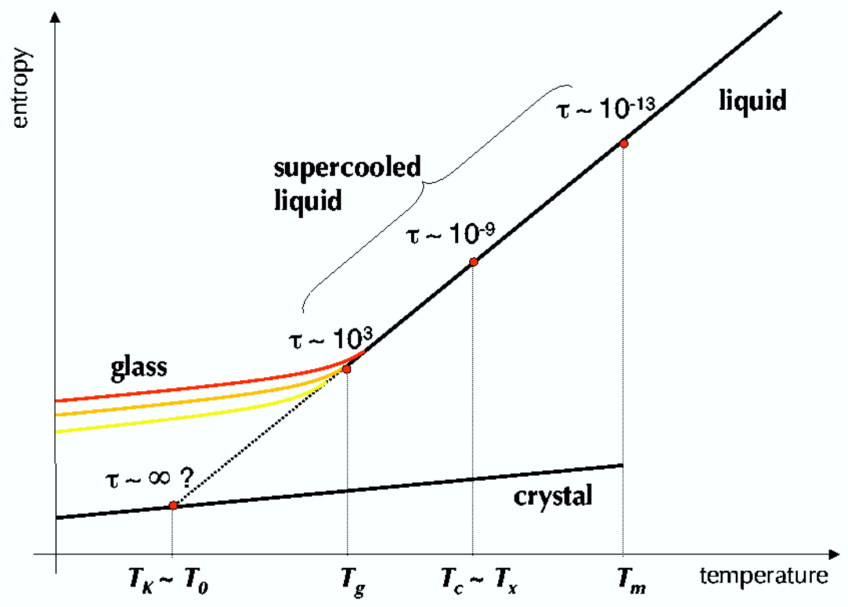

Figure 1.1: Pictorial view of the behavior of the entropy as a function of temperature. For high temperature the system is liquid. The relaxation times τ are indicated in seconds. At the melting point T_m crystallization can be avoided and the system eventually enters in the supercooled liquid phase. At the mode-coupling temperature T_c, the relaxation is dominated by activated dynamics and the relaxation time grows exponentially for decreasing temperature. At the (protocol dependent) glass transition T_g, the relaxation time of the supercooled liquid is longer than the experimental one and the system is frozen in a glass state. The point where the extrapolated entropy of the supercooled liquid meets the one of the crystal is called Kauzmann point T_K. Reprinted from [51].

the crystal has a lower free energy. It shows a sharp increase, at least exponential, of the relaxation time τ_R, in a way that has common features for very different glassy systems, suggesting the presence of some common origin for these phenomena. When the relaxation time exceeds the experimental time, we have reached the glass transition temperature T_g and the system is out of equilibrium. Therefore, T_g depends on the experimental protocol [1] and is not a thermodynamic transition.

For a Maxwell fluid [2], we can write its instantaneous shear modulus as $G(t) = G_\infty e^{-\frac{t}{\tau_R}}$ and relate the (dynamic) viscosity of the fluid η to the relaxation time τ_R using the infinite frequency shear modulus G_∞:

$$\eta = G_\infty \tau_R \tag{1.1}$$

Therefore, the glass transition is often conventionally defined [151] as the temperature T_g for which

$$\eta(T_g) \sim 10^{12} \text{ Pa} \cdot \text{s} \tag{1.2}$$

that, using standard values $G_\infty \sim 10^9 - 10^{10}$ Pa, gives $\tau_R(T_g) \sim 10^2 - 10^3$ s. [3]

[1] By the way, due to the exponential dependence of τ_R from T, the change of T_g with respect to the cooling rate is only logarithmic, corresponding to the Bartenev-Ritland equation.[19, 206]

[2] A Maxwell material is a viscoelastic material having the properties both of elasticity and viscosity. It is represented by a purely viscous damper and a purely elastic spring connected in series.[173, 68]

[3] For comparison, the viscosity of water at $T = 25°C$ is 8.9 10^{-4} Pa·s, and varies between 2.8 10^{-4} Pa·s at $T = 100°C$ and 1.8 10^{-3} Pa · s at $T = 0°C$.

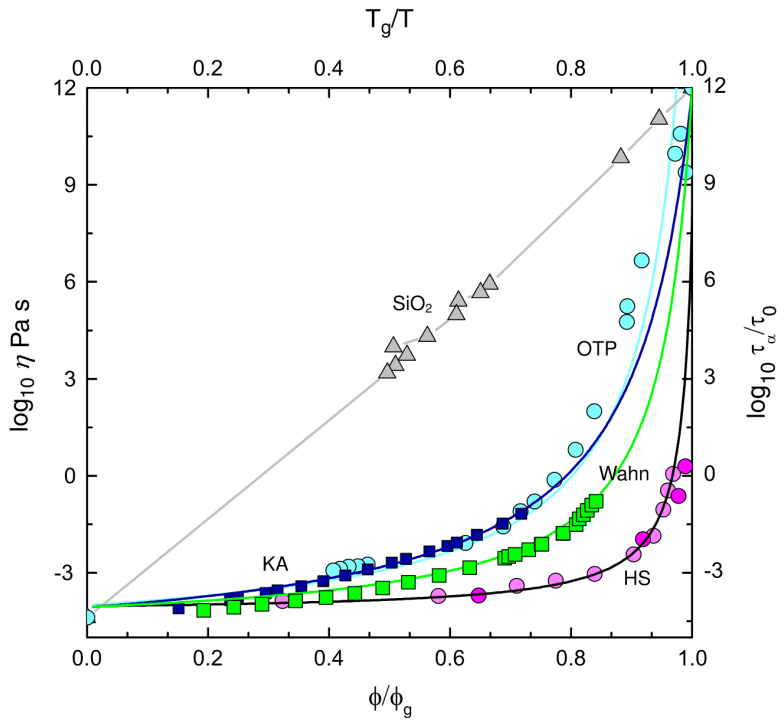

Figure 1.2: Angell plot: behavior of the viscosity/relaxation time for several glass formers with respect to the inverse temperature (or w.r.t. packing fraction ϕ for hard-spheres). OTP=orthoterpheny, KA=Kob-Andersen, Wahn=Wahnström binary Lennard-Jones, HS = hard spheres. Reprinted from [211].

This allows to plot the logarithmic viscosities/relaxation times as function of $\frac{T_g}{T}$ for different glass formers that therefore meet at $\frac{T_g}{T} = 1$: it is called the *Angell plot* [13].

Straight lines in the Angell plot correspond to Arrhenius behavior and the corresponding materials are indicated as *strong* glass formers (e.g. silica SiO_2):

$$\tau_R = \tau_0 \; e^{\frac{E}{k_B T}} \tag{1.3}$$

where k_B is the Boltzmann constant and E is the energy of the barriers to be crossed in order to relax the system. The glass formers defined *fragile* are instead characterized by a super-Arrhenius behavior usually fitted by the Vogel-Fulcher-Tamman law (VFT):

$$\tau_R = \tau_0 \; e^{\frac{KT_0}{T-T_0}} \tag{1.4}$$

where K indicates the index of fragility. The VFT law and the physical meaning of the temperature T_0 are object of debate[127, 92] and other good fitting laws have been proposed, like the Bässler law [20]

$$\tau_R = \tau_0 e^{K \; \left(\frac{T_*}{T}\right)^2} \tag{1.5}$$

One main feature of glasses is that the exponential increase in relaxation time has no signature in simple static correlation functions like the *structure factor*

$$S(q) = \frac{1}{N} \langle \rho_{\mathbf{q}} \rho_{-\mathbf{q}} \rangle \tag{1.6}$$

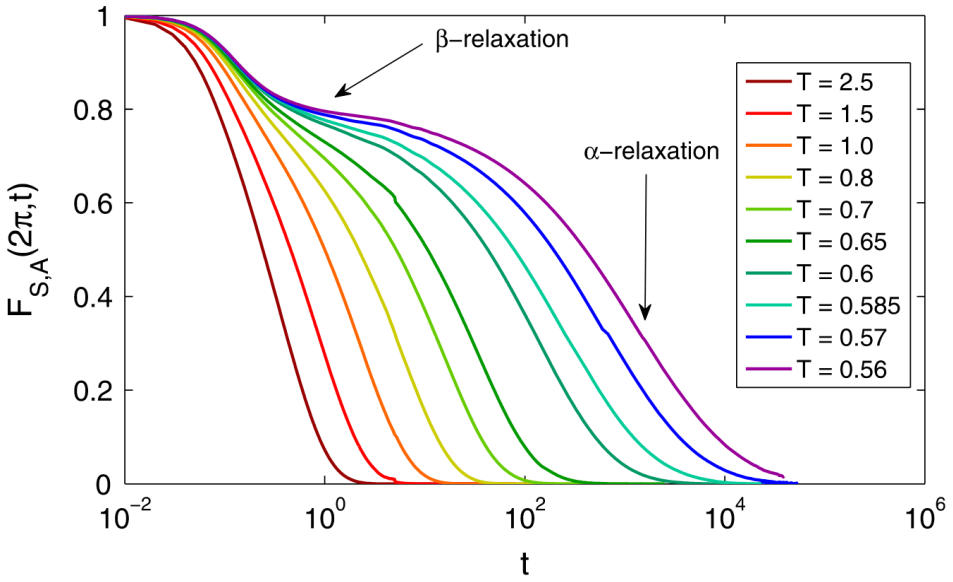

Figure 1.3: Intermediate scattering function at different temperatures in a glass former model (the Wahnström model). Reprinted from [211].

where the average $\langle ... \rangle$ includes averaging over angles and the Fourier component is

$$\rho_{\mathbf{q}} = \sum_{j=1}^{N} e^{i\mathbf{q}\cdot\mathbf{x}_j} \tag{1.7}$$

, where $\mathbf{x}_j$ is the d-dimensional position of particle j. Signals of the glass transition appear in dynamic correlations like the *intermediate scattering function*

$$F(q,t) = \frac{1}{N}\langle \rho_{\mathbf{q}}(t)\rho_{-\mathbf{q}}(0)\rangle \tag{1.8}$$

As pictured in Fig. 1.3, the dynamical correlation functions near the glass transition show a two-step relaxation process: a fast one, called β relaxation, and a slow one, called α relaxation with time-scale τ_α. Between them there exists a plateau whose time extension becomes larger and larger approaching the glass transition. At low temperature, we have a clear separation of time-scales, with τ_β weekly dependent on temperature and τ_α heavily dependent on temperature, so that τ_α dominates the total relaxation time $\tau_R \sim \tau_\alpha$. This behavior is mirrored by the mean-square displacement (MSD) of a particle

$$\langle r(t)^2\rangle = \frac{1}{N}\sum_{i=1}^{N}\langle |\,\mathbf{x}_i(t) - \mathbf{x}_i(0)|^2\rangle \tag{1.9}$$

When approaching the glass transition, $\langle r(t)^2\rangle$ has three regimes: a ballistic one for short times, a localized one for intermediate times and a diffusive one for long times. These have a clear correspondence with the behavior of the dynamical correlation functions. The emergence of the plateau can therefore be pictured as due to the vibrations of the particles inside some "cages", with τ_α being the time scale needed to escape these cages and restore ergodicity. Let's notice that this behavior is observed also in mean field models, where the notion of trapped particles cannot be applied: a better picture is given by thinking of "cages" in the phase space.

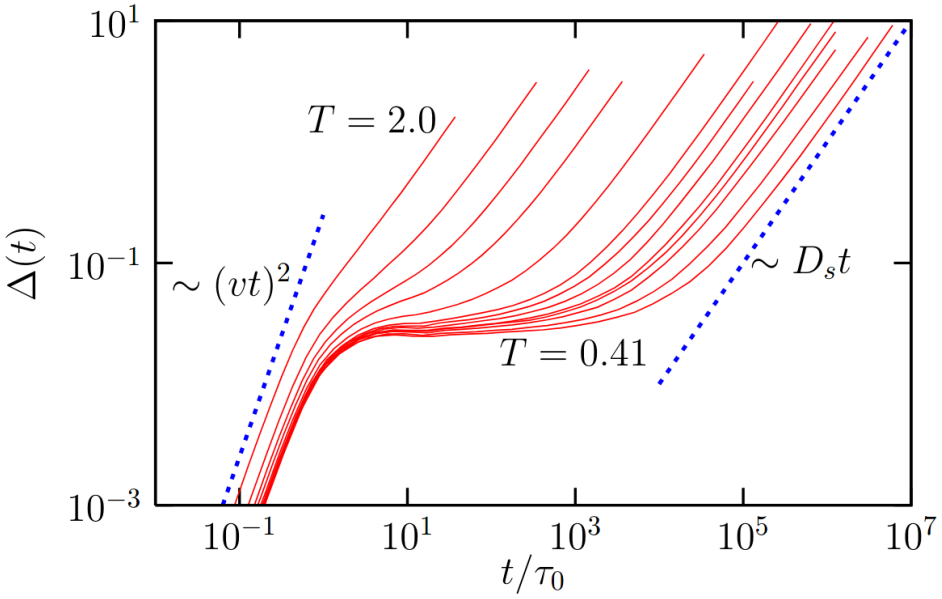

Figure 1.4: Mean-square displacement of particles in time for a liquid of Lennard-Jones particles approaching the glass transition. Reprinted from [27].

The relaxation of supercooled liquids has several features very different from ordinary liquids, in particular the break-down of the Stokes-Einstein relation [230, 221] and the emergence of dynamical heterogeneity [242, 137, 88, 26, 28]. Dynamic heterogeneity refers to the fact that structural relaxation does not happen uniformly in the material, but instead particles rearrange collectively in clusters while the rest of the system remains temporarily frozen. These domains have non-trivial spatio-temporal fluctuations encoded in the *dynamic susceptibility* $\chi_4(t)$ [97, 102, 27], that can hint to a growing dynamical lengthscale [183].

Describing the α-relaxation process from first-principles is very challenging, since it is controlled by *activated dynamics*, meaning rearrangements in real space that involve crossing free-energy barriers whose time-scales are given by the Arrhenius formula. The discussion about what happens near the glass transition in the activated dynamics phase is actually very intense. There exist different approaches and many references that discuss them [211, 27, 161, 150, 213, 229]. One of the main controversies is the role played by thermodynamics.

One perspective is taken by the *dynamical facilitation* approach [52] and *kinetically constrained models* (KCM) [207, 114]. In these models, the interactions between the degrees of freedom are trivial and so the thermodynamics is trivial. On the other hand, the dynamical rules to change a variable are constrained by its local neighborhood. These models are simple enough to be studied analytically and numerically and they consistently show several features of glassy dynamics, like cooperativity of the relaxation with super-Arrhenius relaxation time and the emergence of dynamical heterogeneities in a space-time representation. Their limitation is a lack of explanation of how these dynamical models should emerge from real atomistic liquids [115] and their impossibility to describe thermodynamic features [35].

A different perspective looks at thermodynamics as playing a major role in defining the dynamics. This idea is grounded on the fact that it is correct in mean-field models, but its difficulty consists in dealing with activated processes in finite-dimensional models. These are in fact non-perturbative effects whose presence could jeopardize the mean-field scenario.

In this work, we study glassy models at zero temperature and we do not enter into the discussion of thermally activated processes in real space. Since we make use of mean-field theory, we mention two frameworks that are instrumental for our discussion.

Mode Coupling Theory

Mode Coupling Theory (MCT) [23, 119, 131] is a dynamical theory built on the hypothesis that the structural properties of the glass former are similar to those of the high temperature liquid and that there are two separated time scales, the microscopic (fast) relaxation and a slower one. Therefore it obtains an equation for the time evolution of the dynamical correlation functions which depend on a memory kernel (it is a generalized Langevin equation). The difficulty comes from the fact that the memory kernel depends on higher orders correlations. The standard approach consists in approximating it as a function of two-point correlations: this gives self-consistent integro-differential equations. The input used in this theory is only the static structure factor, therefore it is considered to be close to a first-principles approach.
Solving MCT equations gives a divergent relaxation time for a temperature T_{MCT}. It is not due to local effects, since it involves the divergence of a length scale characterizing the spatial correlations in the dynamics [102, 34]. However, the quantitative predictions are not accurate for real glass formers, since in general $T_{MCT} > T_g$ and the relaxation time diverges as a power-law. It turns out that MCT is a "mean-field like" approximation that can predict the β-relaxation process but not the activated dynamics and its dynamical heterogeneities. In finite dimensions, this singularity is modified both by the fact that its upper critical dimension is $d_u = 8$ [96] and by the presence of activated processes that destroy it altogether.
More recently, a Generalized Mode Coupling Theory (GMCT) [226, 132] has tried to include higher order correlations into the framework: it does improve some quantitative features, like giving a smaller T_{MCT}, and it has potential to give also better qualitative predictions, such as a relaxation time with (super-)Arrhenius behavior [131, 174, 133].

Random First Order Transition

The *Random First Order Transition* (RFOT) [142, 143, 141, 161, 33] is a theory born from the realization that some mean-field models with quenched disorder, like the random p-spin and Potts-glass models with infinite range interactions, have dynamical equations of the same kind as Mode Coupling Theory. In these mean-field models, there exists a dynamical transition temperature T_d corresponding to ergodicity breaking: for $T < T_d$ the dynamics gets trapped in metastable states whose lifetime is infinite, because the energy barriers separating them are infinite in the mean-field setting. Each one of these states is a "glass". Their number is exponential in the system size and they dominate the thermodynamic measure. Therefore it is possible to define the *configurational entropy* Σ

as

$$\Sigma(E) = \lim_{N\to\infty} \frac{1}{N} \log \mathcal{N}(E) \tag{1.10}$$

where $\mathcal{N}(E)$ is the number of glassy states at energy E. For decreasing temperature (i.e. decreasing energy), the number of glassy states diminishes until Σ vanishes at a temperature T_K, called *Kauzmann temperature* [136]. In supercooled liquids, the Kauzmann temperature corresponds to the point where the extrapolation of the entropy of the supercooled liquid below T_g meets with the entropy of the crystal (whose formation was avoided).
Contrary to the dynamical transition, the Kauzmann point is a true thermodynamic phase transition to an *ideal glass* phase. It is a second order transition, since no latent heat is involved, but it is accompanied by a discontinuous jump of the order parameter, corresponding to the correlation between two typical configurations.
In real supercooled liquids, the dynamical transition T_d (corresponding to the Mode Coupling one) is "avoided" and becomes a cross-over, since activated dynamics becomes the dominant relaxation mechanism and restores ergodicity, even if with longer and longer time-scales as temperature decreases. Therefore, in the real-space formulation of RFOT, these non-perturbative processes are added to the theory by a "mosaic state" scenario characterized by a mosaic length diverging at T_K [141, 130, 33, 94, 51]. The last stage of the theory for glass-forming liquids is made by some phenomenological modeling to take into account other experimental phenomena [251, 252, 161].
The validity of the complex landscape scenario in real supercooled liquids is debatable, but it is correct in mean-field models [103, 49, 202]. We use the RFOT framework to understand the mean-field version of the simplest glass former: hard spheres in infinite dimensions.

1.2 Simple structural glass model: dense hard spheres

Let's consider N hard spheres of diameter σ in d dimensions in a volume V. We indicate their center positions at time t by $\mathbf{x}_i(t)$, with $i = 1, ..., N$. The pairwise distances between spheres are given by $h_{ij} = |\,\mathbf{x}_i - \mathbf{x}_j\,| - \sigma$ and the corresponding pair-wise hard sphere potential is simply

$$\nu(h_{ij}) = \begin{cases} 0 & h_{ij} > 0 \\ \infty & h_{ij} < 0 \end{cases} \tag{1.11}$$

Calling $\rho = \frac{N}{V}$ and given the single sphere volume v_σ, the packing fraction is simply $\phi = \rho v_\sigma$. In this problem the temperature is just a rescaling factor for the energy, so we make use of the reduced pressure $p(\phi) = \frac{P}{\rho T}$, where P is the actual pressure. We can understand the glassy phenomenology by using the density ϕ as control parameter, instead of the temperature as it is done in supercooled liquids.
At low density, the system is in a liquid phase with a corresponding equilibrium pressure $p(\phi)$. Increasing the density adiabatically, we get an increasing pressure up to ϕ_f: at this point the system undergoes a first-order phase transition to a crystalline state and the density jumps to ϕ_m. This is true for dimensions $d = 2$ and $d = 3$ where the densest packings are known to be the hexagonal lattice and the face centered cubic (FCC) lattice, respectively; it is true also for those dimensions where the densest packing is known to be

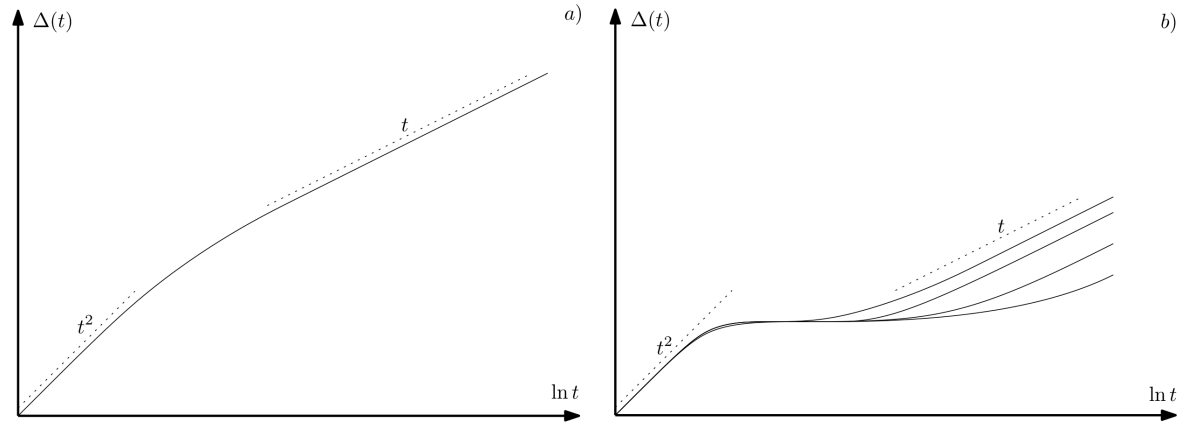

Figure 1.5: Dynamical Mean Square Displacement as a function of time. For low packing fractions a), the liquid phase is characterized by a ballistic regime at short time followed by a diffusive one. For higher packing fractions b), the particles of the supercooled liquid tend to stay trapped in cages for longer times, therefore $\Delta(t)$ develops a plateau after the ballistic regime. The length of the plateau increases exponentially for increasing packing fraction. At the glass transition, the length of the plateau is infinite and ergodicity is broken (with respect to the experimental time-scale).

crystalline [239, 70, 73], even if the crystallization process is more difficult for increasing dimensionality [224, 176, 54, 60]. Once the crystal is formed, it is possible to compress it further to reduce the thermal vibrations and block the system into the perfect crystal, with diverging pressure.
If instead of compressing quasi-statically we do it with a finite compression rate, we can avoid the crystallization and enter in the "supercooled" metastable phase [258, 224, 177, 178]. As a dynamical order parameter we can use the dynamical Mean Square Displacement (MSD)

$$\Delta(t) = \frac{1}{N}\sum_{i=1}^{N} |\,\mathbf{x}_i(t) - \mathbf{x}_i(0)|^2 \tag{1.12}$$

In the liquid phase, the spheres move in a ballistic way for short times, therefore $\Delta(t) \sim t^2$, and in a diffusive manner after they start undergoing collisions, giving $\Delta(t) \sim t$. In the supercooled liquid phase, the ballistic and diffusive regime are separated by a plateau whose length increases for increasing density, due to the fact that the particles stay trapped in "cages" for longer times before managing to get uncorrelated from their initial positions. The time to escape the cages is therefore the α-relaxation time and it increases exponentially upon compression.

Compressing further, the relaxation time eventually becomes larger than the experimental time, the system stays out-of-equilibrium and the glass transition ϕ_g is met. Also in this case, longer experiments, i.e. slower compression protocols, modify the glass transition point and push ϕ_g to higher values. The system gets frozen in an amorphous solid, a hard sphere glass, and it is not able to relax to the metastable supercooled liquid. Experiments with colloidal hard spheres presenting all the glassy phenomenology (i.e. super-Arrhenius relaxation time, two-step relaxation of the dynamical correlation, stretched exponential for the α-process and increasing dynamical heterogeneities) can be

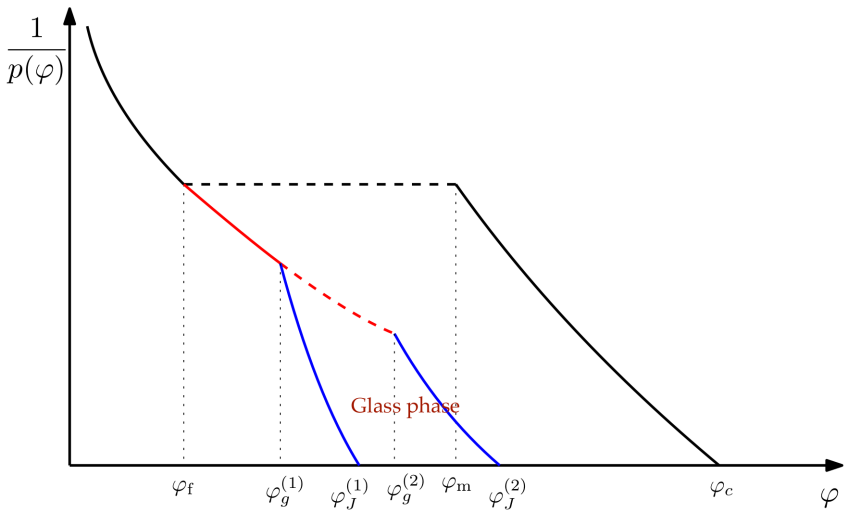

Figure 1.6: Pictorial view of the phase diagram of hard spheres under compression. The black line corresponds to the thermodynamic equilibrium one, which has a first order phase transition from the liquid to the lattice packing, where the density jumps from φ_f to φ_m. The close packing of the crystalline structure corresponds to φ_c, the highest possible density. The red line corresponds to the supercooled liquid. According to the compression rate, a glass transition is met at different φ_g: for a smaller compression rate, an higher φ_g is obtained. Compressing a glass, the infinite pressure point corresponds to the jamming point, with packing fraction φ_J dependent on φ_g. Reprinted from [234].

found in Ref. [42, 69].
If we compress a glass further, the system does not follow any longer the equation of state of the supercooled liquid and the pressure increases sharply and diverges at a density ϕ_J: as ϕ_g, it depends on the compression rate.
The protocol-dependent ϕ_J is the jamming point and its critical properties do not depend on the protocol [135, 147, 66, 165, 192, 259].

1.2.1 Infinite dimensional hard spheres

The theory of a liquid of hard spheres has been solved in infinite-dimensional space $d \to \infty$ [201, 202, 149, 148, 63, 62, 205, 204, 64, 200]. The approach is inspired by the fact that, as for many strongly coupled systems, amorphous materials lack a natural reference for building a perturbative expansion. Therefore, the idea is to solve the problem in $d \to \infty$ and use $\frac{1}{d}$ as a small parameter to approximate the behavior of finite dimensional systems. This approach has little to say about features that strongly depend on the dimensionality, like singularly dense packings due to lattice structures in $d = 2, 3, 8, 24$, but it highlights features of amorphous materials that are weakly dependent, or even independent, of dimensionality [60, 55, 54, 178, 87, 224, 216].
In infinite dimensions, the problem can be solved using techniques developed for mean-field spin glasses. A comprehensive presentation of the theory can be found in the book [200]. Here we discuss the results.
First of all, we have to rescale pressure and packing fraction as $\hat{p} = p/d$ and $\hat{\phi} = 2^d \frac{\phi}{d}$ to have finite quantities in the $d \to \infty$ limit. Starting from the liquid phase at low density, it is possible to follow the equilibrium liquid line upon compression (we think of

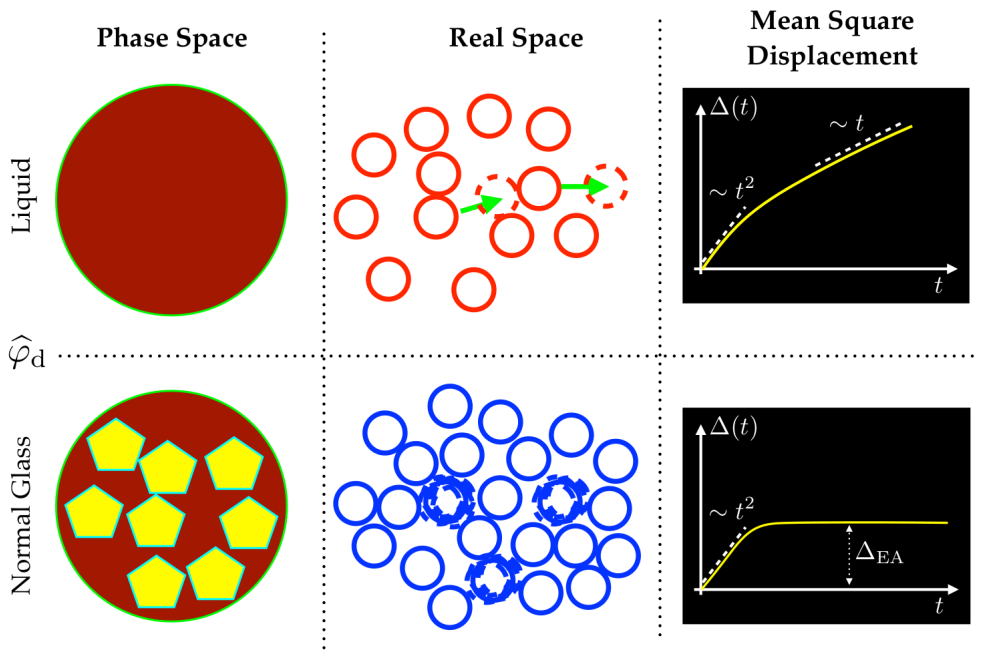

Figure 1.7: Pictorial view of the dynamical transition for hard spheres. Reprinted from [64].

the compression obtained by increasing the spheres' diameters). In infinite dimensions, it is not known if a crystal structure appears.
The infinite dimensional dynamics gives the behavior of the dynamical Mean Square Displacement (MSD) for increasing density [163]. It shows the appearance of a two-step relaxation with τ_α diverging as a power law at the density $\hat{\phi}_d$

$$\tau_\alpha \sim |\hat{\phi} - \hat{\phi}_d|^{-\gamma_{MCT}} \tag{1.13}$$

where the exponent γ_{MCT} can be computed analytically [148]. While in finite dimensions $\hat{\phi}_d$ is just a cross-over, in infinite dimensions it is a true dynamical transition: ergodicity is broken, the landscape gets split in an exponentially large number of glassy states separated by infinite energy barriers and the system gets trapped in one of them. This is revealed by the plateau of the MSD that for long times satisfies

$$\lim_{t\to\infty} \Delta(t) = \Delta_{EA} < \infty \tag{1.14}$$

This transition corresponds to the Mode Coupling (MCT) one discussed for general glass formers [119]. As for usual critical points, the dynamical transition can be detected by the divergence of the dynamical susceptibility $\chi_4(t)$:

$$\chi_4(t) = N\left(\overline{\Delta^2(t)} - \overline{\Delta(t)}^2\right) \tag{1.15}$$

where the average $\overline{\cdots}$ is over the thermal history of the system and the initial configurations. In the glass phase, χ_4 goes to a constant for long times $\lim_{t\to\infty}\chi_4(t) = \chi$ and it diverges as $\chi \sim |\hat{\phi} - \hat{\phi}_d|^{-\frac{1}{2}}$ when approaching the transition from above $\hat{\phi} \to \hat{\phi}_d^+$. When approaching the transition from the liquid phase $\hat{\phi} \to \hat{\phi}_d^-$, $\chi_4(t)$ has peak at $t \sim \tau_\alpha$ similarly diverging [102, 82, 25, 24]. Associated with χ_4 there is a dynamical correlation length diverging at the transition as $\xi_d \sim |\hat{\phi} - \hat{\phi}_d|^{-\frac{1}{4}}$ [96, 98, 99].

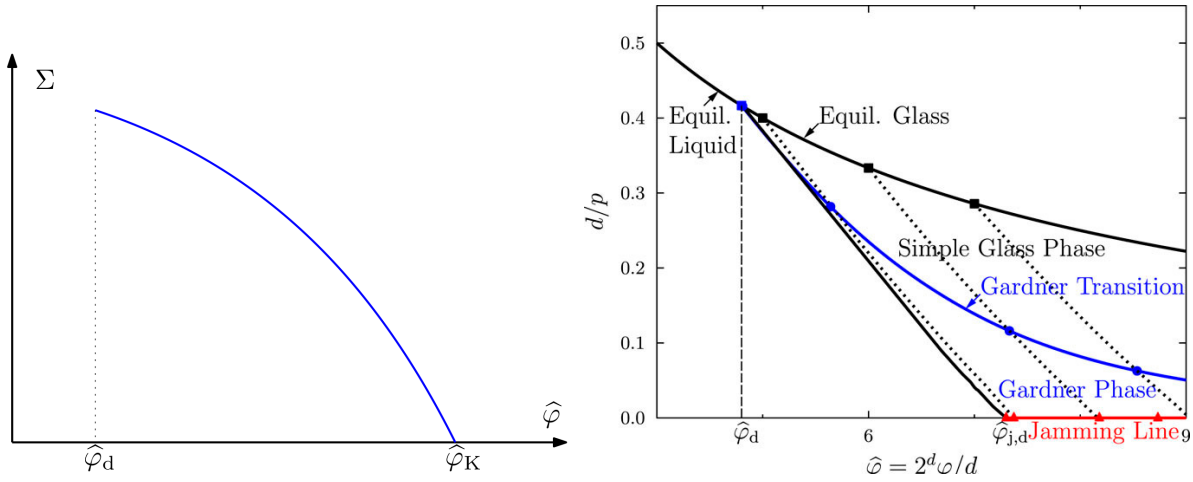

Figure 1.8: *Left panel.* Behavior of the configurational entropy. The glassy states appear at the dynamical transition $\hat{\phi}_d$ and vanish at the Kauzmann point $\hat{\phi}_K$. *Right panel.* Phase diagram of hard spheres in infinite dimensions. The black line is the equilibrium liquid line; the blue line represents the Gardner transition; the red line is the jamming line. Between the blue and red lines, glassy states are marginally stable. Reprinted from [64].

The glassy states emerging above ϕ_d are exponential in number, therefore the configurational entropy can be defined

$$\Sigma(\hat{\phi}) = \lim_{N\to\infty} \frac{1}{N} \log \mathcal{N}(\hat{\phi}) \tag{1.16}$$

with $\mathcal{N}(\hat{\phi})$ being the number of glassy states at packing fraction $\hat{\phi}$. It is maximal at $\hat{\phi}_d$, diminishes for increasing density and vanishes at the Kauzmann point $\hat{\phi}_K$.

For $\hat{\phi} > \hat{\phi}_d$ the system cannot equilibrate. However, if starting from the liquid phase at equilibrium the system is quickly compressed to $\hat{\phi} > \hat{\phi}_d$, it starts *aging*, meaning that $\Delta(t_w, t - t_w)$ relaxes ever more slowly and becomes a function of both the time t_w passed since the rapid compression and the time difference $t - t_w$ [76, 75, 163].

Following a glass state

Notice that $\hat{\phi}_d$ is a singular point only for the dynamics and does not show thermodynamic signatures. However, modifying the measure over the configurations, it is possible to extract dynamical information using only statistical mechanics tools. In disordered systems, this is done using the so called *Franz-Parisi potential* [95, 18, 205, 204]. The construction starts by considering a configuration Y at equilibrium for $\hat{\phi}_g > \hat{\phi}_d$: if a configuration $X(t)$ is let relaxing, with $X(0) = Y$, then their long time mean square displacement behaves like

$$\lim_{t\to\infty} \Delta(X(t), Y) = \lim_{t\to\infty} \frac{d}{N\sigma^2} \sum_i |\,\mathbf{x}_i(t) - \mathbf{y}_i|^2 = \Delta_r \tag{1.17}$$

since $X(t)$ can relax only inside the glassy state of Y but cannot escape it. It is possible also to compress/decompress X to another density $\hat{\phi} \neq \hat{\phi}_g$ (by changing the spheres' diameter σ and keeping the volume constant), where it will relax as

$$\lim_{t\to\infty,\tau\to\infty} \Delta\left(X(t+\tau), X(\tau)\right) \to \Delta \tag{1.18}$$

Assuming that X is sampled by the Boltzmann distribution at $\hat{\phi}$ with the constraint that its average distance from Y is Δ_r, we can define

$$\begin{aligned} P(X, \hat{\phi}\,|Y, \hat{\phi}_g) &= e^{-\beta H\left(X,\hat{\phi}\right)}\ \delta\left(\Delta_r - \Delta\left(X, Y\right)\right) \\ Z[\Delta_r, \hat{\phi}\,|Y, \hat{\phi}_g] &= \int dX\ P(X, \hat{\phi}\,|Y, \hat{\phi}_g) \end{aligned} \tag{1.19}$$

The generalized free-energy of the metastable state selected by Y is therefore

$$f(\Delta_r, \hat{\phi}\,|Y, \hat{\phi}_g) = -\frac{1}{N\beta} \log Z[\Delta_r, \hat{\phi}\,|Y, \hat{\phi}_g] \tag{1.20}$$

Averaging over Y with the equilibrium Boltzmann weight, we obtain the Franz-Parisi potential V_{FP}

$$V_{FP}(\Delta_r, \hat{\phi}\,|\,\hat{\phi}_g) = \int \frac{dY e^{-\beta H[Y;\hat{\phi}_g]}}{Z[\hat{\phi}_g]} f(\Delta_r, \hat{\phi}\,|Y, \hat{\phi}_g) \tag{1.21}$$

V_{FP} can be computed explicitly using the replica method. The value of self mean square displacement Δ of X is chosen so as to minimize the free energy. $V_{FP}(\Delta_r, \hat{\phi}\,|\,\hat{\phi}_g)$ depends explicitly on Δ_r.
For $\hat{\phi}_g < \hat{\phi}_d$ the potential does not have any local minimum at finite Δ_r, therefore Y is unable to trap X at long times and the system is liquid. For $\hat{\phi}_g > \hat{\phi}_d$, instead, there is a local minimum at finite Δ_r and Y is in a metastable state characterized by Δ_r. The transition between these two behaviors corresponds to the dynamical transition $\hat{\phi}_d$.
Notice that we can follow the system at fixed $\hat{\phi}_g$ varying $\hat{\phi}$, and the equation of state of the glass for a given $\hat{\phi}_g$ is obtained by computing the pressure $p(\hat{\phi}\,|\,\hat{\phi}_g) = \frac{\mathrm{d}}{\mathrm{d}\,\hat{\phi}} V_{FP}(\Delta_r, \hat{\phi}\,|\,\hat{\phi}_g)$ [205]. At $\hat{\phi} = \hat{\phi}_g$, the system sits on the line of the equilibrium glasses and therefore $\Delta_r = \Delta_{EA}$ with pressure $p(\hat{\phi}_g\,|\,\hat{\phi}_g)$ corresponding to the analytic continuation of the liquid one. A system prepared in an equilibrium glass state is therefore an amorphous solid: the configurations of its degrees of freedom are confined in a restricted portion of the phase space; inside this basin, the system relaxes with a finite relaxation time τ_β and has a well defined shear modulus and non-linear elastic susceptibilities [36]. Moreover, neglecting the Debye contribution, it has a gapped vibrational density of states [106, 56].

Gardner transition

Considering an equilibrium glass at $\hat{\phi}_g$, we can follow the state when we compress it to $\hat{\phi} > \hat{\phi}_g$. At sufficiently high density $\hat{\phi}_G$ (depending on $\hat{\phi}_g$), the system undergoes a *Gardner phase transition*. Beyond this density the system cannot be described any longer by the two order parameters Δ_r and Δ and it enters in the *Gardner phase* [148, 205, 63, 62]. This phase was first observed in spin-glasses [112, 121] and takes its name from Elisabeth Gardner. It is characterized by the fact that the simple basin of the glass state acquires a complex internal structure of metastable states organized with an ultrametric structure and described by full replica symmetry breaking [168, 63]. At the Gardner transition, the minimum of the glass state flattens causing the divergence of the relaxation time scale $\tau_\beta \sim |\,\hat{\phi}_G - \hat{\phi}\,|^{-a}$ and of the dynamical susceptibility $\lim_{t\to\infty} \chi_4(t) \sim |\,\hat{\phi}_G - \hat{\phi}\,|^{-1}$, where the exponent a is non-universal and depends on $\hat{\phi}_g$ [196, 204, 30, 61]. Moreover, the divergence of χ_4 is associated with a diverging correlation length ξ_G.

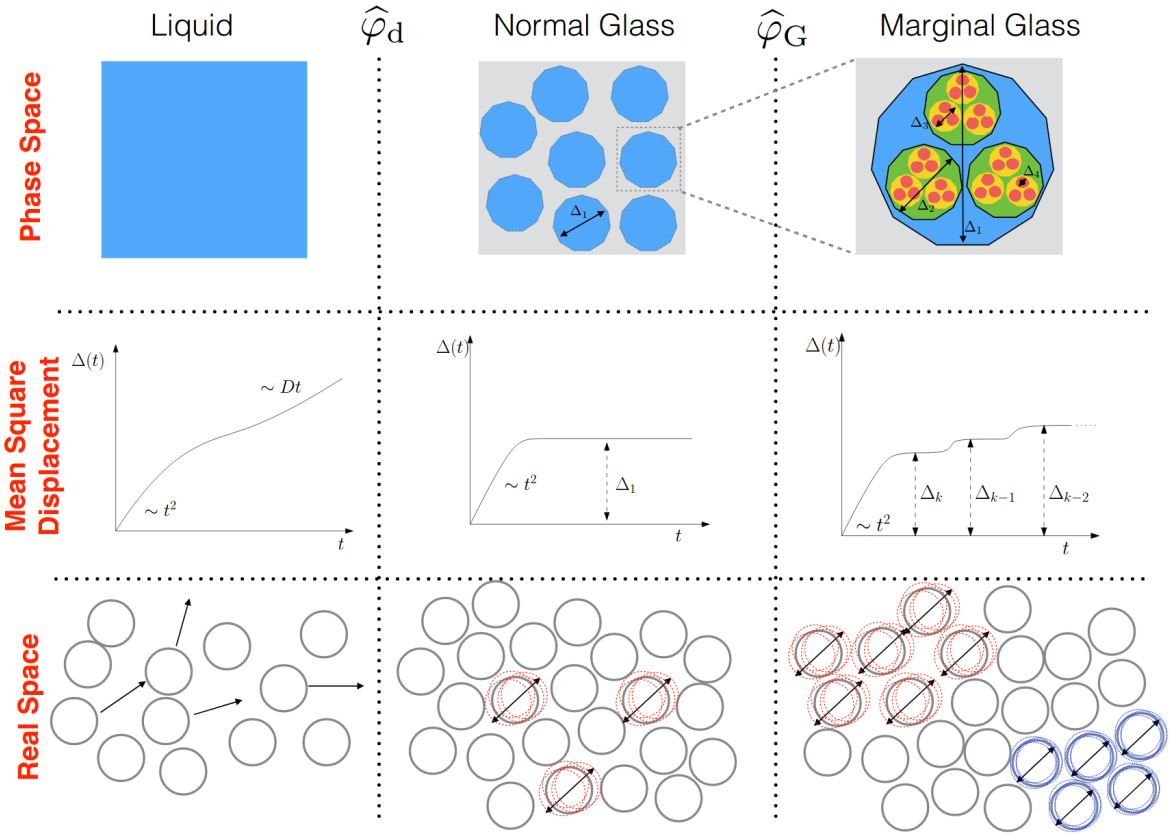

Figure 1.9: For $\hat{\phi} < \hat{\phi}_d$, hard spheres are in a liquid phase: all the phase space can be dynamically explored and the mean-square displacement reaches a diffusive regime that makes it diverge for long times. For $\hat{\phi} \in [\hat{\phi}_d, \hat{\phi}_G]$, the phase space is clustered in an exponential number of metastable states and the system is caged in one of them: it is a normal glass. The particles can only vibrate around an amorphous lattice, therefore the mean-square displacement has a plateau proportional to the amplitude of the vibrations. For $\hat{\phi} > \hat{\phi}_G$, the system is in a marginal glass phase: the basin of the normal glass state gets split in basins of hierarchically organized configurations. The mean-square displacement is not stationary for long times and displays an infinite series of plateaus. Reprinted from [64].

The Gardner transition is of second-order nature and is accompanied by the emergence of soft-modes. They characterize all the Gardner phase that is therefore a *marginal glass* phase. The relaxation of the system is characterized by the rapid vibrations of the spheres around the amorphous lattice positions followed by infinitely slow changes of the amorphous lattice itself [64]. The vibrations of the spheres have heterogeneous amplitudes and are correlated over large regions.
A key feature of the marginal glass phase is the break-down of elasticity [36]. Considering an expansion of the elastic stress in powers of the strain, it is found that the non-linear response coefficient has divergent sample-to-sample fluctuations when approaching the Gardner phase: this is related to *plasticity*, meaning the irreversibility of the elastic response [134], in contrast with the reversibility of the response characterizing the normal glass phase. In the Gardner phase, an infinitesimal variation of density or shear strain produces extensive rearrangements: *avalanches* [188, 153, 110], whose size distribution scales as a power law with universal critical exponents. This is a common signature of marginal stability that emerges in various physical systems like equilibrium mean-field models [187, 77], out-of-equilibrium systems in finite dimensions [188] and self-organized critical models [17, 93]. The presence of avalanches in the response of the system produces the so-called *crackling noise*[218].

The prediction of the existence of a Gardner transition for infinite dimensional hard-spheres is a new non-trivial feature for a structural glass without quenched disorder. The possibility of its existence in finite d is under exploration, both by using renormalization group techniques [235, 65, 59, 10, 184, 256] and numerical simulations (looking for growing correlation length, susceptibility and correlation time) [30, 217, 157]. At the moment, there is consensus on the fact that the lower critical dimension of this transition is $d_l \simeq 2.5$, therefore the exploration is focused on its possible existence in $d = 3$. For a review of Gardner physics, see Ref. [29].

1.3 The jamming transition

1.3.1 Jamming of hard spheres

Considering a glass in the marginal phase of infinite dimensional hard spheres, the compression can be continued: the endpoint is reached when the pressure diverges at a certain $\hat{\phi}_J$ (depending on $\hat{\phi}_g$). That is the jamming point of the glass. It reaches its densest packing and the spheres are in direct mechanical contact with each other. With a hard sphere interaction, the system cannot be compressed any further.
In the case of infinite dimensional hard spheres, we see that the dynamical glass transition happens before approaching the jamming point. Moreover, the jamming point is met in the marginal glass phase: marginal stability is in fact a very important feature of the jamming of spheres [45, 44, 160, 247, 154, 188]. It corresponds to the limit $p \to \infty$ and the exact location $\hat{\phi}_J$ depends on the compression history. Despite this fact, the critical behavior at the jamming point is remarkably universal. In particular, the number of sphere contacts scales like $C \sim dN$, a property called *isostaticity*, and correspondingly the distribution of contact forces f and that of gaps h between particles develop power laws for small argument, i.e. $\rho(f) \underset{f\to 0^+}{\sim} f^\theta$ and $\rho(h) \underset{h\to 0^+}{\sim} h^{-\gamma}$, with irrational critical exponents $\theta = 0.42311...$ and $\gamma = 0.41269...$ [62]. This critical behavior is strongly connected with

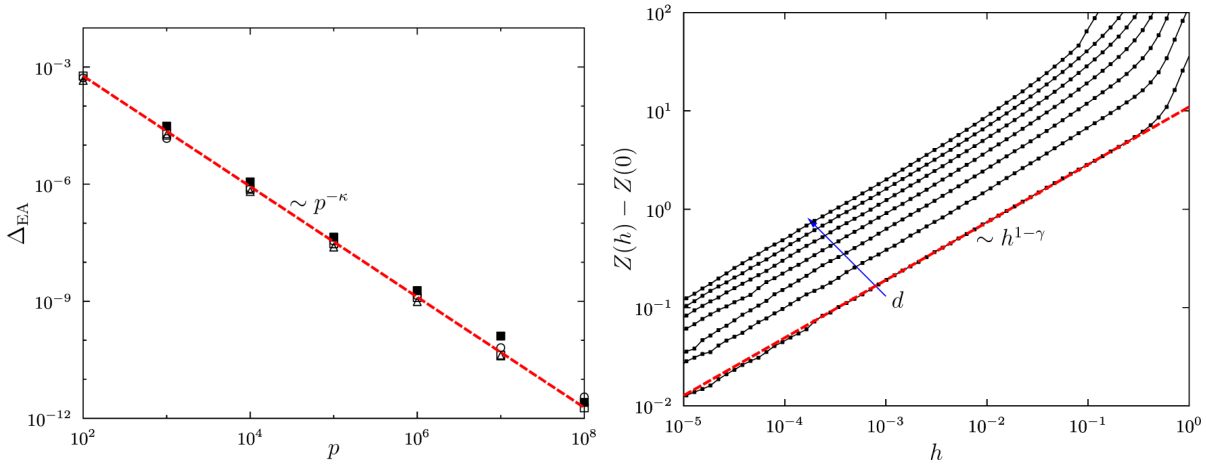

Figure 1.10: Reprinted from [64]. *Left panel.* Decay of the plateau of the mean-square displacement for divergent pressure upon approaching jamming. The scaling $\Delta \sim p^{-\kappa}$ is observed independently of the spatial dimension d ($d = 3, 4, 6, 8$ in the plot). *Right panel.* Cumulative number of spheres at distance h. The critical exponent γ is robust for different dimensions d (represented d from 2 to 12).

the complex structure of the hierarchical metabasins that is fractal with dimension $2/\kappa$, with $\kappa = 1.41574...$. This exponent also controls the scaling of the innermost metabasin that shrinks to a point (i.e. the jamming configuration) giving $\Delta \sim p^{-\kappa}$.
This critical behavior is completely different from what is observed in non-marginal glasses and crystals, where no power law scaling characterizes small forces and gaps and it holds $\Delta \sim p^{-1}$ in normal glasses and $\Delta \sim p^{-2}$ in a crystal [202, 40].
Jamming criticality is strongly linked to the emergence of a large excess of low-frequency modes compared to the Debye scaling for solids, that is a more general feature found in amorphous glasses (even without marginality). This excess of low-frequency modes is called *boson peak* [254, 106]. In fact, the density of vibrational states does not vanish in the limit of zero frequency and it tends to a constant [15, 191, 222, 248, 246]. These soft modes are extended but they have a disordered structure, very different from plane waves [253].
The remarkable feature of jamming criticality is that its universality is very robust with respect to dimensionality, with numerical simulations suggesting that the results of mean-field theory (infinite dimensions) hold down to dimension $d = 2$. This leads to the idea that the upper critical dimension of this universality class is $d_u = 2$ [116, 128, 129].

The jamming point is often studied in the case of athermal systems like grains and foams, where it corresponds to a rigidity transition from a floppy phase to a solid one [159, 190, 191, 160, 233, 158]. Such systems, in fact, can be thought of as athermal soft spheres with pair-wise potential $\nu(h_{ij}) = 0$ if $h_{ij} > 0$ and $\nu(h_{ij}) = |h_{ij}|^a$ if $h_{ij} < 0$, with $a > 1$: in this case the jamming point corresponds to the transition from zero pressure to a positive one (i.e. $p \to 0^+$).

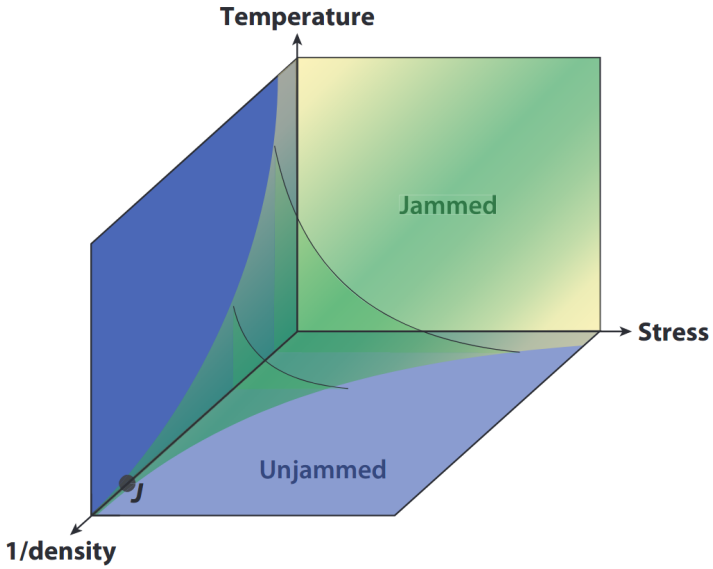

Figure 1.11: Jamming phase diagram proposed by A.J. Liu and S.R. Nagel: inside the shaded green area the system is an amorphous solid (jammed); for high temperature or low density, instead, the system is unjammed and can flow. At zero temperature and zero applied stress there is the jamming transition of ideal spheres. The transition line in the density-temperature phase corresponds to the glass transition, while the one in the density-stress plane is the yield stress. Reprinted form [158].

1.3.2 Jamming in finite dimensions and the marginally jammed solid

Let's consider N spheres in a box of volume V in d spatial dimensions, as before. This time we consider a soft spheres pairwise potential, $H = \sum_{i<j} \nu(h_{ij})$, with

$$\nu(h_{ij}) = \begin{cases} 0 & h_{ij} > 0 \\ \frac{1}{a}|h_{ij}|^a & h_{ij} < 0 \end{cases} \tag{1.22}$$

and $h_{ij} = |\,\mathbf{x}_i - \mathbf{x}_j\,| - \sigma_{ij}$, where $\sigma_{ij} = \sigma_i + \sigma_j$ takes into account the possible polydispersity in the radii σ_i. The case $a = 0$ corresponds to hard spheres. In soft spheres models, differentiable potentials are usually considered, so $a > 1$. Common choices are $a = 2$ (harmonic spheres) and $a = 5/2$ (Hertzian spheres) [191].
We consider the zero temperature case with no applied stress. The control parameter is the packing fraction ϕ.
For small ϕ, the system has zero energy by avoiding overlaps between the spheres, therefore it has no rigidity and flows when a perturbation is applied. Increasing the density, the spheres get more and more closely packed until they start touching: this is the jamming point ϕ_J. Increasing the density produces overlaps between the spheres and the energy and pressure become different from zero. Also the bulk and shear moduli become different from zero, making the jamming point a transition from a liquid-like phase to an amorphous solid one. A further analogy with the glass transition is the fact that the value of ϕ_J depends on the preparation protocol [191, 31, 66, 170]. However, the jamming transition has more peculiar universal properties than generic thermal glass transitions. We list them in the following.

Isostaticity

Since the system is at zero temperature, the contact network formed between the spheres at jamming has to be in mechanical equilibrium. Maxwell's criterion [172] states that, with no frictional forces, the rigidity condition can be satisfied only if the number of inter-particle forces $\frac{Nz}{2}$ (i.e. the number of contacts between the spheres), where z is the average particle connectivity, is at least equal to the number of force balance equations, i.e. the total number of degrees of freedom (d.o.f) which is Nd. Therefore Maxwell criterion gives the condition $z \geq 2d$. At jamming it is found that

$$z = 2d \tag{1.23}$$

meaning that the system is *isostatic* and the number of contacts is the minimal one required by stability [212, 186, 209, 126, 232, 233, 116, 154]. More precisely, the total number of contacts satisfy $Z = Nd + O(d)$, where the order d correction takes into account the choice of the boundary conditions.
In preparing a configuration at jamming, there are other local effects that appear in finite dimensions, for example the presence of *rattlers*, i.e. spheres that are not part of the contact network but rattle inside the cages created by the network. Therefore the isostaticity condition has to be corrected as $Z = dN(1 - f_{ratt}(d)) + O(d)$, where $f_{ratt}(d)$ is the fraction of particles being rattlers which decays exponentially fast for increasing dimensionality [58, 57].

Gap and force distributions

At jamming, the distribution of gaps h_{ij} has a Dirac delta for $h = 0$ that signals the presence of contacts. As discussed for hard spheres, the small gaps between pairs of spheres display a power law scaling

$$\rho(h) \underset{h \to 0^+}{\sim} h^{-\gamma} \tag{1.24}$$

with an exponent $\gamma \simeq 0.4$ [233, 58]. This result holds for all $d \geq 2$ and is compatible with the $d \to \infty$ prediction $\gamma = 0.41269....$

Mechanical marginal stability connects the exponent γ to the power law behavior that is observed for small contact forces [247, 188]. By the way, in finite d a careful analysis of some local effects is necessary. There exist spheres called *bucklers* characterized by a weak connectivity with the rest of the network and that give rise to quasi-localized excitations. We can define bucklers as the spheres with $d + 1$ contacts: they have d contacts that are quasi-coplanar and a remaining weak contact that compensates the asymmetry. These weak forces are characterized by an exponent $\theta_l \simeq 0.18$ [154, 81], different from the critical exponent $\theta \simeq 0.42$ obtained in the infinite dimensional solution. Therefore one can consider the force distribution as a mixture of local and extended components

$$\rho(f) = n_{loc}\rho_{loc}(f) + n_{ext}\rho_{ext}(f) \sim n_{loc}f^{\theta_l} + n_{ext}f^{\theta} \tag{1.25}$$

The analysis of all the contact forces together gives a spurious exponent $\theta_l < \tilde{\theta} < \theta$ and eventually $\tilde{\theta} \simeq \theta_l$ for f small enough. Instead, the analysis of the bucklers separately allows to observe the two exponents θ_l and θ, with θ being compatible with the infinite dimensional value $\theta = 0.4231...$ also for dimensions as small as $d = 2$. Moreover, the number of bucklers, proportional to n_{loc}, vanishes exponentially with increasing d [57].

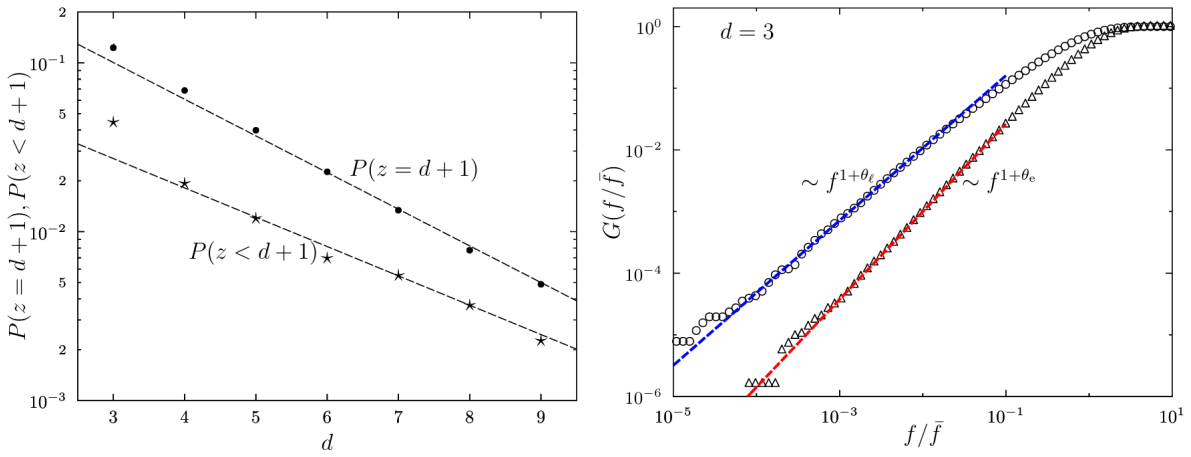

Figure 1.12: *Left panel.* Probability of having a rattler ($z < d+1$) or a buckler $z = d+1$ at jamming as a function of the dimension d. These probabilities decay exponentially for increasing dimensionality, making the presence of rattlers and bucklers a non-perturbative effect with respect to the infinite dimensional solution. *Right panel.* Cumulative distribution of contact forces separating bucklers' contribution ($\sim f^{1+\theta_l}$) from the other forces ($\sim f^{1+\theta_e}$). Their behavior is compatible with the scalings $\theta_l \simeq 0.18$ (blue line) and $\theta_e \simeq 0.42$ (red line). Reprinted from [64].

The values of the critical exponents of gaps and forces satisfy the relation

$$\gamma = \frac{1}{2+\theta} \tag{1.26}$$

that implies *marginal stability* [188]. Studying the fundamental excitations corresponding to opening/closing of contacts, it has been found that stability requires $\gamma \geq 1/(2+\theta)$, where the saturation corresponds to marginal stability [247].

Density of vibrational states

One of the most interesting features of the jamming transition is the anomalous behavior of the density of vibrational states (DOS) $D(\omega)$, where ω is the frequency [248, 246, 253]. For a crystal, or in a general elastic medium, at small energies the Debye dispersion relation $\omega = c\ k$ holds, with c the speed of sound and k the magnitude of the wave vector, which gives a DOS $D(\omega) \sim \omega^{d-1}$ at low frequencies, with d the spatial dimension. As a consequence, the scaling of the specific heat $c_V = \frac{1}{V}\frac{\partial}{\partial T}\int_0^{\omega_D} d\omega D(\omega)\frac{\hbar\omega}{e^{\beta\hbar\omega}-1} \propto T^d$ is obtained, which gives the ubiquitous $c_V \propto T^3$ for three-dimensional crystals at low temperature.
Instead, in amorphous materials it is found that $c_V \propto T$ at low temperature, indicating a DOS that goes to a constant for vanishing frequency: plotting $D(\omega)/\omega^2$ for a three-dimensional glass a peak at low frequency, called *boson peak*, is observed [8, 189, 67, 203, 46, 47, 171, 120].
To study the behavior of the vibrational spectrum, the model is analyzed in an equilibrium jammed configuration at density $\phi > \phi_J$, so that $\Delta\phi = \phi - \phi_J$ is the distance from the jamming point. A second order expansion of the energy of the system gives

$$\Delta H = \sum_c \frac{k_c}{2}|\mathbf{u}_c^{\parallel}|^2 - \frac{f_c}{2r_c}|\mathbf{u}_c^{\perp}|^2 \tag{1.27}$$

where c runs all over the interacting pairs of spheres (i,j) (i.e. $h_{ij} \leq 0$), $k_c = \frac{\partial^2 \nu(h)}{\partial h^2}|_{h=h_{ij}}$ are the stiffnesses, $f_c = \frac{\partial \nu(h)}{\partial h}|_{h=h_{ij}}$ are the exchanged forces, $r_c = |\,\mathbf{x}_i - \mathbf{x}_j\,|$ the distance between the spheres centers, $\mathbf{u}_c = \delta\,\mathbf{x}_i - \delta\,\mathbf{x}_j$ the relative displacement between the spheres. When the system is in the overcompressed phase, $f_c > 0$, the transverse term is destabilizing: it is called *pre-stress*, it has a geometrical origin and the fact it is destabilizing is important to bring about isostaticity at the jamming of spheres [212, 246]. The quadratic expansion of the energy can be written in matrix form

$$\Delta H = \delta x_i^\alpha \mathcal{M}_{ij}^{\alpha\beta} \delta x_j^\beta \tag{1.28}$$

where i,j run over the particles and α,β over the dimensional component. The matrix $\mathcal{M}$ is the dynamical matrix and the spectrum of its eigenvalues λ_k gives the density of vibrational states, with $\omega_k = \sqrt{\lambda_k}$ (assuming spheres of same mass equal to one). Effective medium theory [80] gives

$$D(\omega) = \begin{cases} \omega^{d-1} & \omega << \omega_0 \\ \frac{\omega^2}{\omega_*^2} & \omega_0 << \omega << \omega_* \\ \text{constant} & \omega >> \omega_* \end{cases} \tag{1.29}$$

where the cross-over frequencies ω_0 and ω_* depend on the distance from jamming $\Delta\phi$. The scaling ω^{d-1} corresponds to the Debye one that disappears in the jamming limit because $\omega_0 \to 0$ for $\Delta\phi \to 0$. Interestingly, in mean-field theory [106] it is found that $\omega_0 = 0$ so that the scaling is always non-Debye. This scaling is also found in finite dimensions, close enough to the jamming point [56, 80].
Furthermore, the localization [223, 257] of these modes is studied, for example, by the participation ratio (PR) of each normalized mode $\{\mathbf{u}_i(\omega)\}$

$$PR(\omega) = \left[N \sum_i^N |\mathbf{u}_i(\omega)|^4 \right]^{-1} \tag{1.30}$$

that is $O(1)$ for extended modes and $O(\frac{1}{N})$ for localized ones. While in mean-field theory the low frequency modes are completely delocalized [106], in finite dimensions there are quasi-localized modes at low frequency [167, 243, 253, 166]: they become more delocalized by getting closer to jamming and by increasing dimensionality [56]. At intermediate frequencies, instead, the modes are delocalized, while at high frequency there are localized ones, as it is common in disordered media.

The crossover frequency ω_* vanishes at jamming [250] as

$$\omega_* \sim \Delta z \tag{1.31}$$

where we are using the excess of connectivity with respect to isostaticity $\Delta z = z - z_{iso}$ as a measure of the distance from the jamming point. Therefore, exactly at the jamming transition, the spectrum $D(\omega)$ goes to a constant for vanishing frequency, consistent with the numerical observation [191].

Diverging lengthscales

The vanishing of ω_* can be associated to a diverging length scale following an argument provided by M. Wyart in [250]. In a marginally jammed system, the bonds along a cube of

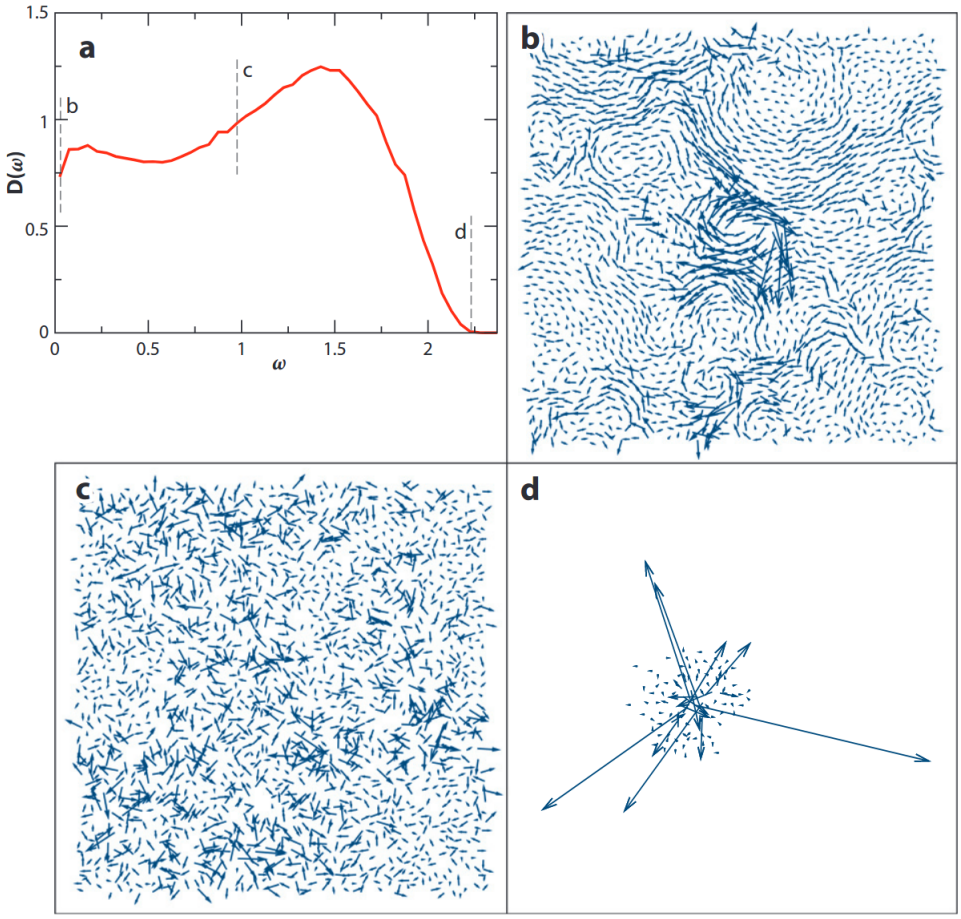

Figure 1.13: Reprinted from [158]. Vibrational modes for $d = 2$ at $\Delta\phi = 10^{-4}$. *a)* The density of states $D(\omega)$, with lines indicating the frequencies of the modes represented in the panels *b,c,d*. *b)* Quasi localized mode at low frequency. *c)* Extended mode at intermediate frequency. *d)* Localized mode at high frequency.

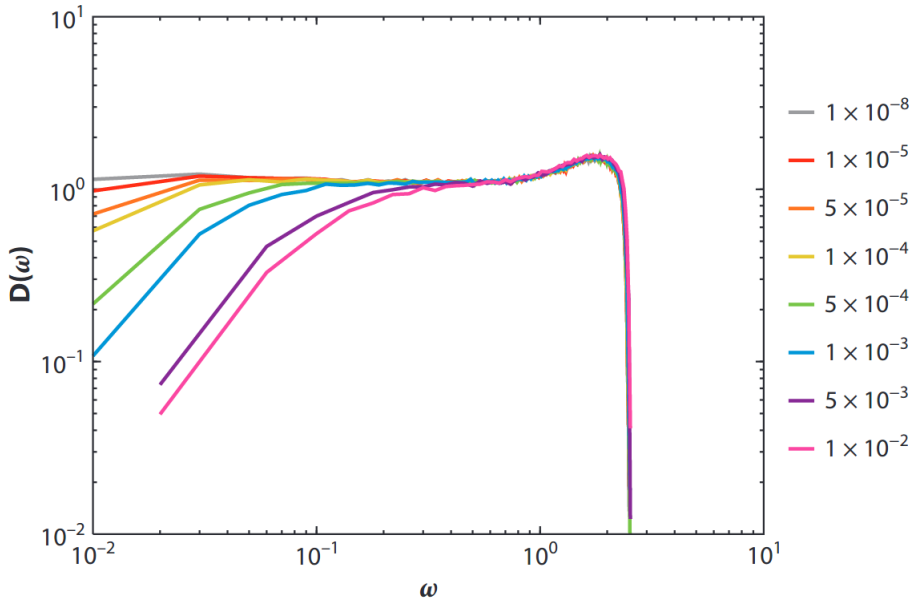

Figure 1.14: Reprinted from [158]. Density of states in log-log scale for three-dimensional harmonic spheres for different values of $\Delta\phi$. At a given density, the lower frequency end of the plateau is the cross-over ω_*. For $\Delta\phi \to 0$, $\omega_* \to 0$ and the density of states tend to a constant at zero frequency.

size l are cut: the number of broken contacts is therefore $\sim l^{d-1}$. On the other hand, the number of the excess contacts in the bulk with respect to isostaticity is $\sim \delta z l^d$. Therefore, the smallest part that can be cut without creating floppy modes is given by equating the two terms:

$$l_* \sim \frac{1}{\Delta z} \tag{1.32}$$

For lengths larger that l_*, the system is comparable to a continuum elastic medium, while for lengths smaller than l_* the modes are anomalous, sensitive to the microscopic structure and form the plateau of the DOS. Therefore at jamming l_* diverges and the anomalous modes control the response of the system. It is difficult to directly measure the length l_* form the data [160], but it has been shown that the cross-over length can be revealed by the response of a jammed system to a point force or an inflation of a local particle [91, 90, 89].
Another lengthscale diverging as $\Delta\phi^{-1/4}$ is associated to the decay length of spatial correlations in modes at frequency ω_*^+ [222, 241, 245].

Scalings at unjamming

When the system is in the jammed phase but close to the unjamming transition, i.e. $\Delta\phi \to 0$, interesting scalings appear [191, 246, 117].
We have seen in the previous section the scaling of the spectrum of vibrational modes, that shows universality at jamming for low frequency.
With a soft potential $\nu(h) = \frac{|h_{ij}|^a}{a}\theta(-h_{ij})$, $a > 1$, the typical amount of overlaps δh_{ij} between spheres created by compressing from the jamming point is proportional to $\Delta\phi$; this happens because the soft potential $a > 1$ makes a contact at jamming (i.e. $h_{ij} = 0$)

become an overlap (i.e. $h_{ij} = \delta h_{ij} < 0$) as soon as an infinitesimal pressure is applied. Therefore, the energy E and the pressure p scale as

$$\begin{aligned} E &\sim \Delta\phi^a \\ p &\sim \Delta\phi^{a-1} \end{aligned} \tag{1.33}$$

since the pressure is proportional to the forces $\nu'(h_{ij}) = |h_{ij}|^{a-1}\theta(-h_{ij})$. The scaling of energy and pressure depends on the soft potential but not on the dimension: in fact it is found also in mean-field theory [105].
The behavior of the excess coordination number with respect to jamming, i.e. the number of overlaps between spheres beyond isostaticity $\Delta z = z - z_{iso}$, has a more universal behavior related to the universality of the density of vibrational states. We have seen that the onset frequency ω_* of the anomalous modes scales as $\omega_* \sim \Delta z$ [250]. Following [246], in the marginally jammed system, the lowest frequency of the anomalous modes is rescaled by a stiffness $\sqrt{k}$ and its energy receives a contribution proportional to the pressure from the destabilizing stress term of Eq. (1.27); therefore, the energy of the mode scales as

$$k\omega_*^2 - Ap \tag{1.34}$$

where k is the stiffness proportional to $\nu''(h) = (a-1)|h|^{a-2}$ and A is an order one constant. Since $k \sim \Delta\phi^{a-2}$, $p \sim \Delta\phi^{a-1}$ and $\omega_* \sim \Delta z$, the stability condition of having a positive energy mode

$$\Delta\phi^{a-2}\omega_*^2 - A\Delta\phi^{a-1} \geq 0 \tag{1.35}$$

gives

$$\Delta z \geq \sqrt{\Delta\phi} \tag{1.36}$$

This stability bound is eventually saturated, giving

$$\Delta z \sim \sqrt{\Delta\phi} \tag{1.37}$$

as it is found in numerical simulations [191, 85, 190].

Another anomalous scaling behavior is found for the elastic moduli: the bulk modulus B and the shear modulus G [191, 85, 190]. They both vanish at the jamming point with power law behavior, but with their ratio

$$\frac{G}{B} \sim \sqrt{\Delta\phi} \tag{1.38}$$

and therefore scaling as Δz. While the bulk modulus is proportional to the stiffness of the potential $B \sim k \sim \Delta\phi^{a-2}$, the shear modulus is smaller and is given by $G \sim k\Delta\phi^{0.5}$. This large difference in shear and bulk modulus is a peculiar property of jamming and it is not found in ordinary solids.

1.4 Jamming criticality in the jammed phase: a full critical and marginally stable phase

In the previous section we have summarized some peculiar characteristics of the jamming transition point. Using a soft potential, the jammed phase corresponds to an amorphous solid whose properties have scaling behavior at the unjamming transition. The discussed soft potentials have the form $\nu(h_{ij}) = \frac{|h_{ij}|^a}{a}\theta(-h_{ij})$ with $a > 1$, where $h_{ij} = |\,\mathbf{x}_i - \mathbf{x}_j\,| - \sigma_{ij}$ are the gaps between the spheres. A legitimate question is what happens to the jammed solid if the potential is considered to have a singular behavior with $a \leq 1$. The technical difficulty of this model comes from the fact that the gradient of the energy has a singularity every time that two spheres are just in contact, i.e. $h_{ij} = 0$. This is an undesired feature, because at zero temperature the equilibrium is given by mechanical stability that simply corresponds to having a zero gradient, i.e. the balance of all the forces acting on a sphere. A good starting point is to note that the critical properties of the jamming point must be unchanged, independently of the exponent a. At the transition point, a certain number of gaps become contacts $h_{ij} = 0$ and are therefore insensitive to the scaling of the soft potential. Moreover, the properties at jamming are well defined also for the hard spheres potential, corresponding to $a = 0$.
We can prepare a configuration of spheres at jamming with some protocol and ask what happens if we try to compress the system having the soft potential scaling linearly: $a = 1$. This *linear potential* is the subject of this work.

A trivial but important observation is that a linear potential $\nu(h_{ij}) = F|h_{ij}|\theta(-h_{ij})$, where F is a constant parameter, gives a constant repulsive force $\nu'(h_{ij}) = -F\ \theta(-h_{ij})$ when an overlap $h_{ij} < 0$, no matter how small, is created. Consequently, two spheres just touching have to be compressed with a force whose intensity is at least F for them to create an overlap. When compressed with a force intensity smaller than F, the spheres continue just touching and exchange a *contact force* $f < F$. The physical consequence is that, even at finite pressure, the spheres have two possible kinds of interaction: forming an overlap $h_{ij} < 0$, with associated force F, or forming a contact $h_{ij} = 0$, with associated force $0 < f < F$. The linear potential is therefore an intermediate case between the purely soft interaction $a > 1$, where the contacts of jamming are destabilized by an infinitesimal compression, and the hard spheres potential, where the contacts can withstand any compression up to infinite pressure without creating overlaps. The linear interaction gives a critical value F to the force needed to destabilize a contact. In the limit $F \to \infty$, the hard spheres case is recovered. Since F is a trivial rescaling factor for the forces and the energy, we simply consider $F = 1$.
The other fundamental ingredients in the system we study are the disorder and the geometry. Let's consider a system of spheres with linear potential in the dense phase, i.e. $\phi > \phi_J$, and let's take their positions $\{\mathbf{x}_i\}$ to be random. We have a set $\mathcal{S}$ of positive gaps $h_{ij} > 0$, meaning pairs of spheres that are not interacting, and a set $\mathcal{O}$ of negative gaps $h_{ij} < 0$, corresponding to pairs of overlapping spheres. The energy landscape is made of linear ramps having some additional curvature due to the spherical geometry of the particles; the linear ramps meet in angular lines and points. If we take the non-linear constraints $h_{ij} > 0$ for $ij \in \mathcal{S}$ and $h_{ij} < 0$ for $ij \in \mathcal{O}$ to be hard constraints, we can minimize the energy inside the portion of phase space defined by $\mathcal{S}$ and $\mathcal{O}$: because of the linear potential, this problem is akin to linear programming in some curved geometry. We

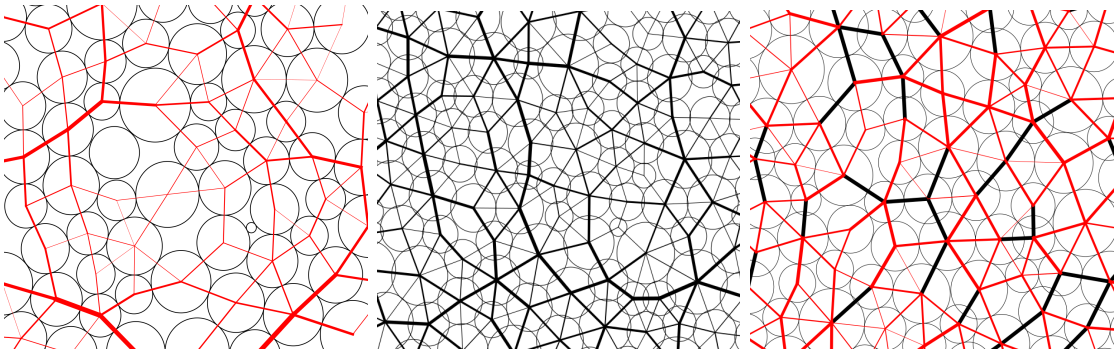

Figure 1.15: Sphere configurations in two dimensions. Red lines correspond to *contacts*, i.e. spheres just touching; black lines corresponds to *overlaps* between the spheres. The thickness of the lines is proportional to the corresponding force intensity. *Left panel.* A snapshot of a configuration of spheres at the jamming point: the spheres form contacts, the energy is zero and the configuration is insensitive to the form of the soft potential. *Central panel.* A snapshot of a jammed configuration with harmonic potential $\nu(h_{ij}) = \frac{|h_{ij}|^2}{2}\theta(-h_{ij})$: there is no contact, only overlaps which provide the mechanical forces necessary to keep the system in mechanical equilibrium. Pressure and energy have positive values. *Right panel.* A snapshot of a jammed configuration with linear potential $\nu(h_{ij}) = |h_{ij}|\theta(-h_{ij})$: the spheres have both contacts and overlaps. The thickness of the black lines is constant because overlaps give constant force intensities. Instead, red lines have various thicknesses, since contact forces do the job of keeping the system in mechanical equilibrium. The critical properties are encoded in the contact network, while the overlap network provides an internal stress. Each sphere needs at least two contacts (d contacts in d dimensions) to be in equilibrium.

know that the solution to this optimization problem is a vertex of the high-dimensional manifold defined by $\mathcal{S}$ and $\mathcal{O}$: this implies that a certain number of constraints will be saturated, therefore $h_{ij} = 0$ for several pairs ij.
This analogy with linear programming suggests that the energy minima in the jammed phase necessarily have an extensive number of contacts. Each of them brings a contact force f_c (i.e. the Lagrange multiplier of the saturated constraint), while instead overlaps give forces of constant intensity. If the system does not have a highly symmetrical configuration, the overlaps cannot give mechanical stability to the system. Stability can be achieved only through the contact forces: following Maxwell's argument, the number of contacts needs to be greater or equal than the number of degrees of freedom Nd. For a system of spheres with continuous polydispersity, the geometry does not allow crystalline configurations and the minima that are found by minimizing the linear potential are *isostatic*. Isostatic configurations at finite pressure display all the critical signatures of the jamming point, but with the important difference that the whole jammed phase is a *critical phase*. Compressing or decompressing the system does not wash out the critical behavior, since other mechanically stable configurations are still isostatic and disordered. These configurations are actually only *marginally stable*: removing a contact creates an unstable mode. The system flows along the unstable modes until isostaticity is restored. As discussed for the jamming transition, marginal stability is accompanied by some peculiar power-law behaviors in the distributions of forces and gaps [188]. As for the jamming point, small positive gaps and small contact forces are controlled by exponents γ and θ respectively, both belonging to the jamming universality class. The jammed phase of the linear potential has also negative gaps (overlaps) and an upper bound $F = 1$ for the intensity of contact forces. Remarkably, it turns out that also small *negative* gaps and contact forces *close to* $F = 1$ have power law behaviors in their distributions with the same exponents γ and θ. This kind of enlarged universality stems directly from marginal stability. One may think that *any* isostatic configuration would be mechanically stable, but this is not the case. The stronger requirement is that the contact network and the overlap network are such that the contact forces can stabilize the configuration with intensities $0 < f_c < 1$. This requirement can be satisfied only by proper contact/overlap networks. The minimization procedure is such that the system *self-organizes* into critical configurations.
The peculiar properties of the system characterize its response to perturbations. Let us imagine taking a (marginally) stable isostatic configuration at finite pressure and compressing it slightly. The additional stress is distributed on the contact forces: those that are the closest to the boundaries 0 and $F = 1$ may fall outside the physical bound $[0, 1]$. Therefore, the corresponding contacts are destabilized and the system starts flowing along the unstable floppy modes. The number of forces near the boundaries 0 and 1, and therefore the exponent θ, controls the excitations of the system. When the spheres move, eventually new pairs meet and form new contacts: when the system has formed again an isostatic network of contacts, the configuration can eventually be stable if $0 < f_c < 1$ for each contact force. The pairs of spheres that form new contacts are those that were already close to one another, i.e. those whose gaps h_{ij} were close to 0. Therefore, the number of small gaps, depending on the exponent γ, controls the relaxation of the system. Let's notice that an infinitesimal pressure variation is sufficient to destabilize one or more contacts: the evolution of the system along the unstable modes corresponds to *avalanches*, whose power-law size distribution is characterized by a critical exponent. This plastic behavior produces the so called *crackling noise*.

The jammed phase with the linear potential is an isostatic, self-organized critical, marginally stable phase whose excitations/relaxations correspond to the opening/closing of contacts. Its universality class is strongly connected to the jamming criticality.

1.5 Organization of the thesis

The presentation of the topics in this thesis follows the logical order in which they have been understood. Some definitions are repeated in order to ease the reading of a single chapter.

In chapter 2 we introduce the perceptron model. After a short historical introduction, the model is defined and its connection to jamming is explained. A mapping between the perceptron and spheres in finite dimensions is provided. The free energy of the model is computed using the replica method, with a generic interaction potential. The obtained equations, both for the replica symmetric and the fullRSB constructions, are therefore general. We solve the model in the SAT phase and we present the scaling solution for the critical jamming transition obtained from the fullRSB equations. At the end of the chapter, the UNSAT phase is briefly discussed using the harmonic potential.
Chapter 3 is the core chapter. It starts with the discussion of an algorithm to find the minima of the perceptron in the UNSAT phase with the linear cost-function. The results are presented both for the critical/non-convex phase and for the non-critical/convex phase. A proper definition of the Hessian of the model is discussed. In the second part of the chapter, the replica theory is used to understand the UNSAT phase of the model and the phase diagram is presented. In the end, a scaling theory, reminiscent of the one known for jamming, is developed for the critical phase starting from the fullRSB equations: it consistently connects with the numerical observations.
In chapter 4 the critical phase is shown to exist also for jammed spheres with linear potential in two and three dimensions. The results are obtained by numerical simulations. The critical behavior is characterized, together with other properties typical of the jamming point like the flat density of soft modes and the hyperuniformity of the contact network.
In chapter 5 we present a compression protocol for the perceptron and we present the results. It shows the crackling noise characterizing the critical phase, with power-law distributed avalanches. Scaling relations are obtained for finite system size. The protocol allows a fine studying of the unjamming transition: it is shown that the scaling laws are different from other soft potentials and an explanation is provided by scaling arguments.
In chapter 6 a variation of the linear potential is studied, consisting in a piece-wise linear one. By numerical simulations, we show that an extended version of isostaticity is in place and that there is a proliferation of excitation/relaxation mechanisms, each one controlled by the same exponents as the jamming universality.

Chapter 2

The perceptron: a simple model for jamming

In this chapter we introduce the perceptron model. Starting with a historical presentation, we clarify the role that this model has acquired in the study of the jamming transition in disordered materials and how the mathematical and conceptual mapping is performed. Therefore, following [105, 234], we develop its theory using the replica method and briefly discuss some features of its phase diagram.

2.1 Introduction to the perceptron

2.1.1 Historical prelude: from Rosenblatt to Gardner

In 1943, McCulloch and Pitts introduced the idea of using networks of "formal neurons" to model some information processing activities of biological brains[175]. Their idea sparked a lot of interest around the subject of artificial neural networks and in 1962 the psychologist Frank Rosenblatt introduced the perceptron, that is the simplest feed-forward neural network[208]. Its task is to perform a binary classification of input patterns, a feature that was soon interpreted as a simplified model of some basic cognitive abilities. However, this euphoria was suddenly interrupted in 1969 when Minsky and Papert pointed out the limitations of the tasks that can be realized using this kind of single layer machine[181]; interestingly, they completely failed in grasping the potential of multilayer architectures. The field got revived in the '80s and a major theoretical achievement was made in a famous paper of 1988 by Elisabeth Gardner [113] where she solved the problem of computing the storage capacity of a perceptron (i.e. how many patterns it can classify) by using techniques from the statistical mechanics of disordered models. Moreover, together with B. Derrida she also studied the phase beyond the limit of capacity[111]: associating an energy cost to the misclassified patterns, an optimization problem is obtained, particularly well suited for a statistical mechanics point of view.

2.1.2 Definition of the perceptron model

The degrees of freedom of a perceptron consist in its "synaptic weights" X_i which are N real numbers forming an N-dimensional vector $\mathbf{X} \in \mathbb{R}^N$. For convenience, this vector belongs to the hypersurface of an N-dimensional hypersphere, that is $\sum_i X_i^2 = N$.

Given a set of M patterns $\boldsymbol{\xi}_\mu \in \mathbb{R}^N$ with their binary labels $y_\mu = \pm 1$, where index μ goes

from 1 to M, the perceptron classifies them according to the rule

$$\hat{y}_\mu = sign\left(\frac{1}{\sqrt{N}}\,\mathbf{X}\cdot\boldsymbol{\xi}_\mu\right) \tag{2.1}$$

To have a correct classification $\hat{y}_\mu = y_\mu$ it is therefore necessary to find $\mathbf{X}$ so that $y_\mu \frac{1}{\sqrt{N}}\,\mathbf{X}\cdot\boldsymbol{\xi}_\mu \geq 0,\ \forall\mu = 1, ..., M$. To have a more robust classification, a *margin* σ can be introduced and the required inequalities become

$$y_\mu \frac{1}{\sqrt{N}}\,\mathbf{X}\cdot\boldsymbol{\xi}_\mu \geq \sigma, \qquad \forall\mu = 1, ..., M \tag{2.2}$$

Equation (2.2) defines a Constraint Satisfaction Problem with Continuous variables (CCSP). In a real classification task, it is required that $\sigma > 0$ so to have a positive margin when the patterns are linearly separated.
In our treatment, we are interested in this model only as a random CCSP. Therefore, we consider the patterns to be made of random variables, independently identically distributed (i.i.d.) according to a normal distribution of zero mean and unit variance: $\xi_{\mu,i} \sim \mathcal{N}(0, 1)$. Choosing random labels y_μ we can absorb them into their respective patterns without changing the statistical properties of the system. Now our CCSP is simply

$$\frac{1}{\sqrt{N}}\,\mathbf{X}\cdot\boldsymbol{\xi}_\mu - \sigma \geq 0, \qquad \forall\mu = 1, ..., M \tag{2.3}$$

in the thermodynamic limit $N \to \infty$, $M \to \infty$, $M/N = \alpha \sim O(1)$.
Gardner's solution to the storage capacity starts by evaluating

$$\Omega_{\boldsymbol{\xi}_\mu} = \int d\mu(\mathbf{X}) \prod_{\mu=1}^{M} \theta\left(\frac{1}{\sqrt{N}}\,\mathbf{X}\cdot\boldsymbol{\xi}_\mu - \sigma\right) \tag{2.4}$$

where $d\mu(\mathbf{X})$ is the uniform measure on the hypersphere $|\,\mathbf{X}\,|^2 = N$ and $\theta(\cdot)$ is the Heaviside step function. This volume is a random variable since it depends on the patterns $\boldsymbol{\xi}_\mu$; it is possible to obtain its typical value by computing the *quenched* entropy

$$\mathrm{v} = \frac{1}{N}\overline{\log \Omega_{\boldsymbol{\xi}_\mu}} \tag{2.5}$$

where the symbol $\overline{\cdots}$ stands for the average over the patterns $\boldsymbol{\xi}_\mu$: it is in performing this computation that the replica machinery comes into use.
As a result of this computation, the typical volume of solutions $\mathbf{X}$ that satisfy the CCSP (2.3) is obtained. Changing the control parameters α and σ, that are the number of patterns and the margin, it is possible to see how the volume of solutions changes accordingly: when it shrinks to a point, the satisfiability threshold is met. This boundary therefore separates a SAT phase where there are solutions to the problem (2.3) from an UNSAT phase where it is not possible to satisfy all the constraints. In figure (2.1) we report the corresponding phase diagram.

To have a lighter notation (and for analogy with the models of sphere packings), it is convenient to define the *gap* variables

$$h_\mu = \frac{1}{\sqrt{N}}\,\mathbf{X}\cdot\boldsymbol{\xi}_\mu - \sigma \tag{2.6}$$

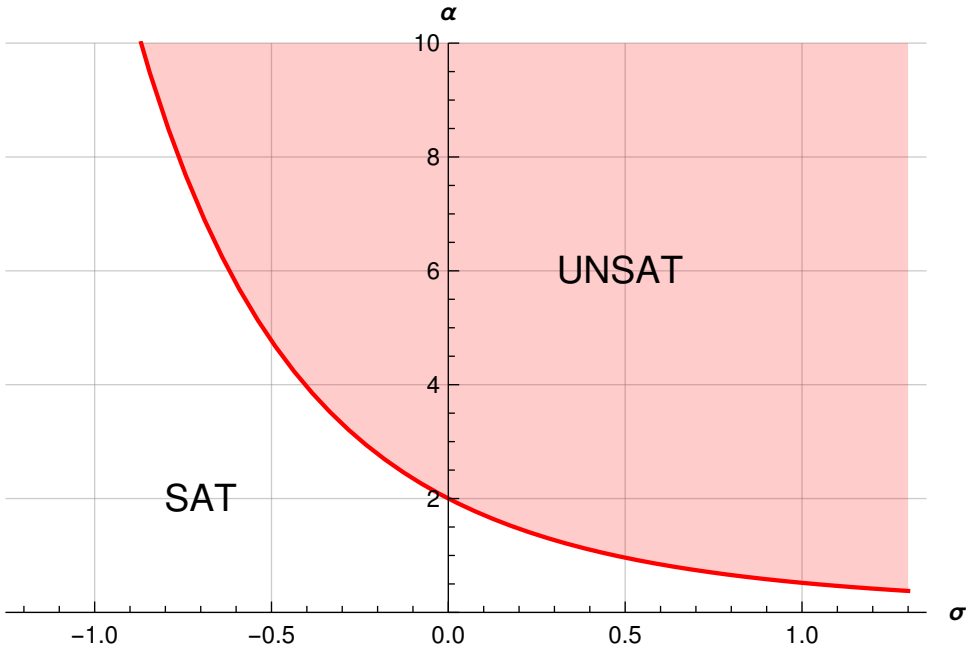

Figure 2.1: SAT-UNSAT phase diagram of the CCSP defined in equation (2.3). The area shaded in red corresponds to the UNSAT phase, the red line is the satisfiability transition.

so that our CCSP (2.3) is simply restated as

$$h_\mu \geq 0, \qquad \forall \mu = 1, ..., M \tag{2.7}$$

When the system enters in the UNSAT phase, it means that all the constraints cannot be satisfied with a single $\mathbf{X}$ and it is necessary to accept that $h_\mu < 0$ at least for some μ. A natural idea from statistical mechanics is to associate a positive energy cost to this UNSAT patterns, say $\nu(h_\mu) = \frac{|h_\mu|^a}{a}\theta(-h_\mu)$, where a is a positive exponent and $\theta(\cdot)$ is the Heaviside step-function. The following Hamiltonian can be defined

$$H(\mathbf{X}) = \sum_\mu \nu(h_\mu) \tag{2.8}$$

whose minima $\mathbf{X}^*$ have positive energy $E = H(\mathbf{X}^*) > 0$ in the UNSAT phase and zero energy $E = H(\mathbf{X}^*) = 0$ in the SAT phase: by looking for the minima of (2.8) we are solving an optimization problem.
Following this statistical mechanics approach, we can introduce a temperature T and its inverse $\beta = \frac{1}{T}$ (the Boltzmann constant is set equal to 1) and the corresponding Gibbs measure

$$e^{-\beta H(\mathbf{X})} \tag{2.9}$$

The quantity (2.4) is generalized with the partition function

$$Z_{\boldsymbol{\xi}_\mu}(T) = \int d\mu(\mathbf{X}) e^{-\beta H(\mathbf{X})} \tag{2.10}$$

which clearly becomes equal to $\Omega_{\boldsymbol{\xi}_\mu}$ in the zero temperature limit, $Z_{\boldsymbol{\xi}_\mu}(T) \underset{T\to 0}{\to} \Omega_{\boldsymbol{\xi}_\mu}$.
The corresponding free energy is given by the average over the patterns of the logarithm

of the partition function

$$\mathrm{f}(T) = \lim_{N\to\infty} -\frac{T}{N}\overline{\log Z_{\boldsymbol{\xi}_\mu}(T)} \tag{2.11}$$

which is often referred to as *quenched average* over the disorder.

2.2 Perceptron as jamming paradigm

The studies started by Gardner on the perceptron were mainly inspired by its use as a binary classifier, which requires the margin σ to be a positive quantity in order to have a stable classification boundary. However, the mathematical problem is perfectly coherent also when the case $\sigma < 0$ is considered. A key observation is that the set $\mathcal{S}_\mu$ of $\mathbf{X}$ satisfying the μ constraint

$$\frac{1}{\sqrt{N}}\,\mathbf{X}\cdot\boldsymbol{\xi}_\mu \geq \sigma \tag{2.12}$$

is a convex set[1] if $\sigma > 0$. Therefore, the solutions of the CCSP live in the set $\mathcal{S} = \cap_\mu \mathcal{S}_\mu$ that is the intersection of convex sets: it is a convex set itself.
When instead $\sigma < 0$, the sets $\mathcal{S}_\mu$ are non-convex and their intersection can be a non-convex set. This situation can lead to the presence of glassy phases, where islands of solutions can be disjoint or connected in a complex structure. The important intuition put forward in 2015 was that the satisfiability threshold of the CCSP inside a glassy phase corresponds to a critical point belonging to the same universality class found in the jamming of hard spheres in infinite dimensions.[104] The importance of this result is twofold: first, it casts the jamming phenomenon in a more general framework since the packing of spheres can be seen as a particular case of CCSP; second, it makes the perceptron the simplest model where to study the jamming universality class, without the need of using the models of spheres and taking the limit of infinite dimensions.

In the following section we present the mapping between CCSP (and specifically the perceptron) and sphere systems. This mapping has been first presented in [106, 105].

2.2.1 Mapping with spheres

- **CCSP.** Continuous constraint satisfaction problem with excluded volume constraints can be defined in an abstract way. One considers first a vector $\mathbf{X} \in \mathbb{R}^N$ and a set of $M = \alpha N$ functions $h_\mu(\mathbf{X}) \in \mathbb{R}$ indexed by $\mu = 1, \ldots, M$. Each function $h_\mu(\mathbf{X})$ is called *gap*. The constraint satisfaction problem is defined by asking to find a configuration of $\mathbf{X}$ that satisfies all the constraints $h_\mu(\mathbf{X}) \geq 0$. If the problem cannot be satisfied one can define an optimization problem by asking to find a configuration of $\mathbf{X}$ that minimizes a cost function. Therefore, a positive cost function $H = \sum_\mu \nu(h_\mu)$ can be defined, with $\nu(h) = 0$ if $h > 0$ and $\nu(h) > 0$ if $h < 0$, where the potential $\nu(h_\mu)$ sets the magnitude of the contribution of the negative gaps to the total cost. The satisfiable (SAT) phase corresponds to an assignment where $H = 0$, while

[1] A set is convex if, given any two points, it contains the whole geodesic that joins them. Since in this case the points belong to the hypersurface of a hypersphere, the corresponding geodesics of spherical geometry must be considered.

we have $H > 0$ in the unsatisfiable (UNSAT) phase. The boundary between the two phases is the SAT/UNSAT transition and will be generically referred to as the jamming point. The precise location of this point as a function of the control parameters of the problem may depend on the precise protocol used to obtain solutions. Marginally satisfied gaps are defined by $h_\mu(\mathbf{X}) = 0$.

- **Spheres.** In this case the degrees of freedom of the problem are the positions of N spheres in $\mathbb{R}^d$ denoted by $\{\mathbf{x}_i \in \mathbb{R}^d\}_{i=1,\dots,N}$. The gap variables are defined for each couple of spheres as $h_{ij} = |\,\mathbf{x}_i - \mathbf{x}_j\,| - \sigma_{ij}$, where $\sigma_{ij} = \sigma_i + \sigma_j$ and $\{\sigma_i\}_{i=1,\dots,N}$ are the values of the radii of the spheres. The constraint satisfaction problem is defined by asking to find a configuration of the spheres such that $h_{ij} \geq 0$ for all couples $\{ij\}$. A contact between two spheres i and j appears if $h_{ij} = 0$, which corresponds to a marginally satisfied gap. The jamming point separates the unjammed (SAT) phase where it is possible to find a SAT configuration for the positions of the spheres, from the jammed (UNSAT) phase where the spheres overlap and an extensive number of gaps are negative. In the jammed phase, a positive cost function $H = \sum_{i<j} \nu(h_{ij})$ can be defined, with $\nu(h_{ij}) > 0$ if $h_{ij} < 0$ and zero otherwise. Usual choices for $\nu(h_{ij})$ are $\nu(h_{ij}) = \frac{1}{a}|h_{ij}|^a \theta(-h_{ij})$. The cases $a = 2, 2.5$ are usually called harmonic and Hertzian soft spheres, respectively.

- **Spherical perceptron.** The degrees of freedom of the spherical perceptron problem are represented by the N-dimensional vector $\mathbf{X} \in \mathbb{R}^N$ subject to the spherical constraint $|\,\mathbf{X}\,|^2 = N$. One then introduces a set of $M = \alpha N$ random vectors $\{\boldsymbol{\xi}_\mu \in \mathbb{R}^N\}_{\mu=1,\dots,M}$ whose components are *i.i.d.* random Gaussian variables with zero mean and unit variance. Given these random vectors, the gaps are defined by $h_\mu(\mathbf{X}) = \boldsymbol{\xi}_\mu \cdot \mathbf{X}/\sqrt{N} - \sigma$. σ is a control parameter in the problem, playing a role similar to the diameter in spheres. The constraint satisfaction problem requires to find a configuration of $\mathbf{X}$ such that $h_\mu \geq 0$ for all $\mu = 1, \dots, M$. In the UNSAT phase, where such configurations cannot be found, one can define an optimization problem by asking to find configurations of $\mathbf{X}$ that minimize a positive cost function given by $H = \sum_\mu \nu(h_\mu)$, where usually $\nu(h_\mu) = \frac{1}{a}|h_\mu|^a \theta(-h_\mu)$. In this thesis we are interested in the case $a = 1$ that defines the linear cost function, while the harmonic case has already been studied [106, 105]. Again, marginally satisfied gaps, analogous to contacts between spheres, correspond to $h_\mu = 0$.

2.3 The replica analysis and the SAT phase

In this section we present the computation of the free-energy of the perceptron model using the replica method. We do it for the generic cost function $H = \sum_\mu \nu(h_\mu)$ and present the general equations that will be the starting point of our analysis. Thereafter, we briefly recapitulate the solution for the harmonic case $\nu(h_\mu) = \frac{1}{2}|h_\mu|^2 \theta(-h_\mu)$ that can be useful to understand our work on the linear case.

2.3.1 The replica analysis

As stated before, from a statistical mechanics point of view we want to compute the free energy

$$\mathrm{f} = \lim_{N\to\infty} -\frac{1}{\beta N}\overline{\log Z_{\boldsymbol{\xi}_\mu}} \tag{2.13}$$

where the partition function defined in (2.10)

$$Z_{\boldsymbol{\xi}_\mu} = \int d\mu(\mathbf{X}) \prod_{\mu=1}^{M} e^{-\beta\,\nu(h_\mu(\mathbf{X}))} \tag{2.14}$$

depends on the disorder given by the random patterns $\boldsymbol{\xi}_\mu$. The complicated task is to perform the average of the log of $Z_{\boldsymbol{\xi}_\mu}$ and the replica method offers a solution to this task by an analytic continuation of the moments $\overline{Z^n_{\boldsymbol{\xi}_\mu}}$:

$$\begin{aligned}
\mathrm{f} &= -\lim_{N\to\infty}\frac{1}{\beta N}\overline{\log Z_{\boldsymbol{\xi}_\mu}} = \\
&= -\lim_{N\to\infty}\lim_{n\to 0}\frac{1}{\beta N}\frac{\overline{Z^n_{\boldsymbol{\xi}_\mu}}-1}{n} = \\
&= -\lim_{N\to\infty}\lim_{n\to 0}\frac{1}{\beta N}\partial_n\overline{Z^n_{\boldsymbol{\xi}_\mu}}
\end{aligned} \tag{2.15}$$

This quantity can be easily computed when n is an integer. Therefore we can think of n as the *number of replicas* of our system that form a set of coordinates $\{\mathbf{X}^a\}_{a=1\dots n}$:

$$Z^n_{\boldsymbol{\xi}_\mu} = \int \left[\prod_{a=1}^{n} \mathrm{d}\,\mathbf{X}^a\right] \prod_{\mu=1}^{\alpha N} e^{-\beta\sum_{a=1}^{n}\nu(h_\mu(\mathbf{X}^a))} \tag{2.16}$$

Remark: only the degrees of freedom get replicated, the random patterns stay the same.

Computation of $\overline{Z^n_{\boldsymbol{\xi}}}$

In the following we integrate over the auxiliary variable r^a_μ that we fix to be equal to $\frac{1}{\sqrt{N}}\boldsymbol{\xi}_\mu\cdot\mathbf{X}^a$ through a Dirac delta, and we use its Fourier representation $\delta(r^a_\mu - z) = \int\frac{d\hat{r}^a_\mu}{2\pi}e^{i\hat{r}^a_\mu(r^a_\mu - z)}$. So we have

$$\begin{aligned}
\overline{Z^n_{\boldsymbol{\xi}}} &= \overline{\int\left[\prod_{a=1}^{n}\mathrm{d}\,\mathbf{X}^a\left[\prod_{\mu=1}^{\alpha N} dr^a_\mu\right]\right] e^{-\beta\sum_{a=1}^{n}\sum_{\mu=1}^{\alpha N}\nu(r^a_\mu-\sigma)}\prod_{a=1}^{n}\prod_{\mu=1}^{\alpha N}\delta\left(r^a_\mu - \frac{1}{\sqrt{N}}\boldsymbol{\xi}_\mu\cdot\mathbf{X}^a\right)} = \\
&= \int\left[\prod_{a=1}^{n}\mathrm{d}\,\mathbf{X}^a\left[\prod_{\mu=1}^{\alpha N}\frac{\mathrm{d}r^a_\mu\mathrm{d}\hat{r}^a_\mu}{2\pi}\right]\right] e^{\sum_{a=1}^{n}\sum_{\mu=1}^{\alpha N}\left[-\beta\,\nu(r^a_\mu-\sigma)+ir^a_\mu\hat{r}^a_\mu\right]}\overline{\exp\left[-\frac{i}{\sqrt{N}}\sum_{\mu=1}^{\alpha N}\sum_{a=1}^{n}\hat{r}^a_\mu\,\boldsymbol{\xi}_\mu\cdot\mathbf{X}^a\right]}
\end{aligned} \tag{2.17}$$

At this point it is easy to perform the Gaussian integral:

$$\overline{\exp\left[-\frac{i}{\sqrt{N}}\sum_{\mu=1}^{\alpha N}\sum_{a=1}^{n}\hat{r}^a_\mu\,\boldsymbol{\xi}_\mu\cdot\mathbf{X}^a\right]} = \exp\left[-\frac{1}{2}\sum_{\mu=1}^{\alpha N}\sum_{a,b=1}^{n}\hat{r}^a_\mu\hat{r}^b_\mu\frac{\mathbf{X}^a\cdot\mathbf{X}^b}{N}\right] \tag{2.18}$$

We see that the quantity $\frac{\mathbf{X}^a \cdot \mathbf{X}^b}{N}$ appears naturally in the computation and measures the overlap between two replicas a and b; consequently we define the $n \times n$ *overlap matrix* $\mathcal{Q}$ as

$$\mathcal{Q}_{ab} = \frac{\mathbf{X}^a \cdot \mathbf{X}^b}{N} \tag{2.19}$$

Let's notice that $\mathcal{Q}_{ab} = 0$ if $\mathbf{X}^a$ and $\mathbf{X}^b$ are orthogonal, while $\mathcal{Q}_{ab} = 1$ if $\mathbf{X}^a \equiv \mathbf{X}^b$. Due to the spherical constraint on $\mathbf{X}$, the diagonal terms are equal to 1, $\mathcal{Q}_{aa} = \frac{|\mathbf{X}^a|^2}{N} = 1$. Putting everything into eq. (2.17) and noticing that the index μ gets factorized, we get:

$$\overline{Z^n_{\boldsymbol{\xi}}} = \int \left[\prod_{a<b} \mathrm{d}\mathcal{Q}_{ab}\right] J(\mathcal{Q}) \left[\int \left[\prod_{a=1}^{n} \frac{\mathrm{d}r^a \mathrm{d}\hat{r}^a}{2\pi}\right] \exp\left(-\frac{1}{2}\sum_{a,b=1}^{n} \mathcal{Q}_{ab}\hat{r}^a\hat{r}^b + i\sum_a r^a\hat{r}^a - \beta\sum_a \nu(r^a - \sigma)\right)\right]^{\alpha N} \tag{2.20}$$

where we have introduced the Jacobian $J(\mathcal{Q}) = \int [\prod_{a=1}^{n} \mathrm{d}\,\mathbf{X}^a] \prod_{a\le b} \delta\left(\mathcal{Q}_{ab} - \frac{\mathbf{X}^a\mathbf{X}^b}{N}\right)$ to transform the integral in $d\,\mathbf{X}$ into an integral in $d\mathcal{Q}$. Let's evaluate this integral by decomposing the Dirac delta into its Fourier representation

$$\begin{aligned} J(\mathcal{Q}) &= N^{n(n-1)/2} \int \left[\prod_{a=1}^{n} \mathrm{d}\,\mathbf{X}^a\right] \prod_{a\le b} \delta\left(N\mathcal{Q}_{ab} - \mathbf{X}^a\,\mathbf{X}^b\right) = \\ &= N^{n(n-1)/2} \int \left[\prod_{a\le b} \frac{\mathrm{d}\hat{\mathcal{Q}}_{ab}}{2\pi}\right] \int \left[\prod_{a=1}^{n} \mathrm{d}\,\mathbf{X}^a\right] e^{iN\sum_{a\le b}\hat{\mathcal{Q}}_{ab}\mathcal{Q}_{ab} - i\sum_{a\le b}\hat{\mathcal{Q}}_{ab}\,\mathbf{X}^a\cdot\mathbf{X}^b} \end{aligned} \tag{2.21}$$

and by performing the Gaussian integration over $d\,\mathbf{X}^a$:

$$\begin{aligned} &\int \left[\prod_{a=1}^{n} \mathrm{d}\,\mathbf{X}^a\right] e^{-i\sum_{a\le b}\hat{\mathcal{Q}}_{ab}\,\mathbf{X}^a\cdot\mathbf{X}^b} = \int \left[\prod_{a=1}^{n} \mathrm{d}\,\mathbf{X}^a\right] e^{-\frac{1}{2}\sum_{ab} i(1+\delta_{ab})\hat{\mathcal{Q}}_{ab}\,\mathbf{X}^a\cdot\mathbf{X}^b} = \\ &= \left(\frac{(2\pi)^{\frac{n}{2}}}{\sqrt{\det\tilde{\mathcal{Q}}}}\right)^N = (2\pi)^{\frac{Nn}{2}} e^{-\frac{N}{2}\log\det\tilde{\mathcal{Q}}} \end{aligned} \tag{2.22}$$

where $\tilde{\mathcal{Q}} = i(1+\delta_{ab})\hat{\mathcal{Q}}$ and δ_{ab} is the Kronecker delta. Now the Jacobian reads

$$J(\mathcal{Q}) = N^{n(n-1)/2}(2\pi)^{\frac{Nn}{2}} \int \left[\prod_{a\le b} \frac{\mathrm{d}\hat{\mathcal{Q}}_{ab}}{2\pi}\right] \exp\left[N\left(i\sum_{a\le b}\hat{\mathcal{Q}}_{ab}\mathcal{Q}_{ab} - \frac{1}{2}\log\det\tilde{\mathcal{Q}}\right)\right] \tag{2.23}$$

and the integral over $\mathrm{d}\hat{\mathcal{Q}}$ can be evaluated by the saddle point method. Noting that $\mathrm{d}\tilde{\mathcal{Q}}_{ab} = i\,\mathrm{d}\hat{\mathcal{Q}}_{ab}$ and that $\frac{\mathrm{d}}{\mathrm{d}\tilde{\mathcal{Q}}}\log\det\tilde{\mathcal{Q}} = \tilde{\mathcal{Q}}^{-1}$, the saddle point equation gives

$$\tilde{\mathcal{Q}} = \mathcal{Q}^{-1} \tag{2.24}$$

and consequently the matrix $\hat{\mathcal{Q}}_{ab} = \frac{\mathcal{Q}^{-1}_{ab}}{i(1+\delta_{ab})}$. Evaluating the integral at the saddle point, we have finally the Jacobian

$$J(\mathcal{Q}) \simeq D_{N,n} \exp\left[\frac{Nn}{2}(1 + \log(2\pi)) + \frac{N}{2}\log\det\mathcal{Q}\right] \tag{2.25}$$

with

$$D_{N,n} = N^{n(n-1)/2}(2\pi)^{-n(n-1)/2} \tag{2.26}$$

Using this expression of the Jacobian in eq. (2.20) we get

$$\overline{Z_{\boldsymbol{\xi}}^n} = D_{N,n} \int \left[\prod_{a<b} \mathrm{d}\mathcal{Q}_{ab}\right] \exp\left[\frac{Nn}{2}(1+\log(2\pi)) + \frac{N}{2}\log\det\mathcal{Q} + \alpha N \log \mathcal{Z}\right] \tag{2.27}$$

where $\mathcal{Z}$ is the expression

$$\mathcal{Z} = \int \left[\prod_{a=1}^{n} \frac{\mathrm{d}r^a \mathrm{d}\hat{r}^a}{2\pi}\right] \exp\left(-\frac{1}{2}\sum_{a,b=1}^{n} \mathcal{Q}_{ab}\hat{r}^a\hat{r}^b + i\sum_a r^a\hat{r}^a - \beta\sum_a \nu\left(r^a - \sigma\right)\right) \tag{2.28}$$

Let's notice that in the exponential of the integral (2.27) only the term $\mathcal{Z}$ depends on the energy of the model, while the other terms coming from the Jacobian $J(\mathcal{Q})$ are entropic terms.

The replicated action

We can further develop the term $\mathcal{Z}$ by using the identity

$$\exp\left[-\frac{1}{2}\sum_{a,b=1}^{n} \mathcal{Q}_{ab}\hat{r}^a\hat{r}^b\right] = \exp\left[\frac{1}{2}\sum_{a,b=1}^{n} \mathcal{Q}_{ab}\frac{\partial^2}{\partial h_a \partial h_b}\right] \left[\prod_{c=1}^{n} e^{-i\hat{r}^c h_c}\right]\Bigg|_{\{h_c=0\}} \tag{2.29}$$

which gives

$$\begin{aligned}\mathcal{Z} &= \exp\left[\frac{1}{2}\sum_{a,b=1}^{n} \mathcal{Q}_{ab}\frac{\partial^2}{\partial h_a \partial h_b}\right] \left[\prod_{c=1}^{n} \int \frac{\mathrm{d}r^c \mathrm{d}\hat{r}^c}{2\pi} e^{-\beta\,\nu(r^c-\sigma)+i\hat{r}^c(r^c-h^c)}\right]\Bigg|_{\{h_c=0\}} = \\ &= \exp\left[\frac{1}{2}\sum_{a,b=1}^{n} \mathcal{Q}_{ab}\frac{\partial^2}{\partial h_a \partial h_b}\right] \left[\prod_{c=1}^{n} e^{-\beta\,\nu(h_c-\sigma)}\right]\Bigg|_{\{h_c=0\}}\end{aligned} \tag{2.30}$$

Now we can write the average replicated partition function as

$$\overline{Z_{\boldsymbol{\xi}}^n} = D_{N,n} \int \left[\prod_{a<b} \mathrm{d}\mathcal{Q}_{ab}\right] \exp\left[N\mathcal{S}\left(\mathcal{Q}\right) + \frac{Nn}{2}(1+\log(2\pi))\right] \tag{2.31}$$

where we have defined the *replicated action*

$$\mathcal{S}\left(\mathcal{Q}\right) = \frac{1}{2}\log\det\mathcal{Q} + \alpha \log \exp\left[\frac{1}{2}\sum_{a,b=1}^{n} \mathcal{Q}_{ab}\frac{\partial^2}{\partial h_a \partial h_b}\right] \left[\prod_{c=1}^{n} e^{-\beta\,\nu(h_c-\sigma)}\right]\Bigg|_{\{h_c=0\}} \tag{2.32}$$

We can now put this expression back into the free-energy of eq. (2.15):

$$\begin{aligned}\mathrm{f} &= -\lim_{N\to\infty}\lim_{n\to 0}\frac{1}{\beta N}\partial_n \overline{Z_{\boldsymbol{\xi}}^n} = \\ &= -\lim_{n\to 0}\lim_{N\to\infty}\partial_n\left[D_{N,n}\int\left[\prod_{a<b}\mathrm{d}\mathcal{Q}_{ab}\right]\exp\left[N\mathcal{S}\left(\mathcal{Q}\right) + \frac{Nn}{2}(1+\log(2\pi))\right]\right]\end{aligned} \tag{2.33}$$

where in the second line we have exchanged the order of the limits so that we can use the saddle point method to evaluate the integral over the $n \times n$ matrices $\mathcal{Q}_{ab}$. The saddle point approximation

$$\int \left[\prod_{a<b} \mathrm{d}\mathcal{Q}_{ab}\right] \exp\left[N\mathcal{S}\left(\mathcal{Q}\right)\right] \simeq \exp\left[N\mathcal{S}(\mathcal{Q}^*)\right] \tag{2.34}$$

requires to find the solution $\mathcal{Q}^*$ of the saddle point equation

$$\frac{\partial \mathcal{S}\left(\mathcal{Q}\right)}{\partial \mathcal{Q}_{ab}} = 0 \tag{2.35}$$

in order to get the free energy

$$\mathrm{f} = -\frac{T}{2}(1 + \log(2\pi)) - T\lim_{n\to 0} \partial_n \mathcal{S}\left(\mathcal{Q}^*\right) \tag{2.36}$$

The first term $-\frac{T}{2}(1+\log(2\pi))$ is an irrelevant factor for our analysis, therefore it will be neglected hereafter.

Solving the replica equations

Solving the saddle point equation (2.35) is a difficult problem. In principle, it could be possible to analyze the equation for each of the $\frac{n(n-1)}{2}$ parameters $\mathcal{Q}_{ab}$ but it is unclear what happens in the limit of $n \to 0$ dimensional matrix. Another possibility is to make an ansatz about the structure of the matrix $\mathcal{Q}$, parametrize it accordingly and compute $\mathcal{S}\left(\mathcal{Q}\right)$ as an analytic function of the parameter n.
The first case we consider is having all the off-diagonal matrix elements equal to the same value: this structure is symmetric under permutation of the replica indexes, therefore it is called the *replica symmetric solution*.

2.3.2 The replica symmetric solution

The replica symmetric ansatz corresponds to assuming that the matrix $\mathcal{Q}$ solving the saddle point equation (2.35) has 1 on the diagonal entries (due to the spherical constraint) and the value q_M in the off-diagonal ones:

$$\mathcal{Q}_{ab} = \delta_{ab} + (1 - \delta_{ab})q_M \tag{2.37}$$

Let's evaluate the replicated action with this matrix structure.
The entropic term becomes:

$$\log\det \mathcal{Q} = \log\left[(1-q_M)^{n-1}(1+(n-1)q_M)\right] = (n-1)\log(1-q_M) + \log\left(1+(n-1)q_M\right) \tag{2.38}$$

The energy term:

$$\begin{aligned}
\alpha \log \mathcal{Z} &= \alpha \log \exp\left[\frac{1}{2}\sum_{a,b=1}^{n} \mathcal{Q}_{ab}\frac{\partial^2}{\partial h_a \partial h_b}\right]\left[\prod_{c=1}^{n}\exp\left[-\beta\,\nu(h_c)\right]\right]\Big|_{\{h_c=-\sigma\}} = \\
&= \alpha \log \exp\left[\frac{q_M}{2}\left(\sum_{a=1}^{n}\frac{\partial}{\partial h_a}\right)^2 + \frac{1}{2}(1-q_M)\sum_{a=1}^{n}\frac{\partial^2}{\partial h_a^2}\right]\left[\prod_{c=1}^{n}\exp\left[-\beta\,\nu(h_c)\right]\right]\Big|_{\{h_c=-\sigma\}} = \\
&= \alpha \log \exp\left[\frac{q_M}{2}\left(\sum_{a=1}^{n}\frac{\partial}{\partial h_a}\right)^2\right]\left[\prod_{c=1}^{n}\exp\left[\frac{1}{2}(1-q_M)\frac{\partial^2}{\partial h_c^2}\right]\exp\left[-\beta\,\nu(h_c)\right]\right]\Big|_{\{h_c=-\sigma\}}
\end{aligned} \tag{2.39}$$

We develop the diffusion operator as a Gaussian convolution

$$e^{\frac{w}{2}\frac{\partial^2}{\partial h^2}} f(h) = \int_{-\infty}^{\infty} \frac{dz}{\sqrt{2\pi w}} e^{-\frac{z^2}{2w}} f(h-z) := \gamma_w * f(h) \tag{2.40}$$

to get

$$\begin{aligned} \alpha \log \mathcal{Z} &= \alpha \log \exp\left[\frac{q_M}{2}\left(\sum_{a=1}^{n}\frac{\partial}{\partial h_a}\right)^2\right]\left[\prod_{c=1}^{n}\gamma_{1-q_M} * \exp\left[-\beta\,\nu(h_c)\right]\right]\Big|_{\{h_c=-\sigma\}} = \\ &= \alpha \log \exp\left[\frac{q_M}{2}\frac{\partial^2}{\partial h^2}\right]\left[\gamma_{1-q_M} * \exp\left[-\beta\,\nu(h)\right]\right]^n\Big|_{\{h=-\sigma\}} = \\ &= \alpha \log \gamma_{q_M} * \left[\gamma_{1-q_M} * e^{-\beta\,\nu(h)}\right]^n\Big|_{\{h=-\sigma\}} \end{aligned} \tag{2.41}$$

The replicated action under the replica symmetric ansatz is:

$$\mathcal{S}(\mathcal{Q}) = \frac{1}{2}\left[(n-1)\log(1-q_M) + \log\left(1+(n-1)q_M\right)\right] + \alpha \log \gamma_{q_M} * \left[\gamma_{1-q_M} * e^{-\beta\,\nu(h)}\right]^n\Big|_{\{h=-\sigma\}} \tag{2.42}$$

To take the limit $n \to 0$, we can expand in n:

$$\mathcal{S}(\mathcal{Q}) \simeq n\tilde{\mathcal{S}}(\mathcal{Q}) = n\left[\frac{1}{2}\log(1-q_M) + \frac{1}{2}\frac{q_M}{1-q_M} + \alpha\gamma_{q_M} * \log\gamma_{1-q_M} * e^{-\beta\,\nu(h)}\Big|_{\{h=-\sigma\}}\right] \tag{2.43}$$

We finally get the RS free energy

$$\begin{aligned} -\beta\,\mathrm{f}_{RS} &= \partial_n \mathcal{S}(\mathcal{Q}_{RS}) = \\ &= \frac{1}{2}\log(1-q_M) + \frac{1}{2}\frac{q_M}{1-q_M} + \alpha\gamma_{q_M} * \log\gamma_{1-q_M} * e^{-\beta\,\nu(h)}\Big|_{\{h=-\sigma\}} \end{aligned} \tag{2.44}$$

Now the only parameter of the overlap matrix is q_M and the saddle point condition (2.35) corresponds to the condition $\frac{\mathrm{d}}{\mathrm{d}q_M}(-\beta f_{RS}) = 0$ that reads:

$$\frac{q_M}{(1-q_M)^2} = \alpha \int \frac{dh}{\sqrt{2\pi q_M}} e^{-\frac{h^2}{2q_M}}\left[\frac{\partial}{\partial h}\log\gamma_{1-q_M} * e^{-\beta\,\nu(h-\sigma)}\right]^2 \tag{2.45}$$

The SAT phase

Studying the SAT phase in the limit $T \to 0$ corresponds to recovering Gardner's analysis. In fact

$$e^{-\beta\,\nu(h)} \underset{\beta\to\infty}{\to} \theta(h) \tag{2.46}$$

and the convolution becomes

$$\gamma_{1-q_M} * \theta(h) = \frac{1}{2}\left[1 + \mathrm{erf}\left(\frac{h}{\sqrt{2(1-q_M)}}\right)\right] = \Theta\left(\frac{h}{\sqrt{2(1-q_M)}}\right) \tag{2.47}$$

where we have defined $\Theta(x) = \frac{1}{2}\left[1 + \mathrm{erf}\,(x)\right]$, with erf being the error function $\mathrm{erf}(x) \coloneqq 2\int_0^x \frac{e^{-t^2}}{\sqrt{\pi}} dt$. So the value of q_M is found by solving numerically the equation

$$\frac{q_M}{(1-q_M)^2} = \alpha \int_{-\infty}^{\infty} \frac{dh}{\sqrt{2q_M}} e^{-\frac{(h+\sigma)^2}{2q_M}} \left[\frac{\mathrm{d}}{\mathrm{d}h} \log \Theta\left(\frac{h}{\sqrt{2(1-q_M)}}\right)\right]^2 \tag{2.48}$$

which is solved for values of $0 < q_M < 1$ when we are in the SAT phase. Intuitively, the value of $1 - q_M$ gives a measure of how large the volume of solutions $\mathbf{X}$ of the CCSP (2.3) is. When we get towards the UNSAT phase, the value of $1 - q_M$ decreases and the transition line is defined by the limit $q_M \to 1$. Taking this limit in eq. (2.48), one obtains the relationship between the control parameters α and σ which defines the transition line, i.e. the *jamming* line (in the RS computation):

$$\alpha_J(\sigma) = \left[\int_{-\infty}^{\sigma} \frac{dh}{\sqrt{2\pi}} e^{-\frac{h^2}{2}} (h-\sigma)^2\right]^{-1} \tag{2.49}$$

Stability of the RS solution

Having found an extremum of the replicated action is not enough: we have to check that it is stable at least against small fluctuations. To do so, we have to consider fluctuations of the overlap matrix around our saddle point solution

$$\mathcal{Q} = \mathcal{Q}^* + \delta\mathcal{Q}_{ab} \tag{2.50}$$

and the corresponding expansion

$$\begin{aligned} \mathcal{S}(\mathcal{Q}) &= \mathcal{S}(\mathcal{Q}^*) + \frac{1}{2}\sum_{a<b}\sum_{c<d} M_{ab;cd}\delta\mathcal{Q}_{ab}\delta\mathcal{Q}_{cd} = \\ &= \mathcal{S}(\mathcal{Q}^*) + \frac{1}{8}\sum_{a\neq b}\sum_{c\neq d} \tilde{M}_{ab;cd}\delta\mathcal{Q}_{ab}\delta\mathcal{Q}_{cd} \end{aligned} \tag{2.51}$$

where

$$M_{ab;cd} = \left.\frac{\delta^2\mathcal{S}(\mathcal{Q})}{\delta\mathcal{Q}_{ab}\delta\mathcal{Q}_{cd}}\right|_{\mathcal{Q}=\mathcal{Q}^*} \tag{2.52}$$

and $\tilde{M}$ is its symmetrized version. At this point it is necessary to compute the terms that contribute to $M_{ab;cd}$ under the RS ansatz and take the limit $n \to 0$. For details of this computation see Ref. [234, 4, 231].
It turns out that there is an eigenspace of the stability matrix whose corresponding eigenvalue can eventually become negative in some parts of the phase diagram and therefore destabilize the RS solution: this eigenspace is usually called the *replicon* and the associated eigenvalue *replicon eigenvalue*. Its expression under the RS ansatz reads:

$$\lambda_{replicon} = -2\left[\frac{1}{(1-q_M)^2} - \alpha\gamma_{q_M} * \left[\frac{\mathrm{d}^2}{\mathrm{d}h^2}\log\gamma_{1-q_M} * e^{-\beta\,\nu(h)}\right]^2\Bigg|_{h=-\sigma}\right] \tag{2.53}$$

RS stability in the SAT phase

To see when the RS solution gets unstable, we can solve for the equation $\lambda_{replicon} = 0$: it gives the boundary line of stability of the RS solution and it is usually called *deAlmeida-Thouless* (dAT) line [4]. Using the expression (2.47) for the convolution in the SAT phase in eq. (2.53), we get

$$\frac{1}{(1-q_M)^2} = \alpha \int_{-\infty}^{\infty} dh \gamma_{q_M}(h+\sigma) \left[\frac{\mathrm{d}^2}{\mathrm{d}h^2} \log \Theta \left(\frac{h}{\sqrt{2(1-q_M)}} \right) \right]^2 \tag{2.54}$$

Analyzing this equation together with eq. (2.48), it turns out that it can be solved only for $\sigma \leq 0$. In fact, this is what we expect: as explained in section (2.2), for $\sigma > 0$ the solutions of the CCSP live in a convex set, therefore they will form a connected island. The existence of a single minimum (or a single basin of solutions) is what is associated to the RS ansatz.
By expanding the convolution for $q_M \to 1$, it is easy to check that the dAT line starts from the point $(\alpha = 2, \sigma = 0)$, that is exactly on the jamming line. Therefore the jamming line for $\sigma < 0$ is in a portion of the phase diagram where the RS ansatz is unstable.

2.3.3 The RSB transition

When the RS solution is unstable, it is necessary to find another ansatz for the matrix $\mathcal{Q}_{ab}$. This problem was first addressed in the context of spin-glasses, trying to solve the low-temperature phase of the Sherrington-Kirkpatrick model [140, 39]. The solution was then found by Parisi who proposed an iterative scheme of replica symmetry breaking (RSB). This construction has been mathematically proven to be correct for the Sherrington-Kirkpatrick model [227, 194, 122, 193] and it is believed to give a correct physical picture in disordered mean-field models like the perceptron. In the following we study the Parisi RSB solution.

RSB scheme

The central hypothesis is that the structure of the overlap matrix $\mathcal{Q}$ is a hierarchical one. The simplest is the replica symmetric, which has the diagonal equal to 1 (due to the spherical constraint) and the off-diagonal entries equal to q_0.
The 1-step RSB is given by dividing the n replicas into n/m_0 groups, each one of size m_0. Then the diagonal blocks have the diagonal equal to 1 and the off-diagonal entries equal to q_1, while the off-diagonal blocks are filled with the value q_0. So the parameters of the 1-RSB matrix are the three numbers m_0, q_0, q_1.
The 2-step RSB is constructed starting from the 1-step RSB matrix, considering its diagonal blocks of size m_0 and dividing them in sub-blocks of size m_1: the diagonal sub-blocks are filled with the value 1 in the diagonal and the value q_2 in the off-diagonal entries, while the off-diagonal sub-blocks are left filled with the value q_1. Therefore the 2RSB hierarchical matrix has 5 parameters: m_0, m_1, q_0, q_1, q_2.

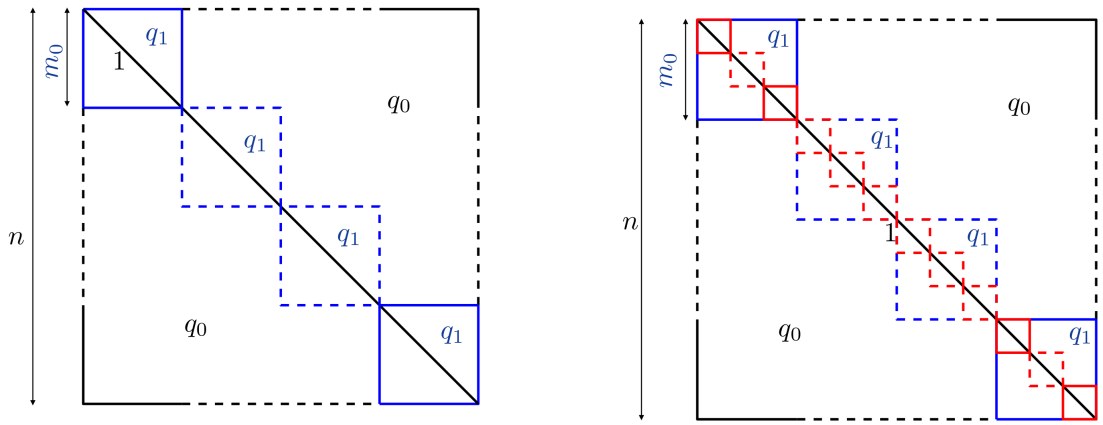

Figure 2.2: Hierarchical matrices following the 1RSB (left) and 2RSB (right) constructions.

It is possible to continue this process creating a kRSB matrix starting from a (k-1)RSB one, each time increasing the number of parameters: $m_0, ...m_{k-1}$, $q_0, ...q_k$. It is worth noting that this kind of hierarchical matrices form an algebra: given two kRSB matrices A and B with the same parameters $\{m_i\}_{i=0,...,k-1}$, their product $C = AB$ is still a kRSB matrix.
By this construction, the parameters m_i satisfy the inequalities

$$n > m_0 > m_1 > ... > m_{k-1} > m_k = 1 \tag{2.55}$$

The limit $n \to 0$ requires some care. The parameters m_i are inside the interval $[1, n)$, but when $n \to 0$ the bounds get exchanged and $m_i \in (0, 1]$. In particular, the inequalities (2.55) exchange their direction as

$$n < m_0 < m_1 < ... < m_{k-1} < m_k = 1 \tag{2.56}$$

A more detailed discussion of this passage can be found in [168].
In the kRSB scheme with $n \to 0$, considering the parameters q_i as functions of $m_i \in (0, 1]$, a stepwise function $q(x)$ is obtained. Repeating this scheme iteratively for $k \to \infty$, the function $q(x)$ becomes a continuous one with $x \in [0, 1]$: this is the *order parameter of a RSB phase* [199]. The k-step RSB construction is simply referred to as kRSB, while the limit $k \to \infty$ is usually called $full$RSB.

The fullRSB equations of the perceptron

Now we have to compute the replicated action (2.32) using an overlap matrix $\mathcal{Q}$ that has a hierarchical structure parametrized by the function $q(x)$. We remind that there are two terms to compute: the entropic one

$$\mathcal{S}_E = \frac{1}{2} \log \det \mathcal{Q} \tag{2.57}$$

and the energy one

$$\mathcal{S}_I = \alpha \log \exp \left[\frac{1}{2} \sum_{a,b=1}^{n} \mathcal{Q}_{ab} \frac{\partial^2}{\partial h_a \partial h_b} \right] \left[\prod_{c=1}^{n} e^{-\beta \nu(h_c - \sigma)} \right] \Bigg|_{\{h_c = 0\}} \tag{2.58}$$

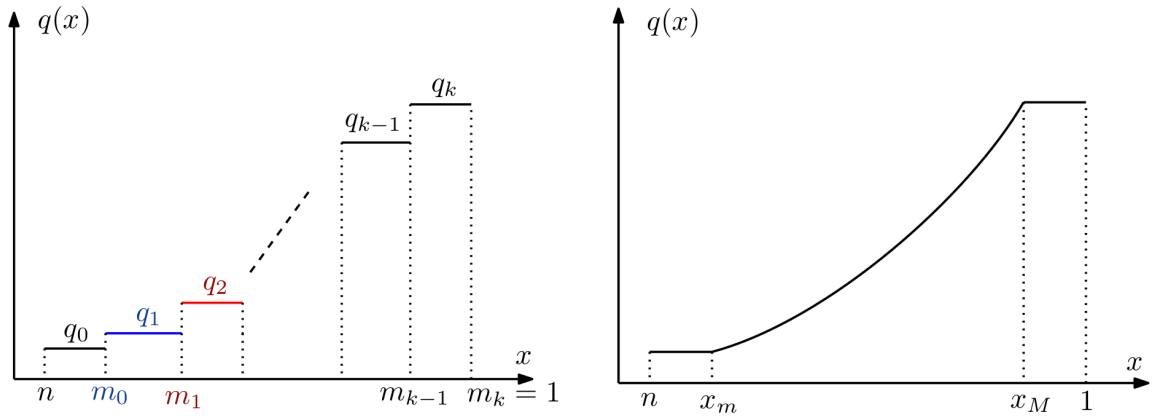

Figure 2.3: Function $q(x)$ in the kRSB case (left) and in the $full$RSB case (right).

Starting with the entropic one, it turns out to be [234, 179]

$$\frac{1}{2}\lim_{n\to 0}\partial_n \log\det \mathcal{Q} = \frac{1}{2}\left[\log\left(1-\langle q\rangle\right) + \frac{q(0)}{\left(1-\langle q\rangle\right)^2} - \int_0^1 \frac{dx}{x^2}\frac{\lambda(x)}{1-\langle x\rangle}\right] \tag{2.59}$$

with

$$\lambda(x) = 1 - xq(x) - \int_x^1 dy q(y) \qquad \langle q\rangle = \int_0^1 dy q(y) \tag{2.60}$$

To compute the energy term, we proceed by finding a general formulation for the kRSB scheme and then taking the limit $k\to\infty$. Let's introduce the $n\times n$ matrix $\mathbf{1}^{(n,m_i)}$ that has diagonal blocks of size $m_i\times m_i$ filled with ones and off-diagonal blocks with all entries equal to 0. With this definition we can write the kRSB $\mathcal{Q}$ matrix as

$$\mathcal{Q} = \sum_{i=0}^{k+1}(q_i - q_{i-1})\mathbf{1}^{(n,m_{i-1})} \tag{2.61}$$

with the conventional choice $q_{k+1}=1$ and $q_{-1}=0$. Therefore the energy term

$$\mathcal{S}_I = \alpha\log\exp\left[\frac{1}{2}\sum_{i=0}^{k+1}(q_i-q_{i-1})\sum_{a,b=1}^{n}\mathbf{1}_{a,b}^{(n,m_{i-1})}\frac{\partial^2}{\partial h_a\partial h_b}\right]\left[\prod_{c=1}^{n}e^{-\beta\,\nu(h_c-\sigma)}\right]\Bigg|_{\{h_c=0\}} \tag{2.62}$$

Making the term $i=k+1$ explicit:

$$\begin{aligned}\mathcal{S}_I &= \alpha\log\exp\left[\frac{1}{2}\sum_{i=0}^{k}(q_i-q_{i-1})\sum_{a,b=1}^{n}\mathbf{1}_{a,b}^{(n,m_{i-1})}\frac{\partial^2}{\partial h_a\partial h_b}\right]\exp\left[\frac{1}{2}(1-q_k)\sum_{a=1}^{n}\frac{\partial^2}{\partial h_a^2}\right]\left[\prod_{c=1}^{n}e^{-\beta\,\nu(h_c-\sigma)}\right]\Bigg|_{\{h_c=0\}} = \\ &= \alpha\log\exp\left[\frac{1}{2}\sum_{i=0}^{k}(q_i-q_{i-1})\sum_{a,b=1}^{n}\mathbf{1}_{a,b}^{(n,m_{i-1})}\frac{\partial^2}{\partial h_a\partial h_b}\right]\left[\prod_{c=1}^{n}\gamma_{1-q_k} * e^{-\beta\,\nu(h_c-\sigma)}\right]\Bigg|_{\{h_c=0\}}\end{aligned} \tag{2.63}$$

Let's rename the convolution as

$$g(1,h)\equiv g(m_k,h) \coloneqq \gamma_{1-q_k} * e^{-\beta\,\nu(h-\sigma)} \tag{2.64}$$

and make explicit the term $i = k$:

$$\begin{aligned}
\mathcal{S}_I = \alpha \log \exp & \left[\frac{1}{2} \sum_{i=0}^{k-1} (q_i - q_{i-1}) \sum_{a,b=1}^{n} \mathbf{1}_{a,b}^{(n,m_{i-1})} \frac{\partial^2}{\partial h_a \partial h_b} \right] \\
& \exp \left[\frac{1}{2} (q_k - q_{k-1}) \sum_{a,b=1}^{n} \mathbf{1}_{a,b}^{(n,m_{k-1})} \frac{\partial^2}{\partial h_a \partial h_b} \right] \left[\prod_{c=1}^{n} g(m_k, h_c - \sigma) \right] \Bigg|_{\{h_c=0\}} = \\
= \alpha \log \exp & \left[\frac{1}{2} \sum_{i=0}^{k-1} (q_i - q_{i-1}) \sum_{a,b=1}^{n/m_{k-1}} \mathbf{1}_{a,b}^{\left(\frac{n}{m_{k-1}}, \frac{m_{i-1}}{m_{k-1}}\right)} \frac{\partial^2}{\partial h_a \partial h_b} \right] \\
& \exp \left[\frac{1}{2} (q_k - q_{k-1}) \sum_{a,b=1}^{n/m_{k-1}} \mathbf{1}_{a,b}^{\left(\frac{n}{m_{k-1}}, 1\right)} \frac{\partial^2}{\partial h_a \partial h_b} \right] \left[\prod_{c=1}^{n/m_{k-1}} g^{m_{k-1}}(m_k, h_c - \sigma) \right] \Bigg|_{\{h_c=0\}} = \\
= \alpha \log \exp & \left[\frac{1}{2} \sum_{i=0}^{k-1} (q_i - q_{i-1}) \sum_{a,b=1}^{n/m_{k-1}} \mathbf{1}_{a,b}^{\left(\frac{n}{m_{k-1}}, \frac{m_{i-1}}{m_{k-1}}\right)} \frac{\partial^2}{\partial h_a \partial h_b} \right] \left[\prod_{c=1}^{n/m_{k-1}} \gamma_{q_k - q_{k-1}} * g^{m_{k-1}}(m_k, h_c - \sigma) \right] \Bigg|_{\{h_c=0\}} \\
= \alpha \log \exp & \left[\frac{1}{2} \sum_{i=0}^{k-1} (q_i - q_{i-1}) \sum_{a,b=1}^{n/m_{k-1}} \mathbf{1}_{a,b}^{\left(\frac{n}{m_{k-1}}, \frac{m_{i-1}}{m_{k-1}}\right)} \frac{\partial^2}{\partial h_a \partial h_b} \right] \left[\prod_{c=1}^{n/m_{k-1}} g(m_{k-1}, h_c - \sigma) \right] \Bigg|_{\{h_c=0\}}
\end{aligned} \tag{2.65}$$

where we have defined

$$g(m_{k-1}, h) \coloneqq \gamma_{q_k - q_{k-1}} * g^{m_{k-1}}(m_k, h) \tag{2.66}$$

This process can be iterated defining at each step the function

$$g(m_{i-1}, h) \coloneqq \gamma_{q_i - q_{i-1}} * g^{m_{i-1}/m_i}(m_i, h) \tag{2.67}$$

We can rewrite this definition in the continuum limit. Using the relationships

$$m_i = x \qquad m_{i-1} \simeq m_i - dx = x - dx \qquad q_i - q_{i-1} = \dot{q}(x) dx \tag{2.68}$$

it becomes the differential equation

$$g(x, h) - dx \dot{g}(x, h) = g(x, h) + \frac{1}{2} \dot{q}(x) g''(x, h) - \frac{1}{x} g(x, h) \log g(x, h) \tag{2.69}$$

that we can recast as

$$\dot{g}(x, h) = -\frac{\dot{q}(x)}{2} g''(x, h) + \frac{1}{x} g(x, h) \log g(x, h) \tag{2.70}$$

where we are using the dot to indicate the derivative with respect to x and the prime for the derivative with respect to h. The boundary condition of the partial differential equation (2.70) is given by

$$g(1, h) = \gamma_{1 - q(1)} * e^{-\beta \nu(h)} \tag{2.71}$$

For convenience, this equation is usually written for the function

$$f(x, h) = \frac{1}{x} \log g(x, h) \tag{2.72}$$

and takes the name of *Parisi's flow equation*:

$$\begin{cases} \dot{f}(x,h) & = -\frac{\dot{q}(x)}{2}\left[f''(x,h) + x(f'(x,h))^2\right] \\ f(1,h) & = \log \gamma_{1-q(1)} * e^{-\beta\,\nu(h)} \end{cases} \tag{2.73}$$

This equation was first derived in the context of the Sherrington-Kirkpatrick model [199]. In fact, the form of the differential equation (2.73) is generic since it is due to the differential operator; the details of the model enter in the initial condition of the equation. To conclude the computation of the energy term, at the end of the iteration we get

$$\mathcal{S}_I = \alpha \log e^{\frac{q(0)}{2}\partial_h^2} g^{n/m_0}(m_0,h)|_{h=-\sigma} \to n\alpha\gamma_{q(0)} * f(0,-\sigma) \qquad n \to 0 \tag{2.74}$$

Finally we can write the free energy of the perceptron in the $full$RSB ansatz:

$$\begin{aligned} -\beta\,\mathrm{f}\,[q(x)] &= \lim_{n\to 0}\partial_n \mathcal{S}(\mathcal{Q}) = \\ &= \frac{1}{2}\left[\log\left(1-\langle q\rangle\right) + \frac{q(0)}{\left(1-\langle q\rangle\right)^2} - \int_0^1 \frac{dx}{x^2}\frac{\lambda(x)}{1-\langle x\rangle}\right] + \alpha\gamma_{q(0)} * f(0,-\sigma) \end{aligned} \tag{2.75}$$

where $f(0,-\sigma)$ is obtained from the solution of the flow equation (2.73): therefore this expression depends both explicitly and implicitly on $q(x)$.

FullRSB saddle point

To find the saddle point, we should take the functional derivative of the $full$RSB free energy with respect to the function $q(x)$: this step is not straightforward since the function $f(x,h)$ depends implicitly on $q(x)$ through the flow equation (2.73). Following [225], a way to solve this task is by introducing the function $P(x,h)$ as a Lagrange multiplier to enforce the flow equation:

$$\begin{aligned} \mathcal{S}(\mathcal{Q}) = &\frac{1}{2}\left[\log(1-\langle q\rangle) + \frac{q(0)}{\left(1-\langle q\rangle\right)^2} - \int_0^1 \frac{dx}{x^2}\frac{\lambda(x)}{1-\langle x\rangle}\right] + \alpha\gamma_{q(0)} * f(0,-\sigma) + \\ &- \alpha\int_{-\infty}^{\infty} dh P(1,h)\left[f(1,h) - \log e^{-\beta\,\nu(h)}\right] + \\ &+ \alpha\int_0^1 dx\int_{-\infty}^{\infty} dh P(x,h)\left[\dot{f}(x,h) + \frac{\dot{q}(x)}{2}\left[f''(x,h) + x\left(f'(x,h)\right)^2\right]\right] \end{aligned} \tag{2.76}$$

Taking the functional derivative with respect to $P(x,h)$ gives back the flow equation. Instead, the functional derivative with respect to $f(x,h)$ and $f(0,h)$ gives a new differential equation for $P(x,h)$:

$$\begin{cases} \dot{P}(x,h) & = \frac{\dot{q}(x)}{2}\left[P''(x,h) - 2x\left(f'(x,h)P(x,h)\right)'\right] \\ P(0,h) & = \frac{1}{\sqrt{2\pi q(0)}} e^{-\frac{(h+\sigma)^2}{2q(0)}} \end{cases} \tag{2.77}$$

Taking the derivative with respect to $q(x)$ [234, 225], we get the final equation

$$\frac{q(0)}{\left(1-\langle q\rangle\right)^2} + \int_0^x dy \frac{\dot{q}(y)}{\lambda^2(y)} = \alpha\int_{-\infty}^{\infty} dh P(x,h)\left(f'(x,h)\right)^2 \tag{2.78}$$

The function $P(x,h)$ for $x \to 1$ is related to the probability distribution of gaps $\rho(h)$. Using $q(x)$ as a variable instead of x, with $q(1) = q_M$, the relation reads

$$\rho(h) = \frac{1}{\alpha}\frac{\mathrm{d}\,\mathrm{f}}{\mathrm{d}\,\nu(h)} = e^{-\beta\nu(h)} \int dz\ P(q_M, z) e^{-f(q_M,z)} \gamma_{1-q_M}(z-h) \tag{2.79}$$

The expression for $\rho(h)$ in terms of $P(q,h)$ is expressed explicitly for the linear potential case in appendix A.

Marginal stability

We can obtain an important equation by deriving eq. (2.78) on both sides w.r.t. x:

$$\frac{1}{\lambda^2(x)}\dot{q}(x) = \dot{q}(x)\alpha \int_{-\infty}^{\infty} dh P(x,h) \left(f''(x,h)\right)^2 \tag{2.80}$$

When $\dot{q}(x) > 0$ it becomes

$$\frac{1}{\lambda^2(x)} = \alpha \int_{-\infty}^{\infty} dh P(x,h) \left(f''(x,h)\right)^2 \tag{2.81}$$

To understand the physical meaning of this equation, it is useful to notice that in the replica symmetric case it just becomes eq. (2.54) that defines the deAlmeida-Touless line where there is the transition between the RS and RSB phase. In fact, it is related to the stability of the saddle point and actually implies the *marginal stability* of the $full$RSB solution, related to the Hessian

$$\frac{\delta^2 \mathcal{S}(\mathcal{Q})}{\delta q(x) \delta q(y)} \tag{2.82}$$

Marginal stability is a crucial feature in the context of the jamming universality class. We will show how equation (2.81) is the connection between the replica formalism and the property of *isostaticity* that is a landmark of the critical jamming transition.

Another useful relationship is obtained by deriving equation (2.81) for x:

$$x = \frac{\lambda(x)}{2} \frac{\int_{-\infty}^{\infty} dh P(x,h) \left(f'''(x,h)\right)^2}{\int_{-\infty}^{\infty} dh P(x,h) \left(f''(x,h)\right)^2 \left(1 + \lambda(x) f'(x,h)\right)} \tag{2.83}$$

Computing this quantity in the limit of approaching the RS phase from the RSB one, gives the so called *breaking point* of $q(x)$, that is the point x^* where the profile of $q(x)$ that is constantly equal to q_M in the RS phase starts to break in the smooth profile typical of the $full$RSB phase. The breaking point is useful to understand what kind of RSB transition takes place. Its study in the case of the linear potential is done in appendix C.

2.3.4 The jamming line

We are now able to study the portion of the phase diagram where the RS solution is unstable and we need the $full$RSB ansatz. Computing the thermodynamic quantities in this phase requires solving the partial differential equations (2.73-2.77), a task that can be done only numerically. The most interesting part, however, is studying the solution of

the problem when approaching the jamming line in the RSB phase: in this regime it is possible to have an interesting theoretical description from an analytical point of view; in particular, a scaling theory of the jamming transition is obtained.
The saddle point equations are

$$\begin{aligned}
&\begin{cases} \dot{f}(x,h) &= -\frac{\dot{q}(x)}{2}\left[f''(x,h) + x(f'(x,h))^2\right] \\ f(1,h) &= \log \gamma_{1-q(1)} * e^{-\beta\,\nu(h)} \end{cases} \\
&\begin{cases} \dot{P}(x,h) &= \frac{\dot{q}(x)}{2}\left[P''(x,h) - 2x\left(f'(x,h)P(x,h)\right)'\right] \\ P(0,h) &= \frac{1}{\sqrt{2\pi q(0)}} e^{-\frac{(h+\sigma)^2}{2q(0)}} \end{cases} \\
&\frac{q(0)}{(1-\langle q\rangle)^2} + \int_0^x dy \frac{\dot{q}(y)}{\lambda^2(y)} = \alpha \int_{-\infty}^{\infty} dh P(x,h)\left(f'(x,h)\right)^2 \\
&\lambda(q) = 1 - q_M + \int_q^{q_M} dp x(p)
\end{aligned} \tag{2.84}$$

where q_m and q_M stand for $q(0)$ and $q(1)$ respectively. In addition, marginal stability implies

$$\begin{aligned}
\frac{1}{\lambda^2(x)} &= \alpha \int_{-\infty}^{\infty} dh P(x,h)\left(f''(x,h)\right)^2 \\
x &= \frac{\lambda(x)}{2} \frac{\int_{-\infty}^{\infty} dh P(x,h)\left(f'''(x,h)\right)^2}{\int_{-\infty}^{\infty} dh P(x,h)\left(f''(x,h)\right)^2\left(1+\lambda(x)f'(x,h)\right)}
\end{aligned} \tag{2.85}$$

In the SAT phase, the typical cluster of solutions has size $1 - q_M$; in the jamming limit, each one of these clusters shrinks to a point, corresponding therefore to the limit $q_M \to 1$. We can call ϵ the (small) distance from the jamming line (it can be $|\alpha - \alpha_J|$ or $|\sigma - \sigma_J|$) and correspondingly the maximum overlap behaves like

$$q_M = 1 - \epsilon^{\kappa} \tag{2.86}$$

Looking at the functions appearing in our equations, it is convenient to rescale them as

$$\begin{aligned}
y(q) &= \frac{x(q)}{\epsilon} \\
\hat{f}(q,h) &= \epsilon f(q,h) \\
\hat{\lambda}(q) &= \frac{\lambda(q)}{\epsilon}
\end{aligned} \tag{2.87}$$

from which it follows that $y(q) \in [0, \frac{1}{\epsilon}]$. From eq. (2.86) we also get that in the limit $q \to 1$

$$y(q) \underset{q\to 1}{\simeq} \bar{y}(1-q)^{-\frac{1}{\kappa}} \tag{2.88}$$

The form of the equations we are guessing is actually very reminiscent of the scaling solution of hard-spheres close to jamming in infinite dimensions [62, 200].

Scaling of the flow equation for $f(q,h)$

Remembering that in the SAT phase $e^{-\beta\nu(h)} = \theta(h)$, the boundary condition for the function $f(q,h)$ is given by

$$f(q_M,h) = \log\gamma_{1-q_M} * \theta(h) = \log\Theta\left(\frac{h}{\sqrt{2(1-q_M)}}\right) = \begin{cases} 0 & h\to+\infty \\ -\frac{h^2}{2(1-q_M)} & h\to-\infty \end{cases} \tag{2.89}$$

We can also show that the flow equation for $f(q,h)$ in (2.84) has an asymptotic solution

$$f(q,h) = \begin{cases} 0 & h\to+\infty \\ -\frac{h^2}{2\lambda(q)} & h\to-\infty \end{cases} \tag{2.90}$$

that is compatible with the condition (2.89). The regime $h\to+\infty$ is a trivial solution, while the one for $h\to-\infty$ can be checked by plugging it into the flow equation. In fact, the left hand side becomes

$$\dot{f}(q,h) = -\frac{x(q)}{\lambda^2(q)}h^2 \tag{2.91}$$

that is equal to the right hand side

$$-\frac{1}{2}\left[f''(q,h) + x(q)\left(f'(q,h)\right)^2\right] = -\frac{1}{2}\left[-\frac{1}{\lambda(q)} + x(q)\frac{h^2}{\lambda^2(q)}\right] \simeq -\frac{x(q)}{2\lambda^2(q)}h^2 \qquad h\to-\infty \tag{2.92}$$

It is convenient to define the function

$$m(q,h) = \lambda(q)f'(q,h) \tag{2.93}$$

so that the flow equation for $f(q,h)$ becomes a flow equation for $m(q,h)$:

$$\dot{m}(q,h) = -\frac{1}{2}m''(q,h) - \frac{y(q)}{\hat{\lambda}(q)}m(q,h)\left[1+m'(q,h)\right] \tag{2.94}$$

with boundary conditions

$$m(q,h) = \begin{cases} -h & h\to-\infty \\ 0 & h\to+\infty \end{cases} \tag{2.95}$$

To find the scaling equation of $m(q,h)$ for $q\to1$, it is necessary to see what happens to the ratio $y(q)/\hat{\lambda}(q)$ in this limit:

$$\frac{y(q)}{\hat{\lambda}(q)} = \frac{y(q)}{(1-q_M)/\epsilon + \int_q^{q_M} dpy(p)} = \frac{\bar{y}(1-q)^{-1/\kappa}}{\epsilon^{\kappa-1}(1-\bar{y}\frac{\kappa}{1-\kappa}) + \bar{y}\frac{\kappa}{\kappa-1}(1-q)^{(\kappa-1)/\kappa}} \tag{2.96}$$

where we have used the scalings (2.86-2.88). In the regime $1-q << \epsilon^\kappa$ we get

$$\frac{y(q)}{\hat{\lambda}(q)} \simeq \frac{\kappa-1}{\kappa}\frac{1}{1-q} \tag{2.97}$$

Let's notice that we are studying the solution in the regime $q_M \to 1$, $q \to 1$ and $1 - q >> 1 - q_M$.

We can finally consider the scaling ansatz for $m(q, h)$ in the limit $q \to 1$ as having the form

$$m(q,h) = -\sqrt{1-q}\,\mathcal{M}\left(\frac{h}{\sqrt{1-q}}\right) \qquad \mathcal{M}(t \to \infty) = 0 \qquad \mathcal{M}(t \to -\infty) = t \tag{2.98}$$

Plugging this ansatz into the equation (2.94) and using the scaling (2.97) we get

$$\mathcal{M}(t) - t\mathcal{M}'(t) = \mathcal{M}''(t) + 2\frac{\kappa - 1}{\kappa}\mathcal{M}(t)\left(1 - \mathcal{M}'(t)\right) \tag{2.99}$$

This is the first of our equations describing the universality of the jamming transition. It depends on the only parameter κ and admits a unique solution with the boundary conditions (2.98).

Scaling of the flow equation for $P(q, h)$

The flow equation for the function $P(q, h)$ has boundary condition

$$P(q_m, h) = \gamma_{q_m}(h + \sigma) \tag{2.100}$$

As before, we can find the asymptotic solutions

$$P(q,h) = \begin{cases} \gamma_q(h+\sigma) & h \to +\infty \\ \propto \sqrt{D(q)}e^{-D(q)h^2} & h \to -\infty \end{cases} \tag{2.101}$$

In fact, for $h \to \infty$ we have $f(q, h) \simeq 0$ and therefore the flow equation for $P(q, h)$ becomes

$$\dot{P}(q,h) \simeq -\frac{P''(q,h)}{2} \qquad h \to +\infty \tag{2.102}$$

For $h \to -\infty$, we have $f(q, h) \simeq \frac{h^2}{2\hat{\lambda}(q)}$ which gives

$$\dot{P}(q,h) = \frac{P''(q,h)}{2} + \frac{y(q)}{\hat{\lambda}(q)}\left[hP'(q,h) + P(q,h)\right] \tag{2.103}$$

that is solved by the form (2.101) given that $D(q)$ solves the equation

$$\dot{D}(q) = -2D^2(q) + 2D(q)\frac{\kappa - 1}{\kappa}\frac{1}{1-q} \tag{2.104}$$

where again we are using the scaling (2.97) for $y(q)/\hat{\lambda}(q)$. If $\kappa < 2$, as we will check it is the case, equation (2.104) provides the scaling for $q \to 1$

$$D(q) \simeq \overline{D}(1-q)^{-2(\kappa-1)/\kappa} \qquad q \to 1 \tag{2.105}$$

This is very useful because it allows us to see the scaling variable of $P(q, h)$ for h negative; so we should have

$$P(q,h) = \begin{cases} P_+(h) & h >> \sqrt{1-q} \\ (1-q)^{-\frac{\kappa-1}{\kappa}} P_-\left(\frac{h}{(1-q)^{(\kappa-1)/\kappa}}\right) & h \sim -(1-q)^{(\kappa-1)/\kappa} \end{cases} \tag{2.106}$$

Looking at this expression, there should me a matching regime between P_+ and P_-; therefore, we conjecture that the complete scaling solution for $P(q,h)$ when $q \to 1$ has the form

$$P(q,h) = \begin{cases} P_+(h) & h >> \sqrt{1-q} \\ (1-q)^{-\frac{a}{\kappa}} P_0\left(\frac{h}{\sqrt{1-q}}\right) & |h| \sim \sqrt{1-q} \\ (1-q)^{-\frac{\kappa-1}{\kappa}} P_-\left(\frac{h}{(1-q)^{(\kappa-1)/\kappa}}\right) & h \sim -(1-q)^{(\kappa-1)/\kappa} \end{cases} \tag{2.107}$$

where a is a scaling exponent. The scaling variable $t = \frac{h}{\sqrt{1-q}}$ is chosen to be equal to the one of the equation (2.99) and in fact it gives a non-trivial differential equation for $P_0(t)$. The three scaling regimes should match and so the functions P_-, P_0, P_+. For $h < 0$, supposing

$$\begin{aligned} P_-(t) &\sim |t|^\theta \qquad t \to 0^- \\ P_0(t) &\sim |t|^\theta \qquad t \to -\infty \end{aligned} \tag{2.108}$$

we get the relationship between the exponents

$$\theta = \frac{2\,(1-\kappa+a)}{\kappa-2} \tag{2.109}$$

Similarly, for $h > 0$ assuming

$$\begin{aligned} P_0(t) &\sim t^{-\gamma} \qquad t \to +\infty \\ P_+(t) &\sim t^{-\gamma} \qquad t \to 0^+ \end{aligned} \tag{2.110}$$

we get

$$\gamma = \frac{2a}{\kappa} \tag{2.111}$$

Putting the matching part of the scaling ansatz (2.107) into the flow equation for P, we get a non-trivial equation for P_0:

$$\begin{aligned} &\frac{a}{\kappa} P_0(t) + \frac{1}{2} t P_0'(t) = \frac{1}{2} P_0''(t) + \frac{\kappa-1}{\kappa} \left[P_0(t)\mathcal{M}(t)\right]' \\ &P_0(t \to -\infty) \sim |t|^{2(1-\kappa+a)/(\kappa-2)} \qquad P_0(t \to +\infty) \sim t^{-2a/\kappa} \end{aligned} \tag{2.112}$$

Having fixed κ and found the solution $\mathcal{M}(t)$, there is a unique solution $P_0(t)$ for equation (2.112) that satisfies both the boundary conditions for a unique value of $a(\kappa)$.

Fixing the exponent κ

Up to now, the scaling equations (2.99) and (2.112) depend on a parameter κ: it can be fixed internally by $\mathcal{M}(t)$ and $P_0(t)$ by using equation (2.85):

$$\frac{\kappa-1}{\kappa} = \frac{1}{2} \frac{\int_{-\infty}^{\infty} dt P_0(t) \mathcal{M}''(t)^2}{\int_{-\infty}^{\infty} dt P_0(t) \mathcal{M}'(t)^2 \left[1 + \mathcal{M}'(t)\right]} \tag{2.113}$$

By solving the equations (2.99), (2.112) and (2.113) iteratively, the exponent κ converges to the value

$$\kappa = 1.4157... \tag{2.114}$$

and, correspondingly, the exponent a converges to

$$a = 0.2921... \tag{2.115}$$

which satisfies, up to numerical precision, the relationship

$$a = 1 - \frac{\kappa}{2} \tag{2.116}$$

This last equality (2.116) is found empirically and no theoretical explanation is yet available [200, 62].
In section 3.3.3 we report the plots of the functions obtained by numerically solving these equations and we confirm the values of the critical exponents reported in the literature.

Physical meaning of the scaling solution

By solving the CCSP given by the perceptron, it is possible to study the distribution $\rho(h)$ of gaps h_μ. This distribution can be obtained from the function $P(q, h)$ for $q \to 1$. At the critical jamming line, there is a number of marginally satisfied gaps $h_\mu \equiv 0$ equal to $N-1$ (a degree of freedom is blocked by the spherical constraint for the $\mathbf{X}$): there is therefore the emergence of *isostaticity*, as in the jamming of hard spheres. This property corresponds to equation (2.81) in the language of replica symmetry breaking, that corresponds to *marginal stability*. This correspondence is made explicit in section 3.3.3 for the linear potential case (particularly in equation 3.165).
Looking at the distribution of small positive gaps, it exhibits a power law

$$\rho(h) \sim h^{-\gamma} \qquad h \to 0^+ \tag{2.117}$$

that is exactly the scaling solution $\rho(h) \sim P_+ \sim h^{-\gamma}$ we have found in (2.110). The value of the exponent γ is fixed by κ to

$$\gamma = 0.41269... \tag{2.118}$$

A set of Lagrange multipliers, that play the role of *contact forces* f_c, is associated to the marginally satisfied gaps $h_c \equiv 0$, in analogy with the case of sphere packings. The distribution of these forces $\rho(f)$ has a pseudo-gap appearing for small values of f

$$\rho(f) \sim f^\theta \qquad f \to 0^+ \tag{2.119}$$

that is exactly the scaling solution $\rho(f) \sim P_-(f) \sim f^\theta$ appearing in eq. (2.108) (the conncetion between $\rho(f)$ and $P_-(f)$ is made explicit in appendix A). Also the value of θ depends on κ and turns out to be

$$\theta = 0.42311... \tag{2.120}$$

Between these two exponents there is the relationship

$$\gamma = \frac{1}{2+\theta} \tag{2.121}$$

which was found in the context of jamming of hard spheres using scaling arguments[247, 248]. This argument tells that stability in a jammed packing is achieved if $\gamma \geq \frac{1}{2+\theta}$, while the equality (2.121) implies marginal stability. There is no direct way of obtaining this

relationship in the context of the $full$RSB equations, but it is actually implied indirectly by the equality $a = 1 - \frac{\kappa}{2}$ that is verified empirically.
There is also a physical interpretation of the exponent κ. In fact, in the context of hard spheres, the order parameter is given by the mean-square displacement Δ_{ab} between two different configurations. In the infinite dimensional limit, where the mean-field replica formalism applies, these mean-square displacements are distributed according to a function $\Delta(x)$ whose maximum value is Δ_{EA}, describing the size of a typical cluster of solutions. In the jamming limit, these clusters shrink to a point, corresponding to $\Delta_{EA} \to 0$, exactly what happens in the perceptron with $1 - q_M \to 0$. Since in the jamming of hard spheres the pressure diverges, the relationship becomes

$$\Delta_{EA} \sim p^{-\kappa} \tag{2.122}$$

Interestingly, the exponent κ is the same both for spheres and the perceptron, and consequently also the other exponents γ and θ. This is due to the emergence of *universality* of the jamming transition.

2.4 The harmonic perceptron

Up to now we have explored the phase diagram of the perceptron below the satisfiability line. However, the replica equations derived in section (2.3) with the factor $e^{-\beta\,\nu(h)}$ are completely general for a potential of the form $\sum_\mu \nu(h_\mu)$. Now we study the perceptron above the saturation line, with a harmonic cost function for the unsat gaps

$$H = \sum_\mu \frac{1}{2} h_\mu^2 \theta(-h_\mu) \tag{2.123}$$

We will generally refer to this model as the *harmonic perceptron*. After Elisabeth Gardner, other attempts of studying the perceptron above the satisfiability line with different potentials were done in the '90s[164, 41, 124, 125]. Here we present the results as presented in [105].

2.4.1 The UNSAT replica symmetric phase

We can start by rewriting the replica symmetric free energy of the perceptron

$$-\beta\, \mathrm{f}_{RS} = \frac{1}{2}\log(1 - q_M) + \frac{1}{2}\frac{q_M}{1 - q_M} + \alpha \gamma_{q_M} * f(q_M, h)|_{\{h=-\sigma\}} \tag{2.124}$$

with

$$f(q_M, h) = \log \gamma_{1-q_M} * e^{-\beta \frac{h^2}{2}\theta(-h)} \tag{2.125}$$

We want to study the model in the UNSAT phase in the limit of zero temperature: therefore, the system sits in the only minimum which gives

$$q_M \underset{T\to 0}{\to} 1 \tag{2.126}$$

and the replica symmetric ansatz implies the validity of linear response theory (i.e. the square displacements $< |\delta \mathbf{X}|^2 >$ grow linearly in T) which corresponds to

$$q_M \sim 1 - \chi T \tag{2.127}$$

where χ is a constant fixed by the saddle point equation. χ is clearly a susceptibility.

Expansion of $f(q_M, h)$ for $T \to 0$

The first step is to compute $f(q_M, h)$ in the zero temperature limit $\beta \to \infty$ using the linear response relation

$$\beta(1 - q_M) = \chi \tag{2.128}$$

We get

$$\begin{aligned} f(q_M, h) &= \log \gamma_{1-q_M} * e^{-\beta \frac{h^2}{2}\theta(-h)} = \\ &= \log \int_{-\infty}^{\infty} \frac{dz}{\sqrt{2\pi\chi T}} e^{-\frac{\beta}{2}\left[\frac{(h-z)^2}{\chi} + z^2\theta(-z)\right]} \end{aligned} \tag{2.129}$$

Since $\beta \to \infty$, we can use the saddle point method by finding z^* defined by

$$\frac{\mathrm{d}}{\mathrm{d}z}\left[\frac{(h-z)^2}{2\chi} + \frac{z^2}{2}\theta(-z)\right]\Bigg|_{z^*} = 0 \tag{2.130}$$

which gives

$$z^* = \begin{cases} h & h > 0 \\ \frac{\chi}{1+\chi} h & h < 0 \end{cases} \tag{2.131}$$

Therefore we have

$$\begin{aligned} f(q_M \to 1, h) &= \log e^{-\frac{\beta}{2}\left[\frac{(h-z^*)^2}{\chi} + z^{*2}\theta(-z^*)\right]} \int_{-\infty}^{\infty} \frac{dz}{\sqrt{2\pi\chi T}} e^{-\frac{\beta}{2}\left(\frac{1}{\chi} + \theta(-z^*)\right)(z-z^*)^2} = \\ &\simeq \begin{cases} 0 & h > 0 \\ -\beta \frac{h^2}{2(1+\chi)} & h < 0 \end{cases} \end{aligned} \tag{2.132}$$

It's worth noting that there is a matching region around $h \sim 0$ between these two behaviors. In particular, the matching part is for $h \sim \sqrt{\chi T}$, so we can rescale the variables $z' = \frac{z}{\sqrt{\chi T}}$ and $h' = \frac{h}{\sqrt{\chi T}}$ and define

$$f(q_M, h) = \log \int_{-\infty}^{\infty} \frac{dz'}{\sqrt{2\pi}} e^{-\frac{1}{2}\left[(h'-z')^2 + \chi z'^2 \theta(-z')\right]} := \mathcal{F}\left(\frac{h}{\sqrt{\chi T}}\right), \qquad h \sim \sqrt{\chi T} \tag{2.133}$$

Wrapping everything up, we have

$$f(q_M \to 1, h) = \begin{cases} 0 & h >> \sqrt{\chi T} \\ \mathcal{F}\left(\frac{h}{\sqrt{\chi T}}\right) & |h| \sim \sqrt{\chi T} \\ -\beta \frac{h^2}{2(1+\chi)} & h << -\sqrt{\chi T} \end{cases} \tag{2.134}$$

The replica symmetric saddle point

We can now easily solve the saddle point equation (2.45) that fixes the value of q_M:

$$\frac{q_M}{(1-q_M)^2} = \alpha \int \frac{dh}{\sqrt{2\pi q_M}} e^{-\frac{h^2}{2q_M}} \left[f'(q_M, h)\right]^2 \tag{2.135}$$

In the limit $T \to 0$, $q_M \simeq 1 - \chi T$, it becomes

$$\frac{1}{\chi^2} = \frac{\alpha}{(1+\chi)^2} \int_{-\infty}^{\sigma} \frac{dh}{\sqrt{2\pi}} e^{-\frac{h^2}{2}} (h-\sigma)^2 \tag{2.136}$$

We see that the equation fixes the value of the susceptibility χ, since q_M is required to take the value 1. The last equation can be rewritten using the relation (2.49) for the transition line $\alpha_J(\sigma) = \left[\int_{-\infty}^{\sigma} \frac{dh}{\sqrt{2\pi}} e^{-\frac{h^2}{2}} (h-\sigma)^2\right]^{-1}$:

$$\left(1 + \frac{1}{\chi}\right)^2 = \frac{\alpha}{\alpha_J(\sigma)} \tag{2.137}$$

Energy

In the limit $T \to 0$, the ground state energy is simply given by

$$e_{RS} = \lim_{T\to 0} \mathrm{f}_{RS}(q_M \to 1) = -\frac{1}{2\chi} + \frac{\alpha}{2(1+\chi)} \int_{-\infty}^{\sigma} \frac{dh}{\sqrt{2\pi}} e^{-\frac{h^2}{2}} (h-\sigma)^2 \tag{2.138}$$

Using again the expression for $\alpha_J(\sigma)$ and the saddle point condition (2.137), it reads

$$e_{RS} = \frac{1}{2\chi^2} = \frac{1}{2}\left(\sqrt{\frac{\alpha}{\alpha_J(\sigma)}} - 1\right)^2 \tag{2.139}$$

Stability of the RS solution in the UNSAT phase

To check in which parts of the phase diagram the RS solution is stable, we have to compute the *replicon* eigenvalue defined in equation (2.53) and check when it is positive. We can write the equation for the *dAT line* in the UNSAT phase as

$$\frac{1}{(1-q_M)^2} = \alpha \int_{-\infty}^{\infty} dh \gamma_{q_M} f''(q_M, h)^2 \tag{2.140}$$

Using the asymptotic limit $T \to 0$, $q_M \to 1$, it becomes

$$\frac{1}{\chi^2} = \frac{\alpha}{(1+\chi)^2} \int_{-\infty}^{\sigma} \frac{dh}{\sqrt{2\pi}} e^{-\frac{h^2}{2}} \tag{2.141}$$

Substituting the saddle point condition (2.137):

$$1 = \alpha_J(\sigma) \int_{-\infty}^{\sigma} \frac{dh}{\sqrt{2\pi}} e^{-\frac{h^2}{2}} \tag{2.142}$$

This equation is solved only for $\sigma = 0$. Therefore, we have obtained that also in the UNSAT phase the RS solution is stable for $\sigma > 0$ and in the region $\sigma < 0$ we need to break the replica symmetry.
While in the SAT phase this condition is easy to understand due to convexity arguments, in the UNSAT phase this condition is less obvious as it will become clear in chapter 3 when discussing the linear perceptron.

Jamming limit

Going towards the transition line from the UNSAT phase for $\sigma > 0$, it is possible to study the (non-critical) jamming transition. Since, for $T \simeq 0$, in the SAT phase we have $q_M < 1$ and in the UNSAT phase $q_M \simeq 1 - \chi T$, the matching between the two conditions is made asking that

$$\text{jamming line: } \chi \to \infty \tag{2.143}$$

In fact, the saddle point equation (2.137) gives $\alpha \to \alpha_J(\sigma)$ for $\chi \to \infty$.
Expanding for $\chi \to \infty$ and $\alpha = \alpha_J(\sigma) + \delta\alpha$, the following scaling relationships are obtained:

$$\begin{aligned} \frac{1}{\chi} &\simeq \delta\alpha \\ e_{RS} &\simeq \delta\alpha^2 \end{aligned} \tag{2.144}$$

Equivalently, expanding for $\sigma = \sigma_J + \delta\sigma$, we can approximate the integral as

$$\int_{-\infty}^{\sigma} \frac{dh}{\sqrt{2\pi}} e^{-\frac{h^2}{2}} (h-\sigma)^2 \simeq \int_{-\infty}^{\sigma_J} \frac{dh}{\sqrt{2\pi}} e^{-\frac{h^2}{2}} (h-\sigma_J)^2 + \left[\sqrt{\frac{2}{\pi}} e^{-\frac{\sigma_J^2}{2}} + \sigma_J \left(1 + \text{erf}(\frac{\sigma_J}{\sqrt{2}}) \right) \right] \delta\sigma \tag{2.145}$$

and get:

$$\begin{aligned} \frac{1}{\chi} &\simeq c_J \ \delta\sigma \\ e_{RS} &\simeq \frac{c_J^2}{2} \ \delta\sigma^2 \end{aligned} \tag{2.146}$$

where we have defined $c_J = \frac{e^{-\sigma_J^2/2}}{\sqrt{2\pi}} + \frac{\sigma_J}{2} \left(1 + \text{erf}(\frac{\sigma_J}{\sqrt{2}}) \right)$.

Looking at the gap distribution $\rho(h)$ (derived from eq. (2.79)), in the limit $\chi \to \infty$ it is obtained that the number of zero gaps is still extensive but less than N:

$$c = \alpha \int_{-\infty}^{0} dh \rho(h) \underset{\chi \to \infty}{\to} \alpha_J(\sigma) \Theta \left(\frac{\sigma}{\sqrt{2}} \right) < 1 \tag{2.147}$$

where c stands for the *isostaticity index*. Therefore, the jamming in the RS phase, i.e. when $\sigma > 0$, is not isostatic: it is actually *hypostatic* and non-critical. It is in fact a stable line, and not a marginally stable one.
The crossing point between the RS jamming and the RSB critical jamming transition is for $\sigma = 0$. In fact, the isostaticity index in eq. (2.147) becomes 1 for $\sigma = 0$, that is also where the dAT line starts, signaling the transition to a glassy phase.

2.4.2 The UNSAT RSB phase

In the UNSAT $full$RSB phase, it is necessary to solve the partial differential equations (2.84) to get the physical quantities. However, in the limit $T \to 0$ it is possible to find a scaling solution inside the UNSAT phase, and then studying the matching with the scaling solution studied in section 2.3.4 when moving towards the jamming line. The details of

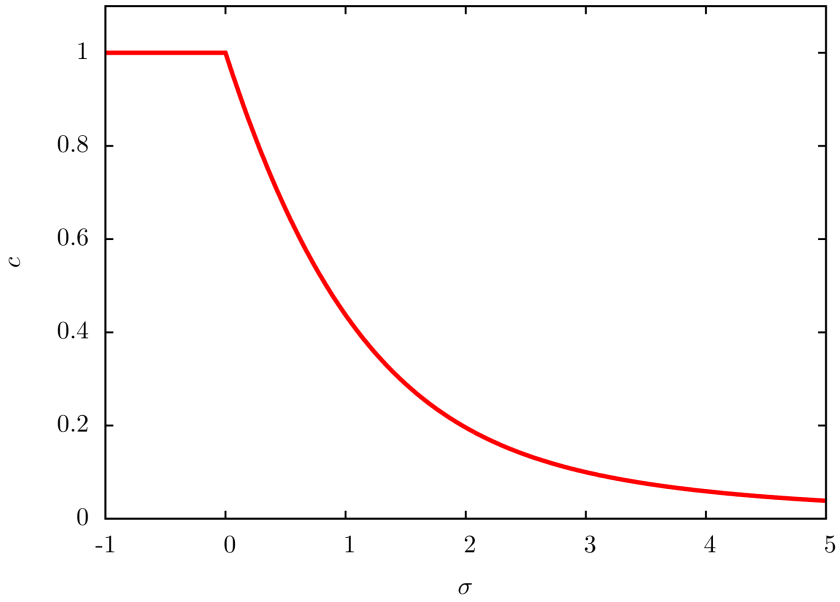

Figure 2.4: Behavior of the isostaticity index c along the jamming line. The jamming is isostatic and critical for $\sigma < 0$ and is hypostatic and non-critical for $\sigma > 0$.

this computation are not discussed here and the interested reader can find them in Ref. [105].
The same reference discusses also another feature of the phase diagram: for σ negative enough, that is for $\sigma < \sigma_{RFOT}$, the system gets into a discontinuous 1RSB solution, which is analogous of the random first order transition of glasses. The details of this discussion are found in [105].

2.4.3 Hessian spectrum of the harmonic perceptron

The perceptron is very well suited for the analytical study of the vibrational spectrum. In [106], the analysis is made for the harmonic perceptron in the UNSAT phase, showing it reproduces the non-Debye scaling observed in soft-spheres near the jamming transition [80, 56]. The Hessian of the harmonic perceptron reads

$$\frac{\partial^2 H}{\partial X_i \partial X_j} = \frac{1}{N}\sum_{\mu=1}^{M} \xi_{\mu,i}\xi_{\mu,i}\theta(-h_\mu) + \eta\,\delta_{ij} \tag{2.148}$$

where η is the Lagrange multiplier associated to the spherical constraint $|\,\mathbf{X}\,|^2 = N$. The Hessian is therefore a Wishart random matrix [244] with quality factor $\frac{1}{o}$, where $o = \frac{\sum_{\mu=1}^{M}\theta(-h_\mu)}{N}$, plus a constant shift η on the diagonal. Therefore the eigenvalue spectrum follows the modified Marchenko-Pastur law [169]

$$\rho(\lambda) = \begin{cases} (1-o)\delta(\lambda-\eta) + \frac{1}{2\pi}\frac{\sqrt{(\lambda-\lambda_-)(\lambda_+-\lambda)}}{\lambda-\eta} & o < 1 \\ \frac{1}{2\pi}\frac{\sqrt{(\lambda-\lambda_-)(\lambda_+-\lambda)}}{\lambda-\eta} & o > 1 \end{cases} \tag{2.149}$$
$$\lambda_\pm = (\sqrt{o} \pm 1)^2 + \eta$$

Three regimes can be distinguished:

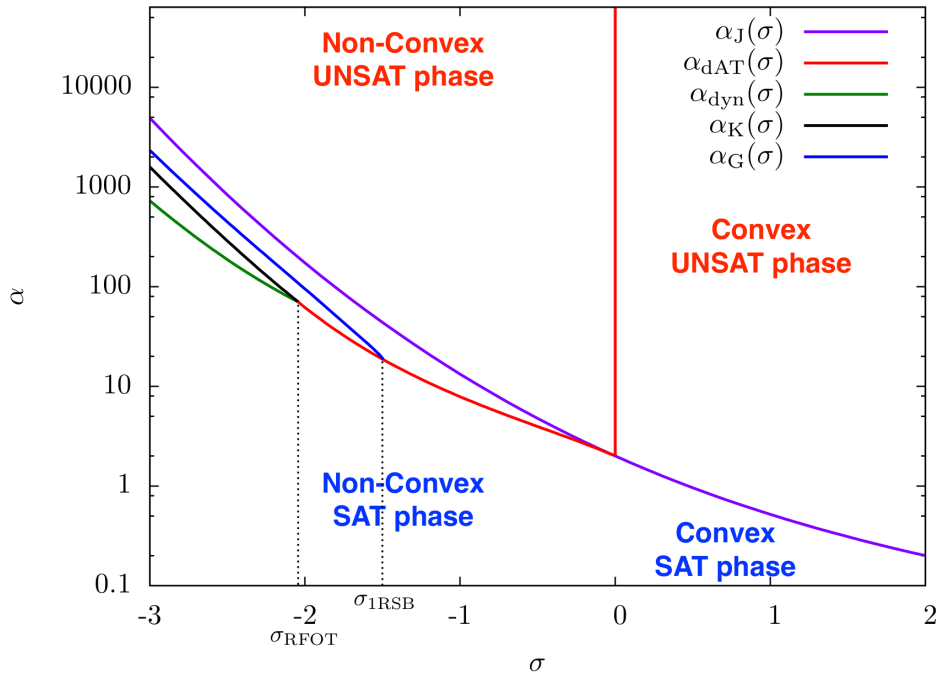

Figure 2.5: The phase diagram of the harmonic perceptron, reprinted from [105].

- in the RS phase $\lambda_- > 0$ and the spectrum is gapped;
- in the RSB phase $\lambda_- = 0$ and the spectrum is gapless, with a pseudogap $\rho(\lambda) \sim \sqrt{\lambda}$ for $\lambda \to 0$;
- in the RSB phase near the jamming transition, the spectrum develops a divergence $\rho(\lambda) \sim \frac{1}{\sqrt{\lambda}}$ for $\lambda \to 0$ because $\eta \to 0^-$.

In frequency terms, $\omega = \sqrt{\lambda}$, the density of states $D(\omega)$ in the fullRSB phase repro-

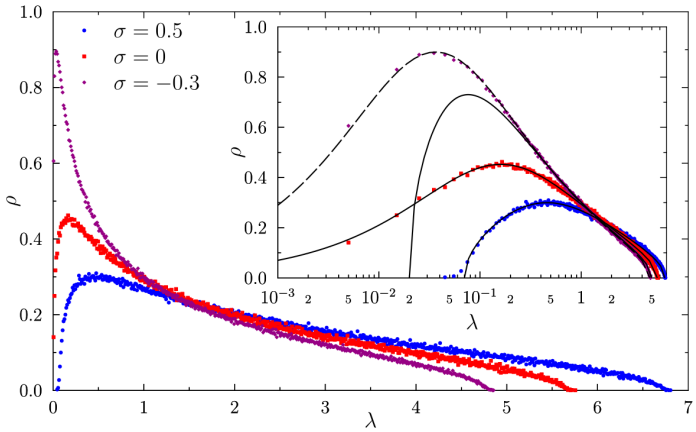

Figure 2.6: Reprinted from [106]. Spectrum of the Hessian obtained for $\alpha = 4$ and $\sigma = -0.3, 0, 0.5$, with $N = 1600$.

duces the boson peak observed in soft spheres models near jamming [80, 56]:

$$D(\omega) = \frac{1}{\pi}\frac{\omega^2\sqrt{\omega_{max}-\omega^2}}{\omega^2+\omega_*^2} \sim \begin{cases} \omega^2 & \omega << \omega_* \\ \text{constant} & \omega_* < \omega < \omega_{max} \end{cases} \tag{2.150}$$

with $\omega_* = \sqrt{|\,\eta\,|} \to 0$ at jamming.
Studying the Hessian in the SAT phase is less straightforward since the minima of the systems are found in clusters of zero energy configurations. This is true also when approaching the jamming point in hard spheres system, where a jammed-UNSAT phase is not defined. A possible approach is using an effective potential derived from the TAP free energy [7, 5, 6].

Chapter 3

The spherical perceptron with linear cost function

A short version of the results of this chapter is published in [108].

In this chapter we study the UNSAT phase of the perceptron with linear cost function, that means substituting the potential $\nu(h_\mu)$ of chapter 2 with $\nu(h_\mu) = |h_\mu|\theta(-h_\mu)$, so that the Hamiltonian reads

$$H(\mathbf{X}) = \sum_\mu |h_\mu|\theta(-h_\mu) \tag{3.1}$$

The most important feature of this potential $\nu(h) = |h|\theta(-h)$ is that its derivative $\nu'(h) = -\theta(-h)$ is piecewise constant with a discontinuity in the origin, therefore the Hamiltonian (3.1) is non-differentiable. Moreover, the second derivative is a Dirac delta $\nu''(h) = \delta(h)$ which makes the Hessian a singular quantity. We will see that this singularity in $h = 0$ has striking physical consequences.

The first studies of this model were made in the paper *Perceptrons above saturation* [164] by P. Majer, A. Engel and A. Zippelius in 1993 where they focus on the UNSAT phase of the perceptron in three different cases, namely with the potentials

- $\nu(h) = \theta(-h)$, that is the Gardner-Derrida case [111];
- $\nu(h) = |h|\theta(-h)$, the linear case which they simply call *Perceptron cost function*;
- $\nu(h) = h^2\theta(-h)$, the harmonic case called *Adatron cost function.*

It is very interesting to note fig. (3.2) reprinted from [164]: the authors studied the linear cost-function and obtained that the distribution $\rho(h)$ of gaps h_μ (*stabilities* in their language) has a Dirac delta for $h = 0$. They also studied the model beyond the dAT instability line, where the RS solution is unstable, using a 1RSB approximation: they obtained a smaller weight of the Dirac delta and a modification of $\rho(h)$ in the neighborhood of $h = 0$. We will show in this chapter that the correct procedure to study the linear cost-function beyond the stability line is to use a $full$RSB scheme, that gives a weight of the Dirac delta equal to $\frac{1}{\alpha}$ (i.e. 0.25 in the case of fig. 3.2), where α is the number of patterns divided by N, and a divergence of the distribution in its neighborhood as $\rho(h) \sim |h|^{-\gamma}$ for $h \to 0$.

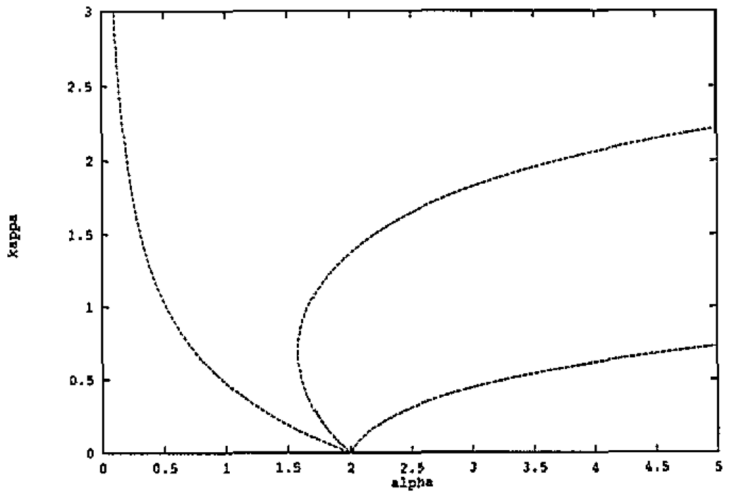

Figure 1. Storage capacity and AT lines. The leftmost line is the critical line of storage capacity. Next, to the right, is the line of local instability of the RS ansatz for the Gardner–Derrida cost function; the rightmost line is that for the Perceptron cost function. The line of instability for the Adatron cost function is the $\kappa = 0$ axis.

Figure 3.1: Reprinted from [164]: in their notation, *kappa* corresponds to σ in our model and *alpha* to our α. The leftmost line corresponds to our jamming line for $\sigma > 0$. The stability lines for the three cost functions they study are reported: the ones for the linear (*Perceptron*) case and for the quadratic (*Adatron*) case are correct, while the stability line of the Gardner-Derrida cost-function is wrong and it should instead coincide with the capacity line (see ref. [41] for a discussion about this instability).

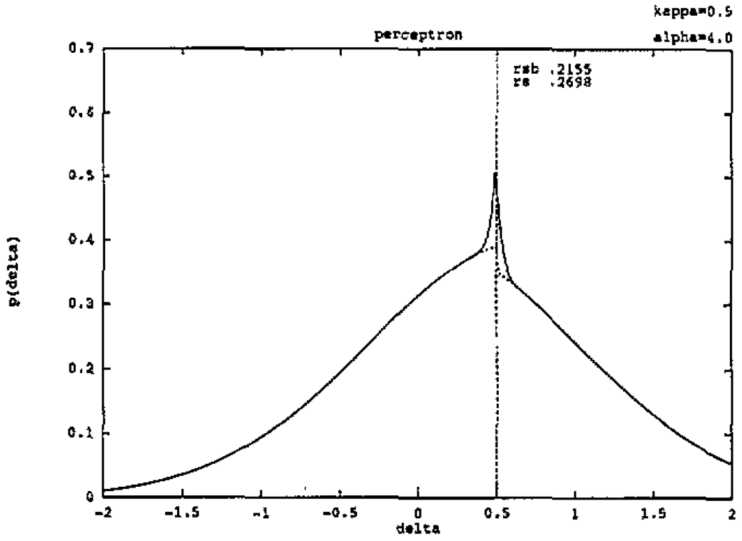

Figure 7. Distribution of stabilities for the perceptron cost function at $\alpha = 4$ and $\kappa = 0.5$. The RSB curve is shown by the full line, and the RS curve is dotted. The δ-peak has weights 0.270 and 0.215 in RS and RSB, respectively.

Figure 3.2: Reprinted from [164]: distribution of the quantities $h_\mu + \sigma = \frac{1}{\sqrt{N}} \mathbf{X} \cdot \boldsymbol{\xi}_\mu$ (*delta* or *stabilities* in their notation) for the linear cost-function. They notice that the distribution has a Dirac delta in $h = 0$. Beyond the dAT stability line, the RS solution is unstable and they use the 1RSB approximation: it decreases the weight of the Dirac delta w.r.t. the RS case and it increases the values of the distribution around it.

3.1 Numerical simulations

We start the study of the linear cost-function by performing numerical simulations.
We run a gradient descent algorithm starting from a random initialization, which corresponds to a zero temperature quench from an infinite temperature configuration. If the landscape of the function to minimize is convex, then we obtain the unique minimum of the function, that corresponds to the ground state of our system; otherwise, if the landscape is glassy, a more thorough discussion about the accessible configurations is needed. We keep this fundamental discussion for a later section when we compare the results of the minimization with the computations describing the ground state.

For fixed values of α and σ, we want to minimize the function

$$H(\mathbf{X}) = \sum_{\mu} \left(\sigma - \frac{1}{\sqrt{N}} \mathbf{X} \cdot \boldsymbol{\xi}_{\mu} \right) \theta \left(-h_{\mu} \right) \tag{3.2}$$

with the spherical constraint $|\,\mathbf{X}\,|^2 = N$. Let's notice that the gradient of this function is discontinuous for every $h_\mu = 0$:

$$\nabla_i H(\mathbf{X}) = \frac{\partial}{\partial X_i} H(\mathbf{X}) = -\frac{1}{\sqrt{N}} \sum_{\mu} \xi_{\mu,i} \theta \left(-h_{\mu} \right) \tag{3.3}$$

The gradient of $H(\mathbf{X})$ is therefore the sum of all the UNSAT patterns at the given $\mathbf{X}$. We see that the condition of stationary point

$$\nabla H(\mathbf{X}) = 0 \tag{3.4}$$

with the gradient defined in eq. (3.3) is not a good condition to define a minimum of the function. To address this issue we propose to regularize the function $H(\mathbf{X})$ so that it becomes differentiable (i.e. its derivative becomes continuous).

3.1.1 The smoothed potential

Regularization of the linear potential in $h = 0$

To regularize $H(\mathbf{X})$ we introduce a smoothed linear potential $\nu_\epsilon(h)$ depending on a smoothing parameter ϵ, defined as

$$\nu_\epsilon(h) = |h| \theta \left(-h - \frac{\epsilon}{2} \right) + \frac{1}{2\epsilon} \left(h - \frac{\epsilon}{2} \right)^2 \mathbb{I} \left(-\frac{\epsilon}{2} < h < \frac{\epsilon}{2} \right) \tag{3.5}$$

where $\mathbb{I}$ is the indicator function

$$\mathbb{I}(a) = \begin{cases} 1 & \text{if } a \text{ is true} \\ 0 & \text{if } a \text{ is false} \end{cases} \tag{3.6}$$

This smoothed potential has a continuous derivative:

$$\nu'_\epsilon(h) = -1 \theta \left(-h - \frac{\epsilon}{2} \right) + \frac{h - \frac{\epsilon}{2}}{\epsilon} \mathbb{I} \left(-\frac{\epsilon}{2} < h < \frac{\epsilon}{2} \right) \tag{3.7}$$

and has a discontinuous second derivative

$$\nu_\epsilon''(h) = \frac{1}{\epsilon}\mathbb{I}\left(-\frac{\epsilon}{2} < h < \frac{\epsilon}{2}\right) \tag{3.8}$$

It is clear that in the limit $\epsilon \to 0$ this smoothed potential becomes the linear potential we want to study:

$$\lim_{\epsilon\to 0}\nu_\epsilon(h) = \nu(h) = |h|\theta(-h) \tag{3.9}$$

We can now use the smoothed Hamiltonian

$$H_\epsilon(\mathbf{X}) = \sum_\mu \nu_\epsilon(h_\mu) = \sum_\mu |h_\mu|\theta\left(-h_\mu - \frac{\epsilon}{2}\right) + \frac{1}{2\epsilon}\left(h_\mu - \frac{\epsilon}{2}\right)^2 \mathbb{I}\left(-\frac{\epsilon}{2} < h_\mu < \frac{\epsilon}{2}\right) \tag{3.10}$$

It is interesting to notice that when a gap h_μ has value in the interval $(-\frac{\epsilon}{2}, \frac{\epsilon}{2})$, then its energy contribution is only of order ϵ since

$$\frac{1}{2\epsilon}\left(h_\mu - \frac{\epsilon}{2}\right)^2 \sim \frac{O(\epsilon^2)}{2\epsilon} \sim O(\epsilon) \tag{3.11}$$

while its contribution to the gradient is of order 1, since

$$\frac{1}{\epsilon}\left(h_\mu - \frac{\epsilon}{2}\right) \in (-1, 0) \tag{3.12}$$

The quantity of equation (3.12) turns out to be particularly important for the stability of the system and has a precise physical meaning that will be explained in the following. For ease of notation, let's define the set $\mathcal{O}$ of all the patterns μ so that $h_\mu \leq -\frac{\epsilon}{2}$ and the set $\mathcal{C}$ of all the patterns μ whose gap is inside the ϵ-window around 0, i.e.

$$\begin{aligned} \mathcal{O} &= \left\{\mu \ : \ h_\mu \leq -\frac{\epsilon}{2}\right\} \\ \mathcal{C} &= \left\{\mu \ : \ -\frac{\epsilon}{2} < h_\mu < \frac{\epsilon}{2}\right\} \end{aligned} \tag{3.13}$$

Now we can write the smoothed Hamiltonian and its gradient as

$$H_\epsilon(\mathbf{X}) = \sum_{o\in\mathcal{O}} |h_o| + \sum_{c\in\mathcal{C}} \frac{1}{2\epsilon}\left(h_c - \frac{\epsilon}{2}\right)^2 \tag{3.14}$$

and

$$\nabla H_\epsilon(\mathbf{X}) = -\frac{1}{\sqrt{N}}\sum_{o\in\mathcal{O}} \boldsymbol{\xi}_o - \frac{1}{\sqrt{N}}\sum_{c\in\mathcal{C}} \boldsymbol{\xi}_c \frac{\frac{\epsilon}{2} - h_c}{\epsilon} \tag{3.15}$$

Based on the observations made in equations (3.11-3.12), we can argue that

$$\lim_{\epsilon\to 0} H_\epsilon(\mathbf{X}) = H(\mathbf{X}) \tag{3.16}$$

but

$$\lim_{\epsilon\to 0} \nabla H_\epsilon(\mathbf{X}) \neq \nabla H(\mathbf{X}) \tag{3.17}$$

if the number of patterns in the set $\mathcal{C}$ does not go to 0 for vanishing ϵ.

Enforcing the spherical constraint $|\mathbf{X}|^2 = N$

Before describing the minimization algorithm, let's add the spherical constraint on $\mathbf{X}$ to the function to be minimized (3.14). It can be done simply by adding a term

$$\frac{\zeta}{4}\left(\sum_{i=1}^{N} X_i^2 - N\right)^2 \tag{3.18}$$

with the constant ζ chosen to be large (it needs to be tuned numerically). We notice also that

$$\lim_{\zeta\to\infty} \zeta\left(\sum_{i=1}^{N} X_i^2 - N\right) = \eta \tag{3.19}$$

with η being the Lagrange multiplier associated to the spherical constraint: this quantity is very important since it turns out to control the convexity of the function we are minimizing.
Putting everything together, we look for minima of the function

$$\mathcal{L}_\epsilon(\mathbf{X}) = \sum_{o\in\mathcal{O}} |h_o| + \sum_{c\in\mathcal{C}} \frac{1}{2\epsilon}\left(h_c - \frac{\epsilon}{2}\right)^2 + \frac{\zeta}{4}\left(\sum_{i=1}^{N} X_i^2 - N\right)^2 \tag{3.20}$$

whose gradient reads

$$\nabla\,\mathcal{L}_\epsilon(\mathbf{X}) = -\frac{1}{\sqrt{N}}\sum_{o\in\mathcal{O}} \boldsymbol{\xi}_o - \frac{1}{\sqrt{N}}\sum_{c\in\mathcal{C}} \boldsymbol{\xi}_c\,\frac{\frac{\epsilon}{2} - h_c}{\epsilon} + \zeta\left(\sum_{i=1}^{N} X_i^2 - N\right)\mathbf{X} \tag{3.21}$$

3.1.2 The minimization algorithm

We minimize (3.20) by **annealing the regularization parameter** ϵ.
When ϵ is bigger than the typical smallest non-zero gaps $|h_\mu|$, the landscape is smoothened by the quadratic contribution. When ϵ is smaller than the smallest non-zero gap, then the function (3.20) is equivalent to its original non-regularized counterpart. Therefore, we start with a large regularization ϵ_1 (we choose $\epsilon_1 \sim 10^{-2}$), perform the gradient-descent minimization, reduce the regularization parameter to ϵ_2 (we choose $\epsilon_i = \epsilon_{i-1}/2$) and perform again the gradient-descent minimization starting from the previously found configuration. We repeat this step n times until the regularization ϵ_n is small (we choose $\epsilon_n \sim 10^{-8}$).

Algorithm 1: Smoothed minimization

$\mathbf{X}^{(0)} \leftarrow$ random point on the $N-$sphere (with $|\mathbf{X}^{(0)}|^2 = N$);
$\epsilon_1 \leftarrow \epsilon_{initial}$;
for *i in* $\{1, ..., n\}$ **do**
  $\mathbf{X}^{(i)} \leftarrow$ minimize $\mathcal{L}_{\epsilon_i}(\mathbf{X})$ starting from $\mathbf{X}^{(i-1)}$;
  $\epsilon_{i+1} \leftarrow \epsilon_i/2$;
end
Result: $\mathbf{X}^* \leftarrow \mathbf{X}^{(n)}$

This minimization procedure is performed for fixed values of the control parameters α and σ.
For the gradient-descent minimization, we actually choose a quasi-Newton method to improve the performance.

Numerical and algorithm details

We explore the following intervals for the parameters in our computer simulations:

- N takes values from 64 to 2048;
- α takes values up to 5;
- σ can vary from -0.6 to 5;
- the constant of the term enforcing the spherical constraint can be chosen as an arbitrary number much bigger than 1; we set it to $\zeta = 500$;
- our starting regularization is $\epsilon_{initial} = 10^{-2}$ and we perform $n = 20$ steps, halving ϵ at each step, to arrive at a final $\epsilon_{final} = \epsilon_{initial}\ 2^{-19} \simeq 1.91 \cdot 10^{-8}$.

The choices of $\epsilon_{initial}$, ϵ_{final} and the ϵ-decreasing rate at each step depend on N and on the minimizer. We have chosen $\epsilon_{initial}$ and the decreasing rate in an empirical manner, based on the fact that they work reasonably well for the values of N we explore and the minimizer we use.
The choice of ϵ_{final} is more important: ideally, we want it to be as small as possible. In particular, the minimum configuration $\mathbf{X}^*$ we want to reach has a gap distribution $\rho(h)$ with minimal non-zero gap h_{min} defined as

$$h_{min} = \min_{\mu:\ |h_\mu|>0} |h_\mu| \tag{3.22}$$

For large N, the value of h_{min} scales according to a power law depending on $\rho(h)$ for $h \sim 0$. With the quite general assumption that

$$\rho(h) \sim |h|^p \text{ for } |h| \to 0, \tag{3.23}$$

the condition $\int_0^{h_{min}} \rho(h) \sim \frac{1}{N}$ gives

$$h_{min} \sim N^{-\frac{1}{1+p}} \tag{3.24}$$

Therefore, our condition on ϵ_{final} is

$$\epsilon_{final} << N^{-\frac{1}{1+p}} \tag{3.25}$$

On the other hand, as previously observed, when a gap in the ϵ-window h_c has a variation δh_c of order $O(\epsilon)$, the corresponding Hamiltonian variation δH_ϵ is of order $O(\epsilon^2)$; for this variation to be detectable, it has to be larger than the machine precision $\varepsilon_{machine}$ (in our computer simulations $\varepsilon_{machine} \sim 10^{-16}$). Therefore, the condition

$$\delta H_\epsilon \geq \varepsilon_{machine} \tag{3.26}$$

gives the bound

$$\epsilon_{final} \geq \sqrt{\varepsilon_{machine}} \sim 10^{-8} \tag{3.27}$$

For this reason, we choose $\epsilon_{final} \sim 10^{-8}$. Let's notice that the condition

$$\sqrt{\varepsilon_{machine}} \leq \epsilon_{final} << N^{-\frac{1}{1+p}} \tag{3.28}$$

gives the limit of usability of the smoothed potential; eventually, for N large enough, we may not be able to use this technique to study the minima of the linear cost-function. Empirically, we do not run into this problem for the linear perceptron model with the values of N we study. In the case of linear spheres, some care is needed, as we discuss in chapter 4.

The quasi-Newton method we use for the gradient-descent-like minimization is the *Limited-memory Broyden–Fletcher–Goldfarb–Shanno algorithm* (L-BFGS) [48]. We use a Fortran implementation of this algorithm [260, 185] available through a Python interface in the library SciPy [240].

3.1.3 Results of the numerical simulations

In this section, we present the numerical results obtained from the algorithm described in the previous section 3.1.2.
To get a glimpse of how the minima of our system look like, we report a plot of the distribution $\rho(h)$ of gaps h_μ for a minimal configuration in the UNSAT phase, let's say $\alpha = 2$, $\sigma = 0.31$.

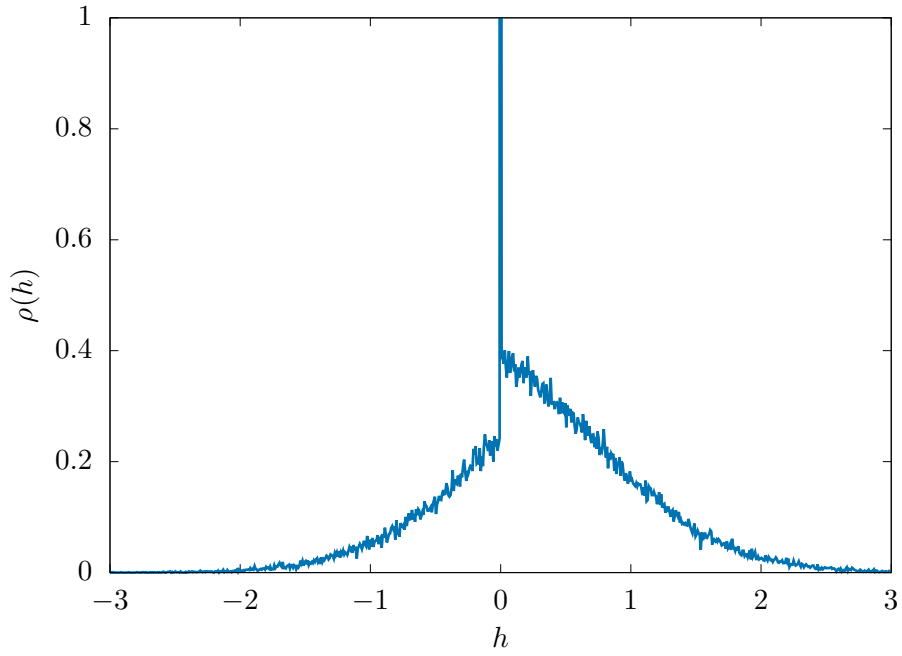

Figure 3.3: gap distribution for $\alpha = 2$, $\sigma = 0.31$, $N = 2048$, averaged over 5 samples.

From figure 3.3, we see a concentration of gaps at the value $h = 0$. This peak in the distribution comes from an extensive number of gaps in the ϵ-window around 0, meaning that the set $\mathcal{C}$ has a number of elements proportional to N. We refer to the gaps in $\mathcal{C}$ as **contacts**, in analogy to sphere models where a couple of touching spheres has zero gap between them. We call

$$C = |\mathcal{C}| = number\ of\ contacts \tag{3.29}$$

In the numerical simulations $h_c \in (-\frac{\epsilon}{2}, \frac{\epsilon}{2})$, so in the limit $\epsilon \to 0$ we get $h_c \to 0$. The value of C converges to an extensive number when decreasing ϵ. In particular, since C is

a discrete quantity, we notice that it reaches its convergence for ϵ smaller than a certain value (dependent on N).

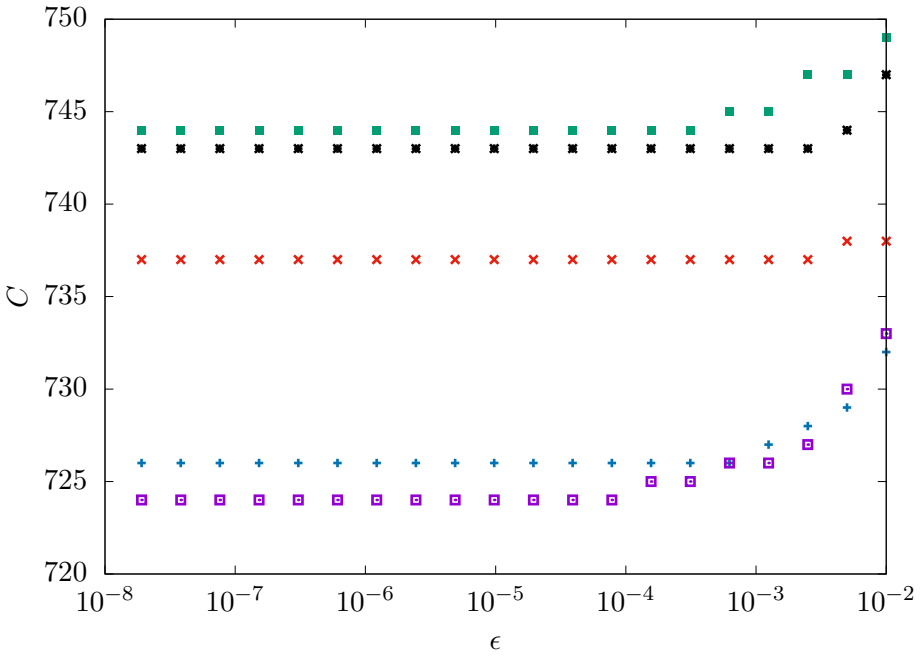

Figure 3.4: Dependence of the number of contacts C with respect to the smoothing parameter ϵ during minimization. Each color represents a different sample with the same parameters $N = 1024$, $\alpha = 1.5$, $\sigma = 0.6$.

We can therefore define an **isostaticity index** c

$$c = \frac{C}{N} \tag{3.30}$$

that measures how many contacts are present in a given configuration.

We make two remarks:

- in the harmonic potential case, discussed in section 2.4, a peak of zero gaps appears only at the satisfiability threshold (the jamming transition), while here it appears also deep inside the UNSAT phase;
- this behavior is in line with the results of [164] as replotted in figure 3.2, where their distribution of stabilities (corresponding to our h_μ) has a Dirac delta.

Why there are *contacts* in the minima of the linear potential

In the harmonic potential case, a peak of zero gaps can appear only at the jamming transition for rigorously zero pressure. This is true for any convex potential of the kind $\nu(h) = |h|^a\theta(-h)$ with $a > 1$. In fact, let's consider such a configuration at jamming and let's say that we want to apply an infinitesimal compression. To destabilize a contact and make it a slightly negative gap, that is changing a gap from $h = 0$ to $h = \delta h < 0$, we need to increase the energy of the system by a quantity $\delta E = |\delta h|^a$. It means we need to provide a work $\delta W = f|\delta h|$ with a force of order $f \sim |\delta h|^{a-1}$, which is an infinitesimal

quantity for $a > 1$.
In the linear case $\nu(h) = F|h|\theta(-h)$, with a slope $F \sim O(1)$, the energy increase $\delta E = F|\delta h|$ and the work $\delta W = f|\delta h|$ requires a force at least bigger than the slope of the linear potential, i.e. $f \geq F$. It means that an infinitesimal compression is not sufficient to destabilize a contact. Indeed, a contact can sustain a compression force whose intensity is in the interval $(0, F)$.
In our model, the slope of the linear energy is $F = 1$ and the contacts are always present in the UNSAT phase, therefore we expect the presence of associated **contact forces**. In fact, they appear quite naturally in the gradient of the smoothed Hamiltonian we have defined: in equation (3.15), it is possible to recognize the terms

$$f_c = \frac{\epsilon/2 - h_c}{\epsilon} \in (0, 1) \tag{3.31}$$

that are exactly the forces associated to the contacts. Making these contact forces explicit in the gradient of the energy and including the term enforcing the spherical constraint $|\,\mathbf{X}\,|^2 = N$, we get

$$\nabla\,\mathcal{L}(\mathbf{X}) = -\frac{1}{\sqrt{N}}\sum_{o\in\mathcal{O}}\boldsymbol{\xi}_o - \frac{1}{\sqrt{N}}\sum_{c\in\mathcal{C}}\boldsymbol{\xi}_c\, f_c + \eta\,\mathbf{X} \tag{3.32}$$

The Lagrange multiplier of the spherical constraint η is very important since the convexity of the energy landscape depends on its sign. Its value is fixed by the condition $\nabla\,\mathcal{L}(\mathbf{X}) = 0$ and is an observable of the system. We discuss further its role in section 3.2.2 looking at the Hessian of the model. For the moment, we simply state that

- for $\eta > 0$ we have a convex phase (described by the replica symmetric ansatz);
- for $\eta < 0$ we have a non-convex phase (described by a replica symmetry breaking ansatz).

In the following we present the numerical results in two different sections of the UNSAT phase. In particular, we report the isostaticity index c, the Lagrange multiplier η, the energy, the number of negative gaps (overlaps), the empirical distributions of gaps $\rho(h)$ and of contact forces $\rho(f)$.

The convex/Replica-symmetric phase

Fixing the value of $\alpha = 1.5$, we study minima of the systems for different values of σ in the UNSAT phase. According to equation (2.49), the satisfiability (jamming) transition for $\alpha = 1.5$ is at $\sigma_J \simeq 0.186$, therefore we consider $\sigma > \sigma_J$. We know that the jamming at $\alpha = 1.5$ is hypostatic, since from equation (2.147)

$$c|_{\sigma_J} \simeq 0.86 < 1 \tag{3.33}$$

At the RS jamming line, the system is convex and has a single minimum. These properties remain valid when entering in the UNSAT phase by increasing σ.

In figure 3.5, we see that the isostaticity index c remains smaller than 1 and is a decreasing function of σ. This means that the number of contacts in the system, that is smaller than N at σ_J, decreases further when increasing σ. The system is therefore **hypostatic**. We also notice that the Lagrange multiplier of the spherical constraint η is

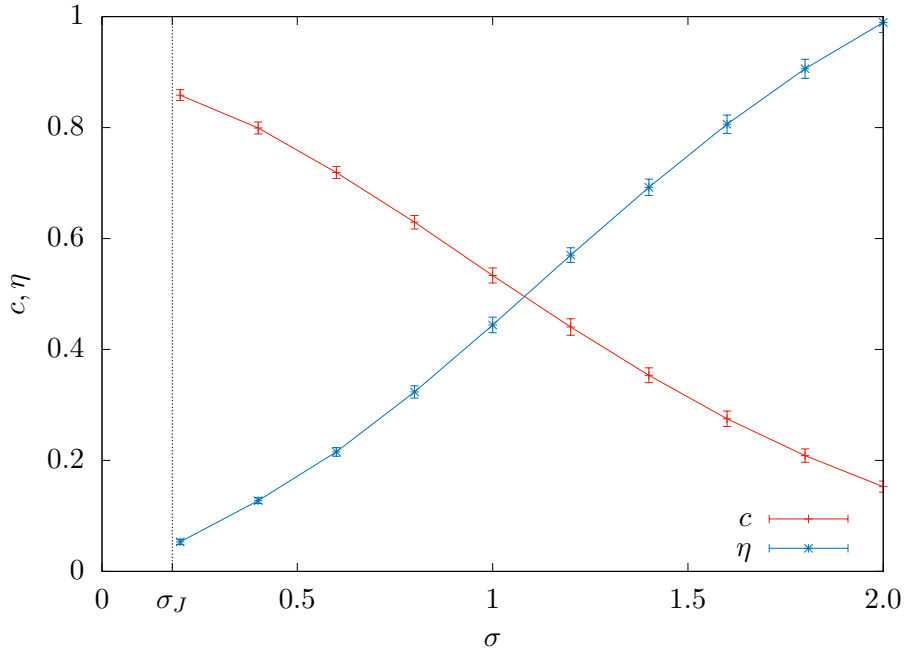

Figure 3.5: Isostaticity index c and Lagrange multiplier of the spherical constraint η for $\alpha = 1.5$ and different values of σ. Values averaged over 69 samples with $N = 2048$. This plot shows that in this region of the phase diagram the system is hypostatic $c < 1$ and that $\eta > 0$ which implies convexity (see section 3.2).

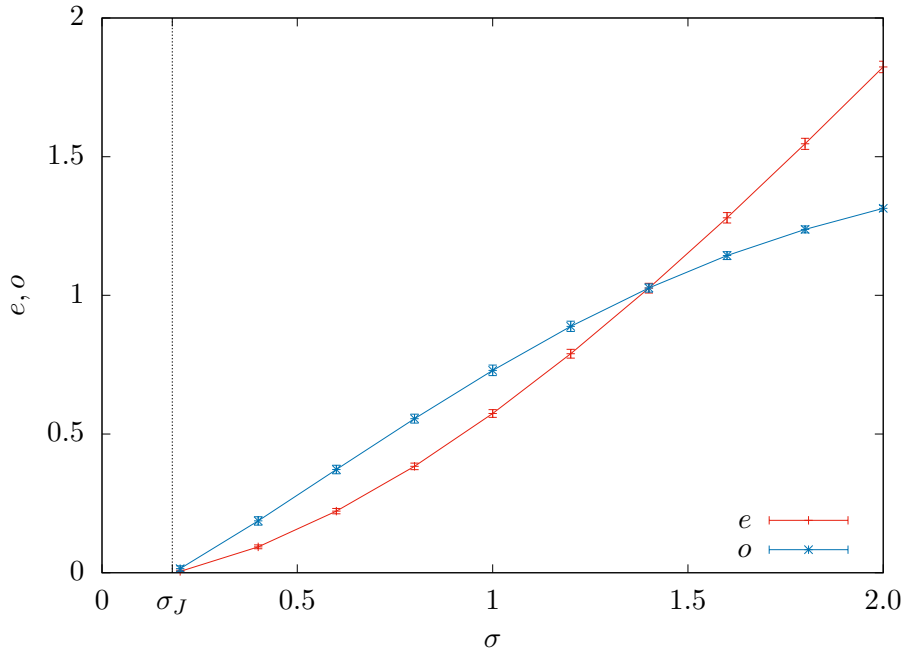

Figure 3.6: Intensive energy $e = H(\mathbf{X}^*)/N$ and number of overlaps O divided by N, $o = O/N$. Values averaged over 69 samples with $N = 2048$. As expected, e and o tend to 0 for σ going to σ_J.

positive and is an increasing function of σ, implying that the model is convex. In this phase, hypostaticity and positive η come together.
In figure 3.6, we see the increase of the energy and of the number of overlaps with respect to σ. As expected, they tend to 0 when approaching the unjamming transition at σ_J. The detailed study of their behavior for $\sigma \to \sigma_J$ is very interesting and it is performed in chapter 5 where we use the pressure as control parameter instead of σ.
In the plots of fig. 3.7-3.10, we report the evolution of the distributions of gaps and contact forces. Going deeper into the UNSAT phase increases the number of negative gaps (overlaps) and pushes the bulk of the distribution of contact forces from 0 towards 1. In section 3.3.1, we show that these distributions in the replica symmetric phase are Gaussian.

Plots of the gap distribution $\rho(h)$ and contact force distribution $\rho(f)$ at $\alpha = 1.5$, $N = 2048$, averaged over 69 samples.

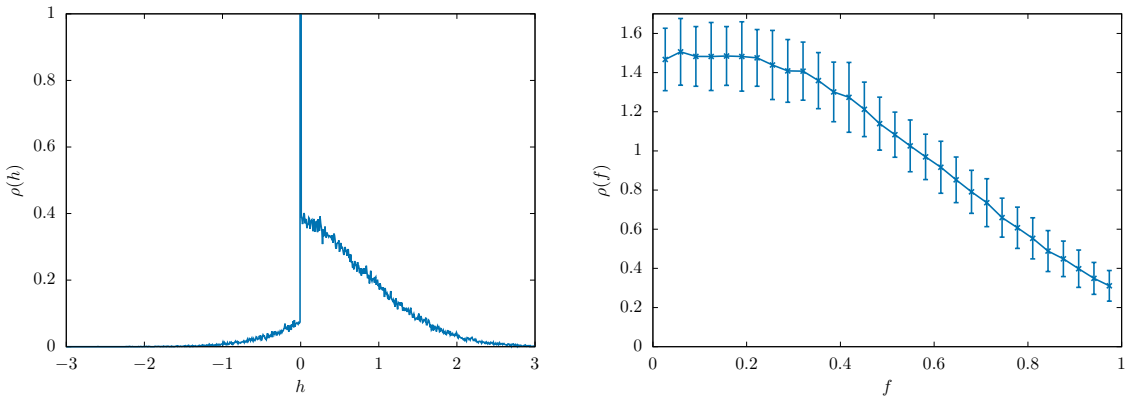

Figure 3.7: $\sigma = 0.25$, energy $e = 0.02$

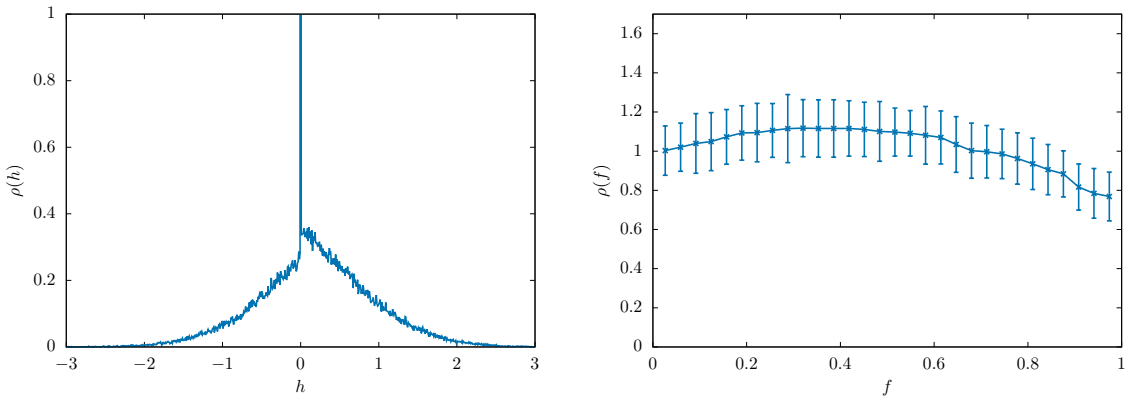

Figure 3.8: $\sigma = 0.5$, energy $e = 0.15$

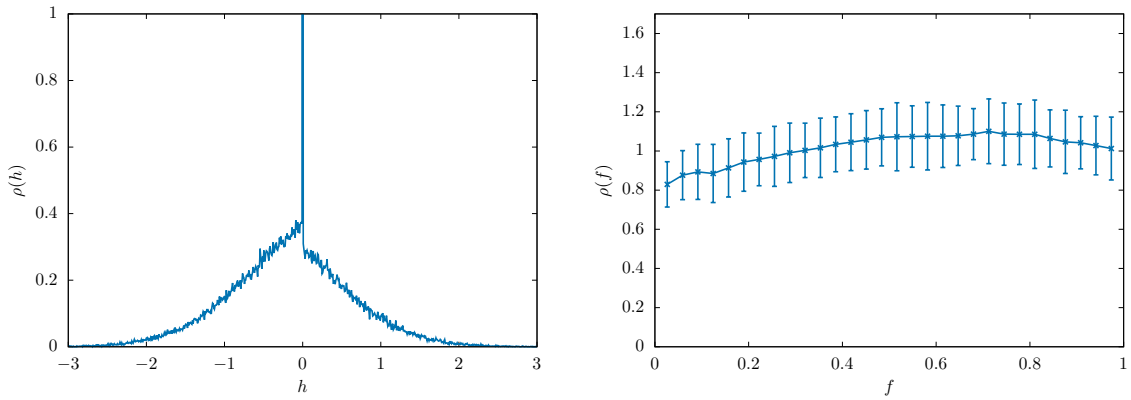

Figure 3.9: $\sigma = 0.75$, energy $e = 0.33$

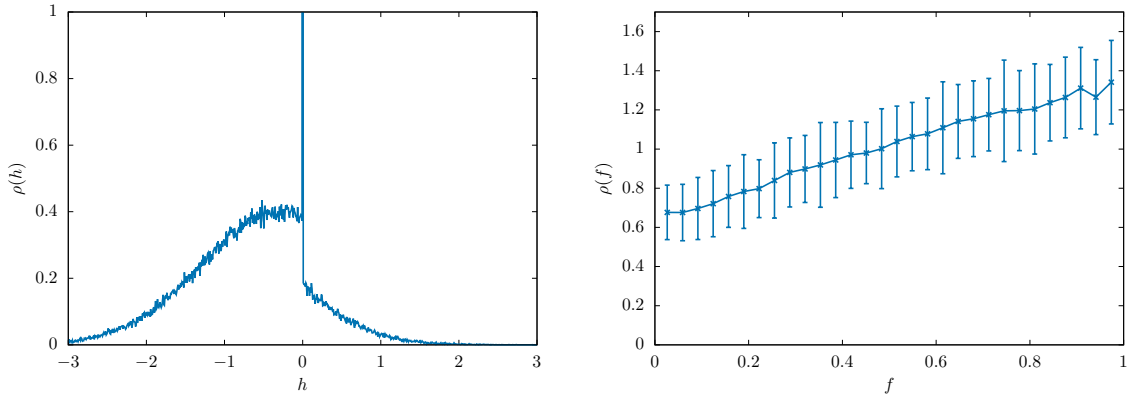

Figure 3.10: $\sigma = 1.25$, energy $e = 0.85$

We complete this data analysis by checking the behavior of the distribution $\rho(h)$ for $h \to 0^+$ and $h \to 0^-$ and of the distribution $\rho(f)$ for $f \to 0^+$ and $f \to 1^-$. From the figs. 3.7-3.10, we expect them to go to constant values. In fact, as shown in fig. 3.11, their respective cumulative distributions have a linear behavior. Therefore, this phase is stable (not just marginally) and there is no critical behavior.

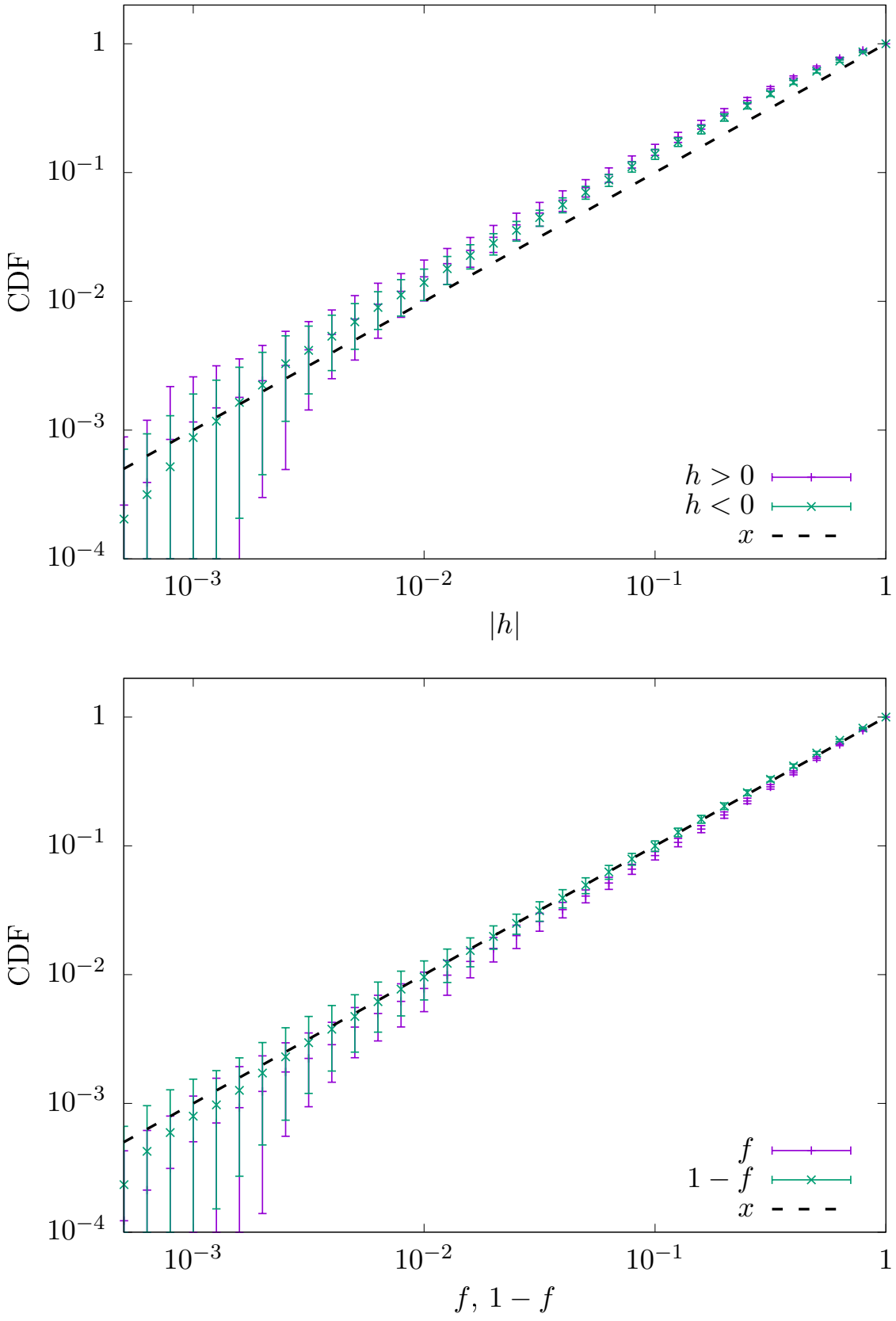

Figure 3.11: *Left panel.* Cumulative distribution functions (CDF) of positive/negative gaps, defined as $\int_0^h \rho(h')dh'$ and $\int_h^0 \rho(h')dh'$ respectively. *Right panel.* Cumulative distribution functions (CDF) of forces f and $1-f$, defined as $\int_0^f \rho(f')df'$ and $\int_{1-f}^1 \rho(f')df'$ respectively.

The non-convex/RSB phase

Fixing the value $\alpha = 4$, we study the minima for different values of σ inside the UNSAT phase. We know that for $\alpha = 4$ the jamming transition occurs at $\sigma_J \simeq -0.4$ (it is possible to use equation (2.49) as an approximation). As discussed in chapter 2, the jamming line for $\sigma < 0$ is a critical line belonging to the universality class of the jamming of spheres. The energy landscape is glassy, with many marginally stable minima, and the system is isostatic at the transition:

$$c|_{\sigma_J} = 1 \tag{3.34}$$

The data we present in this section show that the isostaticity and the criticality do not disappear when the system enters in the UNSAT phase with the linear potential, very differently from other common potentials where the critical behavior is washed out.
Performing the minimization with the smoothed Hamiltonian, we see that the number of contacts C converges to exactly $N - 1$, with basically no fluctuations [1].

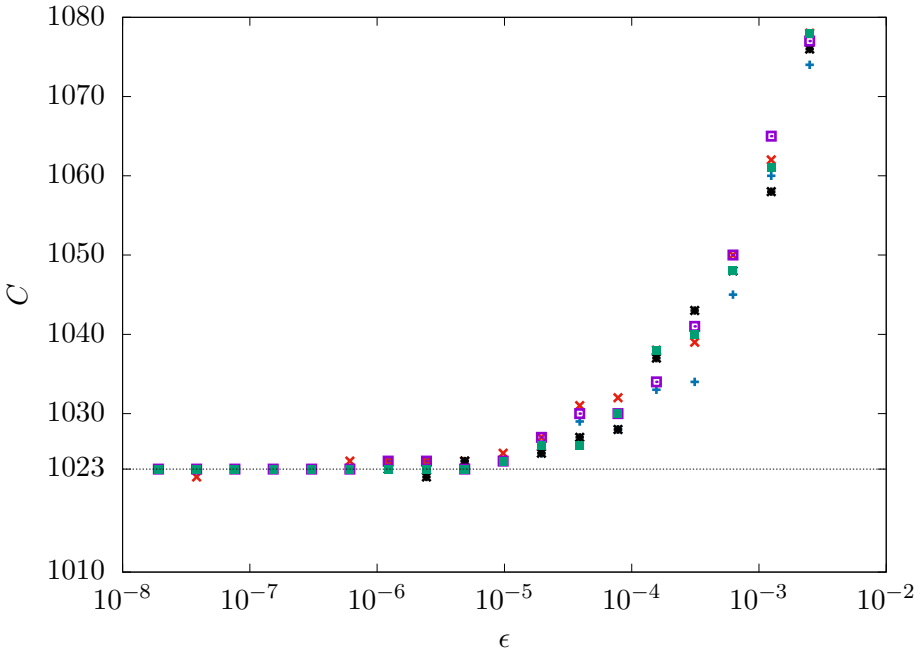

Figure 3.12: Evolution of the number of contacts C with respect to ϵ, for $\alpha = 4$, $\sigma = 0$, $N = 1024$. It shows that C converges to $N - 1 = 1023$. Each color represents a different sample.

The reason why C converges to exactly $N - 1$ is that the number of free degrees of freedom is $N - 1$: one constraint is given by the spherical condition $|\mathbf{X}|^2 = N$. In fact, this constraint provides the Lagrange multiplier η which is basically a reaction force, and together with the contact forces f_c they form a complete set of N forces stabilizing the configuration. Therefore, in a portion of the UNSAT phase the system is **isostatic**.
The reason for isostaticity comes from the fact that in this phase the energy landscape is non-convex. This can be seen from the fact that $\eta < 0$. In figure 3.13, we plot the behavior of c and η at $\alpha = 4$ for increasing σ. We see that the system is isostatic as

[1] Numerically, C can have fluctuations of $O(1)$, but the associated gradient deteriorates abruptly. Equilibrium configurations (i.e. with zero gradient) are found only for $C = N - 1$.

long as η is negative, and finally becomes hypostatic when η becomes positive. We can therefore state that

$$c = 1 \text{ for } \eta < 0 \quad (\textit{non-convexity}) \tag{3.35}$$

The reason why (3.35) is true is that, in a non-convex landscape and a linear potential, the only way to stabilize the configuration is to constrain all the degrees of freedom. This argument will become apparent in section 3.2.2.

In figure 3.14, we report the behavior of the energy and of the number of overlaps. It is surely very interesting to understand the scaling of these quantities at the unjamming transition. We study it in detail in chapter 5. Here we anticipate that the number of overlaps o (usually called Δz in the jamming literature) does not behave according to the universal scaling $o \sim \sqrt{\sigma - \sigma_J}$.

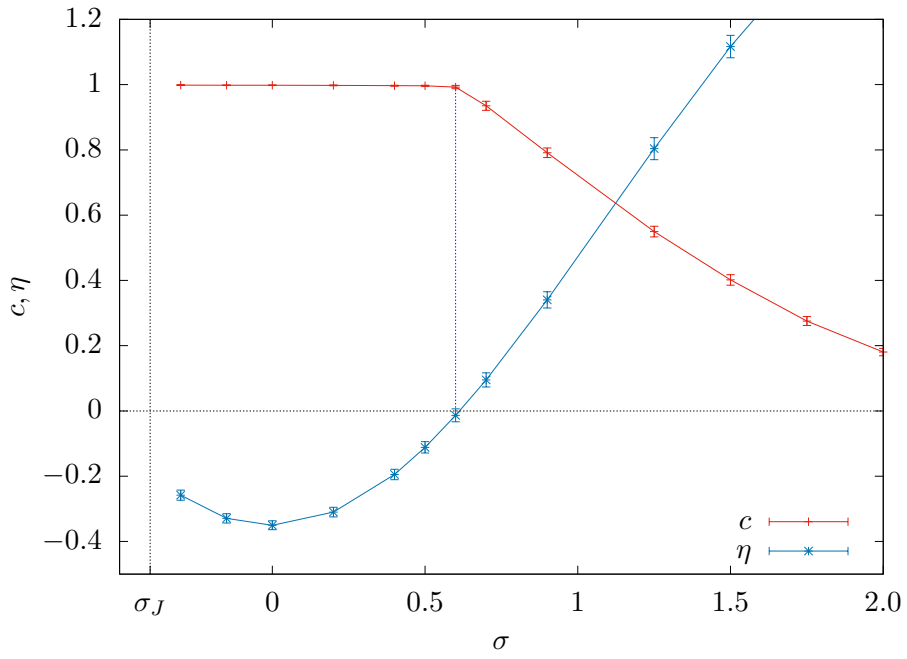

Figure 3.13: Isostaticity index c and Lagrange multiplier of the spherical constraint η at $\alpha = 4$ for increasing σ in the UNSAT phase. It shows the existence of an isostatic phase (with $\eta < 0$) and then the transition to a hypostatic one (with $\eta > 0$). Data for $N = 1024$ averaged over 100 samples.

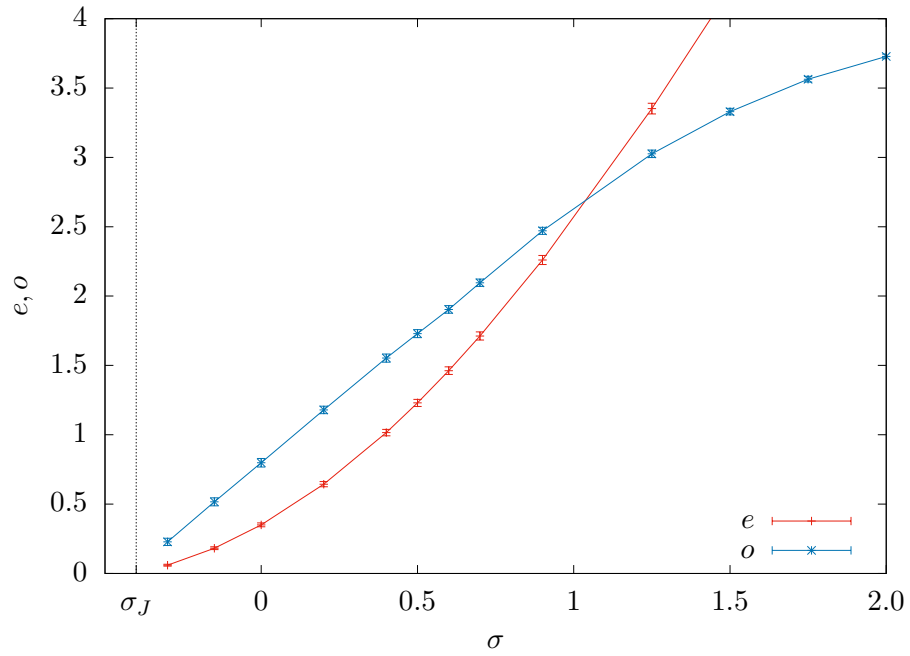

Figure 3.14: Energy e and number of negative gaps (overlaps) o at $\alpha = 4$ for increasing σ. For $\sigma \to \sigma_J$, they tend to 0 with a non-trivial behavior: the energy goes linearly with logarithmic corrections, while the overlaps have a power-law exponent between 0.5 and 1 (discussed in 5). Data for $N = 1024$ averaged over 100 samples.

The connections of this non-convex phase with the critical jamming transition are not limited to isostaticity. Surprisingly, also the critical exponents appear all over the non-convex/UNSAT phase. Even more strikingly, the criticality appears to be richer than what was known. In fact, at the jamming transition a power law divergence of the distribution of small positive gaps $\rho(h) \underset{h\to 0^+}{\sim} h^{-\gamma}$ is observed together with a pseudo-gap in the distribution of small forces $\rho(f) \underset{f\to 0}{\sim} f^{\theta}$, with the two non-trivial exponents $\gamma \simeq 0.41269$ and $\theta \simeq 0.4231$ discussed in section 2.3.4.
In the critical phase of the linear cost-function, not only we observe both this behavior for $h \to 0^+$ and $f \to 0^+$ but also a similar one for $h \to 0^-$ and $f \to 1^-$. In fact, we have

$$\rho(h) \sim |h|^{-\gamma} \quad \text{for } h \to 0^{\pm} \tag{3.36}$$

and

$$\begin{aligned} \rho(f) &\sim f^{\theta} && \text{for } f \to 0^+ \\ \rho(f) &\sim (1-f)^{\theta} && \text{for } f \to 1^- \end{aligned} \tag{3.37}$$

This richer criticality was never observed before. It is due to the fact that in this model there are two kinds of excitations related to a contact $h_c = 0$: making it positive $h_c = \delta h > 0$ or making it negative $h_c = \delta h < 0$. In the same manner, there are two ways of forming a contact: taking a positive gap $h_\mu > 0$ and closing it, or taking a negative gap $h_\mu < 0$ and relaxing it to zero. These four processes are related to the four exponents appearing for positive/negative small gaps and contact forces close to zero/one. The interesting aspect is that these exponents only take the values γ and θ known for the jamming universality. The reason why this holds is connected to marginal stability,

discussed in section 3.4.1. Moreover, their equality appears naturally through a mapping in the scaling solution of the model presented in section 3.4.
In the figures 3.15-3.21 we present the gap and force distributions for $\alpha = 4$ and increasing values of σ. We see that in the isostatic/non-convex phase the gap distribution has a power law divergence for $h \to 0$ from both sides and the contact force distribution has two pseudogaps, one for $f \to 0$ and one for $f \to 1$. For $\sigma > 0.6$ the system enters into the hypostatic phase, where the critical behavior and the corresponding power laws disappear.

Plots of the gap distribution $\rho(h)$ and contact force distribution $\rho(f)$ at $\alpha = 4$, $N = 1024$, averaged over 100.

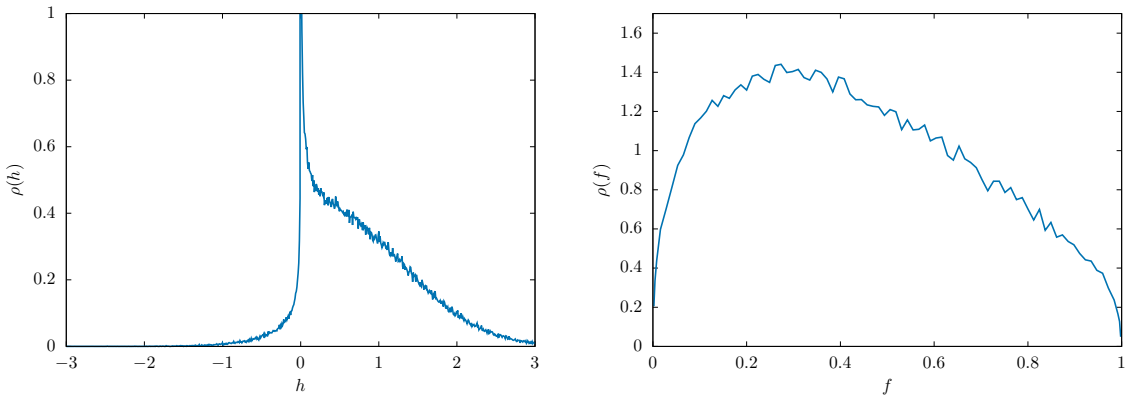

Figure 3.15: $\sigma = -0.3$, energy $e = 0.06$.

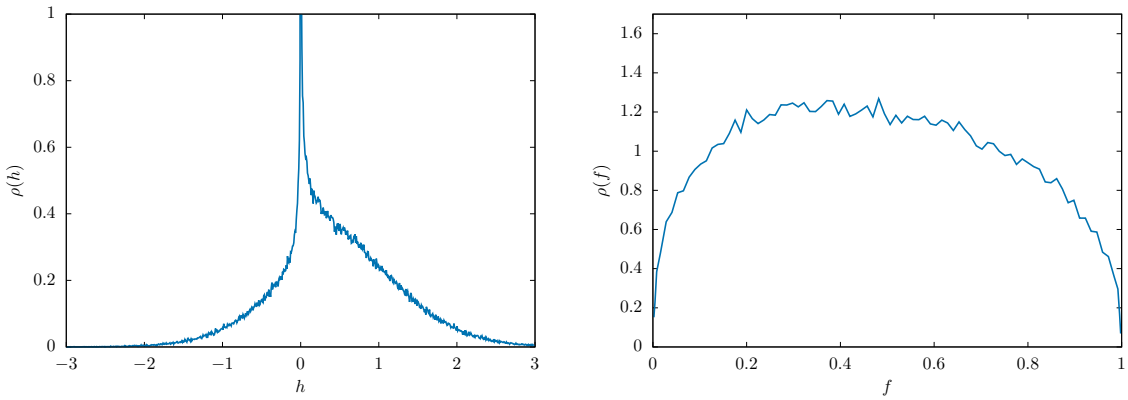

Figure 3.16: $\sigma = 0$, energy $e = 0.35$.

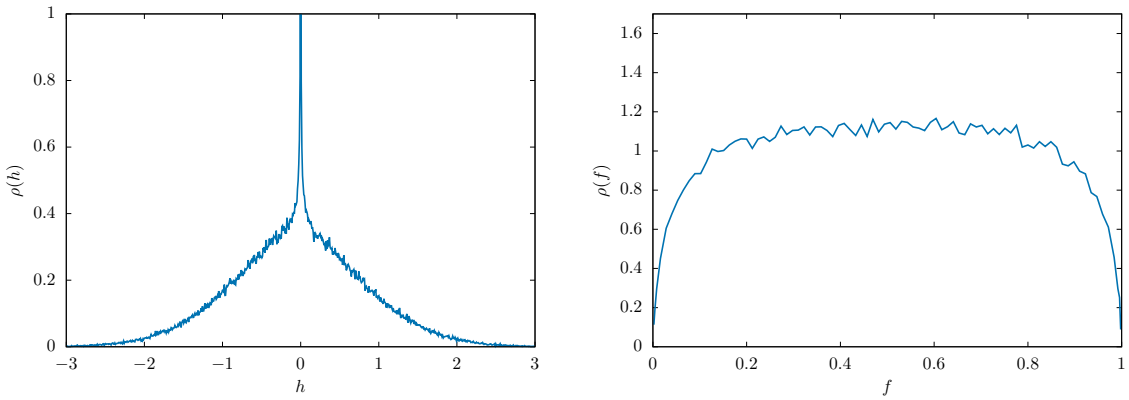

Figure 3.17: $\sigma = 0.4$, energy $e = 1.02$.

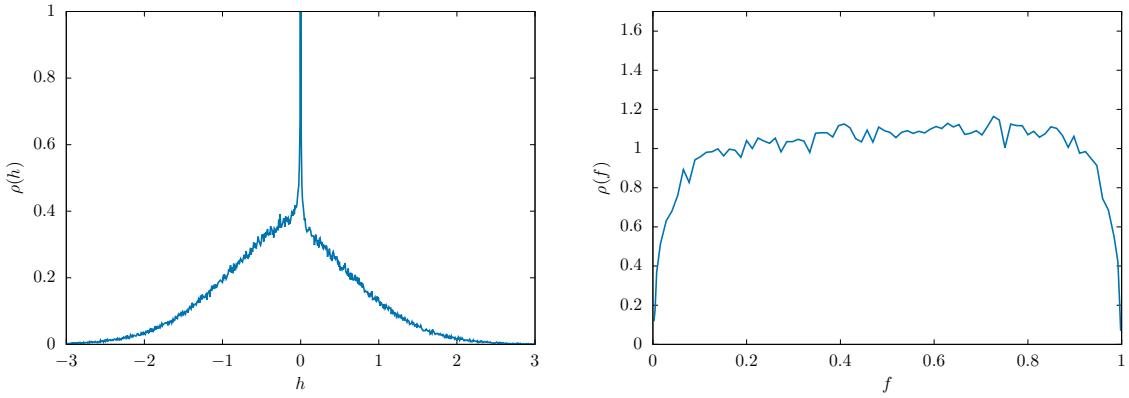

Figure 3.18: $\sigma = 0.5$, energy $e = 1.23$.

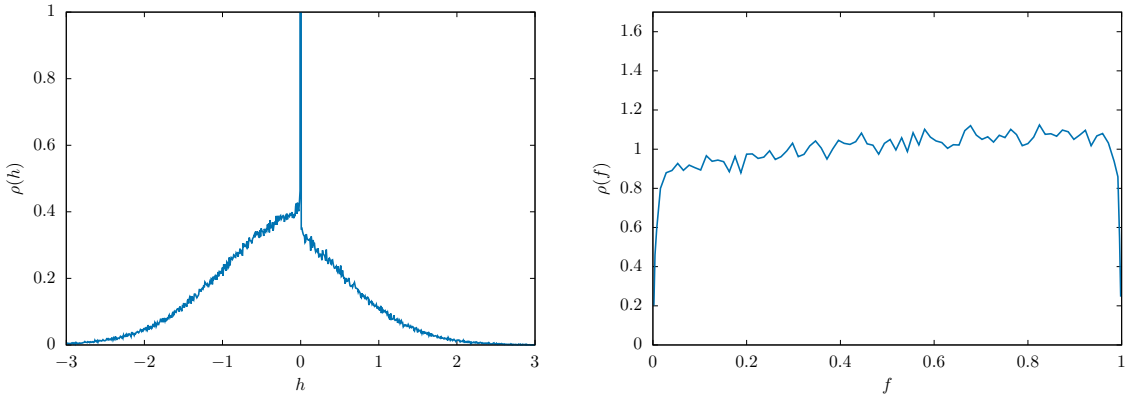

Figure 3.19: $\sigma = 0.6$, energy $e = 1.46$.

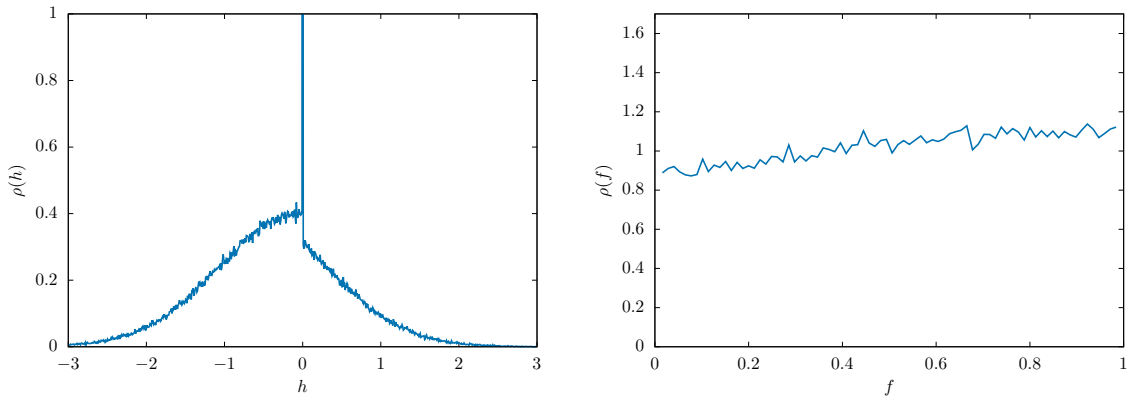

Figure 3.20: $\sigma = 0.7$, energy $e = 1.71$.

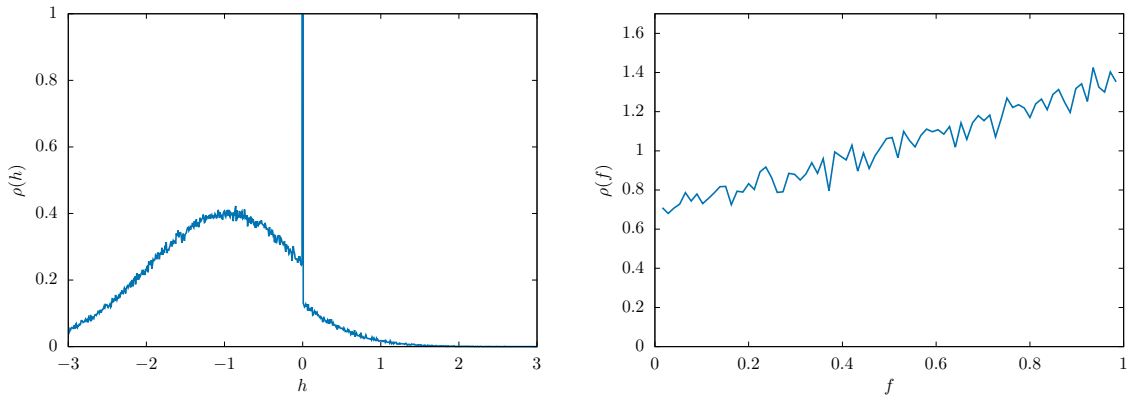

Figure 3.21: $\sigma = 1.5$, energy $e = 4.21$.

We conclude this section by measuring the critical exponents through their respective cumulative distribution functions and showing that they are compatible, up to numerical precision, with the exponents γ and θ of the jamming of spheres.

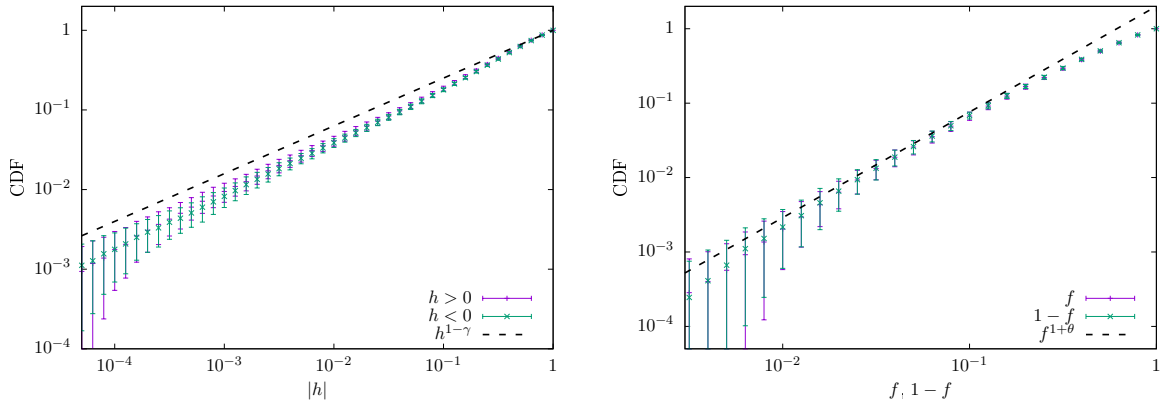

Figure 3.22: Cumulative distribution functions (CDF) of positive/negative gaps (left panel) and of forces close to 0 or 1 (right panel). In both cases, the exponents appear to be compatible with the jamming ones $\gamma \simeq 0.41$ and $\theta \simeq 0.42$. Data for $\alpha = 4$, $\sigma = 0.4$, $N = 1024$, averaged over 100 samples.

3.2 Making sense of the linear potential

In this section, we use the evidence obtained from the numerical simulations to get a better understanding of the model.
First of all, we have understood that the correct Hamiltonian (or, more precisely, the Lagrangian) describing the system reads

$$\mathrm{H}(\mathbf{X}) = \sum_{o\in\mathcal{O}} |h_o| - \sum_{c\in\mathcal{C}} f_c h_c + \frac{\eta}{2}\left(|\,\mathbf{X}\,|^2 - N\right) \tag{3.38}$$

whose gradient is

$$\nabla\,\mathrm{H}(\mathbf{X}) = -\frac{1}{\sqrt{N}}\sum_{o\in\mathcal{O}} \boldsymbol{\xi}_o - \frac{1}{\sqrt{N}}\sum_{c\in\mathcal{C}} \boldsymbol{\xi}_c\, f_c + \eta\,\mathbf{X} \tag{3.39}$$

with

$$f_c \in (0,1), \qquad \forall c \in \mathcal{C} \tag{3.40}$$

Equation (3.38) corresponds to its simpler version $H(\mathbf{X}) = \sum\limits_{o\in\mathcal{O}} |h_o|$ with the addition of the constraints $h_c = 0$ and $|\,\mathbf{X}\,|^2 = N$ and their respective Lagrange multipliers. In fact, the stationarity condition with respect to f_c and η gives

$$\begin{aligned} \frac{\partial\,\mathrm{H}}{\partial f_c} = h_c = \frac{1}{\sqrt{N}}\,\boldsymbol{\xi}_c\cdot\mathbf{X} - \sigma = 0, \qquad \forall c\in\mathcal{C} \\ \frac{\partial\,\mathrm{H}}{\partial\,\eta} = |\,\mathbf{X}\,|^2 - N = 0 \end{aligned} \tag{3.41}$$

which are $C+1$ constraints to be satisfied by $\mathbf{X}$. Moreover, we can derive H with respect to X_i for each component $i = 1, ..., N$ and impose the equilibrium condition

$$\nabla\,\mathrm{H}(\mathbf{X}) = 0 \tag{3.42}$$

to get

$$-\frac{1}{\sqrt{N}}\sum_{o\in\mathcal{O}} \xi_i^o - \frac{1}{\sqrt{N}}\sum_{c\in\mathcal{C}} \xi_i^c f_c + \eta\, X_i = 0 \tag{3.43}$$

Given the two sets of overlaps $\mathcal{O}$ and contacts $\mathcal{C}$, (3.43) represents a set of N equations, to be solved together with the constraints (3.41).
The conditions (3.43) plus (3.41) form a set of $N + C + 1$ equations to be solved for the unknowns

$$\begin{aligned} &X_i, && \text{with } i = 1, ..., N \\ &f_c, && \text{with } c = 1, ..., C \text{ and } f_c \in (0,1) \\ &\eta \end{aligned} \tag{3.44}$$

whose total number is therefore $N + C + 1$.
Having the same number of equations and unknowns, one could think that, choosing randomly two sets of linearly independent contact patterns $\boldsymbol{\xi}^c$ and unsat patterns $\boldsymbol{\xi}^o$, it is always possible to find the X_i, f_c, η by solving the equations (3.43)-(3.41) and thus obtaining a stable configuration of the system. The flaw in this statement is overlooking the condition (3.40) on contact forces: there is no reason why a randomly chosen set $\mathcal{C}$ would satisfy (3.43)-(3.41) with $f_c \in (0, 1)$.
The minimization procedure is therefore essential to find the sets $\mathcal{C}$ and $\mathcal{O}$ which allow (3.43)-(3.41) to be solved with the constraint (3.40). Once $\mathcal{C}$ and $\mathcal{O}$ are known, finding X_i, f_c and η becomes a linear algebra procedure.

3.2.1 Equilibrium equations

Projecting equation (3.43) on the contact patterns $-\frac{1}{\sqrt{N}}\boldsymbol{\xi}^{c'}$ (i.e. multiplying (3.43) by $-\frac{1}{\sqrt{N}}\xi_i^{c'}$ and summing over i), we get

$$\frac{1}{N}\boldsymbol{\xi}^{c'} \cdot \sum_{o\in\mathcal{O}} \boldsymbol{\xi}^o + \frac{1}{N}\sum_{c\in\mathcal{C}} \boldsymbol{\xi}^{c'} \cdot \boldsymbol{\xi}^c \, f_c - \eta \, \frac{1}{\sqrt{N}}\boldsymbol{\xi}_{c'} \cdot \mathbf{X} = 0 \tag{3.45}$$

Calling

$$\begin{aligned} \frac{1}{N}\boldsymbol{\xi}^{c'} \cdot \sum_{o\in\mathcal{O}} \boldsymbol{\xi}^o &= \mathrm{v}_{c'} \\ \frac{1}{N}\boldsymbol{\xi}^{c'} \cdot \boldsymbol{\xi}^c &= \Xi_{c'c} \end{aligned} \tag{3.46}$$

and noticing that $\frac{1}{\sqrt{N}}\boldsymbol{\xi}^{c'} \cdot \mathbf{X} = \sigma$ for all $c' \in \mathcal{C}$, we can write (3.45) as

$$\sum_c \Xi_{c'c} \, f_c - \sigma \, \eta = \mathrm{v}_{c'} \tag{3.47}$$

The $C \times C$ matrix $\Xi_{c'c} = \frac{1}{N}\boldsymbol{\xi}^{c'} \cdot \boldsymbol{\xi}^c$ is a Wishart matrix since ξ_i^c is a standard normally distributed random variable. $\Xi_{c'c}$ is full rank, since $C \leq N$.

In a similar manner, projecting 3.43 on $\mathbf{X}$, we get

$$-\frac{1}{\sqrt{N}}\sum_{o\in\mathcal{O}} \boldsymbol{\xi}^o \cdot \mathbf{X} - \frac{1}{\sqrt{N}}\sum_{c\in\mathcal{C}} f_c \, \boldsymbol{\xi}^c \cdot \mathbf{X} + \eta \, |\, \mathbf{X} \,|^2 = 0 \tag{3.48}$$

where we can substitute $\frac{1}{\sqrt{N}}\boldsymbol{\xi}^c \cdot \mathbf{X} = \sigma$, $|\, \mathbf{X} \,|^2 = N$, $-\frac{1}{\sqrt{N}}\sum_{o\in\mathcal{O}} \boldsymbol{\xi}^o \cdot \mathbf{X} = \sum_{o\in\mathcal{O}} |h_o| - \sigma \, \mathrm{N_o}$, with $\mathrm{N_o}$ the number of overlaps $|\mathcal{O}|$, and get

$$\eta = \frac{1}{N}(\sum_c f_c + \mathrm{N_o})\sigma - e \tag{3.49}$$

where e is the intensive energy $e = \frac{1}{N}\sum_{o\in\mathcal{O}} |h_o|$. We can define the *pressure* p of the system as

$$p = \frac{1}{N}\frac{\partial H}{\partial \sigma} = \frac{1}{N}(\sum_c f_c + \mathrm{N_o}) \tag{3.50}$$

and finally recast (3.49) as

$$\eta = p\sigma - e \tag{3.51}$$

The quantity $p\sigma - e$ is clearly the Legendre transform of the energy with respect to σ, that at equilibrium turns out to be equal to η. Eventually, one could think to change ensemble by using p as control parameter, letting σ become a variable and studying the potential $p\sigma - \mathrm{H}$. We use this approach in chapter 5.

Equilibrium in the isostatic phase

We have seen in section 3.1.3 the existence of a critical isostatic phase with

$$C = N - 1 \tag{3.52}$$

The constraints (3.41)

$$\begin{aligned} h_c = \frac{1}{\sqrt{N}}\,\boldsymbol{\xi}_c \cdot \mathbf{X} - \sigma = 0, \qquad \forall c \in \mathcal{C} \\ |\,\mathbf{X}\,|^2 - N = 0 \end{aligned} \tag{3.53}$$

are therefore N equations that completely define $\mathbf{X}$ (except for a sign $\pm$). In fact, the linear system (we are summing on repeated indices)

$$\frac{1}{\sqrt{N}} \xi_i^c X_i = \sigma \tag{3.54}$$

has an affine space of solutions of dimension 1, since the matrix ξ_i^c of dimension $(N-1)\times N$ has a singular value equal to 0 with corresponding null-space (right singular vector) w_i. The solution to (3.54) is given by

$$X_i = \frac{\sigma}{\sqrt{N}} \xi_i^c \sum_{c'} \Xi^{-1}_{cc'} + k\ w_i \tag{3.55}$$

where we use Ξ^{-1} to indicate the inverse of the matrix $\Xi_{cc'} = \frac{1}{N}\,\boldsymbol{\xi}^c \cdot \boldsymbol{\xi}^{c'}$; k is a constant whose absolute value is fixed by the condition $|\,\mathbf{X}\,|^2 = N$. The sign of k is determined by requiring that $h_o = \frac{1}{\sqrt{N}} \xi_i^o X_i - \sigma < 0$ for the unsat patterns $o \in \mathcal{O}$.
Once $\mathbf{X}$ is known, it is straightforward to compute the energy $e = \frac{1}{N} \sum\limits_{o \in \mathcal{O}} |h_o|$.
At this point, the equations 3.47-3.49 form a linear system

$$\begin{cases} \Xi_{c'c}\, f_c - \sigma\, \eta & = \mathrm{v}_{c'} \\ \frac{\sigma}{N} \sum\limits_c f_c - \eta & = e - \frac{N_o}{N}\sigma \end{cases} \tag{3.56}$$

of $C + 1$ equations that can be solved for the $C + 1$ unknowns f_c and η.
It is interesting to notice that in the isostatic phase, given the sets $\mathcal{C}$ and $\mathcal{O}$ realizing a stable configuration, it is possible to solve the equations for X_i independently of the equations for f_c and η. In the hypostatic case, instead, the equations for f_c, η and X_i have to be solved together and they are quadratic.

Equilibrium in the hypostatic phase

The equations for f_c and η

$$\begin{cases} \Xi_{c'c}\, f_c - \sigma\, \eta & = \mathrm{v}_{c'} \\ \frac{\sigma}{N} \sum_c f_c - \eta & = e - \frac{N_o}{N}\sigma \end{cases} \tag{3.57}$$

depend on $\mathbf{X}$ through the energy term e. To find all the components X_i, it is not sufficient to use the contacts and spherical constraints (3.41) since they constitute $C + 1 < N$ conditions. Therefore it is necessary also to use the stationarity condition with respect to X_i

$$-\frac{1}{\sqrt{N}} \sum_{c \in \mathcal{C}} \xi_i^c f_c + \eta\, X_i = \frac{1}{\sqrt{N}} \sum_{o \in \mathcal{O}} \xi_i^o \tag{3.58}$$

that has a non-linear coupling between the unknowns $\eta\, X_i$. Therefore, in the hypostatic phase, even knowing the contacts and overlaps sets $\mathcal{C}$ and $\mathcal{O}$, finding the stable configuration is a quadratic problem and not a linear one.

3.2.2 Hessian of the linear potential

Since the potential is a piece-wise linear function, its second derivative is a singular quantity. Anyway, interesting insights can be obtained by looking at the smoothed Hamiltonian we have used for the numerical simulations

$$\begin{aligned} H_\epsilon = & \sum_o \left(\sigma - \frac{1}{\sqrt{N}}\, \boldsymbol{\xi}^o \cdot \mathbf{X} \right) \theta \left(-h_\mu - \frac{\epsilon}{2} \right) + \\ & + \frac{1}{2\epsilon} \sum_c \left(\frac{\epsilon}{2} - \sigma + \frac{1}{\sqrt{N}}\, \boldsymbol{\xi}^c \cdot \mathbf{X} \right)^2 \mathbb{I} \left(-\frac{\epsilon}{2} < h_c < \frac{\epsilon}{2} \right) + \\ & + \frac{\eta}{2} \left(|\, \mathbf{X}\, |^2 - N \right) \end{aligned} \tag{3.59}$$

where we have made explicit the expressions of the gaps. If we compute the Hessian, we get

$$\frac{\partial^2 H_\epsilon}{\partial X_i \partial X_j} = \frac{1}{\epsilon} \sum_{c \in \mathcal{C}} \frac{1}{N} \xi_i^c \xi_j^c + \eta\, \delta_{ij} \tag{3.60}$$

Notice that we are always considering taking the limit $\epsilon \to 0$ before $N \to \infty$, also because we have asked ϵ to be smaller than the minimal non-zero gap h_{min} that is $h_{min} \sim N^{-1}$ in the hypostatic phase and $h_{min} \sim N^{-\frac{1}{1-\gamma}} \simeq N^{-1.7}$ in the isostatic phase. To make things clearer, let's say that $\epsilon << N^{-2}$ always.
Looking at eq. 3.60, we recognize the Wishart matrix [244]

$$\mathcal{W} = \sum_{c \in \mathcal{C}} \frac{1}{N} \xi_i^c \xi_j^c \tag{3.61}$$

whose eigenvalue spectrum is given by the well known Marchenko-Pastur distribution [169]. It is important to distinguish between the hypostatic and the isostatic cases.

- In the hypostatic case, $c = \frac{C}{N} < 1$ and $\mathcal{W}$ has $N - C$ eigenvalues equal to 0. The corresponding eigenvalue distribution $\rho(\lambda)$ in the continuum limit reads

$$\rho(\lambda) = (1-c)\delta(\lambda) + \frac{c}{2\pi}\frac{\sqrt{(\lambda_+ - \lambda)(\lambda - \lambda_-)}}{\lambda} \tag{3.62}$$

  with

$$\lambda_\pm = \frac{1}{c}\left(1 \pm \sqrt{c}\right)^2 \tag{3.63}$$

  and $c = \frac{C}{N}$ the usual isostaticity index.

- In the isostatic case, we have $c = 1$ and the eigenvalue distribution becomes

$$\rho(\lambda) = \frac{1}{2\pi}\frac{\sqrt{4-\lambda}}{\sqrt{\lambda}} \tag{3.64}$$

  that therefore diverges for $\lambda \to 0$ as $\rho(\lambda) \sim \frac{1}{\sqrt{\lambda}}$. For finite N, we can get the scale of smallest eigenvalue from

$$\int_0^{\lambda_{min}} \frac{1}{\sqrt{\lambda}} \sim \frac{1}{N} \tag{3.65}$$

  which gives

$$\lambda_{min} \sim N^{-2} \tag{3.66}$$

Therefore, the eigenvalues $\tilde{\lambda}$ of the Hessian

$$\frac{\partial^2 H_\epsilon}{\partial X_i \partial X_j} = \frac{1}{\epsilon}\mathcal{W} + \eta\,\delta_{ij} \tag{3.67}$$

live on two scales:

- the non-zero eigenvalues λ_i of $\mathcal{W}$ get multiplied by $\frac{1}{\epsilon}$ and since $\epsilon << \lambda_{min}$ they all diverge

$$\tilde{\lambda}_i = \frac{1}{\epsilon}\lambda_i \underset{\epsilon\to 0}{\to} \infty \tag{3.68}$$

  irrespective of η;

- the $N - C$ zero eigenvalues of $\mathcal{W}$ stay identical to 0 also when multiplied by $\frac{1}{\epsilon}$, therefore the term $\eta\,\delta_{ij}$ becomes important and shifts the 0 eigenvalues to the value η:

$$\tilde{\lambda}_i = \eta \quad \text{for } i = 1, ..., N - C \tag{3.69}$$

If $\eta > 0$, then a configuration $\mathbf{X}$ can be a stable minimum also if it is hypostatic since all the eigenvalues of the Hessian are positive (or infinite). In fact, in a portion of the UNSAT phase we observe

$$c < 1 \quad \text{AND} \quad \eta > 0 \tag{3.70}$$

If $\eta < 0$, then any hypostatic configuration would get a number of negative eigenvalues $\tilde{\lambda} = \eta$: any hypostatic configuration would be unstable. In fact, we observe that

$$c = 1 \quad \text{AND} \quad \eta < 0 \tag{3.71}$$

In principle, it could be possible to stabilize the system also with a hyperstatic configuration, that is $c > 1$. However, with high-dimensional random vectors $\boldsymbol{\xi}^c$, these configurations are not possible. To see this, one can think of the condition $\frac{1}{\sqrt{N}} \boldsymbol{\xi}^c \cdot \mathbf{X} - \sigma = 0$ as the condition that $\mathbf{X}$ belongs to the affine hyperplane defined by $\boldsymbol{\xi}^c$ and σ. With the number of contacts $C = N - 1$, we get the intersection of $N - 1$ hyperplanes, that defines a line: the configuration is determined by taking one of the two points on this line satisfying $|\,\mathbf{X}\,|^2 = N$. a hyperstatic configuration would require that a certain number of other random hyperplanes $(\boldsymbol{\xi}^\mu, \sigma)$ should pass through the point $\mathbf{X}$ as well, and the probability for this to happen is negligible for large N.

In the non-convex, isostatic phase, the system has actually a number of contacts $C = N - 1$, so the matrix $\mathcal{W}$ should have a 0 eigenvalue that, with negative η, generates an unstable direction. This is not the case, since we have seen that the additional constraint to be added to the $N - 1$ contacts is the spherical one $|\,\mathbf{X}\,|^2 = N$. In fact, the eigenvector associated to the only zero mode of $\mathcal{W}$ is the right singular vector w_i of the matrix ξ_i^c introduced in equation (3.55): the component of the configuration along w_i is fixed by the normalization $|\,\mathbf{X}\,|^2 = N$, therefore w_i cannot be used as an unstable direction. The only way to destabilize the system in the non-convex phase is to break at least one contact, causing the configuration to change until isostaticity is restored.

Analogy with the prestress in spheres and ellipses

The role of the term $\eta\,\delta_{ij}$ in (3.60), whose sign determines isostaticity or hypostaticity, is strongly reminiscent of the role of the *pre-stress* in the models of finite dimensional spheres or ellipses [83, 214]. In these models, the Hessian, usually called *dynamical matrix* M in the condensed matter literature, is decomposed in two terms: the stiffness H, containing the second derivatives of the repulsive potential, and the pre-stress $-S$, depending on the geometry of the particles and on the forces between them:

$$M = H - S \tag{3.72}$$

It happens that exactly at the jamming point $S = 0$, but slightly in the overcompressed phase $-S \neq 0$ and it is

- negative definite in sphere packings;
- positive definite in ellipse packings.

As a result, in the jamming of spheres the stiffness matrix H must be full-rank, otherwise an infinitesimal compression would make the negative eigenvalues of $-S$ destabilize the system: for H to be full rank, the jamming has to be isostatic in spheres.
For ellipses, instead, jamming is hypostatic and the matrix H has $N(z_{iso} - z)$ eigenmodes $\hat{e}_0$ with zero eigenvalues, where N is the number of ellipses, z_{iso} is the average number of contacts per particle needed to get isostaticity and z is the actual number of contacts per particle ($z < z_{iso}$ because of hypostaticity). However, the fact that the prestress $-S$

is positive definite guarantees that $\hat{e}_0$ are not unstable modes: for an infinitesimal compression, the positive eigenvalues of $-S$ make the dynamical matrix M positive definite. Moreover, at the jamming point, a perturbation of magnitude δ along these zero modes $\hat{e}_0$ produces an overlap between ellipses of order δ^2, different from the overlap δ produced by perturbing along the non-zero modes of H. In the harmonic approximation, an overlap δ^2 produces an energy increase $\sim \delta^4$: for this reason, the modes $\hat{e}_0$ are often called "quartic" modes and are associated with collective rotational motions [162, 214].

In our linear perceptron, an analogous mechanism is in place. There is a problem coming from the fact that the minima of the linear potential are corner points that are not suitable for any harmonic approximation. Nevertheless, we can use the smoothed Hamiltonian H_ϵ and apply a perturbation of order $\sim \epsilon$. Considering a normalized non-zero mode δX_i of the matrix $\mathcal{W}$ and a displacement $\delta\tilde{X} \sim \epsilon \delta X_i$, we get

$$\delta H_\epsilon \sim \frac{1}{\epsilon}\mathcal{W}_{ij}\epsilon^2\delta X_i\delta X_j + \eta\,\delta_{ij}\epsilon^2\delta X_i\delta X_j = \lambda\epsilon + \eta\,\epsilon^2 \sim \lambda\epsilon \tag{3.73}$$

where λ is the (positive) eigenvalue of the Wishart matrix $\mathcal{W}$ associated to the eigenvector δX_i. We see that the energy variation is dominated by the linear term in ϵ, that in fact is of the order of the displacement $|\delta\tilde{X}|$. This is in line with the fact that a non-zero mode of $\mathcal{W}$ is associated to breaking at least one contact and the consequent energy increase is linear in the displacement (due to the linear potential).
Let's consider specifically the hypostatic phase, and let's make, instead, a perturbation $\delta\tilde{X} \sim \epsilon\delta X_i$ along a mode δX_i of $\mathcal{W}$ with zero eigenvalue. We get

$$\delta H_\epsilon \sim \frac{1}{\epsilon}\mathcal{W}_{ij}\epsilon^2\delta X_i\delta X_j + \eta\,\delta_{ij}\epsilon^2\delta X_i\delta X_j = \eta\,\epsilon^2 \tag{3.74}$$

The energy increase is positive, due to the positive $\eta > 0$, and it is of order $|\delta\hat{X}|^2$. Noting that in our system the amount of overlap of an unsat gap is exactly its energy contribution, we deduce that in the hypostatic phase:

- moving by an amount δ along a non-zero mode of the matrix $\mathcal{W}$ (i.e. breaking some contacts) generates an overlap of order δ;
- moving by an amount δ along a zero mode of the matrix $\mathcal{W}$ (i.e. leaving the contacts untouched) generates an overlap of order δ^2.

Therefore, we see that the zero modes of the matrix $\mathcal{W}$ in the hypostatic phase are completely analogous to the "quartic" modes of hypostatic jamming in ellipses and ellipsoids. The peculiar feature of our system is that the argument is valid all over the hypostatic UNSAT phase, and not only at the jamming onset.

The extended modes

In section 3.2.2 we have studied a Hessian for the linear potential using the regularized model H_ϵ. Anyway, in the limit $\epsilon \to 0$, the Hessian is still a singular quantity because of the term $\frac{1}{\epsilon}$. To obtain something that is well defined in the $\epsilon \to 0$ limit, we can consider the quantity

$$\lim_{\epsilon\to 0}\epsilon\frac{\partial^2 H_\epsilon}{\partial X_i \partial X_j} = \sum_{c\in\mathcal{C}}\frac{1}{N}\xi_i^c\xi_j^c = \mathcal{W}_{ij} \tag{3.75}$$

that is the Wishart matrix we have already introduced. As discussed in section 3.2.2, it is full rank in the isostatic phase with a divergent spectrum for small, positive eigenvalues. In this phase, the breaking of a contact causes the creation of a zero-eigenvalue mode, that is an unstable direction due to $\eta < 0$. The system follows this direction until a new contact is formed and isostaticity is restored.
In the jamming of spheres, this role is played by the stiffness matrix. Its eigenvalue spectrum is usually discussed in terms of the physical frequencies ω that are the square root of its eigenvalues. In particular, it provides a density $D(\omega)$ of low energy vibrational modes that is flat at jamming: $D(\omega)$ goes to a constant for $\omega \to 0$ [191]. This is very different from the Debye law of crystalline solids (i.e. $D(\omega) \sim \omega^{d-1}$ in d dimensions) and the excess number of low-frequency vibrational modes is associated to important properties of glasses. The flat $D(\omega)$ for soft spheres, however, is present only at the jamming point: a slight compression creates a cut-off frequency ω^* that increases with compression. The vibrational modes appearing at ω^* have an associated length scale $l^* \sim \frac{1}{\omega^*}$ that diverges at the jamming point. Therefore, these low frequencies modes are system spanning and the divergent lengthscale l^* is often called *isostatic lengthscale* [248].
In the linear perceptron, we have a very similar scenario in all the isostatic phase, with $\mathcal{W}$ playing the role of the stiffness matrix. It provides a flat density of states $D(\omega)$, even if these are not properly harmonic vibrational modes. They are system-spanning modes, associated with broken contacts. In this case, $\omega^* \equiv 0$ in all the isostatic phase and therefore the associated lengthscale is always infinite. A detailed discussion of the excitations of the system given by breaking contacts is provide in chapter 5.
An additional observation that can be made is about the energy variation (3.73) along a non-zero mode of the matrix $\mathcal{W}$: through the use of the smoothed potential, we have argued that the energy variation is order $\delta E \sim \lambda |\delta \tilde{X}|$, therefore linear in the perturbation $\delta \tilde{X}$ as it is expected for the linear cost-function. The slope of this linear increase is given by λ, that is the eigenvalue of the mode of $\mathcal{W}$ we are exciting. When the system is hypostatic, the non-zero eigenvalues have a lower bound given by $\lambda_- = \frac{1}{c}(1 - \sqrt{c})^2$ introduced in eq. (3.63). When the system is isostatic, instead, the lower bound for λ is 0 and we have seen there is an abundance of close-to-zero eigenvalues. This suggests that, in the isostatic phase, there exist modes obtained by breaking contacts whose linear energy increase $\delta E \sim \lambda |\delta \tilde{X}|$ has a vanishingly small slope. In other words, the minima in the isostatic phase are corner points surrounded by ramps of increasing energy that, in some directions, are *nearly flat*. This is related to *marginal stability* that is discussed in section 3.4.

In the figures 3.23-3.26 we report the eigenvalue spectra of the Wishart matrix $\mathcal{W}$ as obtained from the numerical minimizations of section 3.1.2 in the isostatic and hypostatic phases. We also plot the same spectra as a function of the frequencies $\omega = \sqrt{\lambda}$, corresponding to the density of states $D(\omega)$. We see that for $c = 1$, the spectrum $\rho(\lambda)$ diverges as $\sim \frac{1}{\sqrt{\lambda}}$ and the corresponding $D(\omega)$ becomes flat for $\omega \to 0$. When $c < 1$, instead, the spectrum is gapped and there is a Dirac delta of zero modes given by the $N - C$ zero-eigenvalues.

Plots of the eigenvalue distribution $\rho(\lambda)$ and corresponding density of states $D(\omega = \sqrt{\lambda})$ of matrix $\mathcal{W}$ (3.75) at $\alpha = 4$, $N = 2048$, averaged over 100 samples.

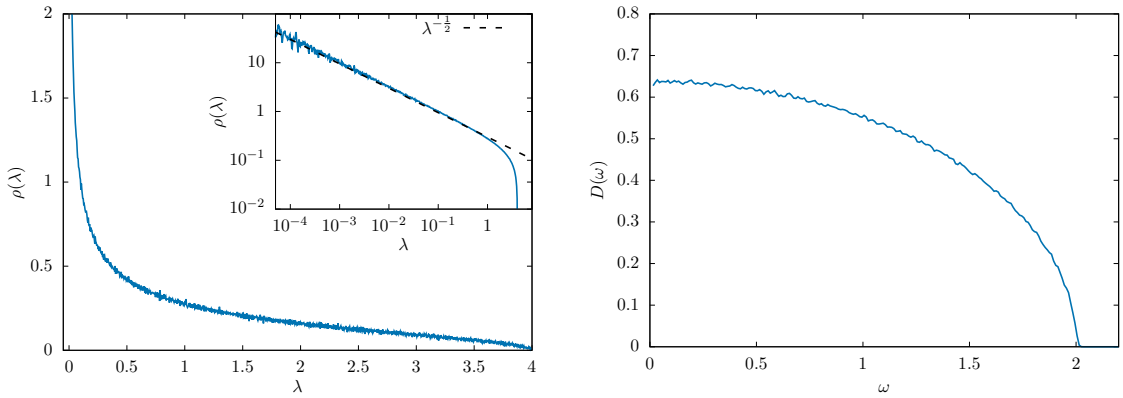

Figure 3.23: $\sigma = -0.3$, energy $e = 0.06$.

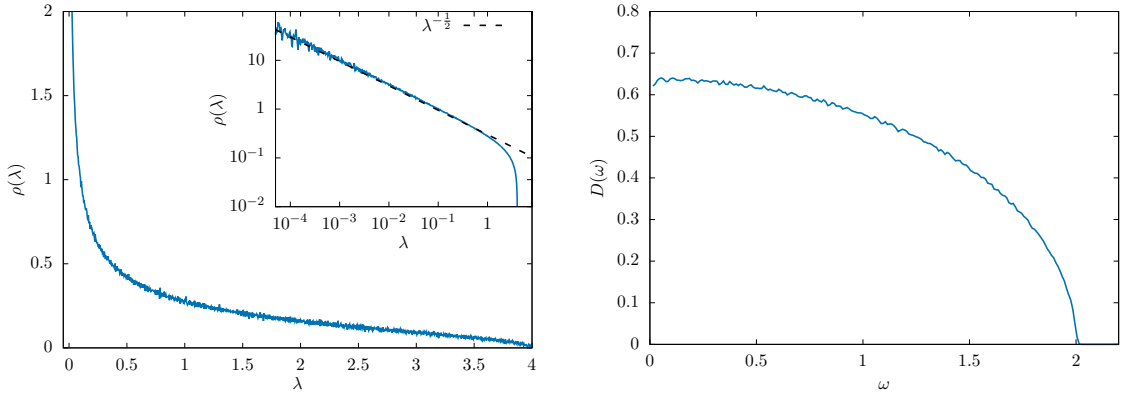

Figure 3.24: $\sigma = 0.6$, energy $e = 1.46$.

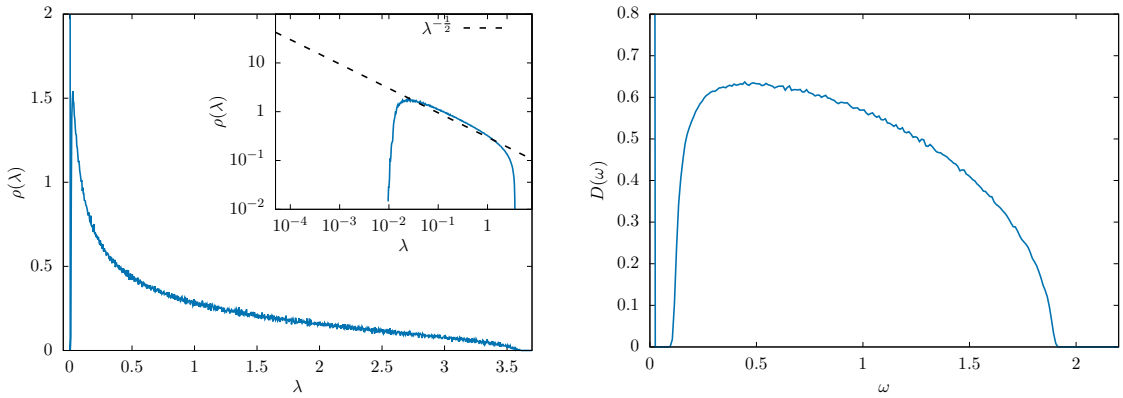

Figure 3.25: $\sigma = 0.9$, energy $e = 2.27$.

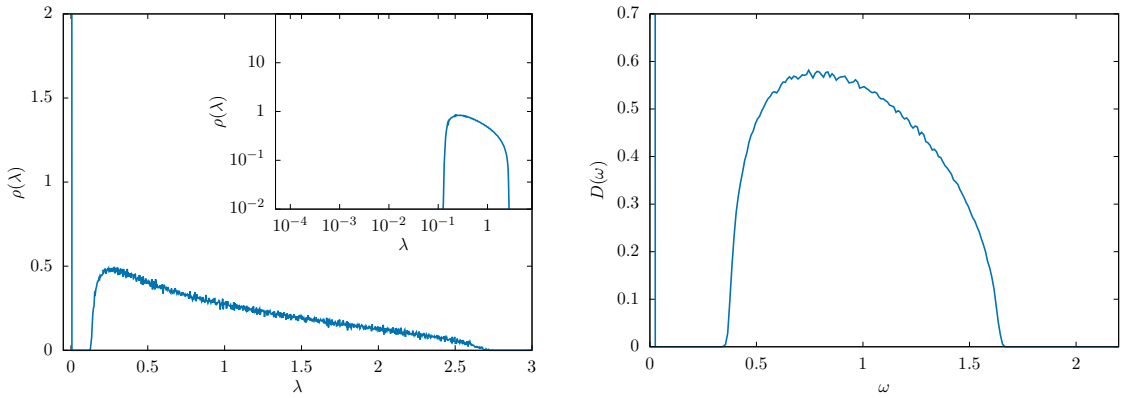

Figure 3.26: $\sigma = 1.5$, energy $e = 4.22$.

3.3 The replica analysis

In this section we solve the replica theory of the linear perceptron. The starting point are the equations obtained in chapter 2 for a perceptron with general potential $\nu(h)$: we set $\nu(h) = |h|\theta(-h)$ and solve the model. We first study the replica symmetric (RS) solution and compute its domain of stability, confirming that it corresponds to the hypostatic phase explored in the simulations of section 3.1.3. We plot the phase diagram of the model. Moreover, we study the unjamming limit in the RS/hypostatic phase, showing the presence of logarithms in the scalings of important quantities like energy and pressure. Thereafter, we investigate the nature of the broken replica symmetry phase, showing it is of a continuous kind ($full$RSB). In particular, the theory establishes a perfect correspondence between isostaticity and marginal stability. We formulate a scaling ansatz for the equations of the $full$RSB theory, showing it provides the same universality class that has been found for the jamming point of spheres (and presented in section 2.3.4 for the perceptron). Therefore, it gives the values of the critical exponents observed in the simulations of section 3.1.3. Very remarkably, this scaling solution provides also a mapping between the distributions of small positive gaps and small negative gaps, predicting that their respective power law divergences must have the same exponents. The same mapping also implies that the pseudogaps at the boundaries of the distribution of contact forces have the same exponents. This is in perfect agreement with our numerical results.

3.3.1 The replica symmetric solution

We can write the RS free energy $\mathrm{f}_{RS}(q_M)$ of the perceptron derived in equation (2.44) making explicit the potential $\nu(h) = |h|\theta(-h)$. We have

$$-\beta f_{RS}(q_M) = \frac{1}{2}\left[\log(1-q_M) + \frac{q_M}{1-q_M}\right] + \alpha\gamma_{q_M} * f(q_M, h)\Big|_{h=-\sigma} \tag{3.76}$$

where

$$f(q_M, h) = \log\left[\int \frac{dz}{\sqrt{2\pi(1-q_M)}} e^{-\frac{z^2}{2(1-q_M)} - \beta|h-z|\theta(-h+z)}\right] \tag{3.77}$$

As a reminder:

- β is the inverse temperature $\beta = \frac{1}{T}$, setting the Boltzmann constant equal to 1;
- q_M is the Edwards-Anderson order parameter;
- α and σ are the usual control parameters of the perceptron model.

Computation of $f(q_M, h)$

$$\begin{aligned} f &= \log\left[\int_{-\infty}^{\infty} \frac{dz}{\sqrt{2\pi(1-q_M)}} e^{-\frac{z^2}{2(1-q_M)} - \beta|h-z|\ \theta(-h+z)}\right] = \\ &= \log\left[\int_{-\infty}^{h} \frac{dz}{\sqrt{2\pi(1-q_M)}} e^{-\frac{z^2}{2(1-q_M)}} + \int_{h}^{\infty} \frac{dz}{\sqrt{2\pi(1-q_M)}} e^{-\frac{z^2}{2(1-q_M)} - \beta(z-h)}\right] = \\ &= \log\left[I_1 + I_2\right] \end{aligned} \tag{3.78}$$

where I_1 and I_2 are the two integrals

$$I_1 = \int_{-\infty}^{h} \frac{dz}{\sqrt{2\pi(1-q_M)}} e^{-\frac{z^2}{2(1-q_M)}} \tag{3.79}$$

$$\begin{aligned} I_2 &= \int_{h}^{\infty} \frac{dz}{\sqrt{2\pi(1-q_M)}} e^{-\frac{z^2}{2(1-q_M)} - \beta(z-h)} = \\ &= e^{\beta h} \int_{h}^{\infty} \frac{dz}{\sqrt{2\pi(1-q_M)}} e^{-\frac{1}{2(1-q_M)}\left[z^2 + 2\beta(1-q_M)z\right]} = \\ &= e^{\beta h + \frac{\beta^2(1-q_M)}{2}} \int_{h}^{\infty} \frac{dz}{\sqrt{2\pi(1-q_M)}} e^{-\frac{1}{2(1-q_M)}[z+\beta(1-q_M)]^2} = \\ &= e^{\beta h + \frac{\beta^2(1-q_M)}{2}}\ \frac{1}{2}\operatorname{erfc}\left(\frac{h+\beta(1-q_M)}{\sqrt{2(1-q_M)}}\right) \end{aligned} \tag{3.80}$$

Defining the function $\Theta(x)$, that already appeared in section 2.3.2, as

$$\Theta(x) = \frac{1}{2}\left[1 + \operatorname{erf}\left(\frac{x}{\sqrt{2}}\right)\right] \tag{3.81}$$

and using the relationship

$$\frac{1}{2}\operatorname{erfc}\left(\frac{x}{\sqrt{2}}\right) = \frac{1}{2}\left(1 - \operatorname{erf}\left(\frac{x}{\sqrt{2}}\right)\right) = \frac{1}{2}\left(1 + \operatorname{erf}\left(-\frac{x}{\sqrt{2}}\right)\right) = \Theta(-x) \tag{3.82}$$

we can write in a compact manner

$$I_1 = \Theta\left(\frac{h}{\sqrt{1-q_M}}\right) \tag{3.83}$$

$$I_2 = e^{\beta\left(h+\frac{\beta(1-q_M)}{2}\right)}\ \Theta\left(-\frac{h+\beta(1-q_M)}{\sqrt{1-q_M}}\right) \tag{3.84}$$

Therefore:

$$f(q_M,h) = \log\left[\Theta\left(\frac{h}{\sqrt{1-q_M}}\right) + e^{\beta\left(h+\frac{\beta(1-q_M)}{2}\right)}\ \Theta\left(-\frac{h+\beta(1-q_M)}{\sqrt{1-q_M}}\right)\right] \tag{3.85}$$

We want to study the zero temperature limit $\beta \to \infty$ in the UNSAT phase, where it holds that $q_M \underset{T\to 0}{\to} 1$.

Asymptotic analysis $T \to 0$, $q_M \to 1$

We know that for $T \to 0$ in the RS phase, the linear response hypothesis

$$q_M \simeq 1 - \chi T \tag{3.86}$$

holds. In the expression (3.85) we can substitute $\beta(1-q_M) = \chi$ and write

$$\begin{aligned} f(q_M,h) &= \log\left[\Theta\left(\frac{h}{\sqrt{1-q_M}}\right) + e^{\beta\left(h+\frac{\chi}{2}\right)}\ \Theta\left(-\frac{h+\chi}{\sqrt{1-q_M}}\right)\right] = \\ &= \log\left[I_1\left(q_M,h\right) + I_2\left(q_M,\chi,h\right)\right] \end{aligned} \tag{3.87}$$

with

$$\begin{aligned} I_1\left(q_M,h\right) &= \Theta\left(\frac{h}{\sqrt{1-q_M}}\right) \\ I_2\left(q_M,\chi,h\right) &= e^{\beta\left(h+\frac{\chi}{2}\right)}\ \Theta\left(-\frac{h+\chi}{\sqrt{1-q_M}}\right) \end{aligned} \tag{3.88}$$

In the limit $q_M \to 1$, we have to study the relative dominance between I_1 and I_2. Noting that $\Theta\left(\frac{h}{\sqrt{1-q_M}}\right) \underset{q_M\to 1}{\to} \theta(h)$ and that $\Theta\left(-\frac{h+\chi}{\sqrt{1-q_M}}\right) \underset{q_M\to 1}{\to} \theta(-h-\chi)$, there is clearly one regime for $h > 0$ where I_1 dominates and a regime $h < -\chi$ where I_2 does.
In between, that is for $-\chi < h < 0$, we need to expand the integrals: it turns out that $I_1 \simeq I_2$.
Therefore we have three regimes:

- $h > 0$ for which $I_1 >> I_2$
- $-\chi < h < 0$ for which $I_1 \simeq I_2$
- $h < -\chi$ for which $I_1 << I_2$

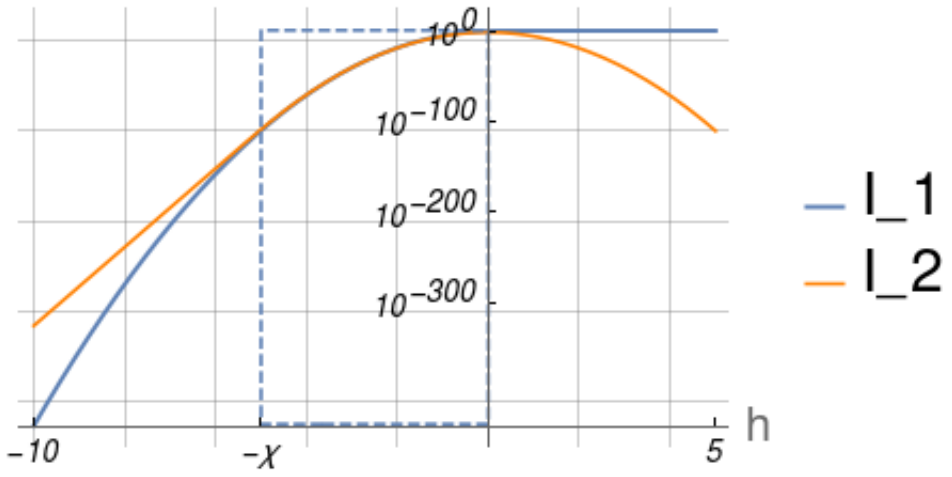

Figure 3.27: Plot of I_1 and I_2 vs h for $q_M = 0.95$, $\beta = 100$ (then $T = 0.01$, $\chi = 5$) with vertical axis in log-scale.

Let's develop $f(q_M, h)$ in these three regions for $q_M \to 1$, $\beta \to \infty$.

- For $h > 0$:

$$f(q_M, h) = \log\left[I_1 + I_2\right] \simeq \log\left[I_1\right] = \log\left[\Theta\left(\frac{h}{\sqrt{1-q_M}}\right)\right] = \\ = \mathcal{F}\left(\frac{h}{\sqrt{1-q_M}}\right) \tag{3.89}$$

where we have defined

$$\mathcal{F}\left(x\right) = \log\left[\Theta\left(x\right)\right] = \log\left[\frac{1+\text{erf}\left(\frac{x}{\sqrt{2}}\right)}{2}\right] \tag{3.90}$$

We see that

$$\mathcal{F}\left(\frac{h}{\sqrt{1-q_M}}\right) \simeq \begin{cases} 0, & h >> \sqrt{1-q_M} \\ -\frac{h^2}{2(1-q_M)}, & h << -\sqrt{1-q_M} \end{cases} \tag{3.91}$$

while it has a non-trivial matching regime for $h \sim O\left(\sqrt{1-q_M}\right)$.

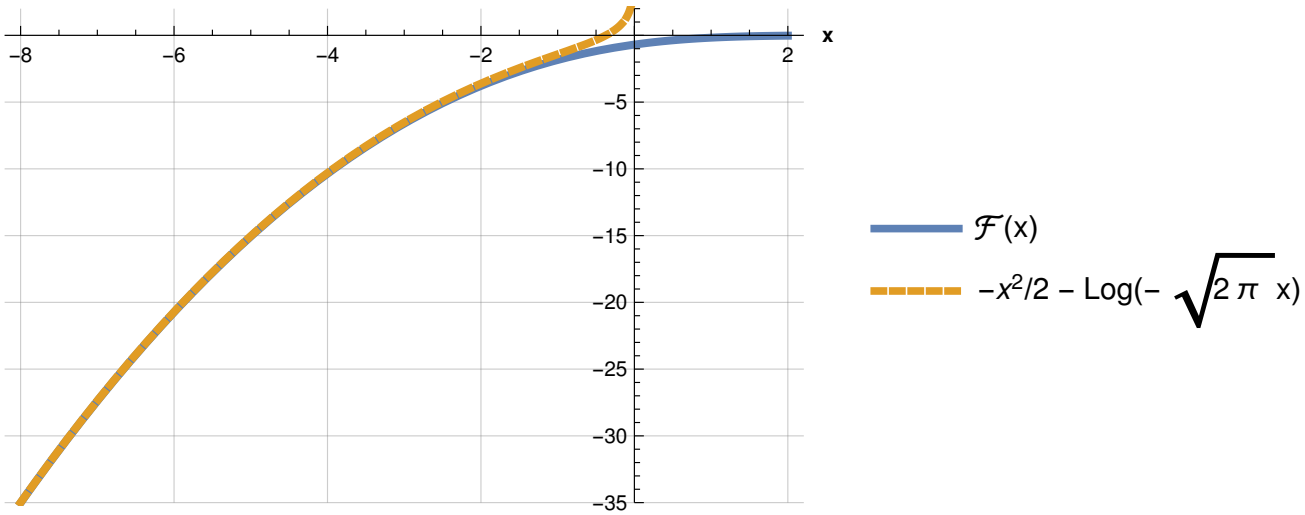

Figure 3.28: Plot of the function $\mathcal{F}(x)$ defined in eq. (3.90) and comparison with the expansion $-\frac{x^2}{2} - \log\left(-\sqrt{2\pi}x\right)$. For $x \to -\infty$, the asymptotic behavior is given by $-\frac{x^2}{2}$.

- For $-\chi < h < 0$, we can use the following development

$$c > 0, \qquad \Theta\left(\frac{-c}{\sqrt{1-q_M}}\right) = \frac{e^{-\frac{c^2}{2(1-q_M)}}}{\sqrt{2\pi}}\left[\frac{\sqrt{1-q_M}}{c} + O\left(\left(\frac{\sqrt{1-q_M}}{c}\right)^3\right)\right] \tag{3.92}$$

that gives

$$I_1 = \frac{e^{-\frac{h^2}{2(1-q_M)}}}{\sqrt{2\pi}}\left[\frac{\sqrt{1-q_M}}{-h} + O\left(\left(\frac{\sqrt{1-q_M}}{h}\right)^3\right)\right] \tag{3.93}$$

$$\begin{aligned} I_2 &= e^{\beta(h+\frac{\chi}{2})}\frac{e^{-\frac{(h+\chi)^2}{2(1-q_M)}}}{\sqrt{2\pi}}\left[\frac{\sqrt{1-q_M}}{\chi+h} + O\left(\left(\frac{\sqrt{1-q_M}}{\chi+h}\right)^3\right)\right] = \\ &= \frac{e^{-\frac{h^2}{2(1-q_M)}}}{\sqrt{2\pi}}\left[\frac{\sqrt{1-q_M}}{\chi+h} + O\left(\left(\frac{\sqrt{1-q_M}}{\chi+h}\right)^3\right)\right] \end{aligned} \tag{3.94}$$

We see that the leading order $e^{-\frac{h^2}{2(1-q_M)}}$ is the same in I_1 and I_2. Therefore we have

$$I_1 + I_2 = \frac{e^{-\frac{h^2}{2(1-q_M)}}}{\sqrt{2\pi}}\left[\sqrt{1-q_M}\frac{\chi}{-h(\chi+h)} + O\left(\left(\frac{\sqrt{1-q_M}}{-h(\chi+h)}\right)^3\right)\right] \tag{3.95}$$

that gives

$$f(q_M, h) = \log\left[I_1 + I_2\right] = -\frac{h^2}{2(1-q_M)} + O\left[\log\left(\frac{\sqrt{1-q_M}}{-h(\chi+h)}\right)\right] \tag{3.96}$$

Also in this case, this development breaks down for $h \sim O\left(\sqrt{1-q_M}\right)$ and $h \sim -\chi + O\left(\sqrt{1-q_M}\right)$

- For $h < -\chi$:

$$f(q_M, h) = \log\left[I_1 + I_2\right] \simeq \log\left[I_2\right] = \log\left[e^{\beta\left(h+\frac{\chi}{2}\right)}\ \Theta\left(-\frac{h+\chi}{\sqrt{1-q_M}}\right)\right] = \\ = \beta\left(h+\frac{\chi}{2}\right) + \log\Theta\left(-\frac{h+\chi}{\sqrt{1-q_M}}\right) = \\ = \beta\left(h+\frac{\chi}{2}\right) + \mathcal{F}\left(-\frac{h+\chi}{\sqrt{1-q_M}}\right) \tag{3.97}$$

  In this case

$$\mathcal{F}\left(-\frac{h+\chi}{\sqrt{1-q_M}}\right) \simeq \begin{cases} 0 & h << -\chi - \sqrt{1-q_M} \\ -\frac{(h+\chi)^2}{2(1-q_M)} & h >> -\chi + \sqrt{1-q_M} \end{cases} \tag{3.98}$$

  with a non-trivial matching regime for $h + \chi \sim O\left(\sqrt{1-q_M}\right)$.

Recapitulating:

$$f(h)\Big|_{q_M\to 1,\beta\to\infty} = \begin{cases} 0 & h >> \sqrt{1-q_M} \\ \mathcal{F}\left(\frac{h}{\sqrt{1-q_M}}\right) & h \sim O\left(\sqrt{1-q_M}\right) \\ -\frac{h^2}{2(1-q_M)} & -\chi < h < 0 \\ \beta\left(h+\frac{\chi}{2}\right) + \mathcal{F}\left(-\frac{h+\chi}{\sqrt{1-q_M}}\right) & h+\chi \sim O\left(\sqrt{1-q_M}\right) \\ \beta\left(h+\frac{\chi}{2}\right) & h << -\chi - \sqrt{1-q_M} \end{cases} \tag{3.99}$$

with $\beta(1-q_M) = \chi$, $\mathcal{F}(x) = \frac{1+\mathrm{erf}\left(\frac{x}{\sqrt{2}}\right)}{2}$.

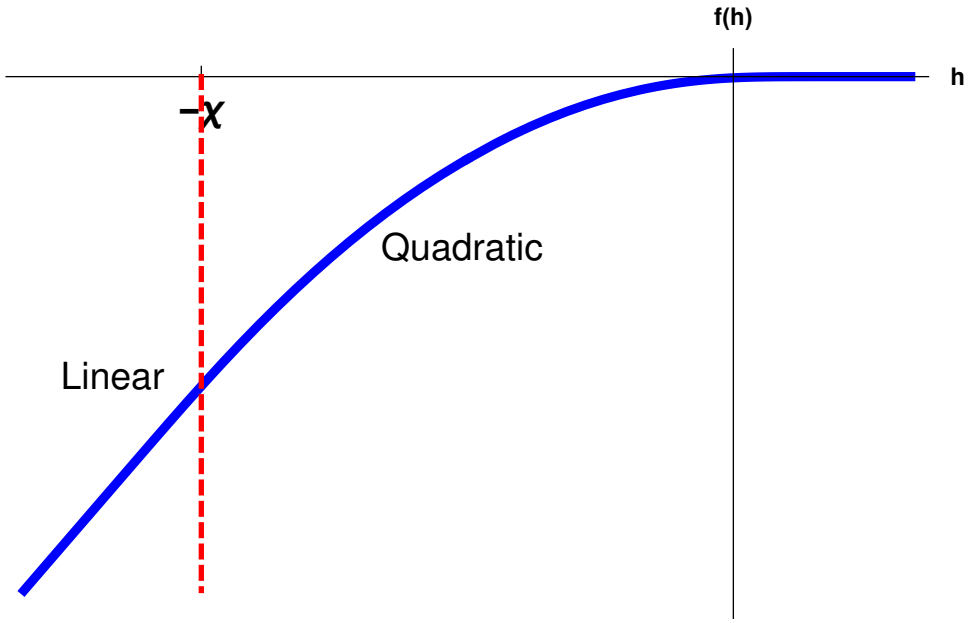

Figure 3.29: Behavior of function f defined in eq. (3.99) for parameters $q_M = 0.95$ and $\chi = 6$. The red dashed line corresponds to $h = -\chi$.

We notice that the asymptotic form has three regions, delimited by $h = 0$ and $h = -\chi$, and two matching regimes between them of width $\sim \sqrt{1-q_M}$.
It is useful to write its derivatives:

$$\frac{d}{dh}f(h)\Big|_{q_M\to 1,\beta\to\infty} = \begin{cases} 0 & h >> \sqrt{1-q_M} \\ \frac{1}{\sqrt{1-q_M}}\mathcal{F}'\left(\frac{h}{\sqrt{1-q_M}}\right) & h \sim O\left(\sqrt{1-q_M}\right) \\ -\frac{h}{1-q_M} & -\chi < h < 0 \\ \beta - \frac{1}{\sqrt{1-q_M}}\mathcal{F}'\left(-\frac{h+\chi}{\sqrt{1-q_M}}\right) & h+\chi \sim O\left(\sqrt{1-q_M}\right) \\ \beta & h << -\chi - \sqrt{1-q_M} \end{cases} \tag{3.100}$$

$$\frac{d^2}{dh^2}f(h)\Big|_{q_M\to 1,\beta\to\infty} = \begin{cases} 0 & h >> \sqrt{1-q_M} \\ \frac{1}{1-q_M}\mathcal{F}''\left(\frac{h}{\sqrt{1-q_M}}\right) & h \sim O\left(\sqrt{1-q_M}\right) \\ -\frac{1}{1-q_M} & -\chi < h < 0 \\ \frac{1}{1-q_M}\mathcal{F}''\left(-\frac{h+\chi}{\sqrt{1-q_M}}\right) & h+\chi \sim O\left(\sqrt{1-q_M}\right) \\ 0 & h << -\chi - \sqrt{1-q_M} \end{cases} \tag{3.101}$$

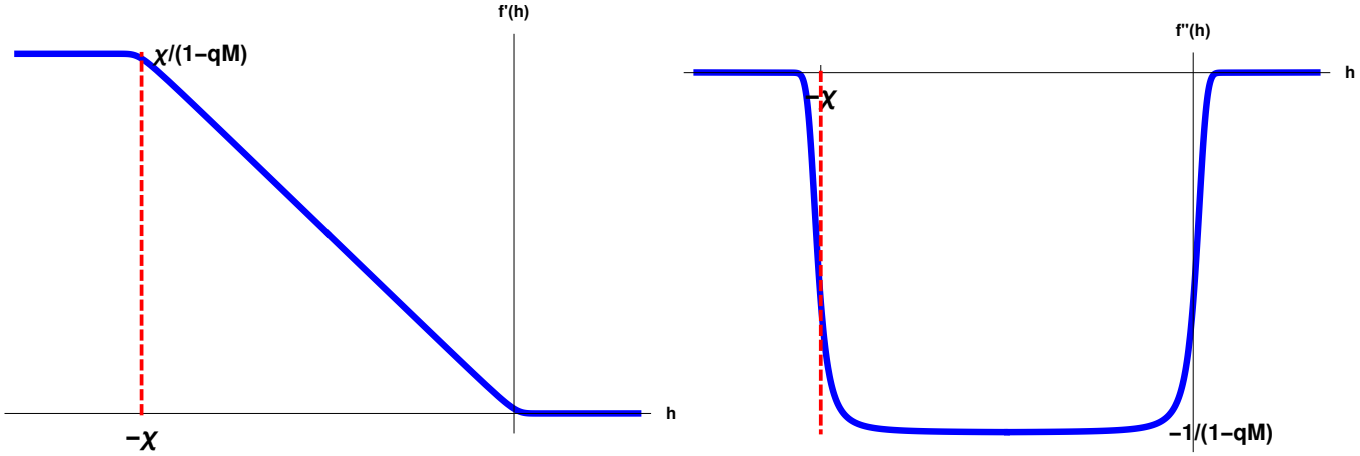

Figure 3.30: First derivative (left) and second derivative (right) of the function $f(h)$ defined in the equations (3.100) and (3.101). The first derivative has a linear behavior for $-\chi < h < 0$ and a plateau at $\beta = \frac{\chi}{1-q_M}$ for $h < -\chi$. The second derivative is different from 0 only in the region $-\chi < h < 0$ and takes the value $-\frac{1}{1-q_M}$. In both cases, the matching regions at $h \sim 0$ and $h \sim -\chi$ can be seen.

The saddle point equation

We can now take the saddle point equation

$$\frac{d}{dq_M}f_{RS}(q_M) = 0 \tag{3.102}$$

We have seen in (2.45) that its general form reads

$$\frac{q_M}{(1-q_M)^2} = \alpha \int_{-\infty}^{\infty} \gamma_{q_M}(h+\sigma)\left[\frac{d}{dh}f(h)\right]^2 \tag{3.103}$$

In the zero temperature limit we have $q_M =\simeq 1-\frac{\chi}{\beta}$ and the equation (3.103) fixes the value of χ as a function of the control parameters α and σ.
Using the expression (3.100), we have

$$\frac{1}{(1-q_M)^2} = \alpha\beta^2 \int_{-\infty}^{-\chi} dh\gamma(h+\sigma) + \alpha \int_{-\chi}^{0} dh\gamma(h+\sigma)\frac{h^2}{(1-q_M)^2} \tag{3.104}$$

Using the relationship $\beta = \frac{\chi}{1-q_M}$:

$$1 = \alpha\chi^2 \int_{-\infty}^{-\chi} dh\gamma(h+\sigma) + \alpha \int_{-\chi}^{0} dh\gamma(h+\sigma)h^2 \tag{3.105}$$

We see that we can take the unjamming limit by sending $\chi \to \infty$, recovering the usual Gardner storage capacity line

$$1 = \alpha_J \int_{-\infty}^{0} dh\gamma(h+\sigma)h^2 \tag{3.106}$$

We can use this expression to rearrange the term $\int_{-\chi}^{0} dh\gamma(h+\sigma)h^2 = \frac{1}{\alpha_J} - \int_{-\infty}^{-\chi} dh\gamma(h+\sigma)h^2$ and write (3.105) in the form

$$\frac{1}{\alpha_J} - \frac{1}{\alpha} = \int_{-\infty}^{-\chi} dh\gamma(h+\sigma)\left(h^2-\chi^2\right) \tag{3.107}$$

This expression allows us to compute χ as a function of the distance from unjamming $\alpha - \alpha_J$ at fixed σ.
In an equivalent manner, we can consider keeping α fixed and varying σ. We can use (3.106) to rewrite $\frac{1}{\alpha} = \int_{-\infty}^{0} dh\gamma(h+\sigma_J)h^2$, so (3.105) becomes

$$\int_{-\infty}^{0} dh\left[\gamma(h+\sigma)-\gamma(h+\sigma_J)\right]h^2 = \int_{-\infty}^{-\chi} \gamma(h+\sigma)\left(h^2-\chi^2\right) \tag{3.108}$$

Defining the distance from unjamming through $\Delta\alpha = \alpha - \alpha_J$ and $\Delta\sigma = \sigma - \sigma_J$, we can now use the following expansions:

$$\frac{1}{\alpha_J} - \frac{1}{\alpha} = \frac{\Delta\alpha}{\alpha_J^2} + O(\Delta\alpha^2) \tag{3.109}$$

$$\int_{-\infty}^{-\chi} \gamma(h+\sigma)\left(h^2-\chi^2\right) \underset{\chi\to\infty}{=} e^{-\frac{(\chi-\sigma)^2}{2}}\sqrt{\frac{2}{\pi}}\left(\frac{1}{\chi}+O\left(\frac{1}{\chi^2}\right)\right) \tag{3.110}$$

$$\int_{-\infty}^{0} dh\left[\gamma(h+\sigma)-\gamma(h+\sigma_J)\right]h^2 = k_J\Delta\sigma + O\left(\Delta\sigma^2\right) \tag{3.111}$$

where we have defined the coefficient

$$k_J = e^{-\sigma_J^2/2}\sqrt{\frac{2}{\pi}} + \sigma_J\left(1+\operatorname{erf}\left(\frac{\sigma_J}{\sqrt{2}}\right)\right) \tag{3.112}$$

From these expansions:

- keeping σ fixed and going to unjamming $\chi \to \infty$ by $\Delta\alpha \to 0$, we get to the leading order

$$\frac{\Delta\alpha}{\alpha_J^2} = \frac{e^{-\frac{(\chi-\sigma)^2}{2}}}{\chi}\sqrt{\frac{2}{\pi}} \tag{3.113}$$

that gives

$$\chi \underset{\Delta\alpha\to 0}{\simeq} \sqrt{2|\log\Delta\alpha|} \tag{3.114}$$

- keeping α fixed and going to unjamming $\chi \to \infty$ by $\Delta\sigma \to 0$, we get to the leading order

$$k_J \Delta\sigma = \frac{e^{-\frac{(\chi-\sigma_J)^2}{2}}}{\chi}\sqrt{\frac{2}{\pi}} \tag{3.115}$$

that gives

$$\chi \underset{\Delta\sigma\to 0}{\simeq} \sqrt{2|\log\Delta\sigma|} \tag{3.116}$$

The logarithmic behavior of χ with respect to the distance from unjamming is very interesting, because it is related to the behavior of the pressure. This link is explained in the next section 3.3.1.

For completeness, we can also take the limit for α or σ going to infinity. From equation (3.105), we get

- keeping σ fixed, for $\alpha \to \infty$

$$\chi \underset{\alpha\to\infty}{\simeq} \frac{1}{\sqrt{\Theta(\sigma)\,\alpha}} \tag{3.117}$$

where $\Theta(\sigma) = \frac{1}{2}(1 + \mathrm{erf}(\sigma))$;

- keeping α fixed, for $\sigma \to \infty$

$$\chi \underset{\sigma\to\infty}{\simeq} \frac{1}{\sqrt{\alpha}} \tag{3.118}$$

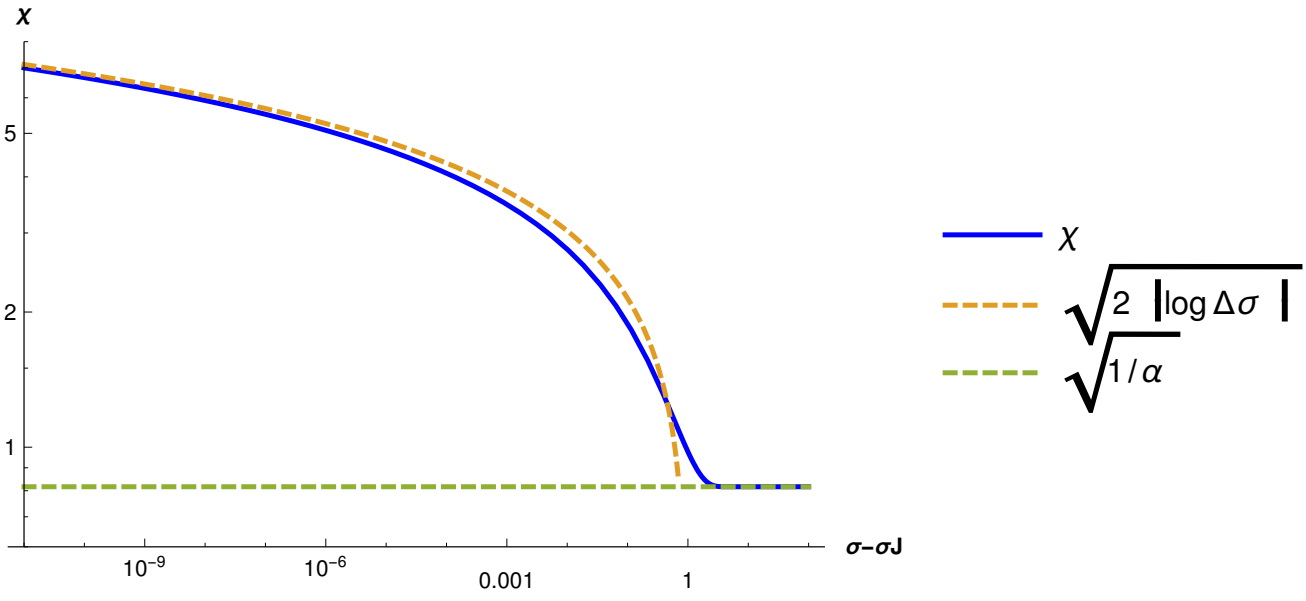

Figure 3.31: Behavior of χ with respect to $\sigma - \sigma_J$ at fixed $\alpha = 1.5$. The dashed lines represent the asymptotic expansions $\chi \underset{\Delta\sigma\to 0}{\simeq} \sqrt{2|\log\Delta\sigma|}$ and $\chi \underset{\sigma\to\infty}{\simeq} \frac{1}{\sqrt{\alpha}}$.

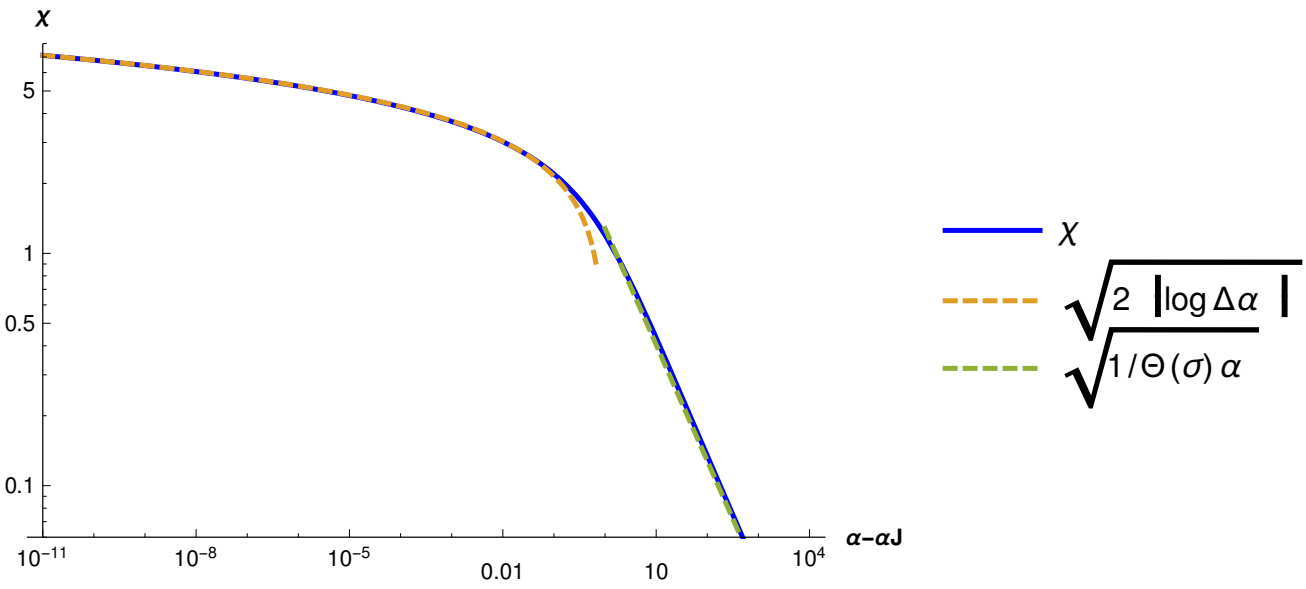

Figure 3.32: Behavior of χ with respect to $\alpha - \alpha_J$ at fixed $\sigma = 0.2$. The dashed lines represent the asymptotic expansions $\chi \underset{\Delta\alpha\to 0}{\simeq} \sqrt{2|\log \Delta\alpha|}$ and $\chi \underset{\alpha\to\infty}{\simeq} \frac{1}{\sqrt{\Theta(\sigma)\ \alpha}}$.

Pressure

In section 3.43 we have defined the pressure p of a configuration as

$$p = \frac{\partial H}{\partial \sigma} = \frac{1}{N}\left(\sum_{o\in\mathcal{O}} 1 + \sum_{c\in\mathcal{C}} f_c\right) \tag{3.119}$$

It is basically the average force in the system, where the overlaps contribute with constant forces equal to 1 and the contacts with forces f_c in the interval $(0, 1)$.
In the RS phase, we can compute its thermodynamic average by

$$p = \frac{\mathrm{d}f_{RS}}{\mathrm{d}\sigma} \tag{3.120}$$

The replica symmetric free energy f_{RS} depends on σ both directly and through the order parameter q_M, therefore

$$p = \frac{\mathrm{d}q_M}{\mathrm{d}\sigma}\frac{\mathrm{d}f_{RS}}{\mathrm{d}q_M} + \frac{\partial f_{RS}}{\partial \sigma} \tag{3.121}$$

We know that the saddle point condition is given by

$$\frac{\mathrm{d}f_{RS}}{\mathrm{d}q_M} = 0 \tag{3.122}$$

so we are left with

$$p = \frac{\partial f_{RS}}{\partial \sigma} \tag{3.123}$$

With f_{RS} given by equation (3.76), we get

$$p = \frac{\alpha}{\beta}\int_{-\infty}^{\infty} dh \gamma_{q_M}(h+\sigma)\frac{d}{dh}f(h) \tag{3.124}$$

In the zero temperature limit $\beta \to \infty$, $q_M \to 1$, we can substitute $f(h)$ with its asymptotic form (3.99):

$$\begin{aligned} p &\underset{\beta\to\infty}{=} \frac{\alpha}{\beta}\int_{-\infty}^{-\chi} dh\gamma(h+\sigma)\beta + \frac{\alpha}{\beta}\int_{-\chi}^{0} dh\gamma(h+\sigma)\frac{-h}{1-q_M} = \\ &= \alpha\int_{-\infty}^{-\chi} dh\gamma(h+\sigma) + \alpha\int_{-\chi}^{0} dh\gamma(h+\sigma)\frac{-h}{\chi} \end{aligned} \tag{3.125}$$

where we have used the fact that $\beta(1-q_M) = \chi$. We can develop further by making simple changes in the dummy variables of the integrals, i.e. $h \to h - \chi$ in the first one and $h \to -\chi\tilde{f}$ in the second one:

$$p = \alpha\int_{-\infty}^{0} dh\gamma(h-\chi+\sigma) + \alpha\chi\int_{0}^{1} d\tilde{f}\gamma(-\chi\tilde{f}+\sigma)\tilde{f} \tag{3.126}$$

Confronting (3.126) with (3.119), there is the strong temptation of identifying $\tilde{f}$ and $\alpha\chi\gamma(-\chi\tilde{f}+\sigma)$ with the contact forces and their distribution, and $\alpha\gamma(h-\chi+\sigma)$ with the distribution of the overlaps $h_o \in (-\infty, 0)$. This interpretation is in fact correct, as we show in appendix A.
To obtain the behavior of p we have to use the saddle point equation for χ (3.105). From (3.125) we can write $\alpha\int_{-\infty}^{-\chi} dh\gamma(h+\sigma) = p - \alpha\int_{-\chi}^{0} dh\gamma(h+\sigma)\frac{-h}{\chi}$ and substitute this expression in (3.105), to obtain

$$p = \frac{1}{\chi^2} - \alpha\int_{-\chi}^{0} dh\gamma(h+\sigma)\frac{h^2}{\chi^2} + \alpha\int_{-\chi}^{0} dh\gamma(h+\sigma)\frac{-h}{\chi} \tag{3.127}$$

We can expand this expression in the unjamming limit $\chi \to \infty$:

$$\begin{aligned} p \underset{\chi\to\infty}{=}\ & \frac{\alpha}{2}\left(e^{-\frac{\sigma^2}{2}}\sqrt{\frac{2}{\pi}} + \sigma\Theta(\sigma)\right)\ \frac{1}{\chi} + \\ & + \left(1 - \alpha\Theta(\sigma) - \frac{\alpha\sigma}{2}\left(e^{-\frac{\sigma^2}{2}}\sqrt{\frac{2}{\pi}} + \sigma\Theta(\sigma)\right)\right)\ \frac{1}{\chi^2} + \\ & + O\left(\frac{e^{-\frac{\chi^2}{2}}}{\chi^3}\right) \end{aligned} \tag{3.128}$$

This relationship establishes the fact that $p \sim \frac{1}{\chi}$ to leading order at unjamming. Therefore we have:

- at σ fixed, when unjamming with $\Delta\alpha = \alpha - \alpha_J \to 0$

$$p \underset{\Delta\alpha\to 0}{=} \frac{k_1}{\sqrt{|\log\Delta\alpha|}} + \frac{k_2}{|\log\Delta\alpha|} + O\left(\frac{\Delta\alpha}{\sqrt{|\log\Delta\alpha|}}\right) \tag{3.129}$$

  with coefficients

$$\begin{aligned} k_1 &= \frac{\alpha_J}{2\sqrt{2}}\left(e^{-\frac{\sigma^2}{2}}\sqrt{\frac{2}{\pi}} + \sigma\Theta(\sigma)\right) \\ k_2 &= \frac{1}{2}\left(1 - \alpha_J\Theta(\sigma) - \frac{\alpha_J\sigma}{2}\left(e^{-\frac{\sigma^2}{2}}\sqrt{\frac{2}{\pi}} + \sigma\Theta(\sigma)\right)\right) \end{aligned} \tag{3.130}$$

- at α fixed, when unjamming with $\Delta\sigma = \sigma - \sigma_J \to 0$

$$p \underset{\Delta\sigma\to 0}{=} \frac{\tilde{k}_1}{\sqrt{|\log\Delta\sigma|}} + \frac{\tilde{k}_2}{|\log\Delta\sigma|} + O\left(\frac{\Delta\sigma}{\sqrt{|\log\Delta\sigma|}}\right) \tag{3.131}$$

with coefficients

$$\begin{aligned} \tilde{k}_1 &= \frac{\alpha k_J}{2\sqrt{2}} \\ \tilde{k}_2 &= \frac{1}{2}\left(1 - \alpha\Theta(\sigma_J) - \frac{\alpha\sigma_J k_J}{2}\right) \\ k_J &= e^{-\sigma_J^2/2}\sqrt{\frac{2}{\pi}} + \sigma_J\left(1 + \mathrm{erf}\left(\frac{\sigma_J}{\sqrt{2}}\right)\right) \end{aligned} \tag{3.132}$$

This result is important because it tells us that the pressure has a logarithmic behavior near the jamming transition:

$$\boxed{p \propto \frac{1}{\sqrt{|\log\delta|}} \qquad \text{@jamming}} \tag{3.133}$$

where δ is the distance from the jamming point, i.e. $\Delta\alpha$ or $\Delta\sigma$ for the perceptron. Notice that this result is valid also for overcompressed sphere packings with linear repulsive potential, where the distance from unjamming is given by $\delta = \phi - \phi_J$, with ϕ the packing fraction [2]. We give an experimental verification of this logarithm for the pressure in chapter 5 for the perceptron and in chapter 4 for finite dimensional linear spheres.

The logarithmic behavior of the pressure could be expected from this reasoning: considering a model with a generic repulsive potential $H = \sum_\mu |h_\mu|^a \theta(-h_\mu)$, with $a > 1$, the perceptron equations give that at unjamming $\frac{1}{\chi} \propto \delta^{a-1}$ and $p \propto \frac{1}{\chi}$, therefore $p \propto \delta^{a-1}$, with δ the distance from unjamming. This scaling is found, theoretically and experimentally, also in finite dimensional overcompressed soft spheres [191, 117, 250, 85]. We see that the exponent $a - 1$ becomes zero for the linear potential $a = 1$: we would expect logarithmic corrections to appear in the scaling, as they do.

We report also the behavior of p when the system is pushed deeply in the UNSAT phase, i.e. $\alpha \to \infty$ or $\sigma \to \infty$.
From the expansions (3.117)-(3.118), we get

$$p \underset{\alpha\to\infty}{=} \alpha + O(\sqrt{\alpha}) \qquad \text{for } \alpha \to \infty \tag{3.134}$$

$$p \underset{\sigma\to\infty}{=} \alpha \qquad \text{for } \sigma \to \infty \tag{3.135}$$

For fixed α, it is clear that the pressure has an upper bound: it reaches the maximum value when all the gaps have become negative. In that case:

$$p = \frac{1}{N}\sum_{o\in\mathcal{O}} 1 = \frac{M}{N} = \alpha \qquad \text{for } \sigma \text{ large} \tag{3.136}$$

[2] In numerical simulations it is easy to see that the pressure has a logarithmic behavior, but it is hard to distinguish between $p \propto \frac{1}{\sqrt{|\log\Delta\phi|}}$ and $p \propto \frac{1}{|\log\Delta\phi|}$.

Energy

The energy corresponds to the UNSAT free energy in the zero temperature limit. Using (3.99) and $\beta(1-q_M)=\chi$ we can write

$$\begin{aligned} f_{RS}\big|_{T=0} &= -\frac{1}{2\chi} - \alpha\int_{-\infty}^{-\chi} dh\gamma(h+\sigma)\left(h+\frac{\chi}{2}\right) + \frac{\alpha}{2\chi}\int_{-\chi}^{0} dh\gamma(h+\sigma)h^2 = \\ &= \frac{1}{2\chi}\left[\alpha\int_{-\chi}^{0} dh\gamma(h+\sigma)h^2 - 1\right] - \alpha\int_{-\infty}^{-\chi} dh\gamma(h+\sigma)\left(h+\frac{\chi}{2}\right) \end{aligned} \tag{3.137}$$

We can now substitute the term 1 in the square brackets of (3.137) with the right hand side of the saddle point equation for χ (3.105):

$$\begin{aligned} f_{RS}\big|_{T=0} &= \frac{1}{2\chi}\left[\alpha\int_{-\chi}^{0} dh\gamma(h+\sigma)h^2 - \chi^2\alpha\int_{-\chi}^{0} dh\gamma(h+\sigma) - \alpha\int_{-\chi}^{0} dh\gamma(h+\sigma)h^2\right] + \\ &- \alpha\int_{-\infty}^{-\chi} dh\gamma(h+\sigma)\left(h+\frac{\chi}{2}\right) = \\ &= -\frac{\chi}{2}\alpha\int_{-\chi}^{0} dh\gamma(h+\sigma) - \alpha\int_{-\infty}^{-\chi} dh\gamma(h+\sigma)\left(h+\frac{\chi}{2}\right) = \\ &= \alpha\int_{-\infty}^{-\chi}\gamma(h+\sigma)|h+\chi| = \\ &= \alpha\int_{-\infty}^{0}\gamma(h-\chi+\sigma)|h| \end{aligned} \tag{3.138}$$

The energy e at zero temperature is therefore

$$e = \alpha\int_{-\infty}^{0}\gamma(h-\chi+\sigma)|h| \tag{3.139}$$

At the unjamming $\chi\to\infty$,

$$e \underset{\chi\to\infty}{=} \alpha\frac{e^{-\frac{(\chi-\sigma)^2}{2}}}{\sqrt{2\pi}\chi^2} + O\left(\frac{e^{-\frac{\chi^2}{2}}}{\chi^3}\right) \tag{3.140}$$

that gives

- for fixed σ, unjamming with $\Delta\alpha=\alpha-\alpha_J\to 0$

$$e \underset{\Delta\alpha\to 0}{\simeq} \frac{1}{\sqrt{2}\alpha_J}\frac{\Delta\alpha}{\sqrt{|\log\Delta\alpha|}} \tag{3.141}$$

- for fixed α, unjamming with $\Delta\sigma=\sigma-\sigma_J\to 0$

$$e \underset{\Delta\sigma\to 0}{\simeq} \frac{\alpha k_J}{\sqrt{2}}\frac{\Delta\sigma}{\sqrt{|\log\Delta\sigma|}} \tag{3.142}$$

This result tells that, with the linear potential, the energy near the jamming transition behaves linearly plus logarithmic corrections:

$$\boxed{e\propto\frac{\delta}{\sqrt{|\log\delta|}} \qquad \text{@jamming}} \tag{3.143}$$

where δ represents the distance from the jamming point (i.e. $\Delta\alpha$ or $\Delta\sigma$ for the perceptron). In chapter 4, we show that this is true also for spheres with linear repulsion in finite dimensions (in that case δ is $\phi - \phi_J$, with ϕ the packing fraction). As already discussed for pressure, a repulsive potential $\nu(h) = |h|^a\theta(-h)$ gives a behavior $e \sim \delta^a$ for the energy near the jamming transition, both in mean-field models (perceptron) and finite dimensional packings [191]. We have shown that in the linear case $a = 1$ the scaling of the energy has logarithmic corrections, necessary to give a logarithmic behavior to the pressure.

Distribution of gaps and forces

As shown in the appendix A, in the replica symmetric phase the distribution of gaps is given by

$$g(h) = \theta(h)\gamma(h+\sigma) + \ \delta(h)\int_{-\chi}^{0} dz\gamma(z+\sigma) + \theta(-h)\gamma(h+\sigma-\chi) \tag{3.144}$$

and the associated contact force distribution (normalized to 1) reads

$$\rho(\tilde{f}) = \frac{\gamma\left(-\chi\tilde{f}+\sigma\right)}{\int_0^1 d\tilde{f}\ \gamma\left(-\chi\tilde{f}+\sigma\right)}, \qquad \tilde{f} \in (0,1) \tag{3.145}$$

We notice that, in the replica symmetric phase, the distributions of gaps and forces are Gaussian distributions restricted to intervals.
As a consistency check, we can compute the energy through this definition of $g(h)$

$$e = \int_{-\infty}^{0} dh g(h)|h| = \int_{-\infty}^{0} dh\gamma(h+\sigma-\chi)|h| \tag{3.146}$$

and we get the same expression as in eq. (3.139), obtained in a different manner.
The interesting quantity is the weight of the Dirac delta in $h = 0$, that gives the number of gaps equal to zero, i.e. the number of contacts. In equation (3.144), $g(h)$ is normalized to 1, therefore it corresponds to $g(h) = \langle \frac{1}{M}\sum_\mu \delta(h - h_\mu)\rangle$, where M is the total number of gaps (i.e. the total number of patterns). To normalize with respect to N instead of M, we can simply multiply by $\alpha = \frac{M}{N}$. Therefore, the weight of $\delta(h)$ in (3.144) multiplied by α corresponds exactly to the isostaticity index $c = C/N$, with C the number of contacts:

$$\boxed{c = \alpha\int_{-\chi}^{0} dh\gamma(h+\sigma)} \tag{3.147}$$

As we have seen in the section 3.1.3 on the numerical simulations, this quantity plays a crucial role in our system. We show in the next section 3.3.2 that it enters directly in determining the stability of the replica symmetric solution.

3.3.2 The replica symmetry breaking transition line

To check the stability of the replica symmetric solution, it is necessary to compute the smallest eigenvalue of the Hessian of the free energy with respect to the overlap matrix: this eigenvalue is called the replicon eigenvalue. As computed for the general case in equation (2.53), we have

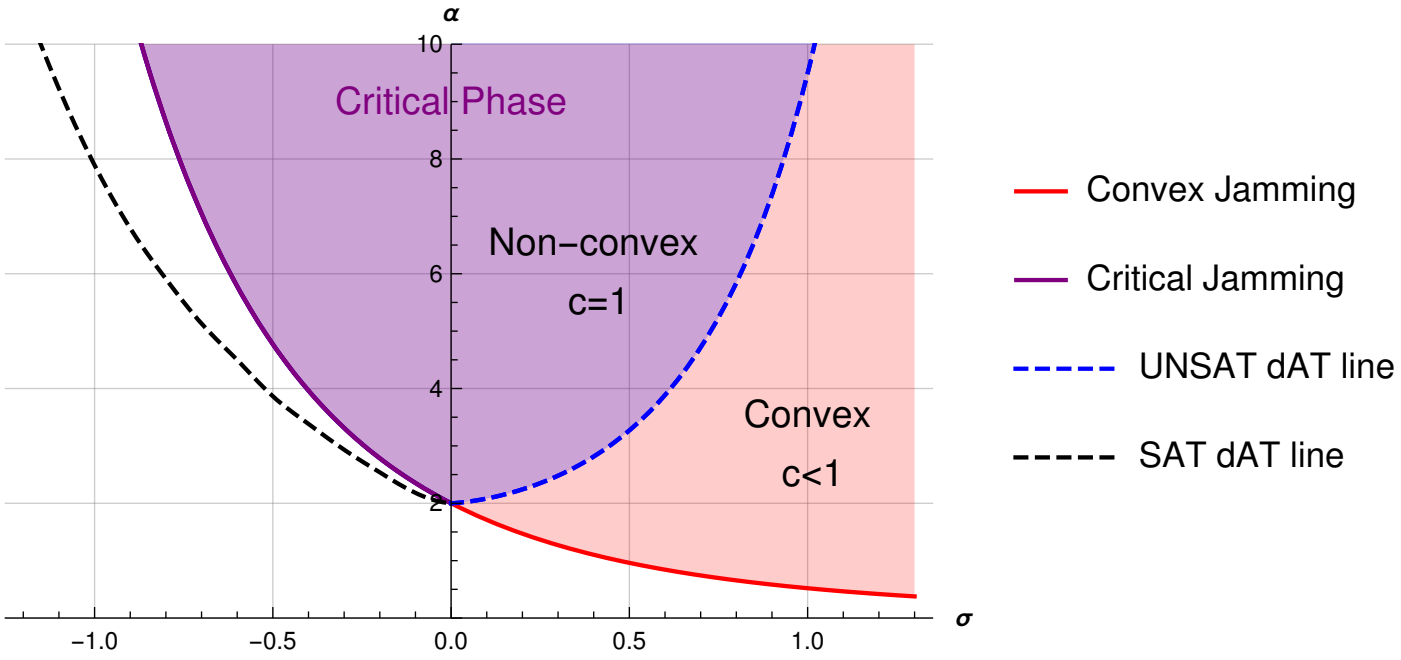

Figure 3.33: Phase diagram of the linear perceptron

$$\lambda_{\text{replicon}} \propto \frac{1}{(1-q_M)^2} - \alpha \int_{-\infty}^{\infty} dh \gamma_{q_M}(h+\sigma) \left[\frac{\mathrm{d}^2}{\mathrm{d}h^2} f(q_M, h)\right]^2 \tag{3.148}$$

In the zero temperature limit, using the expression (3.101), we have

$$\lambda_{\text{replicon}} \propto 1 - \alpha \int_{-\chi}^{0} dh \gamma(h+\sigma) \tag{3.149}$$

We recognize that $\alpha \int_{-\chi}^{0} dh\gamma(h+\sigma)$ is the isostaticity index c obtained in (3.147), therefore

$$\boxed{\lambda_{\text{replicon}} \propto 1 - c} \tag{3.150}$$

This result tell us that the replica symmetric solution is stable as long as the system is hypostatic ($c < 1$). As soon as the system gets isostatic, $c = 1$ and the replicon becomes equal to zero. The deAlmeida-Touless line, defining the limit of stability of the RS solution, is given by the condition $c = 1$:

$$\alpha \int_{-\chi}^{0} dh \gamma(h+\sigma) = 1 \tag{3.151}$$

Solving eq. (3.151) together with the equation for χ (3.105) gives the deAlmeida-Touless line (dAT).

Spherical Lagrange multiplier

To see that the instability of the RS solution and the occurrence of isostaticity coincide with the change of convexity, we need to compute the Lagrange multiplier of the spherical constraint. This can be done using replicas and the computation is reported in the

appendix B. Here we just report the formula for the RS case in the zero temperature limit (B.22):

$$\eta = \frac{1}{\chi}\left[1 - \alpha \int_{-\chi}^{0} \gamma(h+\sigma)\right] \tag{3.152}$$

We recognize the isostaticity index $c = \alpha \int_{-\chi}^{0} \gamma(h+\sigma)$ and write

$$\boxed{\eta = \frac{1}{\chi}(1-c) \qquad \text{in RS phase}} \tag{3.153}$$

This formula implies that the hypostatic/isostatic transition corresponds to the point where the Lagrange multiplier becomes zero and the problem changes from convex to non-convex, since η corresponds to the effective curvature of the energy landscape. In fact, using the RS expression (3.152) as an approximation in the non-convex phase, it gives a negative η, as observed in the simulations.
Equation (3.152) also implies that at the unjamming transition $\eta \to 0$ since $\chi \to \infty$, with the scaling

$$\begin{aligned} &\eta \sim \frac{1}{\chi} \\ &\eta \sim p \qquad \text{@jamming} \end{aligned} \tag{3.154}$$

Therefore η has a logarithmic scaling with respect to the distance from unjamming, as we have found for the pressure (3.133).

3.3.3 A scaling ansatz for the replica-symmetry-broken phase

In the non-convex isostatic phase, the replica symmetry is broken. We show in the appendix C that the transition is to a $full$RSB phase. Therefore the physical quantities have to be computed by solving the partial differential equations found in section 2.3 (in the following, dots are the derivative with respect to q and primes those w.r.t. h):

$$\begin{cases} \dot{f}(q,h) & = -\frac{1}{2}\left[f''(q,h) + x(q)(f'(q,h))^2\right] \qquad q_m < q < q_M \\ f(q_M,h) & = \log \gamma_{1-q_M} * e^{-\beta\,\nu(h)} \end{cases} \tag{3.155}$$

$$\begin{cases} \dot{P}(q,h) & = \frac{1}{2}\left[P''(q,h) - 2\frac{x(q)}{\lambda(q)}\left(f'(q,h)P(q,h)\right)'\right] \qquad q_m < q < q_M \\ P(q_m,h) & = \frac{1}{\sqrt{2\pi q_m}} e^{-\frac{(h+\sigma)^2}{2q_m}} \end{cases} \tag{3.156}$$

$$\begin{aligned} &\frac{q_m}{\lambda(q_m)^2} + \int_{q_m}^{q} dp \frac{1}{\lambda^2(p)} = \alpha \int_{-\infty}^{\infty} dh P(q,h)\left(f'(q,h)\right)^2 \\ &\lambda(q) = 1 - q_M + \int_{q}^{q_M} dp x(p) \end{aligned} \tag{3.157}$$

In addition, marginal stability of the $full$RSB solution implies

$$\begin{aligned} \frac{1}{\lambda^2(q)} &= \alpha \int_{-\infty}^{\infty} dh P(q,h)\left(f''(q,h)\right)^2 \\ x(q) &= \frac{\lambda(q)}{2} \frac{\int_{-\infty}^{\infty} dh P(q,h)\left(f'''(q,h)\right)^2}{\int_{-\infty}^{\infty} dh P(q,h)\left(f''(q,h)\right)^2 \left(1+\lambda(q) f''(q,h)\right)} \end{aligned} \tag{3.158}$$

The equations (3.155)-(3.156)-(3.157) are completely general and the only connection to the model we are studying comes from the initial condition of the function $f(q,h)$ in (3.155), where the potential $\nu(h)$ appears:

$$f(q_M,h) = \log \gamma_{1-q_M} * e^{-\beta|h|\theta(-h)} \tag{3.159}$$

This function is the one we already studied in equation (3.99) for the replica symmetric solution. Using it as initial condition, it is necessary to solve (3.155)-(3.156)-(3.157) to get $P(q_M,h)$. In fact, we have seen in appendix A that the distribution of gaps $g(h)$ is given by

$$g(h) \underset{q\to 1}{=} \theta(h)P(q,h) + \ \delta(h)\int_{-\hat{\lambda}(q)}^{0} dz P(q,z) + \theta(-h)P(q,h-\hat{\lambda}(q)) \tag{3.160}$$

with the isostaticity index

$$c = \alpha \int_{-\hat{\lambda}(q)}^{0} dz P(q,z) \tag{3.161}$$

where $\hat{\lambda}(q)$ is the function $\lambda(q)$ defined in (3.157) scaled by β:

$$\hat{\lambda}(q) = \beta(1-q_M) + \beta\int_{q}^{q_M} dp\ x(p) \tag{3.162}$$

We notice that $\lambda(q_M) = 1-q_M$. Since we have seen in (3.101) that in the zero temperature limit $f''(q_M,h) = -\frac{1}{1-q_M}\mathbb{I}\left(-\chi < h < 0\right)$, we can assume that a good scaling form for $f''(q,h)$ in the limit $q \to q_M \to 1$ is

$$f''(q,h) = -\frac{1}{\lambda(q)}\mathbb{I}\left(-\hat{\lambda}(q) < h < 0\right) \tag{3.163}$$

Plugging this expression into the marginal stability condition (3.157)

$$\frac{1}{\lambda^2(q)} = \alpha\int_{-\infty}^{\infty} dh P(q,h)\left(f''(q,h)\right)^2 \tag{3.164}$$

we get

$$\boxed{c = \alpha\int_{-\hat{\lambda}(q)}^{0} dh P(q,h)\Big|_{q\to 1} = 1} \tag{3.165}$$

where we have recognized the expression (3.161) of the isostaticity index c. This equation makes the connection between the marginal stability of the $full$RSB solution and the isostaticity that is observed in simulations:

$$\text{marginal stability} \longleftrightarrow \text{isostaticity}$$

Scaling form of the solution

There is no obvious way to solve (3.155)-(3.156)-(3.157) analytically and it is necessary to rely on numerical methods. However, we are not interested in getting the complete distribution $g(h)$. Instead, we would like to obtain a scaling theory describing the critical properties of the model in the zero temperature limit. We perform this task in analogy with the jamming solution of the infinite dimensional spheres [62, 200] and the jamming

of the perceptron [105](reported in section 2.3.4).

First of all, the linear response theory $q_M \simeq 1 - \chi T$, valid in the RS phase, does not work in the $full$RSB phase, as it happens also in other models [180]. Now we have

$$q_M \sim 1 - \chi T^{\kappa} \tag{3.166}$$

for an appropriate exponent κ. From the construction of the $full$RSB ansatz, it can be seen that $x(q)$ is proportional to T for low temperatures [195, 237, 180], therefore

$$y(q) = \beta x(q) \tag{3.167}$$

is a finite quantity. Moreover, from the breaking point $x(q_M)\Big|_{dAT\ line}$ (appendix C), we deduce that $x(q_M)$ is finite at zero temperature, implying that $\beta x(q_M)$ is divergent: therefore $y(q)$ has to diverge for $q \to q_M \to 1$. Consistently with (3.166), we make the ansatz

$$y(q) \sim \frac{y_\chi}{(1-q)^{\frac{1}{\kappa}}}, \qquad q \to 1 \tag{3.168}$$

for some constant y_χ. In fact, at $q = q_M$, $y(q_M) \sim y_\chi (1-q_M)^{-\frac{1}{\kappa}} \simeq y_\chi \chi^{-\frac{1}{\kappa}} \frac{1}{T}$, consistent with the fact that $y(q_M) = \beta x(q_M)$ has to diverge as $\frac{1}{T}$.
Now we have

$$\hat{\lambda}(q) = \beta\lambda(q) = \beta(1-q_M) + \int_q^{q_M} dp\ y(p) \tag{3.169}$$

Looking at the asymptotic form of $f(q_M, h)$ (3.99)

$$f(q_M,h)\Big|_{q_M\to 1,\beta\to\infty} = \begin{cases} 0 & h >> \sqrt{1-q_M} \\ \mathcal{F}\left(\frac{h}{\sqrt{1-q_M}}\right) & h \sim O\left(\sqrt{1-q_M}\right) \\ -\frac{h^2}{2(1-q_M)} & -\chi < h < 0 \\ \beta\left(h+\frac{\chi}{2}\right) + \mathcal{F}\left(-\frac{h+\chi}{\sqrt{1-q_M}}\right) & h+\chi \sim O\left(\sqrt{1-q_M}\right) \\ \beta\left(h+\frac{\chi}{2}\right) & h << -\chi - \sqrt{1-q_M} \end{cases} \tag{3.170}$$

we assume the scaling form for $q \to q_M \to 1$:

$$f(q,h) = \begin{cases} 0 & h >> \sqrt{1-q} \\ \hat{\mathcal{F}}\left(\frac{h}{\sqrt{1-q}}\right) & h \sim O\left(\sqrt{1-q}\right) \\ -\frac{h^2}{2\hat{\lambda}(q)} & -\hat{\lambda}(q) < h < 0 \\ \beta\left(h+\frac{\hat{\lambda}(q)}{2}\right) + \hat{\mathcal{F}}\left(-\frac{h+\hat{\lambda}(q)}{\sqrt{1-q}}\right) & h+\hat{\lambda}(q) \sim O\left(\sqrt{1-q}\right) \\ \beta\left(h+\frac{\hat{\lambda}(q)}{2}\right) & h << -\hat{\lambda}(q) - \sqrt{1-q} \end{cases} \tag{3.171}$$

where we have not guessed the scaling of the matching parts $\hat{\mathcal{F}}$ yet. For convenience, instead of using $f(q,h)$, the solution is studied for a rescaled form of $f'(q,h)$:

$$m(q,h) = \lambda(q) f'(q,h) = \begin{cases} 0 & h >> \sqrt{1-q} \\ -\sqrt{1-q}\ \mathcal{M}_+\left(\frac{h}{\sqrt{1-q}}\right) & h \sim O\left(\sqrt{1-q}\right) \\ -h & -\hat{\lambda}(q) < h < 0 \\ \hat{\lambda}(q) + \sqrt{1-q}\ \mathcal{M}_-\left(-\frac{h+\hat{\lambda}(q)}{\sqrt{1-q}}\right) & h+\hat{\lambda}(q) \sim O\left(\sqrt{1-q}\right) \\ \hat{\lambda}(q) & h << -\hat{\lambda}(q) - \sqrt{1-q} \end{cases} \tag{3.172}$$

where now we have inserted two scaling functions $\mathcal{M}_+$ and $\mathcal{M}_-$. They have to satisfy the boundary conditions

$$\begin{array}{ll} \mathcal{M}_+(t\to\infty)=0 & \mathcal{M}_-(t\to\infty)=0 \\ \mathcal{M}_+(t\to-\infty)=t & \mathcal{M}_-(t\to-\infty)=t \end{array} \tag{3.173}$$

to match the other parts of the function. We can write the equation for $m(q,h)$ by substituting $f'(q,h)=m(q,h)/\lambda(q)$ in the equation for $f(q,h)$ (3.155):

$$\begin{cases} \dot{m}(q,h) & = -\frac{1}{2}m''(q,h) - \frac{x(q)}{\lambda(q)}m(q,h)\left[1+m'(q,h)\right] \\ m(q_M,h) & = (1-q_M)\frac{\partial}{\partial h}\ln\gamma_{1-q_M} * e^{-\beta|h|\theta(-h)} \end{cases} \tag{3.174}$$

The presence of the two matching regimes for $m(q,h)$ suggest something similar for the function $P(q,h)$. Therefore, for $q\to 1$ we guess a form of the kind

$$P(q,h)=\begin{cases} p_+(h) & h >> \sqrt{1-q} \\ (1-q)^{-\frac{a}{\kappa}}\ p_0\left(\frac{h}{\sqrt{1-q}}\right) & h\sim O\left(\sqrt{1-q}\right) \\ \frac{1}{\hat{\lambda}(q)}\ p_-\left(\frac{h}{\hat{\lambda}(q)}\right) & -\hat{\lambda}(q)<h<0 \\ (1-q)^{-\frac{\tilde{a}}{\kappa}}\tilde{p}_0\left(-\frac{h+\hat{\lambda}(q)}{\sqrt{1-q}}\right) & h+\hat{\lambda}(q)\sim O\left(\sqrt{1-q}\right) \\ \tilde{p}_+(h) & h << -\hat{\lambda}(q)-\sqrt{1-q} \end{cases} \tag{3.175}$$

that has to satisfy eq. (3.156)

$$\begin{cases} \dot{P}(q,h) & = \frac{1}{2}P''(q,h) - \frac{x(q)}{\lambda(q)}\left(P(q,h)m(q,h)\right)' \\ P(q_m,h) & = \frac{1}{\sqrt{2\pi q_m}}e^{-\frac{(h+\sigma)^2}{2q_m}} \end{cases} \tag{3.176}$$

Both the equations of m and P depend on the ratio $\frac{x(q)}{\lambda(q)}=\frac{\beta x(q)}{\beta\lambda(q)}=\frac{y(q)}{\hat{\lambda}(q)}$. Therefore

$$\begin{aligned} \frac{x(q)}{\lambda(q)} &\simeq \frac{y_\chi(1-q)^{-\frac{1}{\kappa}}}{\beta(1-q_M)+\int_q^{q_M}dp\ y_\chi(1-p)^{-\frac{1}{\kappa}}} = \\ &= \frac{y_\chi(1-q)^{-\frac{1}{\kappa}}}{\left[\chi^{\frac{1}{\kappa}}-\frac{\kappa}{\kappa-1}y_\chi\right](1-q_M)^{\frac{\kappa-1}{\kappa}}+\frac{\kappa}{\kappa-1}y_\chi(1-q)^{\frac{\kappa-1}{\kappa}}} \end{aligned} \tag{3.177}$$

where we have used $1-q_M=\chi T^\kappa$. It is fundamental to clarify that we are studying the regime $q\to 1$ but with $q << q_M$ so that the second term of the denominator dominates. Therefore

$$\frac{y(q)}{\hat{\lambda}(q)}\sim\frac{\kappa-1}{\kappa}\frac{1}{1-q},\qquad q\to 1,\ q<<q_M \tag{3.178}$$

Scaling equations

Now we consider the interval $h \sim O(\sqrt{1-q})$ where the functions $\mathcal{M}$ and p_0 appear. Noticing that for $m(q,h) = -\sqrt{1-q}\mathcal{M}\left(\frac{h}{\sqrt{1-q}}\right)$:

$$\begin{aligned} \dot{m}(q,h) &= \frac{1}{2\sqrt{1-q}}\mathcal{M}_+\left(\frac{h}{\sqrt{1-q}}\right) - \frac{h}{2(1-q)}\mathcal{M}'_+\left(\frac{h}{\sqrt{1-q}}\right) \\ m'(q,h) &= -\mathcal{M}'_+\left(\frac{h}{\sqrt{1-q}}\right) \\ m''(q,h) &= -\frac{1}{\sqrt{1-q}}\mathcal{M}''_+\left(\frac{h}{\sqrt{1-q}}\right) \end{aligned} \tag{3.179}$$

and calling $t = \frac{h}{\sqrt{1-q}}$, we can insert the scaling expression of $m(q,h)$ into its equation (3.174) and, using (3.178), obtain

$$\mathcal{M}_+(t) - t\mathcal{M}'_+(t) = \mathcal{M}''_+(t) + 2\frac{\kappa-1}{\kappa}\mathcal{M}_+(t)\left[1 - \mathcal{M}'_+(t)\right] \tag{3.180}$$

This equation for $\mathcal{M}_+$ is to be solved together with its boundary conditions

$$\mathcal{M}_+(t\to\infty) = 0 \qquad \mathcal{M}_+(t\to-\infty) = t \tag{3.181}$$

We repeat the same procedure plugging $P(q,h) = (1-q)^{-\frac{a}{\kappa}}p_0\left(\frac{h}{\sqrt{1-q}}\right)$ into its equation (3.176) and we obtain

$$\frac{a}{\kappa}p_0(t) + \frac{1}{2}t\ p'_0(t) = \frac{p''_0(t)}{2} + \frac{\kappa-1}{\kappa}\left[p_0(t)\mathcal{M}_+(t)\right]' \tag{3.182}$$

with boundary conditions

$$p_0(t\to\infty) = t^{-2\frac{a}{\kappa}} \qquad p_0(t\to-\infty) = |t|^{2(1-\kappa+a)/(\kappa-2)} \tag{3.183}$$

The universal equations (3.180) and (**??**) are the same as those found at the jamming transition of spheres, and we have obtained them also in section (2.3.4) when presenting the jamming transition in the perceptron. The function p_0 is related to the exponents of the distributions of small positive gaps and small forces.

Now we consider the interval $h + \hat{\lambda}(q) \sim O(\sqrt{1-q})$ where the functions $\mathcal{M}_-$ and $\tilde{p}_0$ appear. Noticing that for $m(q,h) = \hat{\lambda}(q) + \sqrt{1-q}\mathcal{M}_-\left(-\frac{h+\hat{\lambda}(q)}{\sqrt{1-q}}\right)$:

$$\begin{aligned} \dot{m}(q,h) &= -y(q) - \frac{1}{2\sqrt{1-q}}\mathcal{M}_-\left(-\frac{h+\hat{\lambda}(q)}{\sqrt{1-q}}\right) - \frac{h+\hat{\lambda}(q)}{2(1-q)}\mathcal{M}'_-\left(-\frac{h+\hat{\lambda}(q)}{\sqrt{1-q}}\right) + y(q)\mathcal{M}'_-\left(-\frac{h+\hat{\lambda}(q)}{\sqrt{1-q}}\right) \\ m'(q,h) &= -\mathcal{M}'_-\left(-\frac{h+\hat{\lambda}(q)}{\sqrt{1-q}}\right) \\ m''(q,h) &= \frac{1}{\sqrt{1-q}}\mathcal{M}''_-\left(-\frac{h+\hat{\lambda}(q)}{\sqrt{1-q}}\right) \end{aligned} \tag{3.184}$$

and calling $t = -\frac{h+\hat{\lambda}(q)}{\sqrt{1-q}}$, we can insert the scaling expression of $m(q,h)$ into its equation (3.174) and, using (3.178), obtain

$$\mathcal{M}_-(t) - t\mathcal{M}'_-(t) = \mathcal{M}''_-(t) + 2\frac{\kappa-1}{\kappa}\mathcal{M}_-(t)\left[1-\mathcal{M}'_-(t)\right] \tag{3.185}$$

with boundary conditions

$$\mathcal{M}_-(t\to\infty) = 0 \qquad \mathcal{M}_-(t\to-\infty) = t \tag{3.186}$$

We see that the function $\mathcal{M}_-$ is the same as the function $\mathcal{M}_+$.

We have therefore discovered that the equation (3.174) has a structure:

$$\textbf{if } m(q,h) = -\sqrt{1-q}\mathcal{M}\left(\tfrac{h}{\sqrt{1-q}}\right) \textbf{ is a solution,}$$
$$\textbf{then } \tilde{m}(q,h) = \hat{\lambda}(q) + \mathcal{M}\left(-\tfrac{h+\hat{\lambda}(q)}{\sqrt{1-q}}\right) \textbf{ is a solution as well.}$$

This structure has consequences on $P(q,h)$. We repeat the same procedure plugging $P(q,h) = (1-q)^{-\frac{\tilde{a}}{\kappa}}\tilde{p}_0\left(-\frac{h+\hat{\lambda}(q)}{\sqrt{1-q}}\right)$ and $m(q,h) = \hat{\lambda}(q) + \sqrt{1-q}\mathcal{M}_-\left(-\frac{h+\hat{\lambda}(q)}{\sqrt{1-q}}\right)$ into (3.176); calling $t = -\frac{h+\hat{\lambda}(q)}{\sqrt{1-q}}$, we obtain

$$\frac{\tilde{a}}{\kappa}\tilde{p}_0(t) + \frac{1}{2}t\,\tilde{p}'_0(t) = \frac{\tilde{p}''_0(t)}{2} + \frac{\kappa-1}{\kappa}\left[\tilde{p}_0(t)\mathcal{M}_-(t)\right]' \tag{3.187}$$

with boundary conditions

$$\tilde{p}_0(t\to\infty) = t^{-2\frac{\tilde{a}}{\kappa}} \qquad \tilde{p}_0(t\to-\infty) = |t|^{2(1-\kappa+\tilde{a})/(\kappa-2)} \tag{3.188}$$

Since we have seen that $\mathcal{M}_-(t) = \mathcal{M}_+(t)$, this is the same equation as (3.182), therefore

$$\boxed{\begin{array}{c}\tilde{p}_0(t) = p_0(t)\\ \mathcal{M}_-(t) = \mathcal{M}_+(t)\\ \tilde{a} = a\end{array}} \tag{3.189}$$

To complete the picture, we need the equation fixing the exponent κ as a function of $\mathcal{M}_+$ (that now we simply call $\mathcal{M}$) and p_0. This is given by the marginal stability condition (3.158)

$$\frac{y(q)}{\hat{\lambda}(q)} = \frac{1}{2}\frac{\int_{-\infty}^{\infty} dh P(q,h) m''(q,h)^2}{\int_{-\infty}^{\infty} dh P(q,h) m'(q,h)^2\left[1+m'(q,h)\right]} \tag{3.190}$$

that, using (3.178), the scaling forms for $P(q,h)$ and $m(q,h)$, and the equalities (3.189), becomes

$$\frac{\kappa-1}{\kappa} = \frac{1}{2}\frac{\int dt p_0(t)\mathcal{M}''(t)^2}{\int dt p_0(t)\mathcal{M}'(t)^2\left[1-\mathcal{M}'(t)\right]} \tag{3.191}$$

This equation corresponds to the one controlling the exponents of the jamming transition (2.113). Since also the equations (3.180) and (3.182) for $\mathcal{M}$ and p_0 are the same as those found at jamming, then also κ and all the other critical exponents are the same.

The important physical consequence of the equalities (3.189) is that the power laws of the distributions of small positive and negative gaps have the same exponents. The same is valid for the pseudo-gaps of the distribution of contact forces near 0 and near 1 In fact, the matching conditions

$$\begin{aligned} p_0(t)\Big|_{t\to\infty} &\sim t^{-\gamma} \Rightarrow g(h\to 0^+) \sim h^{-\gamma} \\ p_0(t)\Big|_{t\to-\infty} &\sim |t|^{\theta} \Rightarrow \rho(f\to 0^+) \sim f^{\theta} \end{aligned} \tag{3.192}$$

relate the asymptotic behavior of p_0 with the physical distributions. Analogously, we have

$$\begin{aligned} \tilde{p}_0(-t)\Big|_{t\to-\infty} &\sim |t|^{-\tilde{\gamma}} \Rightarrow g(h\to 0^-) \sim |h|^{-\tilde{\gamma}} \\ \tilde{p}_0(-t)\Big|_{t\to+\infty} &\sim t^{\tilde{\theta}} \quad \Rightarrow \rho(f\to 1^-) \sim (1-f)^{\tilde{\theta}} \end{aligned} \tag{3.193}$$

In principle, the functions p_0 and $\tilde{p}_0$ could be different and so also the exponents γ, $\tilde{\gamma}$ and θ, $\tilde{\theta}$ would be different. Because of the structure we have seen in the scaling equations, the equality $p_0 = \tilde{p}_0$ holds and so also the exponents are all equal to the jamming ones [62, 64, 105]:

$$\boxed{\begin{aligned} \kappa &\simeq 1.41574 \\ \theta &\simeq 0.42311 \\ \gamma &\simeq 0.41269 \\ a &\simeq 0.29213 \end{aligned}} \tag{3.194}$$

with the relationships between them

$$\begin{aligned} a &= 1 - \frac{\kappa}{2} \\ \gamma &= \frac{2-\kappa}{\kappa} \\ \theta &= \frac{3\kappa - 4}{2-\kappa} \\ \gamma &= \frac{1}{2+\theta} \end{aligned} \tag{3.195}$$

Solving the scaling equations

We solve numerically the equations (3.201) and we confirm the values of the critical exponents reported in the literature [200, 62].
The ODEs and the boundary conditions for $\mathcal{M}(t)$ and $p_0(t)$ define a boundary value problem for these functions. At fixed κ, we find the solution $\mathcal{M}(t)$. We verify that the solution of the equation for $p_0(t)$ only converges for a single value of a depending on κ. Therefore we solve the boundary value problem with the BVP solver [138, 219] implemented in the library Scipy [240], keeping a as an unknown variable that is found by the algorithm. The last equation of (3.201) is a closure equation that gives κ as a function of $\mathcal{M}(t)$ and $p_0(t)$. We can therefore iterate finding the value of κ that gives $\mathcal{M}$ and p_0 consistent with the closure equation. Our algorithm converges to the values of the exponents:

$$\kappa = 1.4157(3) \qquad a = 0.2921(3) \tag{3.196}$$

where the uncertain digit is in brackets. These values verify the relationship $a = 1 - \frac{\kappa}{2}$ and we confirm the fact that $\kappa \neq \sqrt{2}$.

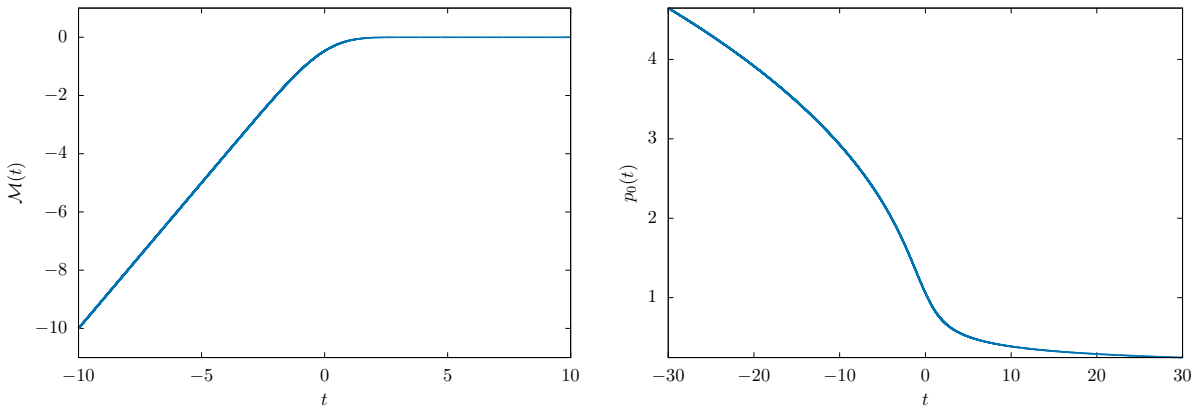

Figure 3.34: Functions $\mathcal{M}(t)$ (left panel) and $p_0(t)$ (right panel) obtained by the numerical solution of the scaling equations (3.201) for the values $\kappa \simeq 1.4157$ and $a \simeq 0.2921$.

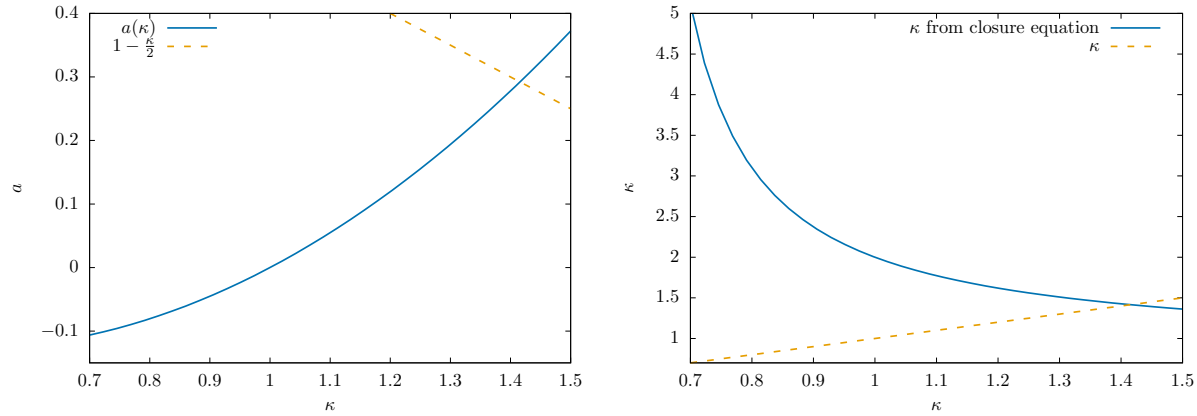

Figure 3.35: Left panel: the value of a, depending on κ, that makes the equation of p_0 solvable; the algorithm converges to the single value satisfying $a = 1 - \frac{\kappa}{2}$. Right panel: the blue line represents κ computed from the closure equation (i.e. the last equation of (3.201)) with respect to the value of κ used for the functions $\mathcal{M}$ and p_0. The two values of κ must be the same: the algorithm converges to the fixed point of the blue line.

3.4 A scaling theory for the critical phase

In the non-convex phase, the perceptron with linear potential displays isostaticity and jamming-like criticality. The distribution of gaps near zero has the form

$$g(h) \sim |h|^{-\gamma} + \frac{1}{\alpha}\delta(h), \qquad h \to 0^{\pm} \tag{3.197}$$

where the factor $\frac{1}{\alpha}$ comes from the normalization over the total number of gaps $M = \alpha N$. The zero-gaps are associated to contact forces $f_c \in (0,1)$ whose distribution has a power-law behavior near the bounds of the domain $f \sim 0^+$ and $f \sim 1^-$:

$$\begin{aligned} &\rho(f) \sim f^{\theta}, && f \to 0^+ \\ &\rho(f) \sim (1-f)^{\theta}, && f \to 1^- \end{aligned} \tag{3.198}$$

The value of these exponents depend on an exponent κ

$$\gamma = \frac{2-\kappa}{\kappa} \tag{3.199}$$

$$\theta = \frac{3\kappa - 4}{2-\kappa} \tag{3.200}$$

that is found by solving the scaling theory

$$\begin{cases} \mathcal{M}(t) - t\mathcal{M}'(t) = \mathcal{M}''(t) + 2\frac{\kappa-1}{\kappa}\mathcal{M}(t)\left[1-\mathcal{M}'(t)\right], \qquad \mathcal{M}(t\to\infty) = 0,\ \mathcal{M}(t\to-\infty) = t \\ \frac{a}{\kappa}p_0(t) + \frac{1}{2}t\ p_0'(t) = \frac{p_0''(t)}{2} + \frac{\kappa-1}{\kappa}\left[p_0(t)\mathcal{M}(t)\right]', \quad p_0(t\to\infty) = t^{-2\frac{a}{\kappa}},\ p_0(t\to-\infty) = |t|^{2\frac{1-\kappa+a}{\kappa-2}} \\ \frac{\kappa-1}{\kappa} = \frac{1}{2}\frac{\int dt p_0(t)\mathcal{M}''(t)^2}{\int dt p_0(t)\mathcal{M}'(t)^2[1-\mathcal{M}'(t)]} \end{cases} \tag{3.201}$$

The exponents γ and θ verify the relationship

$$\gamma = \frac{1}{2+\theta} \tag{3.202}$$

that is connected to marginal stability (and therefore isostaticity).

Meaning of the exponent κ

The exponent κ has a central role in the scaling theory. In replica theory, it appears in the function $y(q)$

$$y(q) \sim \frac{1}{(1-q)^{\frac{1}{\kappa}}} \tag{3.203}$$

that controls the distribution of distances $1-q$ between states in the glassy phase. The divergence of $y(q)$ for $q \to 1$ implies a large number of states close to each other. Marginal stability suggests that, when a zero temperature equilibrium configuration is slightly perturbed, the system starts moving until it falls in a nearby stable state. The availability of nearby states is controlled by the exponent κ, that therefore enters in describing the response of the system to perturbation. The theory of this critical dynamics in the replica framework is done in [110] and it shows that κ enters in the distribution of avalanches of the response of the system. In chapter 5, we use a compression algorithm in the critical phase of the perceptron with linear cost function and we confirm the predictions of the theory, in excellent agreement with the value of $\kappa \simeq 1.416$ being the one obtained in the jamming theory (3.3.3).

3.4.1 Non-linear excitations

The excitations in the critical phase of our model are strictly non-linear. In fact, a stable configuration is defined by the associated $N-1$ zero-gaps, the contacts (plus the spherical constraint). The configuration is therefore the point of intersection of $N-1$ random planes with the N-sphere. Since the cost function is linear, the energy landscape around the point is made of ramps with linearly increasing energy. Such an angular point does not admit a harmonic approximation. Perturbing the system, instead, necessarily breaks some contacts, and the system stabilizes again only when new contacts are formed and isostaticity is restored. The excitations of the system, therefore, cannot be understood in terms of harmonic fluctuations around some minima, but only as a dynamics of opening and closing contacts. This mechanism is akin to excitations of packing of spheres at the jamming point. In fact, scaling arguments about the excitations that can be induced in an isostatic system of spheres [247] can easily be generalized to the critical phase of the linear perceptron.

Marginal stability argument

Consider an isostatic stable configuration $\mathbf{X}$ in the critical phase of the perceptron with linear cost function, with an isostatic number of contacts $h_c = 0$, $c \in \mathcal{C}$, associated to the contact forces f_c, and a certain number of overlaps $h_o < 0$, $o \in \mathcal{O}$:

$$H = \sum_{o\in\mathcal{O}} \left(\sigma - \frac{1}{\sqrt{N}}\boldsymbol{\xi}^o \cdot \mathbf{X}\right) + \sum_{c\in\mathcal{C}} f_c \left(\sigma - \frac{1}{\sqrt{N}}\boldsymbol{\xi}^c \cdot \mathbf{X}\right) + \frac{\eta}{2}\left(|\,\mathbf{X}\,|^2 - N\right) \tag{3.204}$$

$$\frac{\partial}{\partial X_i} H = -\frac{1}{\sqrt{N}}\sum_{o\in\mathcal{O}} \xi_i^o - \frac{1}{\sqrt{N}}\sum_{c\in\mathcal{C}} f_c \xi_i^c + \eta\, X_i = 0, \qquad i = 1, ..., N \tag{3.205}$$

Now we perturb the system with a displacement δX_i so that all the contacts stay in place, except for one contact, of index $c' = 1$, whose gap becomes δ_1:

$$\begin{cases} \frac{1}{\sqrt{N}}\xi_i^c\ \delta X_i & = \delta_{c,1}\delta h_1 \\ X_i\ \delta X_i & = 0 \end{cases} \tag{3.206}$$

where we are summing over repeated indices and the last equation implies that the perturbation is tangent to the surface of the sphere. This system is made of N equations for N unknowns δX_i, therefore our displacement is uniquely defined by δh_1. For simplicity of notation, we can think of including X_i in the matrix ξ_i^c as the "pattern" of index $c = 0$: this has no effect on the spectrum of ξ_i^c and the rest of the discussion. We simply write

$$\delta X_i = \sqrt{N}(\xi^{-1})_{i,1}\delta h_1 \tag{3.207}$$

Since the $N \times N$ random matrix $\frac{1}{\sqrt{N}}\xi_i^c$ has entries of order $O(\frac{1}{\sqrt{N}})$, we would expect its inverse $\sqrt{N}(\xi^{-1})_i^c$ to have entries of order $O(\frac{1}{\sqrt{N}})$: this is not the case, since we have seen when discussing the Hessian in section 3.2.2 that $\frac{1}{N}\xi_i^c\xi_j^c$ has a spectrum divergent in zero with the smallest eigenvalue of order $O(N^{-2})$. It follows that the matrix $\sqrt{N}(\xi^{-1})_i^c$ has entries of order $O(1)$ and that

$$\begin{aligned} \delta X_i &\sim \delta h_1 \\ |\delta X|^2 &= AN\delta h_1^2 \end{aligned} \tag{3.208}$$

for some positive constant $A \sim O(1)$.

Let's say that we want to open the weakest contact, meaning the one whose associated force f_1 is the smallest among the f_c. In doing so, the gradient looses the contribution coming from f_1, therefore it is

$$\left.\frac{\partial H}{\partial X_i}\right|_{c'=1} = -\frac{1}{\sqrt{N}}\sum_{o\in\mathcal{O}}\xi_i^o - \frac{1}{\sqrt{N}}\sum_{c\in\mathcal{C}\setminus 1} f_c\xi_i^c + \eta\, X_i = \frac{1}{\sqrt{N}} f_1\xi_i^1 \tag{3.209}$$

where the last equality comes form (3.205). The energy variation to second order reads:

$$\delta H = \frac{1}{\sqrt{N}} f_1\xi_i^1\delta X_i + \frac{\eta}{2}|\delta X|^2 = f_1\delta h_1 + \frac{\eta}{2}AN\delta h_1^2 \tag{3.210}$$

Since we are in the non-convex phase, $\eta < 0$. Therefore, for $\delta h_1^* > \frac{f_1}{-\eta\, AN}$ the energy would start to decrease, making the system unstable. To have stability, it is necessary that a new contact is formed for $\delta h_1 \leq \delta h_1^*$. Since the variations of the other non-zero gaps is of order $\delta h_\mu \sim \delta h_1$, having a new contact $h_\mu + \delta h_\mu = 0$ for $\delta h_1 \leq \delta h^*$ imposes a condition on the smallest non-zero gaps h_{min}:

$$|h_{min}| \leq \frac{f_1}{-\eta\, AN} \tag{3.211}$$

With $\rho(f \to 0^+) \sim f^\theta$, the minimal force scale as $f_1 \sim N^{-\frac{1}{1+\theta}}$. For $g(h \to 0) \sim |h|^{-\gamma}$, we have $|h_{min}| \sim N^{-\frac{1}{1-\gamma}}$. Therefore, the condition $O(N^{-\frac{1}{1-\gamma}}) \leq O(N^{-\frac{1}{1+\theta}}/N)$, becomes

$$\gamma \geq \frac{1}{2+\theta} \tag{3.212}$$

This relationship becomes an equality for the jamming universality class, which corresponds to marginal stability. In this case, we haven't made a distinction between contacts being formed by positive gaps closing to zero or by overlaps relaxing until becoming contacts. In principle, these are two different mechanisms of stabilizing the system and they could be controlled by different exponents $g(h \to 0^+) \sim h^{-\gamma}$ and $g(h \to 0^-) \sim h^{-\tilde{\gamma}}$. We have seen this is not the case and the small positive gaps have the same scaling as the small negative gaps: $\gamma = \tilde{\gamma}$.

In a very similar way, we could think of taking the strongest contact, meaning the contact associated with the force closest to one, and compress it in order to make it become an overlap. Therefore we are making a perturbation $\delta h_1 < 0$. The corresponding pattern adds to the set $\mathcal{C}$ of unsat patterns, therefore

$$\left.\frac{\partial H}{\partial X_i}\right|_{c'=1} = -\frac{1}{\sqrt{N}}\xi_i^1 - \frac{1}{\sqrt{N}}\sum_{o\in\mathcal{O}}\xi_i^o - \frac{1}{\sqrt{N}}\sum_{c\in\mathcal{C}\setminus 1} f_c\xi_i^c + \eta\, X_i = -\frac{1}{\sqrt{N}}(1-f_1)\xi_i^1 \tag{3.213}$$

The energy variation reads

$$\delta H = -\frac{1}{\sqrt{N}}(1-f_1)\xi_i^1\delta X_i + \frac{\eta}{2}|\delta X|^2 = (1-f_1)(-\delta h_1) + \frac{\eta}{2}AN\delta h_1^2 \tag{3.214}$$

with the linear term being positive, since $\delta h_1 < 0$, and the quadratic term being negative, since $\eta < 0$. Therefore we have the same condition of stability as before

$$|h_{min}| \leq \frac{1-f_1}{-\eta\, AN} \tag{3.215}$$

For $\rho(f \to 1^-) \sim (1-f)^\theta$, the largest force satisfies $1 - f_1 \sim N^{-\frac{1}{1+\theta}}$ and condition (3.212) is found. Like for the small gaps, also small forces and forces close to one could have two different scaling exponents θ and $\tilde{\theta}$ and being associated with different kind of excitations, but this is not the case since $\theta = \tilde{\theta}$.

The critical phase of the perceptron with linear cost-function has all the features of jamming criticality but with a richer physics. The excitations are of two kinds, contacts that are open and contacts that are compressed. Also the relaxation mechanisms are two, since a contact can be formed coming from the positive side or the negative one. Moreover, the system can be compressed/decompressed over a range of pressure values, since there is no need of fine-tuning to see the criticality appearing.

3.5 Discussion

In this chapter we have introduced all the main concepts of the linear cost-function in the jammed phase. The first important feature is the fact that the minima of the system have marginally satisfied gaps, a.k.a. contacts, needed to stabilize the system. This creates an analogy with the problem of optimizing a linear function in a domain, i.e. linear programming, where the minimum sits in one vertex of the polytope, that is where some of the inequalities defining the domain become marginally satisfied. The other important feature comes from the spherical geometry of the problem: when the resulting force pushes the configuration towards the exterior of the hyper-sphere, then the effective geometry in the neighborhood is convex and also a hypostatic configuration can be stable, since the unconstrained directions see an effective positive curvature. When instead the system is in a configuration that is pulled by the resultant force towards the center of the hyper-sphere, then the system lives in a region whose effective curvature is negative. Therefore, the only way to stabilize the configuration is to constrain each degree of freedom with a contact, and this directly leads to the fact that the only stable configurations are (at least) isostatic. This discussion about the "effective curvature" is measurable through the sign of the Lagrange multiplier η of the spherical constraint, that in fact is proportional to the resultant force along the $\mathbf{X}$ direction.
From the algorithmic point of view, the introduction of the smoothed linear potential is a simple solution that can be straightforwardly replicated in other systems having a similar interaction potential, as we do for finite dimensional soft spheres. Pictorially, it is possible to think of the smoothing parameter ϵ as playing the role of the temperature that blurs the irregularity of the linear interaction in the origin.
A remarkable point is the correspondence between the replica theory and the simulations. While in the replica symmetric/convex phase it is expected to hold, in the replica symmetry broken/non-convex phase it is much less obvious. In fact, the fullRSB theory and the scaling solution describe the ground-state, while the local minima we study by gradient-descent-like minimizations from random configurations are not the ground state. Yet, statistical properties like the power law distributions of small gaps and contact forces can be found both in the simulations' local minima and the theoretical scaling solution. A deeper understanding of this fact will be the subject of further research.

Chapter 4

Critical jammed phase of linear soft spheres

The content of this chapter is published in [107].

In this chapter we study the overcompressed phase of finite dimensional soft spheres with linear repulsion. The model is defined similarly to the perceptron with linear cost-function, but now the *gap* variables represent the distances between the spheres. We show that the physics of this model, even in dimension as low as 2 and 3, is the same as the one found in the perceptron counterpart, with the remarkable difference that this defines a physical model in finite dimensions having a novel critical phase.

- Accessible local minima of the potential energy landscape are isostatic. Even if there is a finite fraction of overlapping spheres making the total energy finite, there is also an isostatic number of pairs of spheres that just touch.

- Contacts play a crucial role in the stability of the system. Their number is fixed to be exactly equal to the number of degrees of freedom and its fluctuations are suppressed, as it happens at jamming [128, 129]. In fact the spatial fluctuations of the local connectivity of the contact network are hyperuniform implying that the variance of the number of contacts in a volume V grows more slowly than $|V|$. Conversely, the fluctuations of the number of overlaps follow the central limit theorem and spatial fluctuations of the overlap network are only uniform.

- If we look at gap variables and we focus on strictly positive and negative gaps, we find that their distribution has a power law divergence for small argument (in absolute value). The power law exponents appear to be the same - within numerical precision - for both positive and negative small gaps. The numerical value of the exponent is compatible with the one controlling the divergence of small positive gaps at jamming.

- Contacts can be associated with forces in the interval $(0, F)$, with the maximal force fixed to the value $F = 1$. We measure the empirical distribution of the forces: it displays two singular pseudogaps at the domain boundaries, close to zero and close to $F = 1$. Close to jamming, the pseudogap exponent of forces near to zero appears to depend on the packing fraction. However, if we carefully separate the contribution of "bucklers", namely spheres that have $d + 1$ interacting spheres [57], from the bulk statistics, both the pseudogaps are universal and characterized by the

same exponent in the whole jammed phase, even far from jamming. The value of the critical exponent is compatible with the one of the force distribution at jamming.

4.1 Definition of the model

We consider a set of N spheres in d dimensions whose centers are d-dimensional vectors denoted by $\{\mathbf{x}_i\}_{i=1,\dots,N}$. We define a gap between two spheres, say i and j, as

$$h_{ij} = r_{ij} - \sigma_{ij} \tag{4.1}$$

where we have denoted by σ_{ij} the sum of the radii of the corresponding spheres and by $r_{ij} = |\mathbf{x}_i - \mathbf{x}_j|$ the distance between their centers.
In the overcompressed phase, above jamming, spheres cannot be arranged without creating overlaps between them. Usually, an energy cost is associated to overlapping spheres via a power interaction potential $\nu_a(h_{ij}) = (h_{ij})_+^a$, where $x_+ = |x|\theta(-x)$. Common choices for the penalty exponent a are $a = 2$ or $a = 5/2$, corresponding to harmonic and Hertzian spheres, respectively. If $a > 1$ the interaction potential is convex and differentiable at $r_{ij} = \sigma_{ij}$, i.e. when spheres just touch. As a consequence, given a contact at jamming, an infinitesimal normal force is enough to destabilize it and causes an overlap between the corresponding particles. Therefore, for $a > 1$ jamming is a singular point in the phase diagram: as soon as the spheres overlap, the system stabilizes. This implies that jamming criticality is washed out when the system enters in the overcompressed phase.
Here we present soft spheres interacting through a linear ramp potential, obtained by setting $a = 1$. Therefore the Hamiltonian reads

$$H\left(\{\mathbf{x}_i\}\right) = F \sum_{i<j} |h_{ij}|\theta(-h_{ij}) \tag{4.2}$$

where F is a constant that sets the scale of forces. We set $F = 1$.

The linear ramp potential is at the boundary between convex and non-convex interparticle potentials and presents important qualitative differences from the case $a > 1$. First of all, it is non-differentiable for $h_{ij} = 0$: the consequence is that small forces applied to zero-gaps $h_{ij} = 0$ do not necessarily destabilize them. To induce an overlap $h_{ij} < 0$, a total force greater than F is necessary. In addition, the modulus of the force generated by an overlap does not depend on the extent of the overlap itself. This phenomenology is analogous to the one of the perceptron with linear cost function presented in chapter 3.
We use the following terminology:

- **contacts** are gaps exactly equal to zero: $h_{ij} \equiv 0$. Therefore, the corresponding spheres are *in contact*;
- **overlaps** are negative gaps: $h_{ij} < 0$. Therefore, the corresponding spheres are *overlapping*;
- **interacting** spheres are those that are in contact or overlapping.

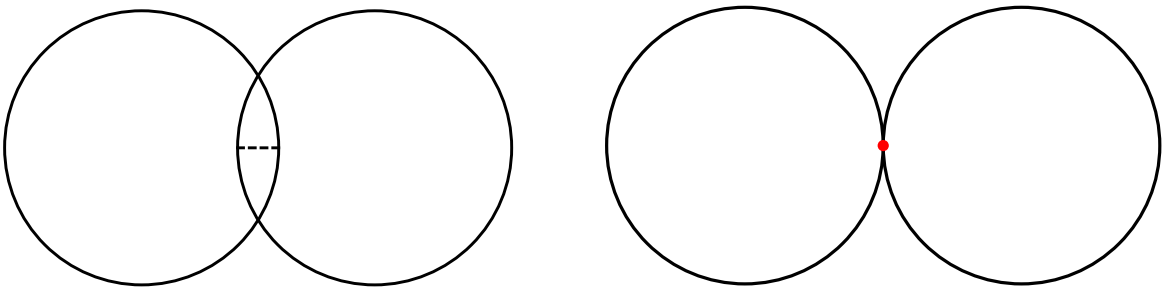

Figure 4.1: On the left, overlapping spheres; the black dashed line indicates the amount of overlap $|h_{ij}|$ between them, with $h_{ij} < 0$. On the right, spheres in contact; the red dot indicates that the gap between them is exactly zero: $h_{ij} = 0$.

We focus on systems of two and three dimensional polydisperse spheres and produce local minima by gradient descent minimization. Isostaticity and critical behavior in the force and gap distributions appear in the unsatisfiable phase of the spherical perceptron with linear cost function, which is a mean field model for linear spheres ([108] and chapter 3). Here we show that these properties appear to survive in a robust way when we go to finite dimensions. Therefore, jammed packings of linear spheres are characterized by diverging isostatic lengthscales and are critical even far from jamming. This provides a new, richer example of self-organized critical, marginally stable, finite dimensional system.

4.2 The emergence of contacts in the jammed phase

Setting the force scale $F = 1$, the gradient of the Hamiltonian defined in (4.2) reads

$$\frac{\partial H}{\partial \mathbf{x}_i} = -\sum_{j \neq i} \mathbf{n}_{ij}\, \theta(-h_{ij}) \tag{4.3}$$

where we are using $\frac{\partial}{\partial \mathbf{x}_i}$ to indicate the partial derivative with respect to each component of the vector $\mathbf{x}_i$, i.e. $x_i^{\alpha=1,\dots,d}$, and $\mathbf{n}_{ij}$ to indicate the unit vector pointing from $\mathbf{x}_j$ to $\mathbf{x}_i$, i.e. $\mathbf{n}_{ij} = \frac{\mathbf{x}_i - \mathbf{x}_j}{|\mathbf{x}_i - \mathbf{x}_j|}$. We see that each sphere j that is overlapped with i pushes it with a force of intensity equal to $F = 1$. If these are the only forces acting in the system, then the mechanical equilibrium is reached only for very symmetric configurations of sphere positions.

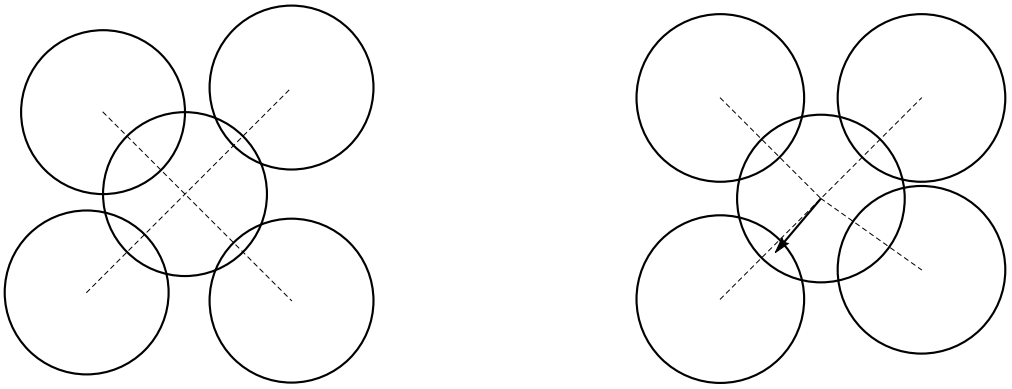

Figure 4.2: In the configuration on the left, the central sphere is at equilibrium: the forces exerted by surrounding spheres counterbalance in couples. Notice that the intensity of the overlapping force is insensitive to the amount of overlap. In the configuration on the right, instead, the resulting force on the central sphere is different from zero: the bottom right sphere is not aligned with the opposite one. The arrow represent the resulting force.

Because we are addressing random configurations of spheres (eventually by inserting polydispersity in their radii), such highly symmetrical configurations are not achievable. Instead, the system gets stabilized by the presence of contacts with the corresponding *contact forces*. By simple energetic arguments it is clear that a pair of spheres in contact can sustain a compression force up to the critical value $F(=1)$, corresponding to the slope of the energy ramp.

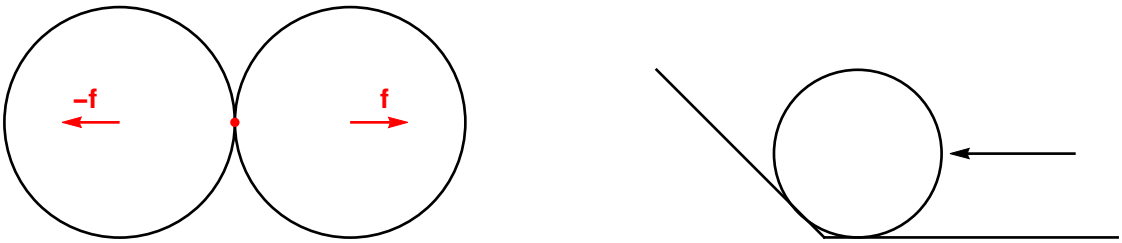

Figure 4.3: A pair of spheres in contact exchange a contact force of intensity between 0 and $F = 1$, keeping the contact in place. Energetically, overlapping a sphere with another is equivalent to pushing a sphere up an inclined plane against gravity: if the energy increases as $F\Delta x$, then the pushing force has to do a work $F\Delta x$ that requires a force (tangent to the plane) of at least F even for an infinitesimal Δx.

The Lagrangian that takes into account the contact forces reads

$$\mathcal{L}\left(\{\mathbf{x}_i\},\{f_{ij}\}\right) = \sum_{i<j} |h_{ij}|\theta(-h_{ij}) - \sum_{i<j} f_{ij}h_{ij}\delta_{h_{ij},0} \tag{4.4}$$

where the forces f_{ij} are defined only for the contacts $h_{ij} = 0$ and the minus sign is chosen so to have $f_{ij} > 0$. To make the notation simpler, we introduce two sets, $\mathcal{C}$ and $\mathcal{O}$:

- $\mathcal{C}$ is the set of all pairs of spheres that are in contact; it contains $C = |\mathcal{C}|$ elements composed of the pairs of indices $c = \langle i, j\rangle$, $i < j$, for $c = 1, ..., C$. The corresponding contact forces form a C-dimensional vector $\mathbf{f} = \{f_{c=1,...,C}\}$.

- $\mathcal{O}$ is the set of all pairs of spheres that are overlapping, i.e. $h_{i,j} < 0$. It contains $O = |\mathcal{O}|$ elements made of the pairs of indices $o = \langle i, j \rangle$, $i < j$, for $o = 1, ..., O$. The corresponding overlap forces have all intensity equal to 1 ($= F$), that we can conveniently indicate via the O-dimensional vector made of 1s: $\mathbf{1} = [1, ..., 1]$.

Therefore we can write

$$\mathcal{L}\left(\{\mathbf{x}_i\}, \{f_c\}\right) = \sum_{o \in \mathcal{O}} |h_o| - \sum_{c \in \mathcal{C}} f_c h_c \tag{4.5}$$

4.3 Static analysis: equilibrium condition for local minima

We can impose the stationary condition of the Lagrangian with respect to its variables. Deriving with respect to the contact forces f_c we simply get the contact condition:

$$\frac{\partial \mathcal{L}}{\partial f_c} = h_c = |\,\mathbf{x}_i - \mathbf{x}_j\,| - \sigma_{ij} = 0, \qquad \langle ij \rangle = c \in \mathcal{C} \tag{4.6}$$

Deriving with respect to the sphere positions $\mathbf{x}_i$, we get the force balance condition

$$\frac{\partial \mathcal{L}}{\partial \mathbf{x}_i} = -\sum_{j \in \mathcal{O}(i)} \mathbf{n}_{ij} - \sum_{j \in \mathcal{C}(i)} f_{ij}\, \mathbf{n}_{ij} = 0 \tag{4.7}$$

where $\mathcal{O}(i)$ indicates the set of spheres overlapping with i and $\mathcal{C}(i)$ the set of spheres in contact with i. Introducing the matrices $\underline{\underline{\mathrm{S}}}$ and $\underline{\underline{\mathrm{T}}}$, with dimensions $C \times Nd$ and $O \times Nd$ respectively, defined as $\underline{\underline{\mathrm{S}}}^{k\alpha}_{\langle ij \rangle} = (\delta_{jk} - \delta_{ik}) n^{\alpha}_{ij}$, with $\langle ij \rangle \in \mathcal{C}$, and $\underline{\underline{\mathrm{T}}}^{k\alpha}_{\langle ij \rangle} = (\delta_{jk} - \delta_{ik}) n^{\alpha}_{ij}$, with $\langle ij \rangle \in \mathcal{O}$, where n^{α}_{ij} is the α-component of the unit vector $\mathbf{n}_{ij} = (\mathbf{x}_i - \mathbf{x}_j)/|\,\mathbf{x}_i - \mathbf{x}_j\,|$, we can write the force balance condition in matrix form:

$$\underline{\underline{\mathrm{S}}}^T \mathbf{f} = -\,\underline{\underline{\mathrm{T}}}^T \mathbf{1}\,. \tag{4.8}$$

We see that, knowing the matrices $\underline{\underline{\mathrm{S}}}$ and $\underline{\underline{\mathrm{T}}}$ (that implies knowing the sphere positions $\mathbf{x}_i$ and the sets $\mathcal{C}$ and $\mathcal{O}$), the contact forces $f_{c=<ij>}$ can be computed algebraically from equation (4.8). In fact, it is always possible to project on the contact directions by $\underline{\underline{\mathrm{S}}}$ and solve the equation

$$\underline{\underline{\mathrm{S}}}\,\underline{\underline{\mathrm{S}}}^T \mathbf{f} = -\,\underline{\underline{\mathrm{S}}}\,\underline{\underline{\mathrm{T}}}^T \mathbf{1} \tag{4.9}$$

Anyway, to have a stable configuration it is necessary that the resultant forces $\mathbf{f} = \{f_{ij}\}$ are in the interval $(0, 1)$ and that the gradient $\underline{\underline{\mathrm{S}}}^T \mathbf{f} + \underline{\underline{\mathrm{T}}}^T \mathbf{1}$ is equal to zero. For this to happen, it is necessary that the configuration of sphere centers is properly organized. In the next section 4.4 we define a minimization algorithm in order to reach a minimum configuration.

A remark can be done about the contact condition (4.6). If we know the isostatic contact network, the number of equations (4.6) is $C = Nd$, therefore equal to the number of unknowns x^{α}_i. Finding the positions of the spheres x^{α}_i from the contact network requires solving for x^{α}_i the system of non-linear equations (4.6). This is a difference with respect to the perceptron with linear cost-function: we have seen in section 3.2.1 that knowing the contact and overlap sets in the isostatic phase provides a linear problem defining the corresponding perceptron configuration.

4.4 Numerical simulations

We want to minimize the Hamiltonian (4.2) or its Lagrangian counterpart (4.5). The presence of a singularity in the first derivative for $h_{ij} = 0$ requires a regularization analogous to the one used for the perceptron in 3.1.2.

4.4.1 Smoothening of the potential

We define a differentiable ϵ-regularized potential between particles:

$$\nu_\epsilon(h) = \begin{cases} 0 & h > \frac{\epsilon}{2} \\ \frac{1}{2\epsilon}(h - \frac{\epsilon}{2})^2 & -\frac{\epsilon}{2} < h < \frac{\epsilon}{2} \\ |h| & h < -\frac{\epsilon}{2} \end{cases} \tag{4.10}$$

which in the limit $\epsilon \to 0$ reduces to the linear ramp potential. More precisely, the limit $\epsilon \to 0$ gives back the Lagrangian (4.5). In fact we have

$$\mathcal{L}_\epsilon\left(\{\mathbf{x}_i\}\right) = \sum_{i<j} \nu_\epsilon(h) = \sum_{o\in\mathcal{O}} |h_o| + \sum_{c\in\mathcal{C}} \frac{\left(h_c - \frac{\epsilon}{2}\right)^2}{2\epsilon} \tag{4.11}$$

where now we have redefined the sets $\mathcal{O}$ as $\mathcal{O} = \{\langle i,j\rangle \ : \ h_{ij} < -\frac{\epsilon}{2},\ i<j\}$ and $\mathcal{C}$ as $\mathcal{C} = \{\langle i,j\rangle \ : \ -\frac{\epsilon}{2} < h_{ij} < \frac{\epsilon}{2},\ i<j\}$.
Now $\mathcal{L}_\epsilon$ is differentiable and the equilibrium condition for each sphere i reads

$$\frac{\partial\, \mathcal{L}_\epsilon\left(\{\mathbf{x}_i\}\right)}{\partial\, \mathbf{x}_i} = -\sum_{j\in\mathcal{O}(i)} \mathbf{n}_{ij} - \sum_{j\in\mathcal{C}(i)} \frac{\frac{\epsilon}{2} - h_c}{\epsilon}\, \mathbf{n}_{ij} = 0 \tag{4.12}$$

We see the natural occurrence of the order one quantity $\frac{\frac{\epsilon}{2}-h_c}{\epsilon} \in (0,1)$ that in the limit $\epsilon \to 0$ is exactly the contact force f_c:

$$\lim_{\epsilon\to 0} \frac{\frac{\epsilon}{2} - h_c}{\epsilon} = f_c \tag{4.13}$$

This recovers the force balance condition (4.8). Notice that, while the smoothed ϵ part of the potential (4.10) gives an $O(1)$ contribution to the force balance condition, its contribution to the energy of the model is $O(\epsilon)$.

4.4.2 Gradient descent protocol and minimization algorithm

We consider a set of polydisperse spheres in d dimensions in a box of side length L with periodic boundary conditions. The radii $\sigma_{i=1,\dots,N}$ of the spheres are uniformly randomly distributed in the interval $[1-p, 1+p]$, with polydispersity $p = 0.2$. The side-length L of the box is set by the volume density $\phi = \sum_{i=1}^N k_d \sigma_i^d / L^d$, with $k_d = \pi^{d/2}/\Gamma(1+d/2)$ where $\Gamma(x)$ is the Euler gamma function.
We minimize (4.11) through an annealing on the regularization parameter ϵ.
Identically to the perceptron case, when ϵ is bigger than the typical smallest non-zero gaps $|h_{min}|$, the landscape is smoothened by the quadratic contribution. When ϵ is smaller than the smallest non-zero gap, then the function (4.11) is equivalent to its original non-regularized counterpart. Therefore, we start with a large regularization ϵ_1 (we choose

$\epsilon_1 \sim 10^{-2}$), perform the gradient-descent minimization, reduce the regularization parameter to ϵ_2 (we choose $\epsilon_k = \epsilon_{k-1}/2$) and perform again the gradient-descent minimization starting from the previously found configuration. We repeat this step n times until the regularization ϵ_n is small (we choose $\epsilon_n \sim 10^{-7}$ or $\epsilon_n \sim 10^{-8}$).

Algorithm 2: Spheres smoothed minimization

$\{\mathbf{x}_{i=1,...,N}\}^{(0)} \leftarrow$ random point in the d dimensional box of side L;
$\epsilon_1 \leftarrow \epsilon_{initial}$;
for k *in* $\{1, ..., n\}$ **do**
  $\{\mathbf{x}_i\}^{(k)} \leftarrow$ minimize $\mathcal{L}_{\epsilon_k}(\{\mathbf{x}_i\})$ starting from $\{\mathbf{x}_i\}^{(k-1)}$;
  $\epsilon_{k+1} \leftarrow \epsilon_k/2$;
end
Result: $\{\mathbf{x}_i\}^* \leftarrow \{\mathbf{x}_i\}^{(n)}$

This minimization procedure is performed for a fixed value of the packing fraction ϕ. For the gradient-descent minimization, we actually choose a quasi-Newton method to improve the performance.
With this procedure we meet the jamming transition at packing fractions $\phi_J\Big|_{d=2} \simeq 0.84$ and $\phi_J\Big|_{d=3} \simeq 0.64$.
This procedure provides the set $\mathcal{C}$ of the $C = |\mathcal{C}|$ particle pairs $c = \langle ij \rangle$, with $i < j$, that are in contact (i.e. $-\epsilon/2 < h_{ij} < \epsilon/2$) and the set $\mathcal{O}$ of the $O = |\mathcal{O}|$ particle pairs $o = \langle ij \rangle$ that are overlapping (i.e. that have negative gaps $h_{ij} < -\epsilon/2$).

Numerical and algorithm details

We explore the following intervals for the parameters in our computer simulations:

- N takes values from 64 to 4096;
- d takes values 2 and 3;
- the packing fraction ϕ can vary from the jamming values $\phi_J\Big|_{d=2} \simeq 0.84$, $\phi_J\Big|_{d=3} \simeq 0.64$ to $\phi = 2$;
- our starting regularization is $\epsilon_{initial} = 10^{-2}$ and we perform n steps, halving ϵ at each step, to arrive at a final $\epsilon_{final} \sim 10^{-7}$ in $n = 17$ steps or $\epsilon_{final} \sim 10^{-8}$ in $n = 20$ steps.

The choices of $\epsilon_{initial}$ and the ϵ-decreasing rate are chosen empirically, based on the fact that they work well with the minimizer we use. The choice of ϵ_{final} depends on N: since for a generic power law distribution of the small gaps $\rho(h \to 0) \sim |h|^p$ the smallest non-zero gap scales as $h_{min} \sim N^{-\frac{1}{1+p}}$, we need

$$\epsilon_{final} << N^{-\frac{1}{1+p}} \tag{4.14}$$

On the other hand, we see that for $\epsilon \sim 10^{-8}$ we have $\delta \mathcal{L}_\epsilon \sim \varepsilon_{machine}$ and we start to loose precision on the control of the contacts (i.e. the gaps in the window $-\frac{\epsilon}{2} < h_{ij} < \frac{\epsilon}{2}$). This is a limiting factor in the sizes of the systems that we explore. In fact, exploring larger

sizes N, we still find the same physics (i.e. isostaticity and the emergence of criticality), but we loose the single contact control for $\epsilon \lesssim 10^{-8}$; by the way, also in this case the fluctuations of the number of contacts are $O(1)$ (therefore the relative fluctuations are $O(\frac{1}{N})$) and get reflected in a strong degradation of the gradient. For sizes up to $N \sim 512, 1024$, instead, the control of the contact network is excellent up to a single contact.

The quasi-Newton method we use for the gradient-descent-like minimization is the *Limited-memory Broyden–Fletcher–Goldfarb–Shanno algorithm* (L-BFGS) [48]. We use a Fortran implementation of this algorithm [260, 185] available through a Python interface in the library SciPy [240]. We have performed some minimizations using the FIRE algorithm [38] for the first step ϵ_1, for performance reasons: changing gradient-based routines is completely irrelevant for the physics of the system.

4.5 Results

Inside the jammed phase, $\phi > \phi_J$, the energy and the pressure in the system are positive and a large number of overlaps is present in the system. In minimum configurations, an extensive number of contacts is also present, as expected from the force balance argument (4.8).

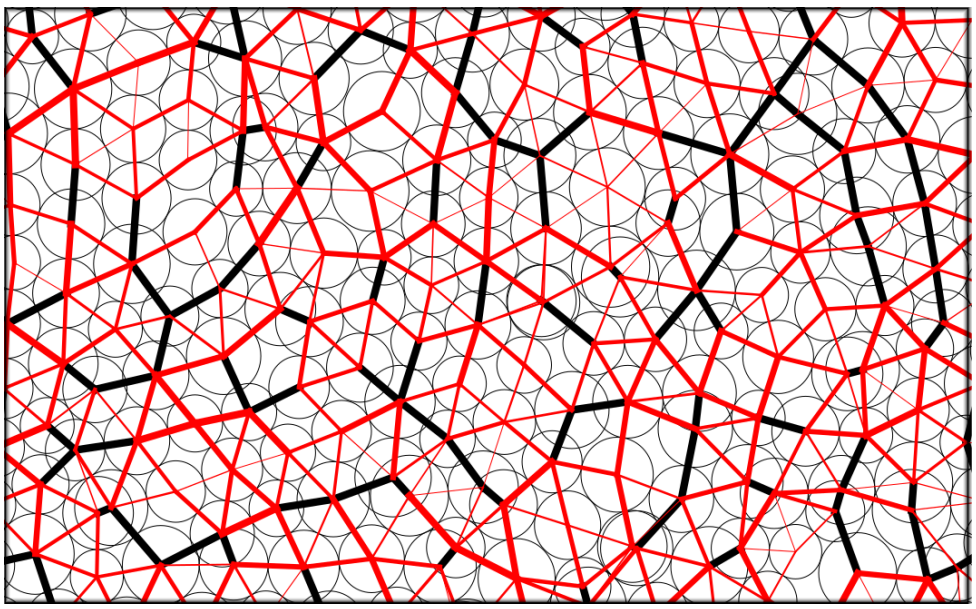

Figure 4.4: A snapshot of a configuration of disks with the linear potential at packing fraction $\phi = 1$. The contact network is in red while the overlap network is in black. The thickness of the lines reflects the intensities of forces. While black lines carry all forces equal to one, red lines, associated to contacts, carry a force that varies in the interval $[0, F = 1]$.

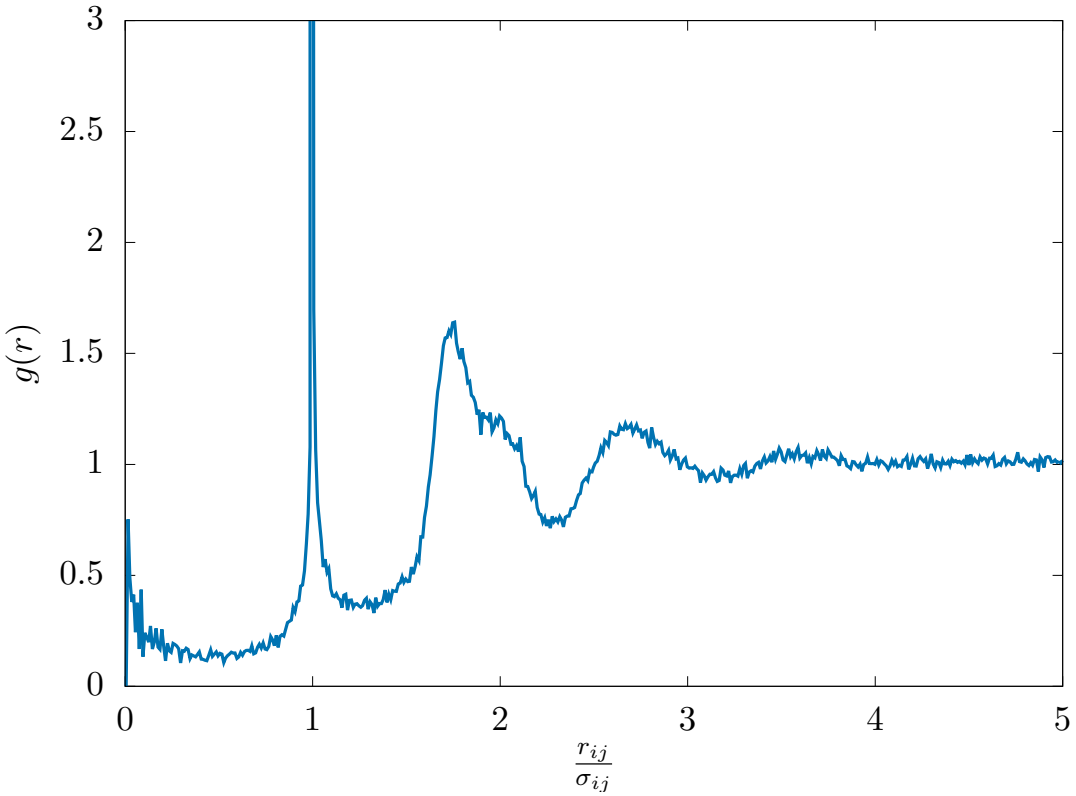

Figure 4.5: Radial distribution function of a system of overcompressed disks in $d = 2$ at $\phi = 1$, as a function of $\frac{r_{ij}}{\sigma_{ij}} = \frac{|\mathbf{x}_i - \mathbf{x}_j|}{\sigma_{ij}}$. It reveals the presence of contacts in the system, meaning pairs of tangent spheres $r_{ij} = \sigma_{ij}$. Data obtained for $N = 2048$, averaged over 14 samples.

4.5.1 Structural properties of the jammed phase

In all the jammed phase, also very far from the jamming transition point, the system is isostatic, meaning there is a number of contacts C equal to the number of degrees of freedom. Due to the periodic boundary conditions, the system is invariant to a global translation, therefore the degrees of freedom are $Nd - d$. We have that

$$C = N^* d - d \tag{4.15}$$

in all the jammed phase, where N^* is the number of spheres minus the number of rattlers, meaning spheres that are out of the interaction network of the system. They are present for densities close to ϕ_J, but they quickly disappear going deeper in the overcompressed phase. Therefore the isostaticity index $c = \frac{C}{Nd-d}$ is always equal to one

$$c = 1 \tag{4.16}$$

While the number of contacts stays constant from the jamming transition, the (intensive) number of overlaps $n_o = \frac{O}{Nd-d}$, the energy e and the pressure p start from zero at

ϕ_J. Having defined

$$\begin{aligned} e &= \sum_{o\in\mathcal{O}} |h_o| \\ p &= \frac{1}{dL^d}\left[\sum_{\langle ij\rangle\in\mathcal{O}} |\,\mathbf{x}_i-\mathbf{x}_j\,| + \sum_{\langle ij\rangle\in\mathcal{C}} |\,\mathbf{x}_i-\mathbf{x}_j\,|f_{ij}\right] \end{aligned} \tag{4.17}$$

we report the quantities c, n_o, e, p in figure 4.6 for dimension $d = 2$ and figure (4.7) for dimension $d = 3$.

In the lower panel of figure (4.6) we report the scaling of the energy, the number of overlaps and the pressure as a function of the distance from unjamming $\phi - \phi_J$. It has been shown [191, 117, 250] for soft-spheres interacting with a power law repulsion

$$H = \sum_{i<j} |h_{ij}|^a \theta(-h_{ij}) \qquad \text{with } a > 1 \tag{4.18}$$

that close to jamming it holds

$$e \sim \Delta\phi^a \qquad p \sim \Delta\phi^{a-1} \qquad \Delta z = \sqrt{\Delta\phi} \tag{4.19}$$

where $\Delta\phi = \phi - \phi_J$ and $\Delta z = z - z_{iso}$ represents the excess average connectivity per particle with respect to the jamming point where isostaticity holds $z_{iso} = 2d$. The scaling of Δz is universal and independent of the power law repulsion a.
In our case, $a = 1$ and the scaling (4.19) for the pressure becomes marginal: we have that logarithmic terms come into play and

$$\boxed{p \sim \frac{1}{|\log\Delta\phi|^b}} \tag{4.20}$$

where b is some positive power. In the case of the perceptron with linear cost-function, we have $b = \frac{1}{2}$. The energy has a linear scaling with logarithmic corrections,

$$\boxed{e \sim \frac{\Delta\phi}{|\log\Delta\phi|^b}} \tag{4.21}$$

The number of overlaps, which is equivalent to Δz for general soft spheres, does not have the known scaling (4.19). Instead, data in figure 4.6 suggest that

$$\boxed{n_o \sim \Delta\phi^\nu} \tag{4.22}$$

with an exponent $0.5 < \nu < 1$. We argue that this is due to the nature of the critical jammed phase induced by the linear potential and it can be understood via mean-field theory, i.e. with the perceptron model. In chapter 5, we define a compression algorithm and obtain by scaling arguments that

$$\nu = 2\frac{1+\theta}{3+\theta} \simeq 0.83 \tag{4.23}$$

where $\theta \simeq 0.42$ is the critical exponent associated to the distribution of small forces at jamming.
Some remarks can be made:

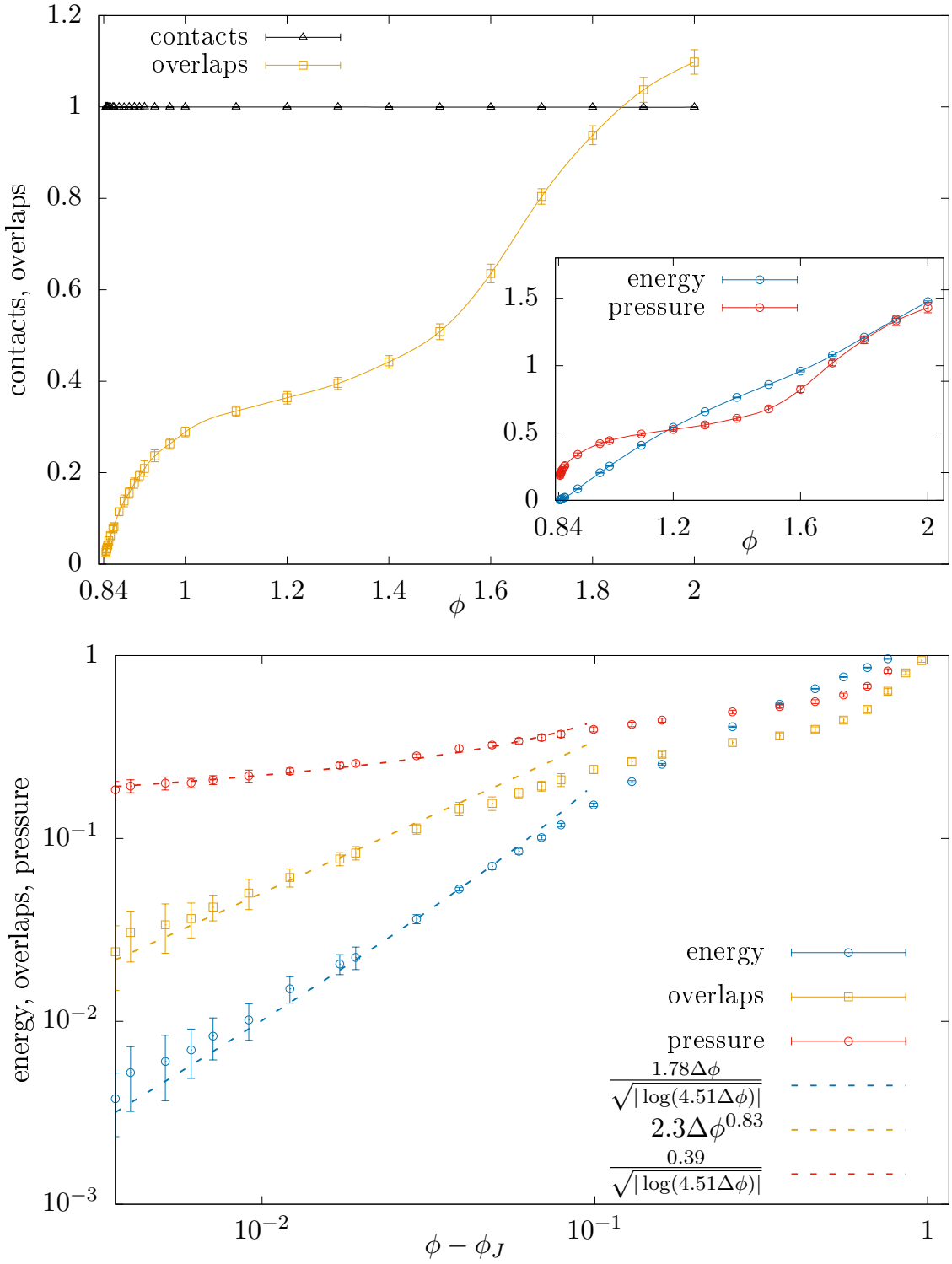

Figure 4.6: *Upper Panel.* Main plot: the isostaticity index defined as $c = C/(Nd - d)$ and the fraction of overlaps defined as $n_O = O/(Nd - d)$ as a function of the packing fraction in dimension $d = 2$ (we find the jamming transition at $\phi_J \simeq 0.84$). Inset: Behavior of energy and pressure for $\phi > \phi_J$. Energy, pressure and number of overlaps are increasing functions continuous at jamming. Data produced with system size $N = 512$, dimension $d = 2$, averaged over ~ 40 samples for each point. *Lower Panel.* The behavior of pressure, energy and overlaps close to the unjamming transition. We attempted some logarithmic fits of the form $e \sim |\Delta\phi|/\sqrt{\log(\Delta\phi/2)}$, $p \sim 1/\sqrt{\log(\Delta\phi/2)}$ and $n_O \sim |\Delta\phi|^{\nu}$. The unjamming packing fraction ϕ_J is extracted from the fit of the energy.

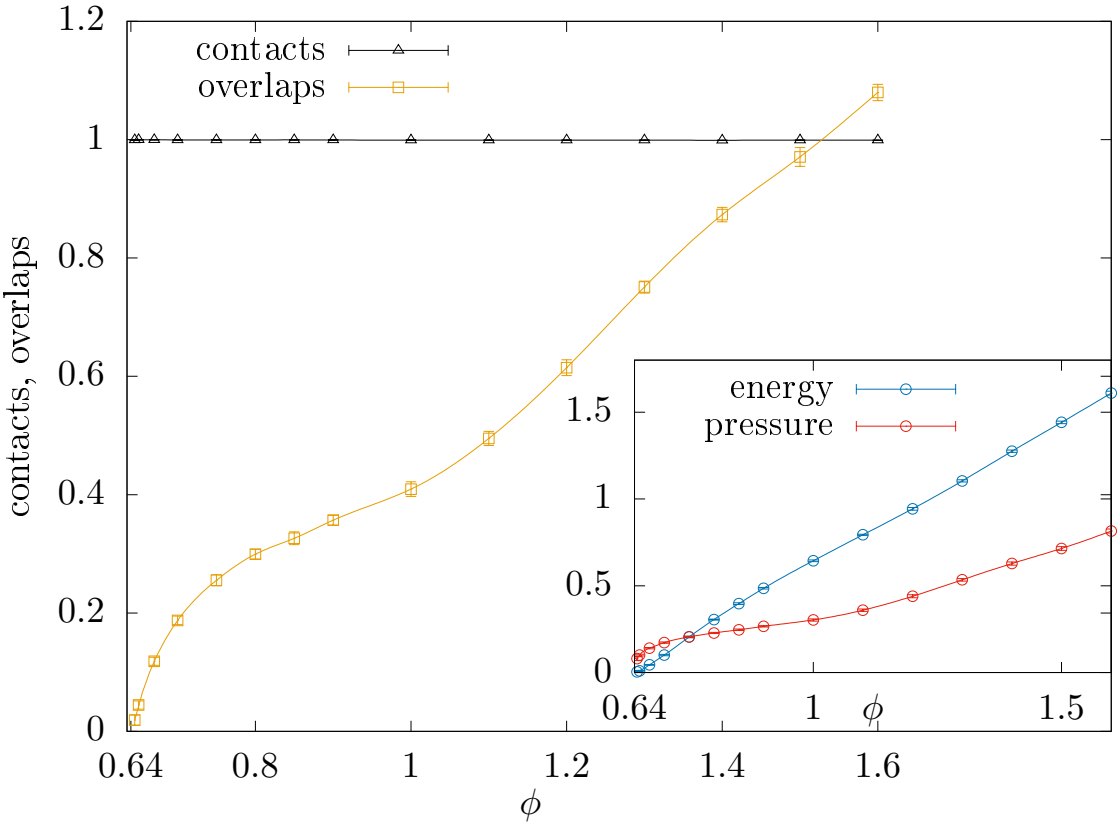

Figure 4.7: Isostaticity index and fraction of overlaps in dimension $d = 3$. While at all densities the minima are isostatic, the number of overlaps increases monotonically. In the inset, the corresponding energy and pressure. Data produced with system size $N = 1024$, dimension $d = 3$, averaged over ~ 30 samples for each density ϕ.

- the scalings for soft spheres (4.19) with $a > 1$ correspond to what is obtained in the corresponding mean-field theory, i.e. the perceptron [105];
- the scalings for energy (4.21) and pressure (4.20) for the linear potential correspond to those found in the perceptron with linear cost-function (3.143)-(3.133) by a replica symmetric computation;
- the scaling of the number of overlaps n_o is also found in the perceptron with linear cost-function, but only in the non-convex/isostatic phase that requires the $full$RSB theory. In the non-critical, replica symmetric phase, in fact, the number of overlaps scales proportionally to the distance from unjamming. Unfortunately, we are not able to compute ν from the $full$RSB theory, but we provide a scaling argument in chapter 5 when studying the avalanches dynamics.

The reason why we do not report in this section a systematic numerical study of the unjamming transition is that the algorithm we are considering is not suited for this kind of analysis. To have good quality data, in fact, it is necessary to follow a configuration by progressively reducing ϕ until ϕ_J, which is a fluctuating point [191] (it depends on the algorithm and on the disorder realization). The problem is that, when an isostatic minimum is found at ϕ, a variation $\delta\phi$ necessarily destroys all the contacts of the configuration: in order to find a new stable packing, it is necessary to proceed with a new annealing in the regularization parameter ϵ. This procedure does not allow to follow a configuration in a fine manner, for example with the objective of addressing a certain value of the energy with arbitrary precision. The way to get a finer control of the structure is by changing ensemble and using the pressure as control parameter while promoting the average radius, therefore the packing fraction, to a variable. In this manner, it is possible to look for configurations of the system at a given pressure, arbitrarily close to the jamming point. A (small) variation of the pressure destabilizes only a part of the contacts, and the configuration evolves by creation of avalanches. This is done in chapter 5.

Gaps and forces

At all jammed packing fractions $\phi > \phi_J$, the distribution of gaps h_{ij} has a divergence in $h = 0$ due to the presence of contacts and a power law behavior for $h \to 0^{\pm}$. The associated exponent is the same both for small positive and small negative gaps, and it is compatible with the exponent $\gamma \simeq 0.41$ [64] of the distribution of small positive gaps at jamming:

$$\rho(h \to 0^{\pm}) \sim |h|^{-\gamma} \tag{4.24}$$

This is shown in fig. 4.8 for $d = 2$ and fig.4.9 for $d = 3$.

The contact forces associated to the contacts are distributed in the interval $(0, F = 1)$ and have two pseudo-gaps at its boundaries:

$$\rho(f) \sim \begin{cases} f^{\theta_0} & f \to 0^+ \\ (1-f)^{\theta} & f \to 1^- \end{cases} \tag{4.25}$$

At low packing fractions local effects are still present and they influence the distribution of forces near 0: these are due to the *bucklers* which carry small forces whose distribution $\rho_{bucklers}(f \to 0) \sim f^{\theta_l}$, with $\theta_l \simeq 0.18$ [154]. These effects vanish when the packing fraction

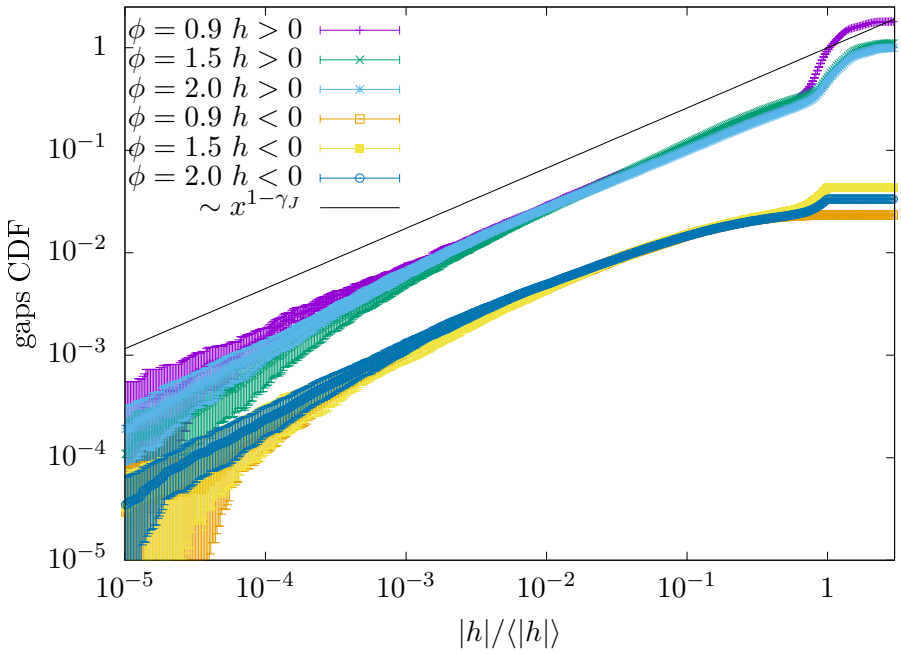

Figure 4.8: The positive and negative cumulative gap distribution. The y-axis of the negative gap is rescaled by an artificial factor 0.1 to improve the readability of the figure. We observe that both cumulative distributions appear to be described by the same power law exponent for small argument.

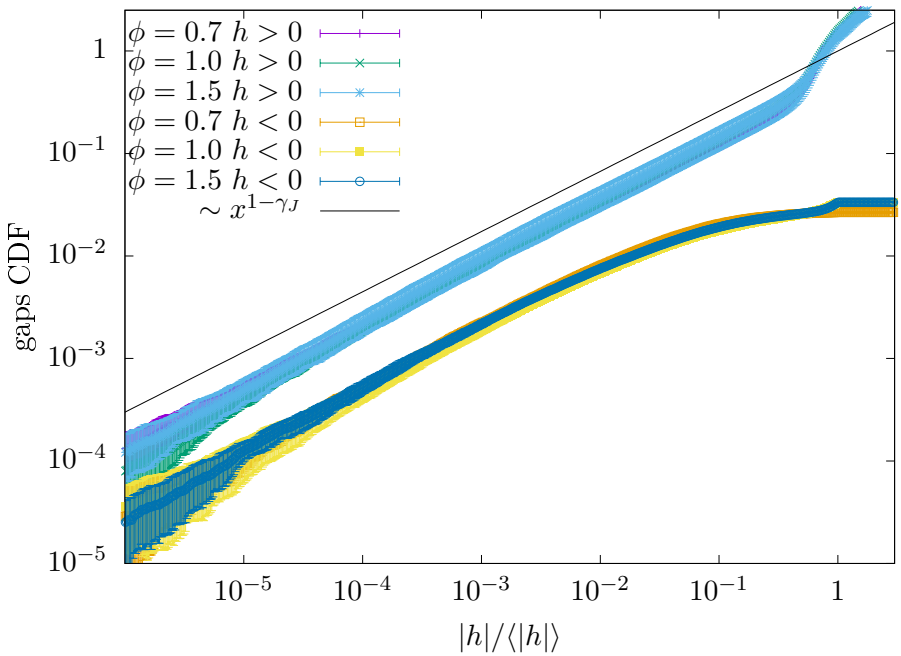

Figure 4.9: Cumulative distribution of small positive and negative gaps for different packing fractions. The solid line represents the mean field theory prediction. Data produced with system size $N = 1024$, dimensions $d = 3$, averaged over 45 samples for density $\phi = 0.7$, 44 samples for $\phi = 1.5$, 27 samples for $\phi = 2.0$.

is increased. Therefore the exponent θ_0 of the distribution of small forces is dependent on ϕ and satisfies $\theta_l < \theta_0 < \theta$, with $\theta \simeq 0.42$ being the critical exponent of small forces at jamming [64]. Deeper in the jammed phase, the effects of the bucklers disappear and $\rho(f \to 0) \sim f^\theta$ with the jamming exponent. Therefore, in this model it is possible to remove local effects already in dimension $d = 2$ by simply increasing the packing fraction ϕ. Notice that this is not possible when studying only the jamming point: in that case it is possible to eliminate local effects only by increasing d [57]. For $f \to 1$, the local effects do not affect the statistics and $\rho(f \to 1) \sim (1 - f)^\theta$ always.

Rattlers and Bucklers

Rattlers are spheres that, for a given stable configuration, do not interact with any other sphere and therefore they do not have any contact or overlap. This can happen for packing fractions near ϕ_J because the interaction network of spheres can form a cage large enough for a sphere to fit in, isolated from the other particles. This is a local effect in finite dimension. In our model, going into the overcompressed phase, the typical size of the cages becomes smaller and all the spheres enter the contact and overlap networks: therefore the rattlers vanish by increasing ϕ.

Bucklers are spheres that, when perturbed, can relax by buckling locally. They carry small contact forces that affect the total distribution of forces, and are characterized by being typically weakly connected with the rest of the system. Therefore, following [57], bucklers can be defined as spheres having only $d + 1$ contacts. In our case, both contacts and overlaps are present in the system, so we define bucklers as spheres having total connectivity equal to $d + 1$:

$$z_{c,i} + z_{o,i} = d + 1 \tag{4.26}$$

where $z_{c,i}$ is the number of spheres in contact with sphere i and $z_{o,i}$ is the number of spheres overlapping with sphere i.

In a packing of spheres at jamming, a sphere (that isn't a rattler) can be in mechanical equilibrium only if it has at least $d + 1$ contacts, so the connectivity constraint is

$$\text{@jamming} \qquad z_{c,i} \geq d + 1 \qquad \text{for all } i \text{ non-rattlers} \tag{4.27}$$

Interestingly, in the overcompressed phase of our model, a sphere can be in mechanical equilibrium even by having 1 overlap and just d contacts: a sphere can have the resultant of the overlapping forces being compensated in the d directions by d contacts. Therefore, the constraint of connectivity for a sphere being in mechanical equilibrium is

$$\boxed{\begin{cases} z_{c,i} + z_{o,i} \geq d + 1 \\ z_{c,i} \geq d \end{cases} \qquad \text{for all non-rattlers } i} \tag{4.28}$$

Hyperuniformity of the contact network

Following [128], we study the fluctuations of the local number of contacts and number of overlaps. Each sphere i has its center in $\mathbf{x}_i$ and a number $z_{c,i}$ of contacts and $z_{o,i}$ of overlaps. Defining by $\overline{z_c}$ the average contact number (that it is equal to $2d$ because of

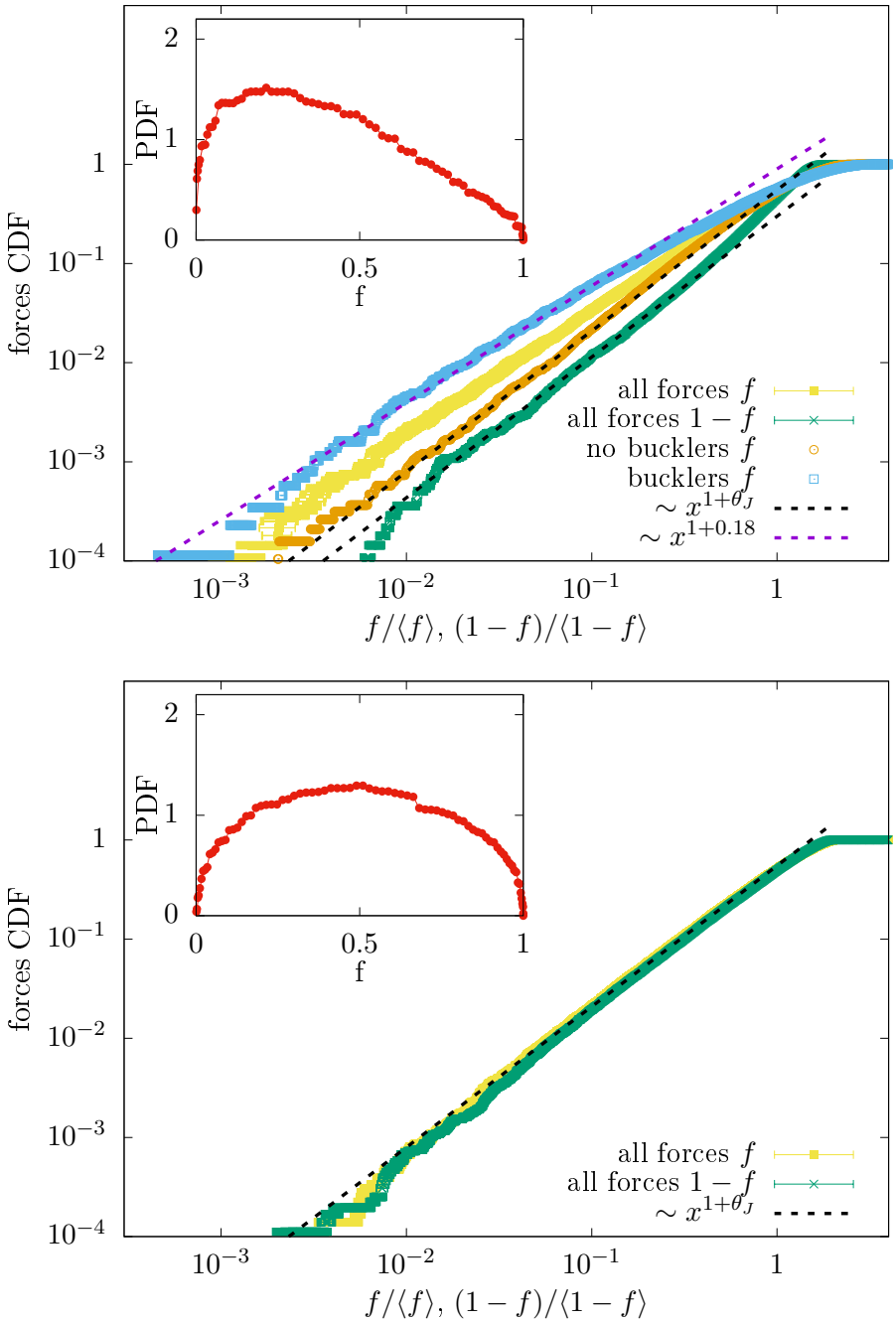

Figure 4.10: Contact force distributions. *Upper panel*: the cumulative of the contact force distribution at $\phi = 0.85$ in $2d$, close to the unjamming transition. We plot the cumulative both starting from the edge at $f = 0$ and at $f = 1$. While a blind statistics of forces is controlled by a hybrid power law exponent, once the effects of bucklers are removed we clearly observe power laws controlled by the mean field exponents, both close to $f = 0^+$ and $f = 1^-$. In the inset we plot the empirical probability distribution function. *Lower panel*: Cumulative distribution of contact forces close to zero and one at $\phi = 2$ in $2d$, far from jamming. We observe that both distributions follow the mean field exponent. Our statistics is not sufficient to detect any localized excitations at this packing fraction and therefore in this case we consider directly all forces without separating the contribution of bucklers from the analysis.

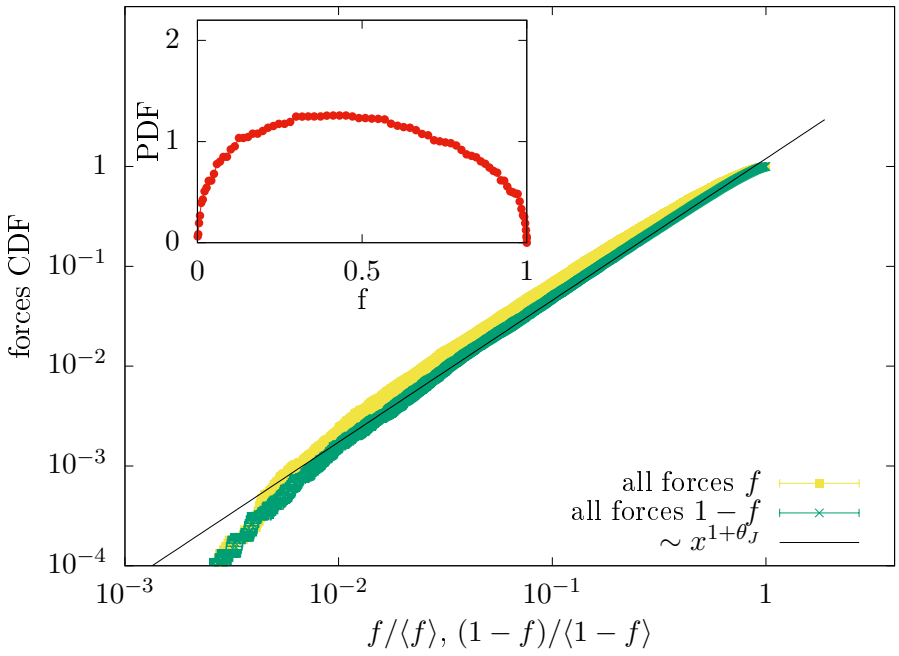

Figure 4.11: Cumulative distribution of contact forces close to the two edges at $\phi = 1.5$. The solid line corresponds to the mean field theory prediction. In the inset we plot the corresponding empirical distribution function. Data produced with system size $N = 1024$, dimensions $d = 3$, averaged over 45 samples for density $\phi = 0.7$, 44 samples for $\phi = 1.5$, 27 samples for $\phi = 2.0$.

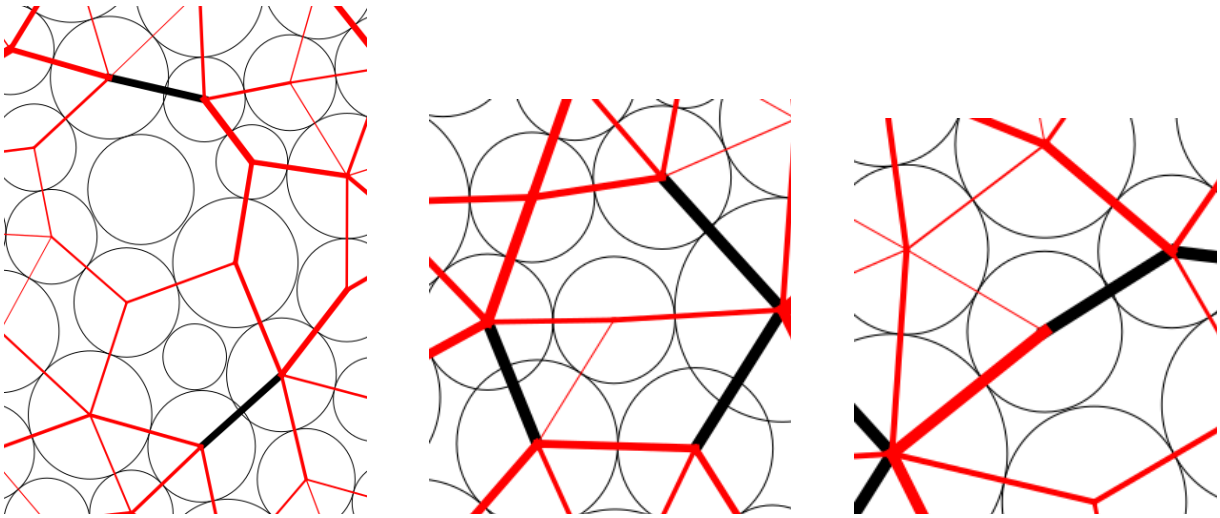

Figure 4.12: Examples of sphere configurations in $d = 2$: black lines represent overlaps, red lines represent contacts and their thicknesses are proportional to the contact force intensities. *Left panel.* Example of two rattlers, i.e. spheres that do not have any contact or overlap and are caged by the other particles. *Central panel.* Example of a buckler with three contacts and no overlap. *Right panel.* Example of a buckler with two contacts and one overlap.

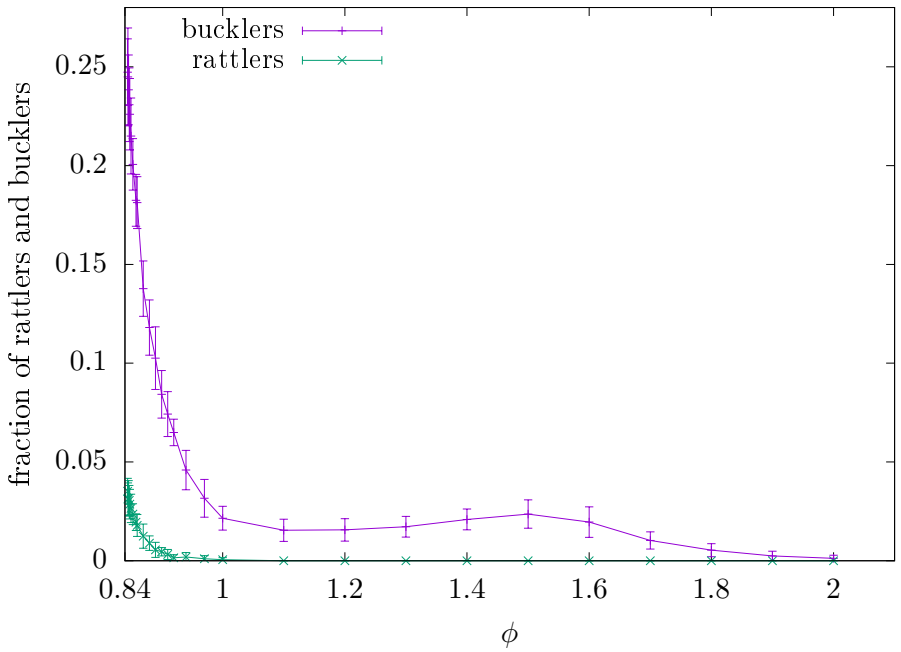

Figure 4.13: Fraction of spheres being rattlers or bucklers (defined in (4.26)) as a function of the packing fraction in dimension $d = 2$.

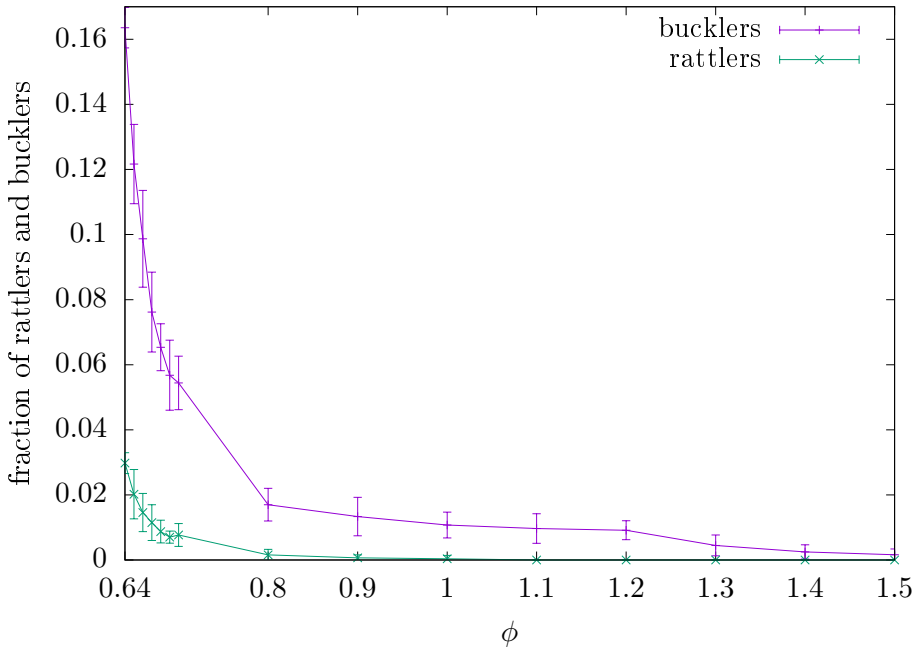

Figure 4.14: Fraction of spheres being rattlers or bucklers (defined in (4.26)) as a function of the packing fraction in dimension $d = 3$.

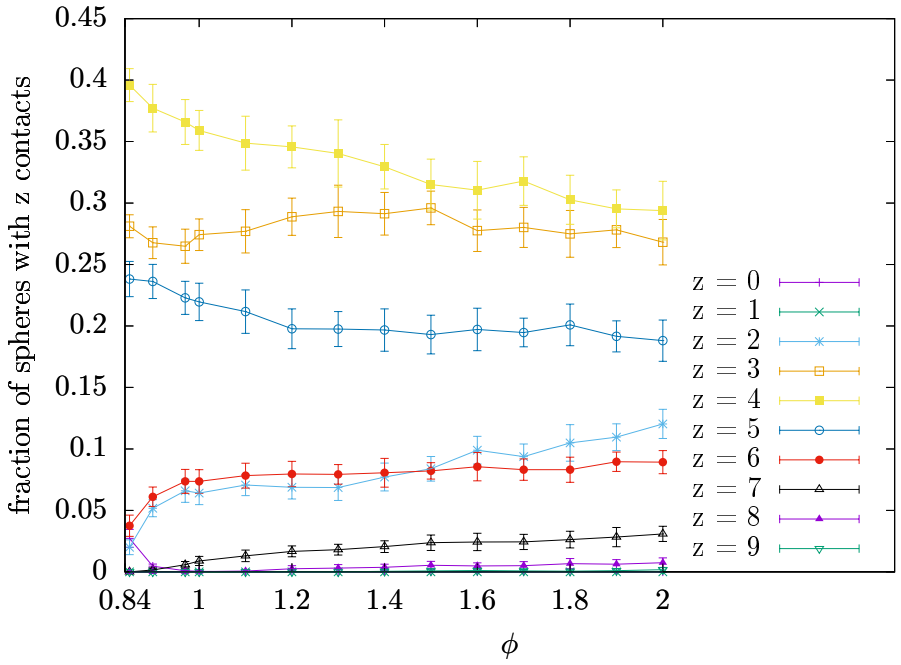

Figure 4.15: Fraction of spheres having z contacts as a function of the packing fraction ϕ, for $d = 2$. At the jamming point, some spheres have $z = 0$ contacts (rattlers) and no sphere has only $z = d = 2$ contacts. Increasing the packing fraction, the rattlers quickly disappear and an extensive number of spheres have just $d = 2$ contacts.

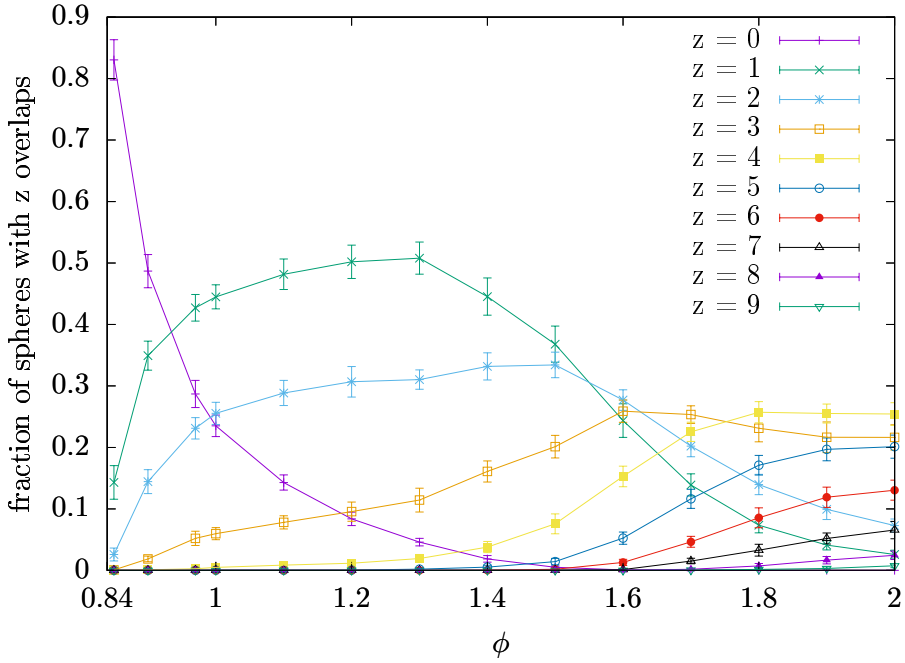

Figure 4.16: Fraction of spheres having z overlaps as a function of the packing fraction ϕ, for $d = 2$. At the jamming point, no sphere has any overlap. Increasing the packing fraction, overlaps start to appear and for $\phi \simeq 1.5$ every sphere has at least one overlap.

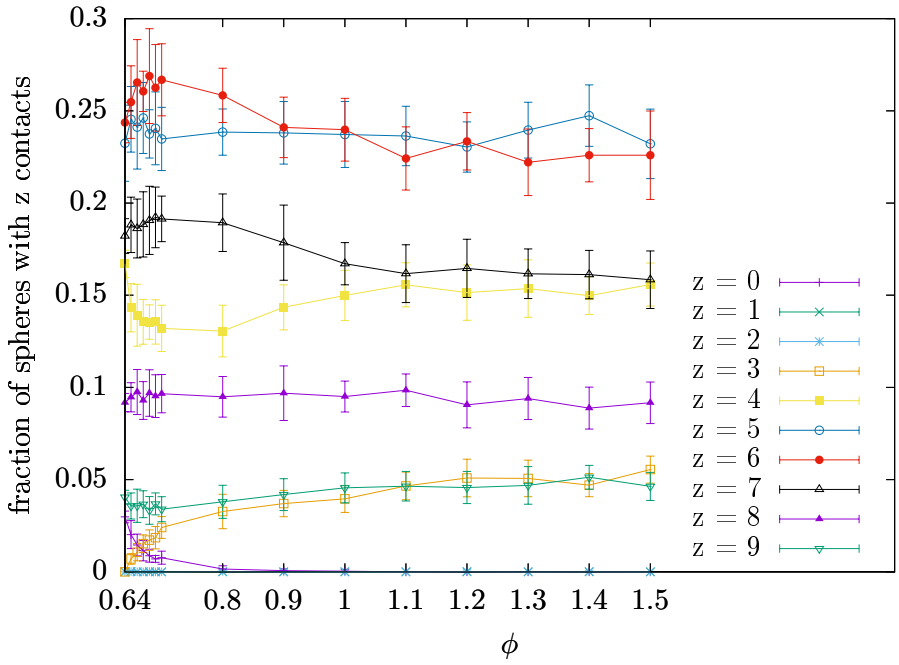

Figure 4.17: Fraction of spheres having z contacts as a function of the packing fraction ϕ, for $d = 3$. At the jamming point, some spheres have $z = 0$ contacts (rattlers) and no sphere has 1, 2 or 3 contacts. Increasing the packing fraction, the rattlers quickly disappear and an extensive number of spheres appear to have only $d = 3$ contacts.

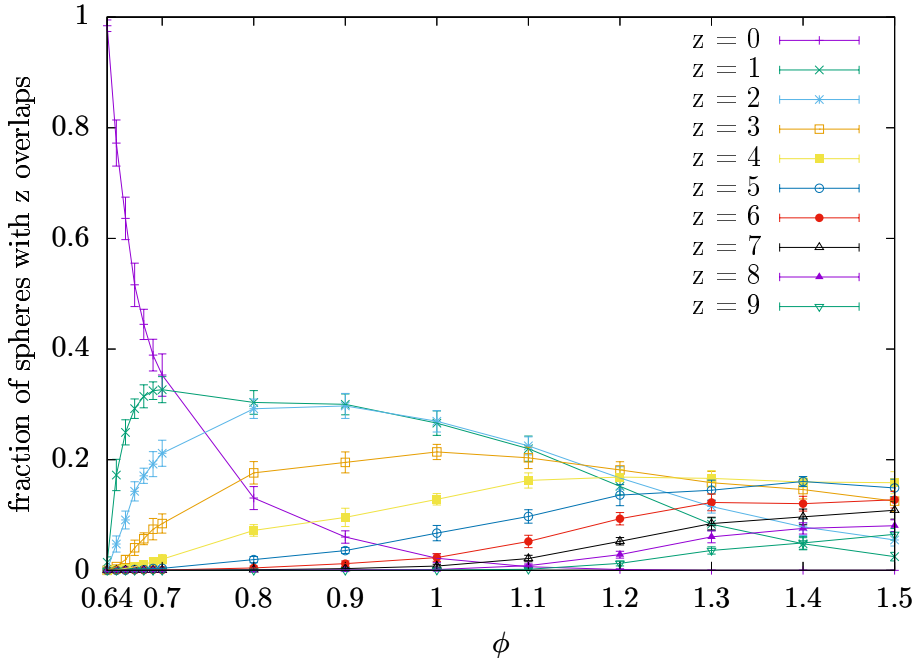

Figure 4.18: Fraction of spheres having z overlaps as a function of the packing fraction ϕ, for $d = 3$. At the jamming point, no sphere has any overlap. Increasing the packing fraction, overlaps start to appear and for $\phi \simeq 1.1$ every sphere has at least one overlap.

isostaticity) and by $\overline{z_o}$ the average overlap number (that it is an increasing function of ϕ), we can define the local fluctuations as $\delta z_{c,i} = z_{c,i} - \overline{z_c}$ and $\delta z_{o,i} = z_{o,i} - \overline{z_c}$. We study their structure factors

$$S_c(q) = \frac{1}{N} \sum_{i,j=1}^{N} \langle \delta z_{c,i} \delta z_{c,j} e^{iq \cdot r_{ij}} \rangle \tag{4.29}$$

and

$$S_o(q) = \frac{1}{N} \sum_{i,j=1}^{N} \langle \delta z_{o,i} \delta z_{o,j} e^{iq \cdot r_{ij}} \rangle \tag{4.30}$$

where the angular brackets represent the average over different minima and $r_{ij} = |\, \mathbf{x}_i - \mathbf{x}_j \,|$. The behavior at small/large q tells about the correlations of connectivity at large/short scale. If the local connectivities are uncorrelated random numbers, their square fluctuations should scale extensively, therefore proportionally to the volume V (or, equivalently, to N), because of the central limit theorem. In that case, we should see $S_{c,o}(q \to 0)$ going to a constant. This is true only for the fluctuations of the overlap numbers.
Differently, the contact number fluctuations are suppressed and they scale sub-extensively: this property is called **hyperuniformity**. Consequently $S_c(q \to 0) \to 0$ and this is possible only with correlations being present at large lengthscales. This is due to the fact that isostaticity is a global condition.
The difference of behavior between S_c and S_o is a manifestation of the different roles that contacts and overlaps play in the stability of the system. As the system is progressively compressed from the jamming point to higher densities, the networks self-organize keeping the number of contacts fixed while increasing the overlaps. As at regular jamming [128], fluctuations of contact numbers away from isostaticity are suppressed and controlled by an infinite lengthscale.
In figure 4.19, we observe the structure factor of the contact numbers and of the overlap numbers in dimension $d = 2$ for different densities ϕ. Interestingly, for small argument $S_c(q)$ goes to zero as a power law whose exponent appears to be compatible with the one measured at the jamming transition [128]. For the overlap numbers, instead, $S_o(q)$ goes to a constant for small argument. The same phenomenon is observed for dimension $d = 3$ in figure 4.20.

4.5.2 A singular Hessian

The linear potential is non-differentiable when a gap is zero and therefore the corresponding Hessian is a singular quantity. However, we can follow the same line of reasoning used for the linear perceptron in section 3.2.2 where we used the smoothed potential to define a Hessian matrix. For a general pairwise potential $\nu(h_{ij})$, the Hessian reads

$$\mathcal{H}_{i\alpha,j\beta} = \begin{cases} -\nu''(h_{ij}) n_{ij}^{\alpha} n_{ij}^{\beta} - \frac{1}{r_{ij}} \nu'(h_{ij})(\delta_{\alpha\beta} - n_{ij}^{\alpha} n_{ij}^{\beta}) & i \neq j \\ -\sum_{k \neq i} \mathcal{H}_{i\alpha,k\beta} & i = j \end{cases} \tag{4.31}$$

where $r_{ij} = |\, \mathbf{x}_i - \mathbf{x}_j \,|$, $n_{ij}^{\alpha} = \frac{x_i^{\alpha} - x_j^{\alpha}}{|\, \mathbf{x}_i - \mathbf{x}_j \,|}$, the indices i and j run over all the spheres $1, ..., N$ and the indices α and β indicate the component $1, ..., d$.
Considering the smoothed Lagrangian (4.11), we have

$$\mathcal{H}_{i\alpha,j\beta} = \begin{cases} -\frac{1}{\epsilon} \sum\limits_{\langle ij \rangle \in \mathcal{C}} n_{ij}^{\alpha} n_{ij}^{\beta} + \sum\limits_{\langle ij \rangle \in \mathcal{C}} \frac{f_{ij}}{r_{ij}} (\delta_{\alpha\beta} - n_{ij}^{\alpha} n_{ij}^{\beta}) + \sum\limits_{\langle ij \rangle \in \mathcal{O}} \frac{1}{r_{ij}} (\delta_{\alpha\beta} - n_{ij}^{\alpha} n_{ij}^{\beta}) & i \neq j \\ -\sum_{k \neq i} \mathcal{H}_{i\alpha,k\beta} & i = j \end{cases} \tag{4.32}$$

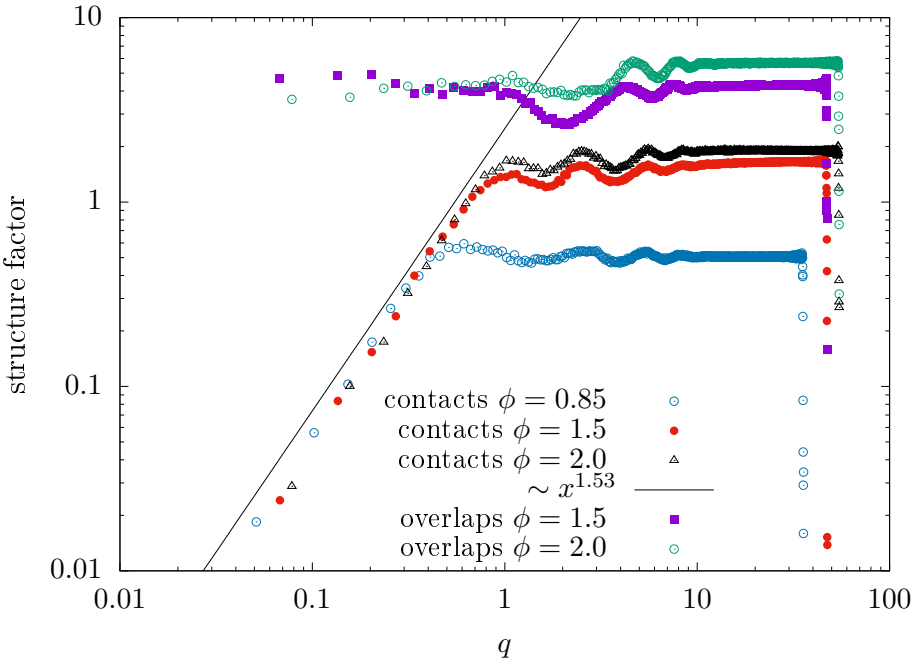

Figure 4.19: Structure factor of the local connectivity of the network of contacts and overlaps for $d = 2$. For small momentum, the structure factor of the contact network decreases down to zero implying hyperuniformity in the fluctuations of connectivity. The exponent controlling the behavior of the structure factor appears to be close to ~ 1.53 which is the same as the one found at jamming [128]. On the contrary, the connectivity of the overlap network is not hyperuniform. These data are produced with system size $N = 4096$.

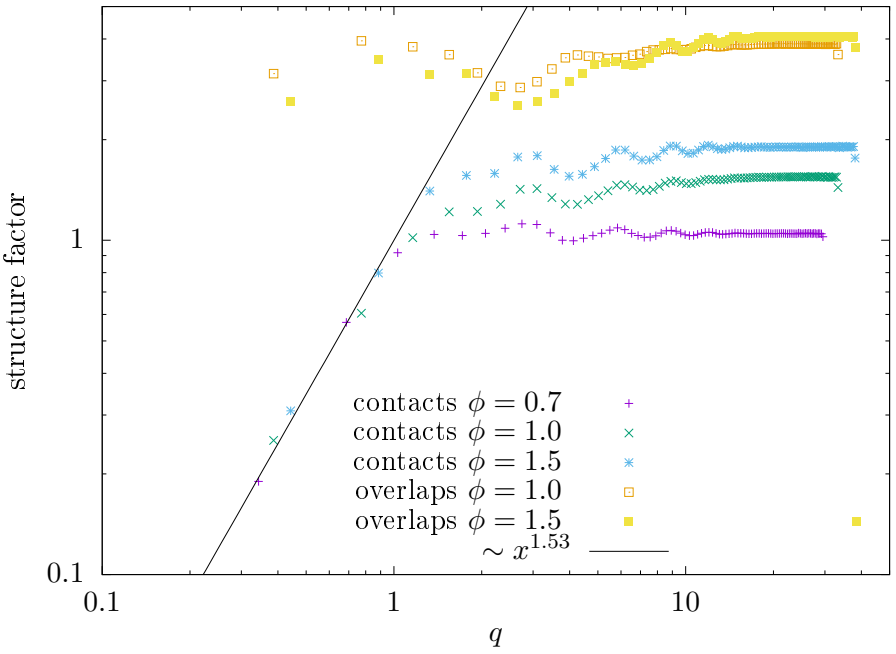

Figure 4.20: Structure factor of the local coordination of the contact and overlap network. While fluctuations of the local connectivity of the overlap network follow the central limit theorem, the ones of the contact network are hyperuniform. Data produced with system size $N = 1024$, dimensions $d = 3$, averaged over ~ 30 samples for each density ϕ.

We can clearly identify the stiffness part

$$-\frac{1}{\epsilon}\sum_{\langle ij\rangle\in\mathcal{C}} n_{ij}^{\alpha}n_{ij}^{\beta} \tag{4.33}$$

that is of order $O(\frac{1}{\epsilon})$, and the pre-stress part

$$\sum_{\langle ij\rangle\in\mathcal{C}}\frac{f_{ij}}{r_{ij}}(\delta_{\alpha\beta}-n_{ij}^{\alpha}n_{ij}^{\beta})+\sum_{\langle ij\rangle\in\mathcal{O}}\frac{1}{r_{ij}}(\delta_{\alpha\beta}-n_{ij}^{\alpha}n_{ij}^{\beta}) \tag{4.34}$$

that is of order $O(1)$ and vanishes at the jamming point. The eigenvalues of the stiffness part are of order $\frac{1}{\epsilon}$, while the pre-stress matrix is negative definite: to have a positive definite Hessian it is necessary that the stiffness matrix is full-rank, since if it has any zero eigenvalue it would receive a contribution from the pre-stress matrix and become negative. Therefore, the system is stable in the limit $\epsilon \to 0$ only if it is isostatic, since that is the only way to have a full-rank stiffness matrix.

The Hessian is therefore dominated by its isostatic random elastic part. Isostatic random matrices are gapless [191, 249, 255, 197, 106, 22] and characterized by an abundance of soft modes. Their spectrum should behave as $\lambda^{-1/2}$ at small argument, where λ represents the eigenvalues. We measure the spectrum of the elastic term matrix, namely the spectrum of

$$\lim_{\epsilon\to 0}\epsilon\ \mathcal{H}_{i\alpha,j\beta} \tag{4.35}$$

In Fig.4.21, we plot the corresponding density of states (DOS) with respect to the vibrational frequency $\omega=\sqrt{\lambda}$. Varying the density from $\phi=0.85$ to $\phi=2.0$, our numerical simulations are compatible with having a constant DOS for $\omega\to 0$.
We see that having a constant DOS for $\omega\to 0$ corresponds to what we observed in the mean-field case, i.e. the perceptron, in section 3.2.2.

4.5.3 The jamming criticality: marginal stability

Further understanding can be obtained by analyzing the marginal stability of the local minima of the energy landscape. They are isostatic, with power-law divergences in the distribution of small gaps and pseudo-gaps at the boundaries of the contact force domain. We realize that the excitations of the system correspond to breaking contacts while the formation of new ones let the system restore isostaticity. Therefore these non-linear excitations dominate the dynamics of the system when it is perturbed away from a minimum. We can generalize the line of thought employed in [247, 154] for the jamming point.

Marginal stability argument

Starting from a configuration in mechanical equilibrium

$$\nabla_i\mathcal{L}=-\sum_{j\in\mathcal{C}(i)}f_{ij}\,\mathbf{n}_{ij}-\sum_{j\in\mathcal{O}(i)}\mathbf{n}_{ij}=0 \tag{4.36}$$

we want to move the particles according to a certain displacement field $\delta\,\mathbf{x}_i$. The second order variation of the energy reads

$$\Delta\,\mathcal{L}\simeq\sum_{i=1}^{N}\nabla_i\,\mathcal{L}\cdot\delta\,\mathbf{x}_i-\sum_{\langle ij\rangle}\frac{F_{ij}(\delta\,\mathbf{x}_{ij}\cdot\mathbf{n}_{ij}^{\perp})^2}{2r_{ij}} \tag{4.37}$$

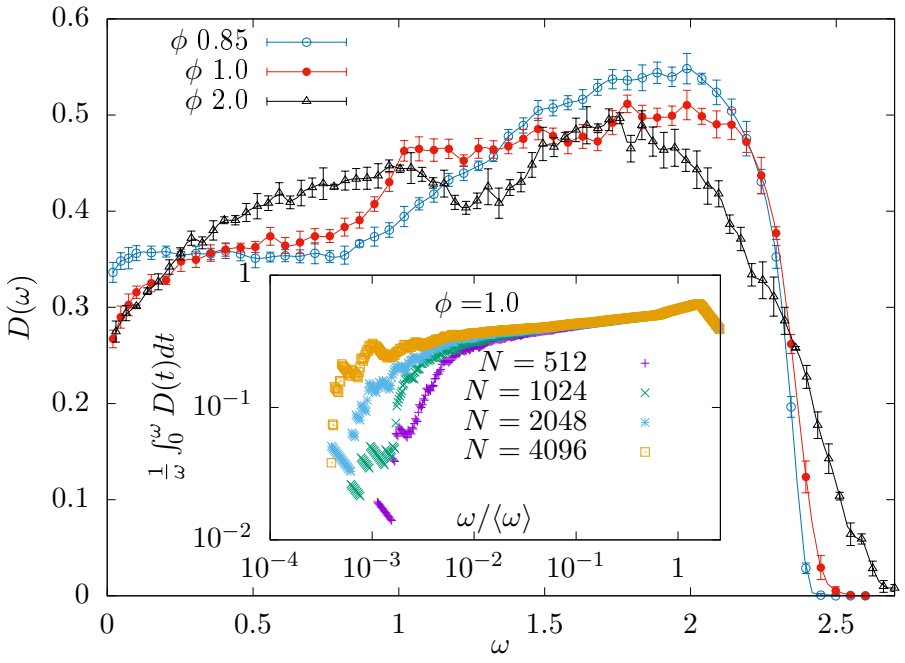

Figure 4.21: Density of states (DOS) of the rescaled elastic part of the Hessian matrix, i.e. eq. (4.35), for different packing fractions above jamming in $d = 2$ and with $N = 4096$, averaged over 44 samples for $\phi = 0.85$, over 40 samples for $\phi = 1.0$, over 48 samples for $\phi = 2.0$. Inset: the finite size behavior of the left tail of the DOS is consistent with having a finite value for $D(\omega = 0)$.

with $\delta\mathbf{x}_{ij} = \delta\mathbf{x}_i - \delta\mathbf{x}_j$, $r_{ij} = |\mathbf{x}_i - \mathbf{x}_j|$, $\delta\mathbf{x}_{ij}\cdot\mathbf{n}_{ij}^{\perp}$ the component of the displacement perpendicular to $\mathbf{n}_{ij}$, $F_{ij} = f_c$ if $\langle ij\rangle \in \mathcal{C}$ or $F_{ij} = 1$ if $\langle ij\rangle \in \mathcal{O}$. The linear term can generically be recast into

$$\sum_{i=1}^{N} \nabla_i \mathcal{L}\cdot\delta\mathbf{x}_i = -\sum_{\langle ij\rangle\in\mathcal{C}} f_{ij}\,\mathbf{n}_{ij}\cdot\delta\mathbf{x}_{ij} - \sum_{\langle ij\rangle\in\mathcal{O}} \mathbf{n}_{ij}\cdot\delta\mathbf{x}_{ij} \tag{4.38}$$

Let's say that we want to open a contact α by pulling apart the two spheres by an amount s, keeping all the other contacts in place. The displacement field is defined by

$$\mathbf{n}_{ij}\cdot\delta\mathbf{x}_{ij}(s) + O(s^2) = s\delta_{\alpha,ij} \qquad \langle ij\rangle \in \mathcal{C} \tag{4.39}$$

Transforming the contact α into a positive gap makes (4.36) loose the contribution coming from f_α, therefore the energy variation with this displacement field reads

$$\Delta\mathcal{L} = f_\alpha s - \sum_{\langle ij\rangle} \frac{F_{ij}(\delta\mathbf{x}_{ij}\cdot\mathbf{n}_{ij}^{\perp})^2}{2r_{ij}} + o(s^2) \tag{4.40}$$

A crucial feature inherited by isostaticity is the fact that the displacements $\delta\mathbf{x}_{ij}\cdot\mathbf{n}_{ij}^{\perp}$ are of order s even very far from the contact opening α (see Ref. [247, 154] for a discussion on this point). The quadratic term in (4.40) can therefore be rewritten as $\sum_{\langle ij\rangle} \frac{F_{ij}(\delta\mathbf{x}_{ij}\cdot\mathbf{n}_{ij}^{\perp})^2}{2r_{ij}} = c_\alpha\langle F\rangle N s^2$, where $\langle F\rangle$ is an average force (proportional to the pressure) and c_α a constant. So we can write

$$\Delta\mathcal{L} = f_\alpha s - c_\alpha\langle F\rangle N s^2 + o(s^2) \tag{4.41}$$

Exactly the same procedure can be followed if, instead of opening a contact, we push the two spheres into each other in order to make them overlap. In this case the displacement field is defined by

$$\mathbf{n}_{ij} \cdot \delta \mathbf{x}_{ij}(s) + O(s^2) = -s\delta_{\alpha,ij} \qquad \langle ij \rangle \in \mathcal{C} \tag{4.42}$$

The gradient in this direction would loose the contribution of f_α but gain the one of the new overlap, therefore

$$\Delta \mathcal{L} = (1 - f_\alpha)s - c_\alpha \langle F \rangle N s^2 + o(s^2) \tag{4.43}$$

In the first case (4.41), the smallest perturbation would correspond to the opening of the weakest contact, i.e. the one with the smallest contact force. With a distribution having a power-law for small forces $\rho(f \to 0^+) \sim f^{\theta_0}$, the smallest force scales as

$$f_{min} \sim N^{-\frac{1}{1+\theta_0}} \tag{4.44}$$

The quadratic term makes the energy variation become negative for $s^* = \frac{f_\alpha}{c_\alpha \langle F \rangle N}$, therefore to have a configuration that is stable against these elementary excitations we need that a new contact is formed for an $s_c \leq s^*$. Since we are opening a contact by pulling two spheres apart, we are reducing the volume available for the other spheres that will tend to get closer: in this setting, a new contact is typically formed by a positive gap that reduces until becoming zero. Therefore s_c is of the order of the smallest positive gap h^+_{min}, that for a power law distribution $\rho(h \to 0^+) \sim h^{-\gamma_+}$ scales as $h^+_{min} \sim N^{-\frac{1}{1-\gamma_+}}$. The condition $h^+_{min} \lesssim s^* = \frac{f_{min}}{c_\alpha \langle F \rangle N}$ gives the relationship between the exponents γ_+ and θ_0

$$\gamma_+ \geq \frac{1}{2 + \theta_0} \tag{4.45}$$

In the second case (4.43), the change in the sign of the energy happens for $s^* = \frac{1-f_\alpha}{c_\alpha \langle F \rangle N}$. The weakest perturbation is obtained by overlapping two spheres whose contact force is the closest to 1. With a power-law $\rho(f \to 1^-) \sim (1 - f)^{\theta_1}$, the following scaling holds

$$(1 - f)_{min} \sim N^{-\frac{1}{1+\theta_1}} \tag{4.46}$$

Since overlapping a pair of spheres makes more volume available for other spheres, new contacts can be formed by relaxing an overlap until it becomes zero. Like in the previous case, for a power-law $\rho(h \to 0^-) \sim |h|^{-\gamma_-}$ the smallest overlap scales as $h^-_{min} \sim N^{-\frac{1}{1-\gamma_-}}$, and the stability condition $h^-_{min} \lesssim s^* = \frac{(1-f)_{min}}{c_\alpha \langle F \rangle N}$ gives

$$\gamma_- \geq \frac{1}{2 + \theta_1} \tag{4.47}$$

By numerical simulations, we have seen that the two stability bounds are saturated and

$$\boxed{\begin{array}{c} \gamma_+ = \gamma_- = \gamma \\ \theta_0 = \theta_1 = \theta \\ \gamma = \dfrac{1}{2 + \theta} \end{array}} \tag{4.48}$$

where $\gamma \simeq 0.41$ and $\theta \simeq 0.42$ are the two critical exponents of small gaps and forces of spheres at jamming, related to marginal stability. To be precise, in small dimension near the jamming onset the exponent θ_0 needs to be considered by properly analyzing local effects (i.e. separating the forces of buckler spheres, presented in section 3.3.1).

4.6 Discussion

We have studied soft spheres with linear repulsion in the jammed phase which we have shown to be a marginally stable, critical phase. As it happens for the jamming transition, this corresponds with our finding in the mean-field version of the model, the perceptron, suggesting once again that the upper critical dimension for the jamming universality class is $d_u = 2$. Since the configurations are isostatic, breaking one contact is enough to destabilize the system and make it flow along the unstable mode; only creating a new contact can restore isostaticity and eventually stabilize the system. Therefore the excitations/relaxations of the system are controlled by the mechanisms of breaking/forming contacts and they are strongly non-linear.
An interesting feature of having a critical phase in finite dimensions is the fact that we can study the jamming criticality in sphere models without the need of looking for the critical point by fine-tuning the control parameters. Moreover, increasing the pressure by going deeper into the jammed phase makes the spheres more connected together and reduces the effects of localized excitations also for finite dimensions.
Since the critical phase is marginally stable, we expect that the response of the system to perturbations is characterized by scale-free avalanches and crackling noise.
Another difference with common soft spheres can be noticed at the unjamming transition, where the pressure has a logarithmic behavior and the number of overlaps scales with a different power-law of the distance from unjamming instead of the typical square-root behavior (more details about this in chapter 5 [109]).

Chapter 5

Surfing on minima of isostatic landscapes: avalanches and the unjamming transition

The content of this chapter is published in [109].

We have seen, both numerically and theoretically, that the UNSAT phase of the perceptron with linear cost-function has a non-convex critical phase related to the jamming universality class. Minima in this phase are isostatic, marginally stable, and their excitation/relaxation mechanisms are controlled by breaking/forming contacts.
Once we have characterized the properties of the static configurations, a natural question is what happens when we perturb the system. In particular, we are interested in studying small compressions of the system, in order to move inside the jammed phase. One way to do so, is to perform small changes of the packing fraction (by changing the average radius or the volume) for spheres or small changes of the parameter σ in the case of the perceptron. The inconvenience of this procedure is that, no matter how small the perturbation, it breaks instantaneously all the contacts. Instead, we perform a Legendre transform over the average-radius for spheres or over σ for the perceptron and we use its conjugate variable, i.e. a pressure p, as a control parameter. The interesting aspect of this procedure is that the contact forces are a linear function of p. Therefore, for finite system size N, we can perform a small variation δp while the contact forces remain in their physical domain $(0, 1)$. For a given configuration, a "critical" value δp_c exists which causes at least one contact force to meet one boundary, be it 0 or 1: it corresponds to the instability point of that contact. Breaking (at least) a contact creates a soft mode that the system can follow until a new isostatic configuration is formed. In this chapter:

- we define the model and its constitutive equations in this transformed ensemble;
- we define an algorithm that performs a compression of the system by triggering small instabilities, both for the perceptron and for spheres;
- we show that this kind of compression gives access to information about the microstructure of the system, like the typical distance between consecutive minima;
- we implement the algorithm for the perceptron, showing that this procedure gives rise to a zero-temperature avalanche dynamics;
- the avalanche dynamics is critical with diverging avalanche sizes;

- we use this fine control to study the unjamming transition in the perceptron and we show it corresponds to a different behavior than the one known for differentiable soft potentials.

5.1 Changing control parameters: a compression algorithm for the perceptron

Let's consider the perceptron with linear cost-function studied in chapter 3.
The configuration is given by an N-dimensional vector $\mathbf{X} \in \mathbb{R}^N$ living on the surface of the hypersphere $|\,\mathbf{X}\,|^2 = N$, subjected to $M = \alpha N$ random soft constraints. They are given by a set of M N-dimensional vectors $\boldsymbol{\xi}_\mu \in \mathbb{R}^N$, with $\mu = 1, ..., M$, called *patterns* that we take as random points on the sphere. Their entries ξ^i_μ, $i = 1, \dots N$ are independent Gaussian random numbers with zero mean and unit variance. The total number of random vectors, M, scales with the dimension of the phase space as $M/N = \alpha$ and α is a $O(1)$ control parameter of the problem. For a given configuration $\mathbf{X}$, each pattern has a corresponding *gap* variable

$$h_\mu = \frac{1}{\sqrt{N}}\,\boldsymbol{\xi}_\mu \cdot \mathbf{X} - \sigma \tag{5.1}$$

with σ being a real number often called *margin* in the machine learning literature. Since in the classification problem the constraints are defined by requiring the positive gaps, $h_\mu \geq 0$, an energy cost is associated to the negative gaps. We are interested in the linear cost-function given by

$$H\left(\mathbf{X}\right) = \sum_\mu |h_\mu| \theta(-h_\mu) \tag{5.2}$$

We have seen in chapter 3 that the minima of this cost-function are characterized by an extensive number $C = cN$ of gaps being exactly zero, called *contacts*, that are associated to their Lagrange multipliers, the *contact forces*. Therefore, the model is better understood by considering the Lagrangian

$$\mathcal{L}\left(\mathbf{X}, \{f_c\}, \eta\right) = \sum_{o \in \mathcal{O}} |h_o| - \sum_{c \in \mathcal{C}} f_c h_c + \frac{\eta}{2}\left(|\,\mathbf{X}\,|^2 - N\right) \tag{5.3}$$

where we have made explicit the spherical constraint $|\,\mathbf{X}\,|^2 = N$ and we have defined the overlap set $\mathcal{O}$ and the contact set $\mathcal{C}$

$$\mathcal{O} = \{o : h_o < 0\} \qquad \mathcal{C} = \{c : h_c = 0\} \tag{5.4}$$

In chapter 3, we have studied the model (5.3) and obtained the phase diagram (fig. 5.1) using the number of patterns α and the margin σ as control parameters.

The UNSAT phase of the model has two main regions:

- a **critical, non-convex, isostatic phase**: the landscape is non-convex due to the fact that $\eta < 0$ and the number of contacts is exactly equal to the number of degrees of freedom (d.o.f.) $N - 1$ (one d.o.f. is set by the spherical constraint). Therefore the isostaticity index $c = 1$, and the minima are marginally stable. The distribution

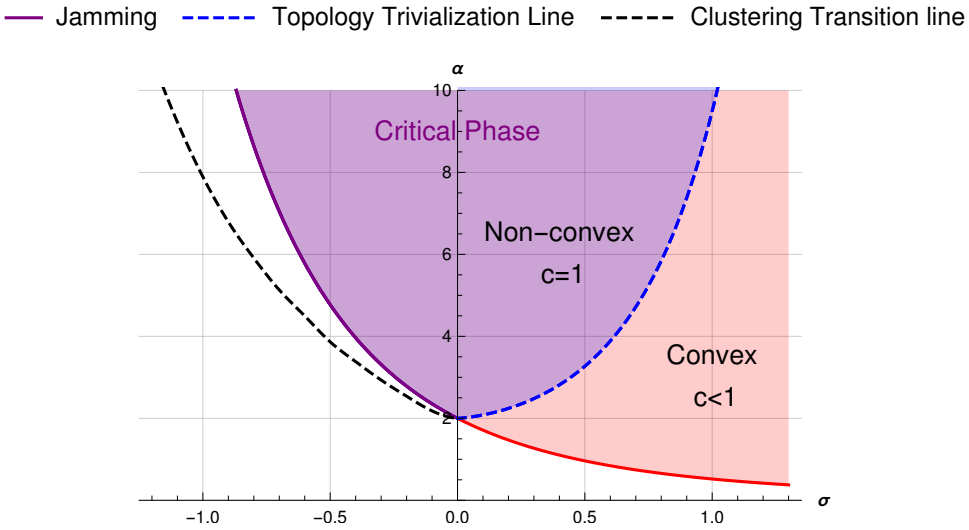

Figure 5.1: The phase diagram of the spherical perceptron problem with linear cost function [108]. The blue dashed curve is a topology trivialization transition line (that coincides with the onset of Replica Symmetry Breaking). Above this line the landscape is non-covex with many local minima while below it is convex with just one unique minimum. The isostaticity index, defined as the number of contacts divided by N is $c = 1$ in the glassy/non-convex phase while $c < 1$ in the convex phase. In the glassy phase one has isostatic minima which are marginally stable. In the SAT phase, we indicated with a black dashed line the point where the solutions to the satisfiability problem become clustered and replica symmetry breaks.

of gaps has a Dirac delta in zero due to the presence of contacts and a power law divergence for small gaps, both positive and negative:

$$g(h \to 0^{\pm}) \sim |h|^{-\gamma} \tag{5.5}$$

The contact forces are distributed in the interval $(0, 1)$ and have pseudogaps near the boundaries of the interval:

$$\rho(f \to 0^{+}) \sim f^{\theta} \qquad \rho(f \to 1^{-}) \sim (1 - f)^{\theta} \tag{5.6}$$

The exponents $\gamma \simeq 0.41$ and $\theta \simeq 0.42$ correspond to the critical exponents of the jamming universality class. The theory of this phase is obtained through the replica formalism and a $full$RSB ansatz.

- a **non-critical, convex, hypostatic phase**: the energy landscape is convex due to $\eta > 0$ and the number of contacts is still extensive but smaller than N, therefore $c < 1$. Due to convexity, there exists a single, stable minimum. The distribution of gaps has a Dirac delta in zero due to the presence of contacts, but no divergence for small gaps. The contact forces are distributed in the interval $(0, 1)$ and have a regular behavior at the boundaries. The distributions of positive/negative gaps and contact forces, in fact, are Gaussian functions (with restricted domains).

Ensemble transformation

We change ensemble by performing a Legendre transform on the parameter σ. We have

$$\mathscr{L} = \mathcal{L} - \sigma \frac{\partial \mathcal{L}}{\partial \sigma} \tag{5.7}$$

We notice that

$$\frac{\partial \mathcal{L}}{\partial \sigma} = \sum_{o \in \mathcal{O}} 1 + \sum_{c \in \mathcal{C}} f_c \tag{5.8}$$

Therefore, we define its intensive version, the pressure p, as done in section 3.3.1, that is basically an average force intensity:

$$p = \frac{1}{N} \frac{\partial \mathcal{L}}{\partial \sigma} = \frac{1}{N} \left(\sum_{o \in \mathcal{O}} 1 + \sum_{c \in \mathcal{C}} f_c \right) \tag{5.9}$$

p is the (intensive) conjugate variable of σ. The transformed Lagrangian becomes

$$\begin{aligned} \mathscr{L}\left(\mathbf{X}, \sigma, \{f_c\}, \mu\right) &= \mathcal{L} - \sigma N p = \\ &= \sum_{o \in \mathcal{O}} \left(\sigma - \frac{\boldsymbol{\xi}_o \cdot \mathbf{X}}{\sqrt{N}} \right) + \sum_{c \in \mathcal{C}} f_c \left(\sigma - \frac{\boldsymbol{\xi}_c \cdot \mathbf{X}}{\sqrt{N}} \right) + \frac{\eta}{2} \left(|\, \mathbf{X} \,|^2 - N \right) - p \sigma N \end{aligned} \tag{5.10}$$

Now σ is a degree of freedom and the control parameters are α and p.

5.1.1 Physical intuition

The addition of the term $-p\sigma N$ in (5.10) is basically tilting the landscape. If the energy part were not present, the term $-p\sigma N$, even for small p, would push σ to ∞. The energy part $H = \sum_{o \in \mathcal{O}} \left(\sigma - \frac{\boldsymbol{\xi}_o \cdot \mathbf{X}}{\sqrt{N}} \right)$, instead, would become zero by making σ small enough so that $h_\mu \geq 0$ for all μ. Therefore, minimizing 5.10 corresponds to finding a trade-off between the two terms, and this is controlled by p.
For $p \to 0$, we get to the jamming transition point where the energy $H \to 0$. For $p > 0$ we enter into the UNSAT/jammed phase. From the definition (5.9), the upper bound for p is given by α, when all the gaps of the system have become negative.

5.1.2 Equilibrium equations for local minima

Once the sets $\mathcal{O}$ and $\mathcal{C}$ are fixed, the extrema of the Lagrangian satisfy the first-order conditions

$$\begin{cases} \partial_{X_i} \mathscr{L} = \sum\limits_o \dfrac{-\xi_{o,i}}{\sqrt{N}} + \sum\limits_c f_c \dfrac{-\xi_{c,i}}{\sqrt{N}} + \eta\, X_i = 0 \\ \partial_\sigma \mathscr{L} = \sum\limits_o 1 + \sum\limits_c f_c - pN = 0 \end{cases} \qquad \begin{cases} \partial_{f_c} \mathscr{L} = -h_c = \sigma - \dfrac{\boldsymbol{\xi}_c \cdot \mathbf{X}}{\sqrt{N}} = 0 \quad \forall c \in \mathscr{C} \\ \partial_\eta \mathscr{L} = \dfrac{1}{2}(\mathbf{X}^2 - N) = 0 \end{cases} \tag{5.11}$$

The first set of these equations states the force balance conditions on each of the variables and the fact that the pressure is the average force due to contacts and overlaps. The second set of equations describes the conditions that $h_c = 0$ for all contacts and the spherical constraint for $\mathbf{X}$. From the constitutive equations (5.11), we can derive a '1st

principle'-like relation between p, σ, η, and the intensive energy due to the overlaps $e = \sum_{o\in\mathcal{O}} |h_o|/N$. Indeed, if we consider $\sum_i X_i \partial_{X_i} \mathscr{L} = 0$ from eq. (5.11), we obtain

$$\eta = p\sigma - e \tag{5.12}$$

This relationship implies that, in a minimum, the value of the Lagrangian is $\frac{\mathscr{L}_*}{N} = -\eta$. Taking the derivatives w.r.t. σ and w.r.t. p keeping the other parameters fixed, we get

$$p = \left.\frac{\mathrm{d}e}{\mathrm{d}\sigma}\right|_{\mathrm{p},\eta} \qquad \sigma = \left.\frac{\mathrm{d}\,\eta}{\mathrm{d}\,\mathrm{p}}\right|_{\sigma,e} . \tag{5.13}$$

The first relation is consistent with the definition of the pressure. The second one tells that η has a minimum for $\sigma = 0$. In fact, let us consider the jamming line, where $\eta = 0$: for $\sigma < 0$, we enter the jammed phase with $\eta < 0$ and we get the non-convex phase; for $\sigma > 0$, instead, η increases and we get $\eta > 0$ defining the convex phase. Moreover, it holds that $e < p\sigma$ in the convex phase and $e > p\sigma$ in the non-convex phase.
Let us notice that (5.11) are $N + C + 2$ equations to be solved for $N + C + 2$ variables, i.e. $X_{i=1,\dots,N}$, σ, $f_{c=1,\dots,C}$, η.
We can write the first set of equations (5.11) in a more compact form by introducing the $C + 1$ dimensional vector

$$\mathbf{f} = \begin{bmatrix} f_1 \\ \dots \\ f_C \\ \eta \end{bmatrix} , \tag{5.14}$$

the $(N + 1) \times (C + 1)$ matrix $\underline{\underline{\mathrm{S}}}$

$$\underline{\underline{\mathrm{S}}} = \begin{bmatrix} \frac{-\boldsymbol{\xi}_1}{\sqrt{N}} & \frac{-\boldsymbol{\xi}_2}{\sqrt{N}} & \dots & \frac{-\boldsymbol{\xi}_C}{\sqrt{N}} & \mathbf{X} \\ 1 & 1 & \dots & 1 & 0 \end{bmatrix} , \tag{5.15}$$

and the $N + 1$ dimensional vector

$$\mathbf{v} = \begin{bmatrix} \frac{1}{\sqrt{N}} \sum_o \boldsymbol{\xi}_o \\ pN - O \end{bmatrix} . \tag{5.16}$$

where $O = |\mathcal{O}|$ is the number of overlaps. We can write

$$\nabla \mathscr{L} = \begin{bmatrix} \partial_{X_1} \mathscr{L} \\ \dots \\ \partial_{X_N} \mathscr{L} \\ \partial_\sigma \mathscr{L} \end{bmatrix} \equiv \underline{\underline{\mathrm{S}}}\, \mathbf{f} - \mathbf{v} = 0. \tag{5.17}$$

We can also rewrite the second set of equations (5.11) through the matrix $\underline{\underline{\mathrm{S}}}$. We have in fact

$$\underline{\underline{\mathrm{S}}}^T \begin{bmatrix} \mathbf{X} \\ \sigma \end{bmatrix} = \begin{bmatrix} \mathbf{0} \\ N \end{bmatrix} \tag{5.18}$$

If the configuration $\begin{bmatrix} \mathbf{X} \\ \sigma \end{bmatrix}$ is known, then it is possible to use equation (5.17) to find the contact forces and the Lagrange multiplier η. A valid physical configuration at equilibrium has to satisfy the condition on the contact forces

$$f_c \in (0, 1) \qquad \forall c \in \mathcal{C} \tag{5.19}$$

that is not automatically satisfied for any set $\mathcal{C}$ and $\mathcal{O}$: they have to be properly found by a minimization algorithm.
In the isostatic phase, we have a number of contacts equal to the number of d.o.f.: considering that a configuration $\begin{bmatrix}\mathbf{X}\\ \sigma\end{bmatrix}$ has $N+1$ d.o.f. and one of them is constrained by the spherical condition $|\,\mathbf{X}\,|^2 = N$, isostaticity in this model is achieved with $C = N$ contacts. Therefore, knowing the sets $\mathcal{C}$ and $\mathcal{O}$ in the isostatic phase, eq. (5.18) alone completely defines the configuration $\begin{bmatrix}\mathbf{X}\\ \sigma\end{bmatrix}$. In fact, considering the matrix $\underline{\underline{\mathrm{S}}}$ without the last column (the one containing $\mathbf{X}$), it will be a rectangular $(N+1)\times N$ matrix with only one left-singular-vector $\begin{bmatrix}\mathbf{w}\\ s\end{bmatrix} \in \mathbb{R}^{N+1}$ having zero singular value:

$$\begin{bmatrix} \frac{-\boldsymbol{\xi}_1}{\sqrt{N}} & 1 \\ \frac{-\boldsymbol{\xi}_2}{\sqrt{N}} & 1 \\ \dots & \dots \\ \frac{-\boldsymbol{\xi}_C}{\sqrt{N}} & 1 \end{bmatrix} \begin{bmatrix}\mathbf{w}\\ s\end{bmatrix} = 0 \tag{5.20}$$

Once $\begin{bmatrix}\mathbf{w}\\ s\end{bmatrix}$ has been found, the configuration is fixed through the spherical constraint $|\,\mathbf{X}\,|^2 = N$:

$$\begin{bmatrix}\mathbf{X}\\ \sigma\end{bmatrix} = \pm\frac{\sqrt{N}}{|\mathbf{w}|}\begin{bmatrix}\mathbf{w}\\ s\end{bmatrix} \tag{5.21}$$

and the sign is chosen so that $h_o < 0$ for all $o \in \mathcal{O}$. Knowing $\mathbf{X}$, we can solve (5.17) to find the contact forces and η.
In the hypostatic phase, knowing $\mathcal{C}$ and $\mathcal{O}$, the condition (5.18) is not enough to find $\begin{bmatrix}\mathbf{X}\\ \sigma\end{bmatrix}$, thus it is necessary to solve it together with (5.17): they do not form a linear problem any longer because of the quadratic coupling $\eta\,\mathbf{X}$ in (5.17).

5.1.3 Instability points and evolution of the configuration

Evolution in the non-convex, isostatic phase

Let us consider what happens when we have an isostatic configuration $\mathbf{X}$, σ, and we vary the pressure $p \to p + \delta p$. For finite size N, an infinitesimal δp does not change $\mathbf{X}$ and eq. (5.17) produces a variation of the contact forces and of μ according to

$$\underline{\underline{\mathrm{S}}}\,\delta\,\mathbf{f} = \begin{bmatrix}\mathbf{0}\\ N\delta p\end{bmatrix} \tag{5.22}$$

As long as every $f_c + \delta f_c$ is in the interval $(0,1)$, the configuration is stable and does not change. When δp reaches a critical value δp^*, one contact force hits a boundary, that is $f_c + \delta f_c = 1$ or $f_c + \delta f_c = 0$ and the corresponding contact becomes unstable: it becomes an overlap (i.e. a negative gap) if $f_c + \delta f_c = 1$, it becomes a positive gap if $f_c + \delta f_c = 0$. Let us say that this destabilized contact has index $c = 1$. At this point, we do not vary δp any longer and we let the system find another stable configuration. The system is

missing one constraint, so the configuration makes a move $\begin{bmatrix}\delta\,\mathbf{X}\\ \delta\sigma\end{bmatrix}$ while keeping the stable contacts in place. Therefore, the movement direction is uniquely defined by:

$$\begin{cases}\frac{1}{\sqrt{N}}\,\boldsymbol{\xi}_c\cdot\delta\,\mathbf{X}-\delta\sigma &= 0 \qquad \forall c\in\mathcal{C}\smallsetminus 1\\ \delta\,\mathbf{X}\cdot\left(\mathbf{X}+\frac{1}{2}\delta\,\mathbf{X}\right) &= 0\end{cases} \tag{5.23}$$

where the first condition ensures that all the contacts except the unstable one stay in place and the second equation, quadratic in $\delta\,\mathbf{X}$, is the spherical constraint. During this evolution, all the gaps, except the stable contacts, have a variation δh_μ

$$\delta h_\mu = \frac{1}{\sqrt{N}}\,\boldsymbol{\xi}_\mu\cdot\delta\,\mathbf{X}-\delta\sigma \tag{5.24}$$

We see that the condition (5.23) ensures that $\delta h_c = 0$ for the stable contacts $c\in\mathcal{C}\smallsetminus 1$, while for all the other gaps $\delta h_\mu\neq 0$. The evolution continues along the direction defined by (5.23) until a positive or negative gap becomes a contact:

$$h_{\tilde{\mu}}+\delta h_{\tilde{\mu}} = 0 \qquad \text{for one } \tilde{\mu}\notin\mathcal{C} \tag{5.25}$$

At this point, we have again an isostatic configuration and the evolution halts. As a net result, the set $\mathcal{C}$ has lost the contact $c=1$ but has acquired a new pattern $\tilde{\mu}$; at the same time, the set $\mathcal{O}$ or the one of the positive gaps have lost the pattern $\tilde{\mu}$ and acquired the ex-contact $c=1$. The new configuration is given by $\mathbf{X}+\delta\,\mathbf{X}$, $\sigma+\delta\sigma$.
Given the new sets $\mathcal{C}$ and $\mathcal{O}$, we can find the new contact forces f_c and the new η by solving equation (5.17). If all the new contact forces are in the interval $(0,1)$, then the configuration is stable. If not, then a further evolution of the configuration is demanded as described in the following section.

Breaking multiple contacts

Let us say that, following the procedure of the last section, we have reached a new configuration that turns out to be unstable because not all the contact forces are in the physical domain $(0,1)$. Then there are two possibilities:

- only one contact force is outside the support $(0,1)$: we have only one unstable contact and we can follow the only direction prescribed by (5.23). Then everything proceeds as in the previous section, until a new contact is formed;
- more than one contact force is outside the support $(0,1)$: then the condition of keeping the stable contacts in place, plus the spherical condition, define a multi-dimensional manifold and the evolution direction is not uniquely defined.

In case of multiple unstable contacts, it is necessary to choose in which direction to move and this is an arbitrary choice. We decide to choose the "softest", or "least-descent", direction, defined by

$$\min_{\mathbf{f}}\ |\nabla\mathscr{L}|^2 \qquad \text{with constraints } f_c\in[0,1] \tag{5.26}$$

where

$$\nabla\mathscr{L} = \underline{\underline{\mathrm{S}}}\,\mathbf{f}-\mathbf{v} \tag{5.27}$$

According to the procedure (5.26), the unstable contacts k get a contact force saturated to the boundary, i.e. $f_k = 0$ or $f_k = 1$, while the stable contacts have $f_c \in (0,1)$. The solution of (5.26) gives the gradient $\nabla^* \mathscr{L}$ that we follow for the evolution of the configuration

$$\begin{bmatrix} \delta \mathbf{X} \\ \delta\sigma \end{bmatrix} \propto -\nabla^* \mathscr{L} \tag{5.28}$$

We should add the spherical condition $\delta \mathbf{X} \left(\mathbf{X} + \frac{1}{2} \delta \mathbf{X} \right) = 0$, but we can actually avoid this non-linear condition and perform a rescaling at the end. The evolution (5.28) induces a variation δh_μ for the non-contact gaps: when one of them becomes a contact, i.e. $h_{\tilde{\mu}} + \delta h_{\tilde{\mu}} = 0$, the evolution stops and the new configuration is given by

$$K \left(\begin{bmatrix} \mathbf{X} \\ \sigma \end{bmatrix} + \begin{bmatrix} \delta \mathbf{X} \\ \delta\sigma \end{bmatrix} \right) \tag{5.29}$$

where K is the rescaling factor $K = \frac{\sqrt{N}}{|\mathbf{X} + \delta \mathbf{X}|}$ needed to ensure the spherical constraint. Note that this rescaling does not change the value of the contact gaps that are zero and does not change the sign of the positive and negative gaps.
At this point we have a new set $\mathcal{C}$: if we still do not have an isostatic and stable configuration, we can compute the new gradient $\nabla^* \mathscr{L}$ by (5.26) and evolve the configuration.

Evolution in the convex, hypostatic phase

The convex phase is hypostatic and the procedure described in the previous section does not apply. In fact, even keeping the contacts in place, an infinitesimal variation of pressure δp, however small, necessarily causes also a variations of the configuration $\begin{bmatrix} \delta \mathbf{X} \\ \delta\sigma \end{bmatrix}$: we have therefore a *state following* scenario. Given a hypostatic configuration and a δp, it is possible to track the evolution by the equilibrium equations (5.11):

$$\begin{cases} \sum_c \delta f_c \frac{-\xi_{c,i}}{\sqrt{N}} + X_i \delta\eta + \eta\, \delta X_i + \delta\eta\, \delta X_i = 0 \\ \sum_c \delta f_c = N \delta p \\ \delta\sigma - \frac{1}{\sqrt{N}} \boldsymbol{\xi}_c \cdot \delta \mathbf{X} = 0 \quad \forall c \in \mathcal{C} \\ \delta \mathbf{X} (\mathbf{X} + \frac{1}{2} \delta \mathbf{X}) = 0 \end{cases} \tag{5.30}$$

The first two equations give the change in δf_c, $\delta\eta$ and $\delta \mathbf{X}$ as a function of δp, while the last two equations impose the contacts staying in place and the spherical condition. As discussed in the isostatic phase, a contact gets destabilized when its force touches a boundary, i.e. $f_c + \delta f_c = 0$ or $f_c + \delta f_c = 1$. At that point, the contact can be removed from $\mathcal{C}$. By the way, the system does not need necessarily to find another contact to stabilize: due to the convexity $\eta > 0$, a proper change $\delta \mathbf{X}$ can be enough to compensate the gradient and restore equilibrium.
Another main difference is that in the isostatic phase it was possible to separate the evolution of δf_c, $\delta\eta$ from that of δX. In fact the algorithm in that case is made of two steps: a pressure variation until the trigger δp^* that destabilizes a contact and a variation $\begin{bmatrix} \delta \mathbf{X} \\ \delta\sigma \end{bmatrix}$ until the stability is restored. In the convex hypostatic case, it is not possible to separate the evolution of δf_c from that of $\delta \mathbf{X}$ since they vary together with δp. However, in the numerical algorithm, we decide to make compression steps with the following routine, that clearly mimics the one of the critical phase.

1 Keeping the configuration $\begin{bmatrix}\mathbf{X}\\ \sigma\end{bmatrix}$, increase δp and compute the approximated variation δf_c, $\delta\,\eta$ from

$$\underline{\underline{\mathrm{S}}}^T\,\underline{\underline{\mathrm{S}}}\,\delta\,\mathbf{f} = N\delta p \tag{5.31}$$

It is an approximation of the correct $\delta\,\mathbf{f}$ since the left hand-side should have an additional term $-\,\eta\,\delta\sigma - \delta\,\eta\,\delta\sigma$. In this way we find a δp^* where one contact force meets one boundary of $(0,1)$ and the corresponding contact gets destabilized.

2 The contact forces $f_c + \delta f_c$ ensure that the gradient $\nabla\,\mathscr{L}\,(\mathbf{X},\mathbf{f}+\delta\,\mathbf{f})$ is orthogonal to the stable contacts, therefore we evolve the configuration according to

$$\begin{bmatrix}\delta\,\mathbf{X}\\ \delta\sigma\end{bmatrix} = -\frac{1}{\eta}\nabla\,\mathscr{L}\,(\mathbf{X},\mathbf{f}+\delta\,\mathbf{f}) \tag{5.32}$$

This evolution makes a variation of the non-contact gaps

$$\delta h_\mu = -\frac{1}{\eta}\begin{bmatrix}\frac{\boldsymbol{\xi}_\mu}{\sqrt{N}}\\ -1\end{bmatrix}\cdot\nabla\,\mathscr{L} \tag{5.33}$$

If there is one non-contact gap that changes sign because of this variation, then we have to reduce the "step" to let this gap potentially become a contact. Giving index $\tilde{\mu}$ to this gap, we have $h_{\tilde{\mu}} + t^*\delta h_{\tilde{\mu}} = 0$ for some $0 < t^* < 1$. Therefore, the actual evolution of the system is

$$\begin{bmatrix}\delta\,\mathbf{X}\\ \delta\sigma\end{bmatrix} = -\frac{t^*}{\eta}\nabla\,\mathscr{L}\,(\mathbf{X},\mathbf{f}+\delta\,\mathbf{f}) \tag{5.34}$$

In this way the gap $\tilde{\mu}$ becomes a contact and enters the set $\mathcal{C}$.

3 The new configuration is given by $K\left(\begin{bmatrix}\mathbf{X}\\ \sigma\end{bmatrix} + \begin{bmatrix}\delta\,\mathbf{X}\\ \delta\sigma\end{bmatrix}\right)$, where K is the rescaling factor $K = \frac{\sqrt{N}}{|\,\mathbf{X}+\delta\,\mathbf{X}\,|}$ needed to ensure the spherical constraint.

4 We use the equilibrium equation (5.17) projected on $\underline{\underline{\mathrm{S}}}^T$ to compute the contact forces f_c in the new configuration

$$\underline{\underline{\mathrm{S}}}^T\,\underline{\underline{\mathrm{S}}}\,\mathbf{f} = \underline{\underline{\mathrm{S}}}^T\,\mathbf{v} \tag{5.35}$$

Since the set $\mathcal{C}$ may have changed, it can happen that some forces are outside the desired physical domain. In that case, we compute the contact forces according to (5.26), i.e. those that minimize the gradient, that is simply a generalization of (5.35).

5 The new set of contact forces gives the new gradient $\nabla\,\mathscr{L}$. If it is still non-zero, then we evolve the configuration according to $-\frac{1}{\eta}\nabla\,\mathscr{L}$ or $-\frac{t^*}{\eta}\nabla\,\mathscr{L}$ as done in step 2. We continue iterating until a configuration $\mathbf{X},\eta,\mathbf{f}$ is found, with the corresponding sets $\mathcal{C}$, $\mathcal{O}$.

5.1.4 The algorithm

We wrap-up the reasoning of the last section by writing the algorithmic procedure used to obtain the data. The compression algorithm is performed at fixed α, from pressure $p = 0^+$, corresponding to the jamming point, to a finite value p_{final}, by "small" variations δp that trigger the instability of one contact at each step, as described in the previous section. As a preliminary step, at fixed α, it is necessary to produce a configuration at the jamming line.

Step 0: producing a configuration at jamming

We consider the smoothed version of the Lagrangian

$$\mathscr{L}_\epsilon = \sum_{o\in\mathcal{O}} \left(\sigma - \frac{\boldsymbol{\xi}_o\cdot\mathbf{X}}{\sqrt{N}}\right) + \sum_{c\in\mathcal{C}} \frac{1}{2\epsilon}\left(\sigma - \frac{\boldsymbol{\xi}_c\cdot\mathbf{X}}{\sqrt{N}}\right)^2 + \frac{\lambda}{4}\left(|\,\mathbf{X}\,|^2 - N\right)^2 - p\sigma N \tag{5.36}$$

where we have introduced a regularization of the interaction for the contacts and the spherical constraint. The extrema of the Lagrangian Eq. (5.10) are recovered from the one of the smoothed one in an appropriate limit $\epsilon \to 0$ and $\lambda \to \infty$. Once the number of patterns α and a value of p *small enough* are chosen, we run a conjugate-gradient descent on the cost function (5.36) with the degrees of freedom $(\mathbf{X}, \sigma)$, repeating the minimization for smaller and smaller values of ϵ (identical to the procedure of section 3.1.2): this produces a configuration $(\mathbf{X}, \sigma)_J$.
In the thermodynamic limit, jamming points are only stable for pressure $p \to 0$. However, as it will become clear in a moment, for finite system size configurations at jamming can sustain small pressures without moving, and they can be compressed till the point where the largest of the contact forces leaves the stability interval $(0, 1)$. Therefore, a finite size configuration at jamming is stable in an interval of pressure values $p \in [0, p_J(N)]$ where $p_J(N) \to 0$ as $N \to \infty$. Given a configuration at jamming, we can compute the contact forces from Eq. (5.11). For p strictly equal to zero all the contact forces are zero. Increasing p, since the set of overlaps is empty $\mathcal{O} = \emptyset$, the solution of the linear system has the form $f_c = p\hat{f}_c$, with $\hat{f}_c$ independent of pressure. The force distribution therefore progressively invades the stability interval $(0, 1)$, and the solution is stable till pressures $p_J(N) = 1/\hat{f}_{\max}$ where the largest contact force exits the stability interval and we enter the jammed phase. In Fig. 5.3, we show the empirical distribution $\rho_f(\hat{f})$ of the rescaled forces $\hat{f} = f/p$ at jamming for $\alpha = 1.5$ and $\alpha = 4$. For $\alpha = 1.5$ the jamming point is in the convex non-critical phase and the isostaticity index is $c = \frac{C}{N} \simeq 0.86$, since we are in the hypostatic phase. The distribution $\rho_f(\hat{f})$ is a Gaussian branch, as expected from the replica symmetric computations for the theory of the linear perceptron in section 3.3.1. For $\alpha = 4$, instead, the jamming point is in the non-convex critical region and the configuration is isostatic, $c = 1$. The force distribution displays the critical pseudogap for $\hat{f} \to 0$ [105] in analogy with hard spheres at jamming [64]. In addition, similarly to what is found in [191] for jamming points in spheres, we empirically observe a large argument tail which is compatible with a Gaussian.
Usual extreme value statistic arguments, supposing independence of the contact forces, imply that $\hat{f}_{\max} \sim \sqrt{\ln N}$, or $p_J(N) = 1/\hat{f}_{\max} \sim (\ln N)^{-1/2}$. Fig.5.2 shows that such a scaling is in agreement with numerical simulations, and gives rise to rather large critical pressures for the system sizes we have studied. When the pressure reaches $p = p_J(N)$, the system becomes unstable because the largest contact force gets to the upper bound of the stability interval $(0, 1)$ and we enter in the jammed phase.

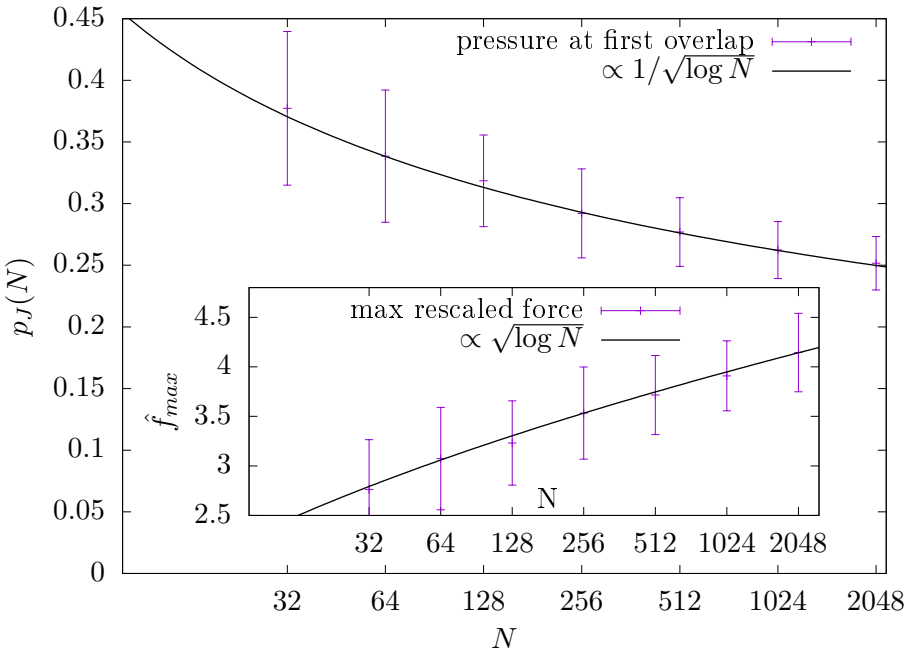

Figure 5.2: The scaling of $p_J(N)$ as a function of the system size at jamming with $\alpha = 4$. In the inset we plot the maximum scaled force $\hat{f}_{\max}$ as a function of the system size. In black lines we show a logarithmic fit.

Notice that the argument for finite volume stability of isostatic configuration under small pressure changes extends without changes into the jammed phase. In fact, also for isostatic jammed configurations, despite the fact that now contact forces have an affine dependence on the pressure, we still have that for fixed $(\mathbf{X}, \sigma)$ a small pressure variation δp induces small force changes $\delta f_c \sim \delta p$. Since generically all forces are strictly smaller than one, this does not cause destabilization if δp is small enough.

Compression in the critical, isostatic phase

Starting with an isostatic stable configuration $(\mathbf{X}, \sigma)$ at pressure p, we proceed with the compression step. The starting configuration can be the isostatic-jamming one: that would be compression step number 1 and the routine works like in the rest of the jammed phase. We rationalize the procedure discussed in section 5.1.3.

1 We compute δp^* for which one contact force gets to the boundary $(0, 1)$, let us say $f_k + \delta f_k = 1$ for a single $k \in \mathcal{C}$. With $p \to p + \delta p^*$ we would have one force at exactly the boundary but still a zero gradient. To make it acquire a component in the unstable direction, we need to add a little push $\delta\delta p << \delta p^*$. Therefore we set $p \leftarrow p + \delta p^* + \delta\delta p$ and we compute the gradient $\nabla^* \mathscr{L}(\mathbf{f}^*) = \underline{\underline{S}}\, \mathbf{f}^* - \mathbf{v}$ according to

$$\nabla^* \mathscr{L} = \nabla \mathscr{L}(\mathbf{f}^*) \text{ with } \mathbf{f}^* = \underset{\mathbf{f}, f_c \in [0,1]}{argmin} |\nabla \mathscr{L}(\mathbf{f})|^2 \tag{5.37}$$

It keeps $f_k = 1$ while the stable contacts compensate for the pressure increment making the gradient $\nabla^* \mathscr{L} \neq 0$ acquire the direction corresponding to breaking only the contact k.

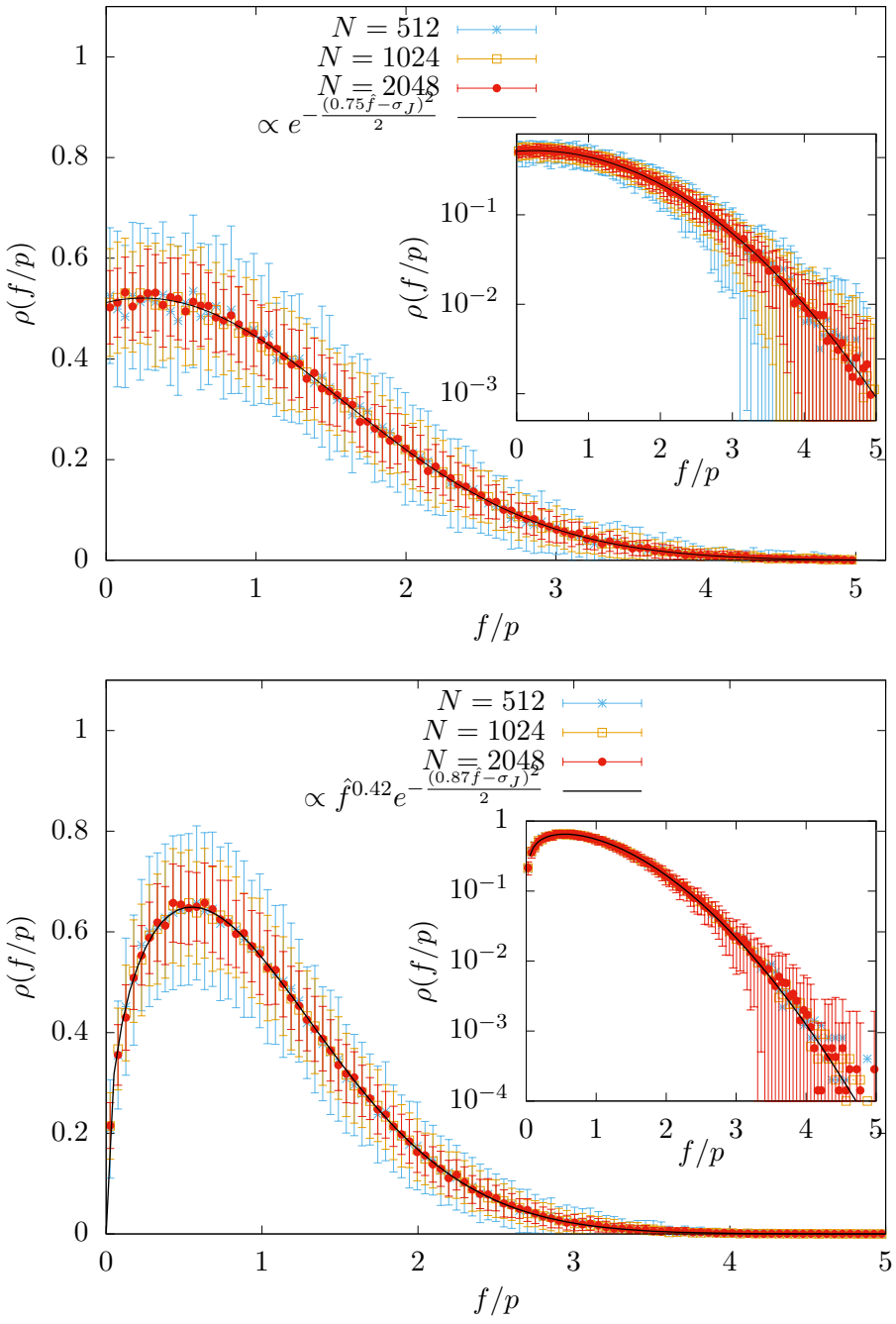

Figure 5.3: The scaled force distribution at jamming for different system sizes at $\alpha = 1.5$ (upper panel) and $\alpha = 4$ (lower panel). Insets: zoom on the tails. The jamming at $\alpha = 1.5$ happens at $\sigma_J \simeq 0.186$ and belongs to the convex, hypostatic phase. The black line represents the functional form $\rho(\hat{f}) = A\ e^{-\frac{(B\hat{f}-\sigma_J)}{2}}$, with the constants A, B fitted, according to the replica symmetric theory developed in section 3.3.1. The jamming at $\alpha = 4$ happens at $\sigma_J \simeq -0.4$ and belongs to the non-convex phase; it manifests the signatures of the jamming criticality, in this case the pseudo-gap $\rho(\hat{f}) \sim \hat{f}^{\theta}$ for small forces, with $\theta \simeq 0.42$ the critical exponent; the black line represents the functional form $\rho(\hat{f}) = A\ \hat{f}^{\theta} e^{-\frac{(B\hat{f}-\sigma_J)}{2}}$, with the constants A, B fitted.

2 We make the move

$$\begin{bmatrix} \delta \mathbf{X} \\ \delta\sigma \end{bmatrix} = -t^* \nabla^* \mathscr{L} \tag{5.38}$$

with

$$t^* = \min_{\mu} \{ t_\mu \ : \ h_\mu + t_\mu \delta h_\mu = 0 \wedge t_\mu > 0 \wedge \mu \notin \mathcal{C} \} \tag{5.39}$$

where $\delta h_\mu = (\frac{\boldsymbol{\xi}_\mu}{\sqrt{N}}, -1) \cdot (\delta \mathbf{X}, \delta\sigma)$.
In this way we move following the gradient until a new contact is formed.

3 We set the new configuration

$$\begin{bmatrix} \mathbf{X} \\ \sigma \end{bmatrix} \leftarrow K \left(\begin{bmatrix} \mathbf{X} \\ \sigma \end{bmatrix} + \begin{bmatrix} \delta \mathbf{X} \\ \delta\sigma \end{bmatrix} \right) \tag{5.40}$$

with the rescaling $K = \frac{\sqrt{N}}{|\mathbf{X} + \delta \mathbf{X}|}$ necessary for ensuring the spherical normalization $|\mathbf{X}|^2 = N$.

4 Given the new configuration, we have two new sets $\mathcal{C}$ and $\mathcal{O}$. If it is isostatic, we can try to solve $\nabla \mathscr{L}(\mathbf{f}) = \underline{\underline{S}} \mathbf{f} - \mathbf{v} = 0$ for $\mathbf{f}$ and check if all the contact forces $f_c \in (0, 1)$; it can happen that now several f_k are outside $(0, 1)$ and we have to break multiple contacts. In any case, if the configuration is unstable we need to find the new gradient $\nabla^* \mathscr{L}(\mathbf{f}^*)$ with the procedure (5.37). We can prescribe to always do (5.37), since it becomes equivalent to solving the linear system $\underline{\underline{S}} \mathbf{f} - \mathbf{v} = 0$ every time that this is possible.
If $\nabla^* \mathscr{L} \neq 0$, we reiterate from point 2. If $\nabla^* \mathscr{L} = 0$, then we have found a new stable configuration for the new pressure value, having all the contact forces $f_c \in (0, 1)$.

Algorithm 3: Linear perceptron: Compression step

$(\mathbf{X}, \sigma)$ starting configuration at p_0;
$\delta p^* \leftarrow$ compute critical pressure variation at fixed $(\mathbf{X}, \sigma)$;
$p \leftarrow p_0 + \delta p^* + \delta\delta p$;
$\mathbf{f}^* \leftarrow \underset{\mathbf{f}, f_c \in [0,1]}{argmin} |\nabla \mathscr{L}(\mathbf{f})|^2$;
$\nabla^* \mathscr{L} \leftarrow \nabla \mathscr{L}(\mathbf{f}^*)$;
while $|\nabla^* \mathscr{L}| > tollerance$ **do**
  $\delta h_\mu = -(\boldsymbol{\xi}_\mu / \sqrt{N}, -1) \cdot \nabla^* \mathscr{L}$;
  $t^* \leftarrow \min_{\mu} \{ t_\mu \ : \ h_\mu + t_\mu \delta h_\mu = 0 \wedge t_\mu > 0 \wedge \mu \notin \mathcal{C} \}$;
  $(\delta \mathbf{X}, \delta\sigma) \leftarrow -t^* \nabla^* \mathscr{L}$;
  $K \leftarrow \sqrt{N} / |\mathbf{X} + \delta \mathbf{X}|$;
  $(\mathbf{X}, \sigma) \leftarrow K [(\mathbf{X}, \sigma) + (\delta \mathbf{X}, \delta\sigma)]$;
  compute the new $\mathcal{C}$, $\mathcal{O}$;
  $\mathbf{f}^* \leftarrow \underset{\mathbf{f}, f_c \in [0,1]}{argmin} |\nabla \mathscr{L}(\mathbf{f})|^2$;
  $\nabla^* \mathscr{L} \leftarrow \nabla \mathscr{L}(\mathbf{f}^*)$;
end
Result: $(\mathbf{X}, \sigma)$ is a stable configuration at pressure $p_0 + \delta p^* + \delta\delta p$

Remarks on the algorithm

- The algorithm 3 can also be applied starting from a jamming configuration $(\mathbf{X}, \sigma)_J$. In that case $p_0 = 0$ and $\delta p^* = p_J(N)$.
- The algorithm 3 simulates plastic events: at $p = p_0 + \delta p^{*+}$ a contact breaks and the system starts moving; it goes thorough intermediate configurations characterized by the formation or the breaking of contacts. Each one of these configurations is a saddle, since it is characterized by stable directions (i.e. the stable contacts) and unstable ones (i.e. the broken contacts). At each intermediate configuration, the system can acquire at most one new stable contact, since the gaps close one by one. Therefore, the unstable directions diminish progressively when approaching a new isostatic stable point.
- In the critical phase, the number of iterations to get a new stable configuration varies a lot: this is due to the avalanche distribution that is a fat-tailed power law, as discussed in the next section.
- The most computational demanding step is the constrained minimization $\underset{\mathbf{f}, f_c \in [0,1]}{argmin} |\nabla \mathscr{L}(\mathbf{f})|^2$ which corresponds to a constrained least-squares problem. To solve it, we use the routine described in reference [152].
- It is possible to avoid the rescaling and implementing directly the spherical condition on the displacement $\delta \mathbf{X} \cdot (\mathbf{X} + \frac{1}{2}\delta \mathbf{X}) = 0$. The direction of the displacement $-\nabla^* \mathscr{L}$ is such that $\nabla^* \mathscr{L} \cdot (\mathbf{X}, 0) = 0$. Since the spherical condition is a non-linear one, we would need to find the correct displacement direction $\nabla^* \mathscr{L}\big|_{\delta \mathbf{X}}$ by iteration using the projector $1 - \underline{\underline{\tilde{\mathrm{S}}}} \left(\underline{\underline{\tilde{\mathrm{S}}}}^T \underline{\underline{\tilde{\mathrm{S}}}} \right)^{-1} \underline{\underline{\tilde{\mathrm{S}}}}^T$, where the matrix $\underline{\underline{\tilde{\mathrm{S}}}}$ is the same as $\underline{\underline{\mathrm{S}}}$ but with $\mathbf{X} + \frac{1}{2}\delta \mathbf{X}$ in the last column (instead of simply $\mathbf{X}$). Therefore $\nabla^* \mathscr{L}\big|_{\delta \mathbf{X}}$ is found by convergence of

$$\nabla^* \mathscr{L}\big|_{\delta \mathbf{X}} = \left[1 - \underline{\underline{\tilde{\mathrm{S}}}} \left(\underline{\underline{\tilde{\mathrm{S}}}}^T \underline{\underline{\tilde{\mathrm{S}}}} \right)^{-1} \underline{\underline{\tilde{\mathrm{S}}}}^T \right] \nabla^* \mathscr{L}\big|_{\delta \mathbf{X}} \tag{5.41}$$

  The role of the projector $1 - \underline{\underline{\tilde{\mathrm{S}}}} \left(\underline{\underline{\tilde{\mathrm{S}}}}^T \underline{\underline{\tilde{\mathrm{S}}}} \right)^{-1} \underline{\underline{\tilde{\mathrm{S}}}}^T$ is simply to eliminate the component of the displacement along $\mathbf{X} + \frac{1}{2}\delta \mathbf{X}$ while keeping all the stable contacts, corresponding to the other columns of $\underline{\underline{\tilde{\mathrm{S}}}}$, intact.

Compression in the convex, hypostatic phase

In the convex phase, the configuration $(\mathbf{X}, \sigma)$ can continuously follow any pressure variation $(\delta \mathbf{X}, \delta\sigma) \propto \delta p$. Anyway, we decide to take steps in δp with the same criteria used in the isostatic phase, i.e. by destabilizing one contact at the time. Therefore, it is possible to use exactly the algorithm (3) modifying only the computation of t^* in the following manner:

$$\begin{aligned} t_{\tilde{\mu}} &= \min_{\mu} \{ t_\mu \ : \ h_\mu + t_\mu \delta h_\mu = 0 \wedge t_\mu > 0 \wedge \mu \notin \mathcal{C} \} \\ t^* &= min\{ \frac{1}{\eta}, t_{\tilde{\mu}} \} \end{aligned} \tag{5.42}$$

In fact, in the convex phase, $\eta > 0$ and the gradient can be compensated by a move $\delta \mathbf{X}$ following the positive curvature $\frac{1}{\eta}$.

5.2 Results of numerical simulations

In this section, we discuss the results obtained by running the algorithm presented in the previous section. We are mainly interested in the case $\alpha > 2$, where the jamming point lies in the non-convex domain of the phase diagram and the system enters in the critical phase characterized by avalanches. For comparison we also consider values $\alpha < 2$. We simulated system sizes $N = 64, 128, 256, 512, 1024$, all quantities were averaged over 100 independent samples. In the step 0, the gradient based minimization has been done with the same L-BFGS minimizer [260, 185, 240] as used in the section 3.1.2.

We first see the behavior of bulk physical quantities across the full compression cycle and then analyze the statistics of avalanches. Finally we will discuss the scalings at the unjamming transition.

5.2.1 Following a jammed configuration across the phase diagram: the topology trivialization transition

Let us consider the case $\alpha = 4$, so the initial configuration is at a non-convex jamming point with $\sigma_J < 0$. Compressing the system, we enter the jammed phase: based on the phase diagram of Fig.5.1, we expect that the system undergoes a transition from the glassy phase to the convex phase where the landscape reduces to a unique minimum.

In Fig.5.4 we plot the evolution of the isostaticity index $c = C/N$, measuring the number of contacts C, and the value of the Lagrange multiplier η for the spherical constraint. We plot the corresponding behavior both as a function of the pressure and as a function of the distance from the algorithmic jamming point σ_J. It is clear from the figure that there are two regimes. For $p < p^*$ the isostaticity index is strictly equal to one. In this regime, the system is isostatic and the compression steps correspond to avalanches between isostatic minima. Correspondingly, the Lagrange multiplier η is negative. In fact, as already discussed in section 3.1.3, the convex or non-convex nature of the problem is self-generated and is detected from the sign of the Lagrange multiplier η. The region where $\eta < 0$ corresponds to the glassy phase where the optimization problem is non-convex while $\eta > 0$ corresponds to the convex phase where the landscape is characterized by a unique attractive minimum. Therefore the replica symmetry breaking transition point at which η changes sign is the point of a topology trivialization: it separates a region where the landscape is very rough and the dynamics surfs on marginally stable states from a region where the landscape is convex.

5.2.2 Statistics of avalanches in the non-convex UNSAT phase

In this section we consider the statistics of jumps in the critical phase where, increasing the pressure, the system undergoes a series of avalanches. As we have discussed, they are triggered by the fact that some of the contact forces exit the support $(0, 1)$ leading to a rearrangement of the contact network, with consequent jumps in σ and energy (see Fig.5.5). In order to quantitatively describe the statistics of avalanches, we need to

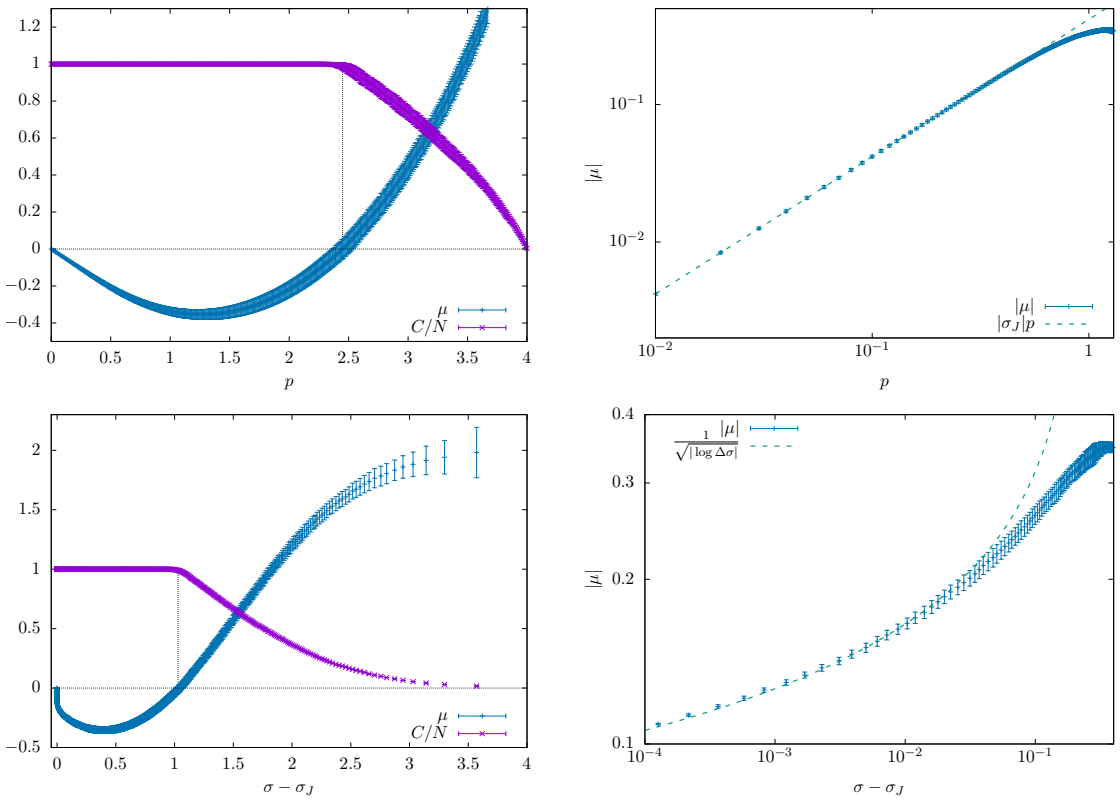

Figure 5.4: *Left panel*: The evolution of the number of contacts normalized by N and the Lagrange multiplier η (indicated as μ in the plot legend) as a function of p (top plot) and $\sigma - \sigma_J$ (bottom plot) at $\alpha = 4$ and $N = 256$. The dotted lines correspond to the topology trivialization transition point (*a.k.a.* the RSB transition) where the landscape changes from being glassy to being convex. *Right panel*: Behavior of the absolute value of the Lagrange multiplier η (indicated as μ in the plot legend) near the unjamming transition with respect to p (top plot) and $\sigma - \sigma_J$ (bottom plot). We observe a linear dependence on η in p, $\eta \simeq \sigma_J p$, and a logarithmic dependence in $\sigma - \sigma_J$, see discussion of section 5.2.3.

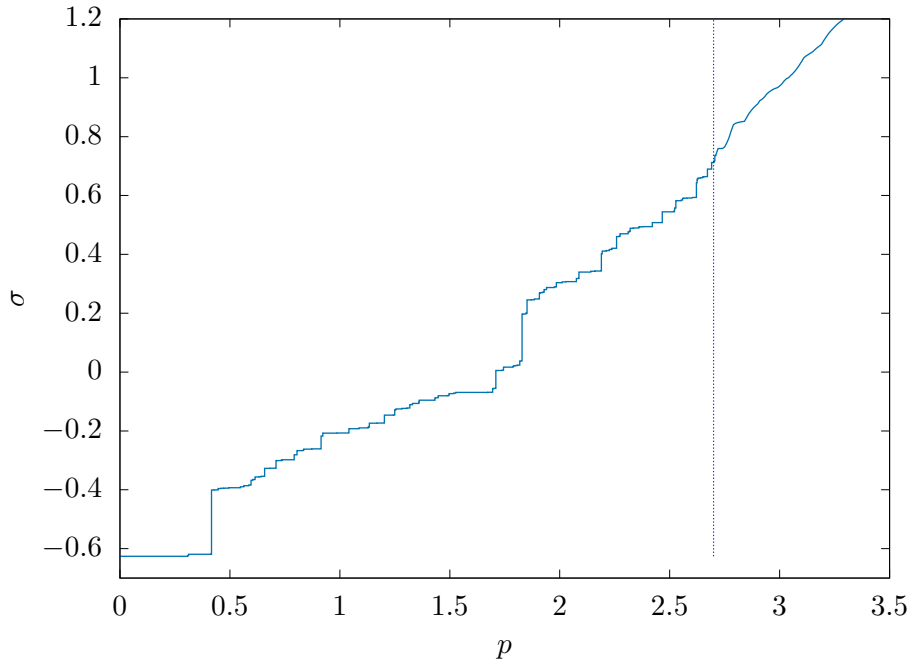

Figure 5.5: The staircase of the values of σ as a function of p for a single sample at $\alpha = 4$ for $N = 32$, starting from jamming. The vertical dashed line signals the point where η changes signs and the landscape of the model becomes convex. Correspondingly, coming from jamming, one looses the jerky staircase profile that characterizes the non-convex phase and signals crackling noise.

establish the typical finite size scale of the pressure variation between two stable isostatic configurations, δp, and also the typical finite size scale of the jumps $\delta\sigma$ that take place when the rearrangements happen.

The jumps of the pressure

As we have seen, minima have a small range of stability when the pressure is changed. We would like to estimate here the order of magnitude of pressure changes δp needed to destabilize a minimum. This is different at jamming and in the jammed phase. We have seen that at jamming, supposing a Gaussian tail of the force distribution, $\delta p_J \sim 1/\sqrt{\log N}$. In the jammed phase, the situation is different. The force distribution has a pseudo-gap rather than an exponential tail, namely $\rho_f(f) \sim (1-f)^\theta$, and one can expect that typically δp scales as an inverse power of N: $\delta p \sim N^{-\beta}$.

In order to estimate the exponent β, we start from Eq. (5.13). Since in the interval $[p, p+\delta p]$ the configuration $(\mathbf{X}, \sigma)$ does not move, we have that

$$\delta\,\eta = \sigma\delta p \tag{5.43}$$

Therefore, the force balance condition, upon increasing pressure by δp, reads

$$-v_i + \sum_c (f_c + \delta f_c)\frac{-\xi_{c,i}}{\sqrt{N}} + (\eta + \sigma\delta p)X_i = 0. \tag{5.44}$$

$$v_i = \sum_o \frac{\xi_{o,i}}{\sqrt{N}}$$

or, defining $\tilde{\xi}_{c,i} = \frac{\xi_{c,i}}{\sqrt{N}}$

$$\delta f_c = \delta p \sigma \sum_i (\tilde{\xi}^{-1})_{c,i} X_i. \tag{5.45}$$

We would like to argue that, while $\frac{1}{N}\sum_c \delta f_c = \delta p$, the typical values of δf_c are of order $O(\delta p\sqrt{N})$. An increase of pressure results in a additional force on each variable i proportional to X_i. These forces need to be compensated by variations in the contact forces f_c. These forces are correlated with the ξ_c by the contact conditions. In order to proceed, we argue that the effect of a pressure change is statistically similar to the application of random forces on the variables [1]. Let us then slightly modify the problem, imagining to perturb the equilibrium equations by a random term ϵY_i with $\mathbf{Y}$ a vector of random variables independent of the patterns with $\langle Y_i^2\rangle$=1. Since the resulting δf_c will have both signs, we can estimate the order of magnitude of each term, by studying

$$\frac{1}{N}\sum_c (\delta f_c)^2 = \epsilon \frac{1}{N} \sum_{i,j} Y_i (M^{-1})_{ij} Y_j \tag{5.46}$$

where the matrix M_{ij} is

$$M_{ij} = \frac{1}{N}\sum_c \xi_{c,i}\xi_{c,j}. \tag{5.47}$$

This matrix is known to be close to a Wishart matrix with quality factor 1 [106]. In the thermodynamic limit its spectral density behaves as $\rho(\lambda) \sim \lambda^{-1/2}$ for small λ, and, for finite N, the minimum eigenvalue is of order $\lambda_{min} \sim N^{-2}$. Moreover, the eigenvectors $|n\rangle$ of M are just random points on the sphere of radius 1 independent on the eigenvalues, orthogonal to each other and weakly correlated with X. Let us use the spectral representation of M and write:

$$\frac{1}{N}\sum_{i,j} Y_i (M^{-1})_{ij} Y_j = \frac{1}{N}\sum_n \frac{1}{\lambda_n}\langle Y|n\rangle^2. \tag{5.48}$$

The random factors $\langle Y|n\rangle$ are Gaussian variables with unit variance, so the expected value over Y of this quantity is

$$\frac{1}{N}\,\mathrm{Tr}\; M^{-1} = \int_{\lambda_{min}}^4 \frac{\rho(\lambda)}{\lambda} \sim \lambda_{min}^{-1/2} \sim N, \tag{5.49}$$

leading to $\delta f_c = O(\epsilon N^{1/2})$. We verified that the calculation of higher moments confirms this scaling. Looking back at the original perturbation $\delta f_c = \delta p \sigma \sum_i (\tilde{\xi}^{-1})_{c,i} X_i$, we want to check that it is equivalent to a random one. To do so, let us notice that the contact forces f_c read

$$f_c = \sum_i (\tilde{\xi}^{-1})_{c,i} v_i + \eta \sum_i (\tilde{\xi}^{-1})_{c,i} X_i \;\in (0,1). \tag{5.50}$$

We notice that the contribution from the overlaps $v_i = \sum_o \tilde{\xi}_{o,i}$ is a random term essentially independent of the choice of the contacts. If $O \sim N$, v_i is of order $O(1)$ and therefore

[1] In infinite dimensions, it is clear that any direction is effectively a random direction from the perspective of the system. While it can be shown analytically for thermodynamic observables [1], it is much less obvious for mesoscopic quantities, meaning quantities that scale in a nontrivial way with the system size as we are showing.

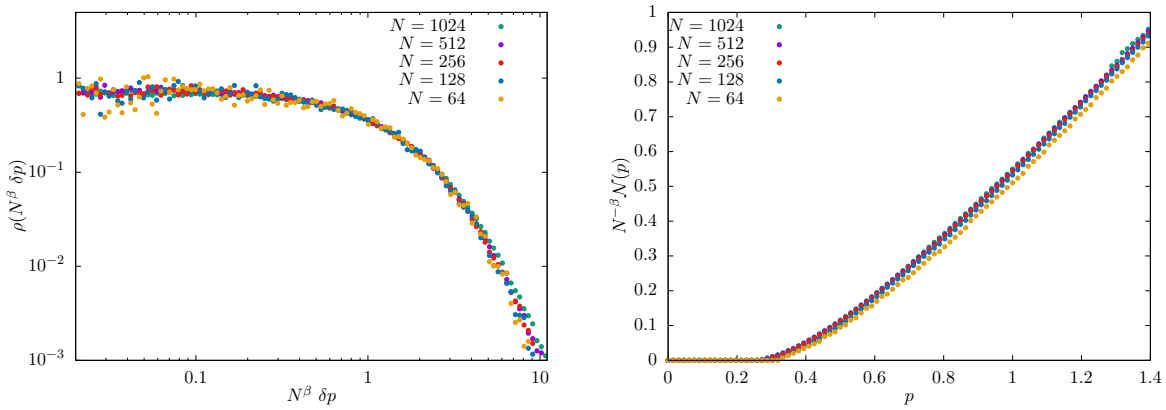

Figure 5.6: *Left panel:* Statistics of the scaled jumps of the pressure $\hat{\delta p} = N^\beta \delta p$. *Right panel:* Average cumulative number of plastic events up to pressure p, rescaled by $N^{-\beta}$, as a function of p. It shows that the number of plastic events scales as N^β for finite pressure variation Δp.

the two terms at the r.h.s. of (5.50) are of order $O(\sqrt{N})$. To have $f_c \in (0,1)$, these two terms have to cancel out at the order $O(\sqrt{N})$. Consequently, the perturbation δf_c, which is proportional to the second term in the r.h.s. of (5.50), can be considered uncorrelated from f_c and we have

$$\delta f_c = O(\delta p N^{1/2}) \tag{5.51}$$

This scaling does not apply close to jamming, where $|v_i| \ll |X_i|$ and there is no cancellation: the second contribution in (5.50) dominates the sum and $\delta f_c = \delta p f_c$.
Let us notice that this argument has an interesting byproduct: it shows that, in the bulk of the jammed phase, the effect of a small compression is statistically equivalent to a random perturbation.

We can now estimate the order of magnitude of a destabilizing pressure variation δp. Following a compression, the first force that exits the stability support $(0,1)$ is one close to the edges in the unperturbed configuration; because of the pseudo-gaps $\rho_f(f \to 0^+) \sim f^\theta$ and $\rho_f(f \to 1^-) \sim (1-f)^\theta$ in the critical phase, standard extreme value statistics tells us that the corresponding δf_c is of the order $\delta f_c \sim N^{-1/(1+\theta)}$. Therefore we obtain the scaling

$$N^{-1/(1+\theta)} \sim N^{1/2}\delta p \tag{5.52}$$

or,

$$\boxed{\delta p \sim N^{-\beta} \qquad \beta = \frac{1}{2} + \frac{1}{1+\theta}} \tag{5.53}$$

In Fig.5.6, we show the histogram of the rescaled pressure jumps $\delta\hat{p} = N^\beta \delta p$ between plastic events, collected from all the jumps taking place when the pressure lies in the interval $p \in [0.2, 1.2]$ [2] for different system sizes and we observe an excellent data collapse. Notice that the tail of the distribution at large argument converge to zero exponentially and in any case much faster than $(\delta\hat{p})^{-2}$. The first moment of $\delta\hat{p}$, $\langle\delta\hat{p}\rangle$ remains finite for

[2] We verified that in this interval of pressure the statistics of jumps is reasonably stationary.

$N \to \infty$, and the number $\mathcal{N}(\Delta p)$ of plastic events that occur when pressure is increased by a finite amount Δp scales as

$$\mathcal{N}(\Delta p) = \frac{\Delta p}{\langle \delta p \rangle} \sim \Delta p N^{\beta} \tag{5.54}$$

The left panel of Fig. 5.7 shows the average $\langle \delta p \rangle$ as a function of pressure. As expected, the scaling $\langle \delta p \rangle \sim N^{-\beta}$ is well respected except for the vicinity of jamming.

Statistics of the jumps of σ

In a similar way, we can relate the order of magnitude of the jumps in σ after a plastic event to the exponent γ of the gap distribution. For $N \to \infty$, the statistics of the small jumps of σ shrinks to zero as $\delta\sigma \sim N^{-\omega}$. To determine ω, let us consider the variation of σ that ensues a process where a weak single contact, say contact c, becomes a small positive gap or overlap. Therefore we have a configuration movement $(\delta \mathbf{X}, \delta\sigma)$ that conserves all the contacts $c' \neq c$ and modifies the contact c by an amount δh_c:

$$\sum_i \tilde{\xi}_{c',i} \delta X_i - \delta\sigma = \delta_{c,c'} \delta h_c \tag{5.55}$$

The movement stops when a new contact is formed, therefore δh_c is of the order of the smallest gap present in the system. Because of the divergences in the distribution of small gaps $\rho_h(h \to 0^{\pm}) \sim |h|^{-\gamma}$, extreme value statistics gives an estimation of the smallest gaps $\delta h_c \sim N^{-1/(1-\gamma)}$. Being full rank, $\tilde{\xi}_{c',i}$ can be inverted and we get

$$\delta X_i = \sum_{c'} \tilde{\xi}^{-1}_{i,c'} \left(\delta_{c,c'} \delta h_c + \delta\sigma \right) \tag{5.56}$$

Multiplying both sides by X_i and summing over i

$$\mathbf{X} \cdot \delta \mathbf{X} = \sum_i X_i \left(\tilde{\xi}^{-1}_{i,c} \delta h_c + \delta\sigma \sum_{c'} \tilde{\xi}^{-1}_{i,c'} \right) \tag{5.57}$$

Because of the spherical condition $\mathbf{X} \cdot \delta \mathbf{X} = -\frac{1}{2} \delta \mathbf{X} \cdot \delta \mathbf{X}$, the l.h.s. of (5.57) is of order $O(|\delta \mathbf{X}|^2)$ and the two terms at the r.h.s. have to compensate each other at their leading order. Therefore they are of the same order and we get

$$\boxed{\delta\sigma \sim N^{-\omega} \qquad \omega = \frac{1}{2} + \frac{1}{1-\gamma}} \tag{5.58}$$

Using the scaling relation $\gamma = (2+\theta)^{-1}$ [247] we get

$$\boxed{\omega = \frac{3}{2} + \frac{1}{1+\theta} = 1 + \beta \,.} \tag{5.59}$$

Our argument could be extended to compression of jammed configurations of soft linear spheres giving rise to identical exponents. In fact, we notice that both Eq. (5.53) and Eq. (5.59) coincide with the ones obtained for hard spheres at jamming under shear strain [210, 79]. This indicates that any destabilizing perturbation that leads isostatic states to new isostatic states with self-similar distributions of forces and gaps close to the edges gives rise to the same kind of avalanche statistics. Notice that the scaling of (5.58) is

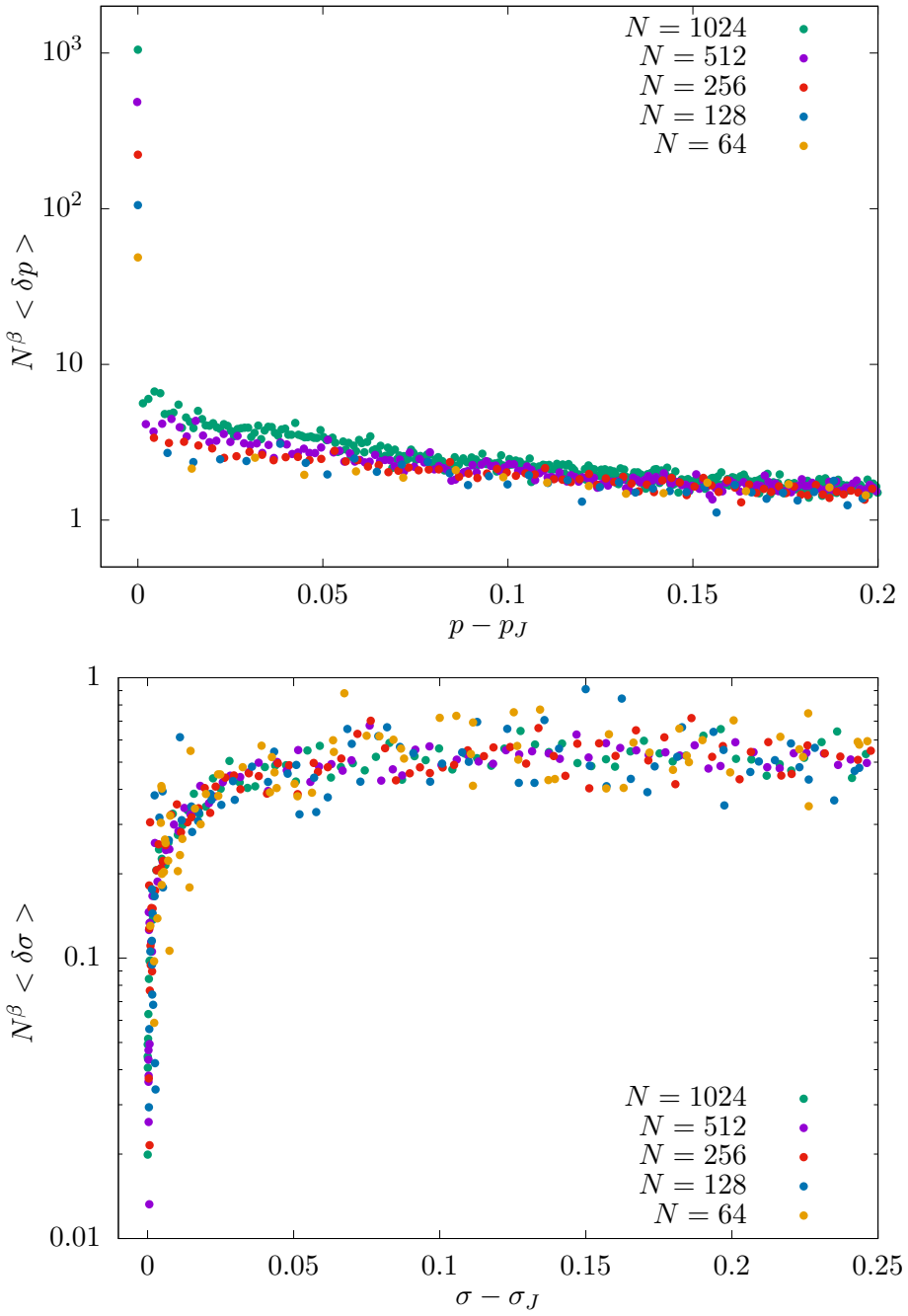

Figure 5.7: *Upper panel:* Average jump $\langle \delta p \rangle$, rescaled by N^β as a function of $p - p_J(N)$ for $N = 64, 128, 256, 512, 1024$. The first point is the pressure jump at jamming $p_J \sim \frac{1}{\sqrt{\log N}}$. All the subsequent jumps are much smaller. Notice that the scaling $\langle \delta p \rangle \sim N^{-\beta}$ is very well verified far away from jamming. Close to jamming there are small deviations to this behavior. It is not clear to us if these are due to next to leading finite-size corrections or to genuine changes in the leading behavior. *Lower Panel:* Average rescaled avalanche size $\langle \delta \sigma \rangle N^\beta$ as a function of $\Delta\sigma = \sigma - \sigma_J$ for the same values of N. The scaling is well respected untill the jamming point.

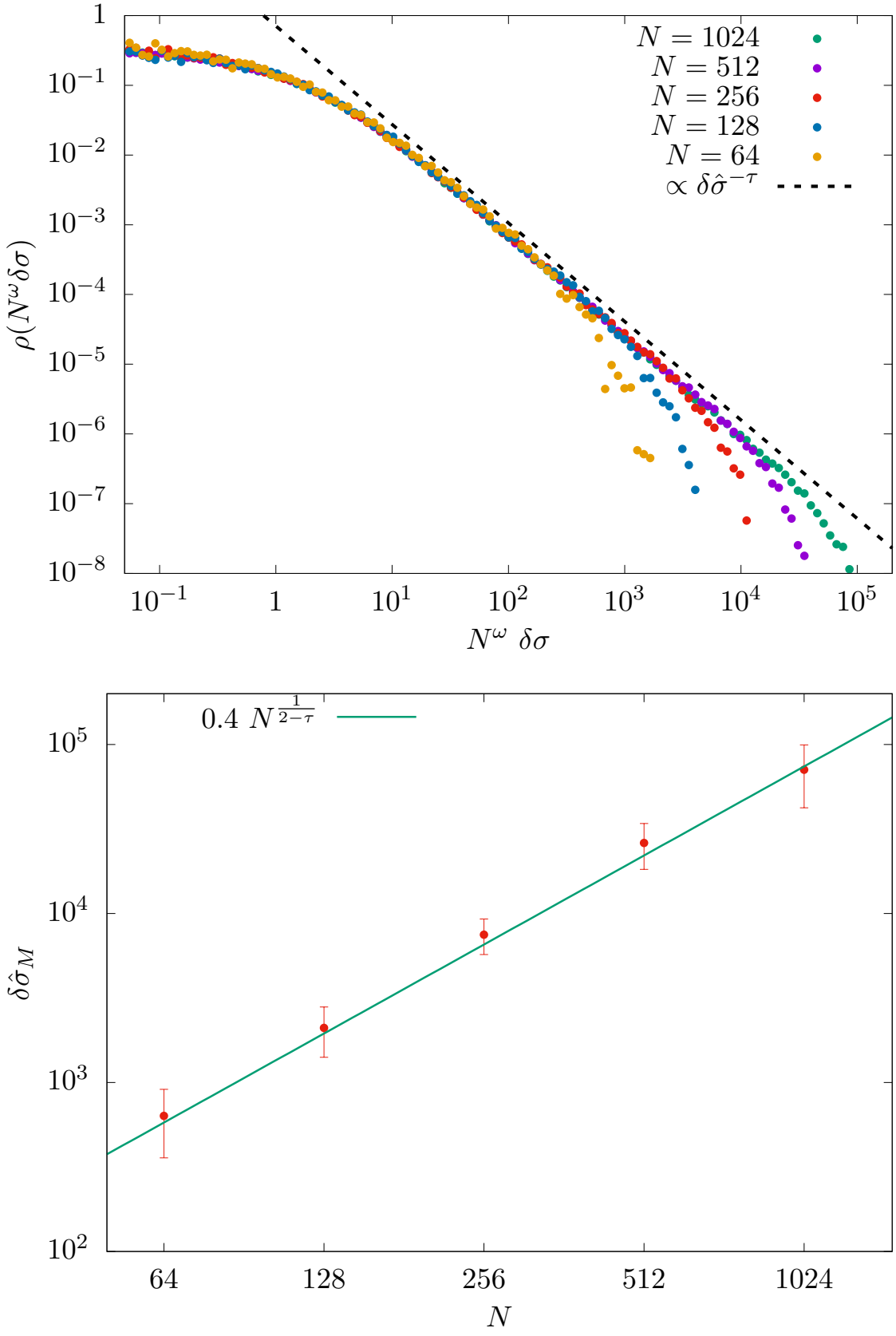

Figure 5.8: *Upper Panel.* Statistics of the scaled avalanche size $\hat{\delta\sigma} = N^{\omega}\delta\sigma$. The dotted line is the power law $\rho(\hat{\delta\sigma}) \sim \hat{\delta\sigma}^{-\tau}$. *Lower Panel.* The scaling of $\hat{\delta\sigma}_M$ as a function of the system size. The green dashed line is a fit to $\hat{\delta\sigma}_M \sim N^{\frac{1}{2-\tau}}$.

incompatible with a distribution of the rescaled jumps $\delta\hat{\sigma}$ which admits a finite first moment in the thermodynamic limit. In fact, a finite pressure increase $\Delta p = \mathcal{N}\langle\delta p\rangle$, should correspond to a finite jump $\Delta\sigma = \mathcal{N}\langle\delta\sigma\rangle$. This tells that $\langle\delta\sigma\rangle = N^{-\omega}\langle\delta\hat{\sigma}\rangle \sim N^{-\beta}$ and that the finite N average of $\delta\hat{\sigma}$ should diverge as $\langle\delta\hat{\sigma}\rangle \sim N$ for large N. As can be seen in the upper panel of Fig. 5.7, the scaling $\langle\delta\sigma\rangle \sim N^{-\beta}$ is observed already right after jamming. The divergence of the first moment indicates that the distribution of avalanches $\delta\hat{\sigma}$ should exhibit, in the thermodynamic limit, a power law at large argument

$$\rho(\delta\hat{\sigma}) \sim \delta\hat{\sigma}^{-\tau} \qquad \delta\hat{\sigma} >> 1. \tag{5.60}$$

The exponent τ should be in the interval $1 < \tau \leq 2$, so that the distribution has a divergent first moment. For finite N, however, the distribution should be cut-off around a value $\delta\hat{\sigma}_M$ so that

$$\langle\delta\hat{\sigma}\rangle \sim \int_0^{\hat{\delta\sigma}_M} d\hat{\delta\sigma}(\hat{\delta\sigma})^{1-\tau} \sim (\hat{\delta\sigma}_M)^{2-\tau} \sim N. \tag{5.61}$$

Therefore we get

$$\hat{\delta\sigma}_M \sim N^{\frac{1}{2-\tau}} \tag{5.62}$$

The statistics of avalanches in mean-field disordered systems has been fully characterized using equilibrium techniques [153, 110], where instead of studying the change of local minima following a destabilizing perturbation, one studies the discontinuities in the evolution of the actual ground state of the system when it is in a fullRSB region. In this case, the exponent τ can be related to the force pseudogap exponent by the relation

$$\tau = \frac{3+\theta}{2+\theta} \simeq 1.41. \tag{5.63}$$

Differently from the scaling with N, that we have obtained by purely local considerations, this form for the avalanche distribution with the specific value of τ depends on the statistical properties of the neighborhood of the ground state, something that is captured by the replica solution. Remarkably, we find that within numerical precision, the value (5.63) coincides with the one found for avalanches of sheared hard spheres at jamming [74] and soft spheres close to jamming [110]. Our simulations indicate that the remarkable coincidence between static and dynamic avalanche statistics also holds in this case. In Fig.5.8-Upper Panel we show the statistics of the rescaled jumps of $\hat{\delta\sigma} = N^{\omega}\delta\sigma$ collected from all the plastic events taking place for pressures in the interval $[0.2, 1.2]$. We notice a very good collapse of the numerical results for different sizes and we observe the expected power law distribution (5.60). In the lower panel we show that the maximum $\delta\hat{\sigma}_M$ corresponding to the cut-off of the power law respects the expected scaling with N.

Ultimately, the results of Fig.5.8 strengthen the observation that the non-convex jammed phase of the linear perceptron is marginally stable, self-organized critical and belongs to the jamming universality class.

Energy avalanches and squared displacement

A similar analysis as in the previous section allows to analyze the jumps in energy and in position. It is easy to see that the jumps in energy density follow exactly the same scaling as the ones in σ, namely

$$\delta e \sim N^{-\omega} \tag{5.64}$$

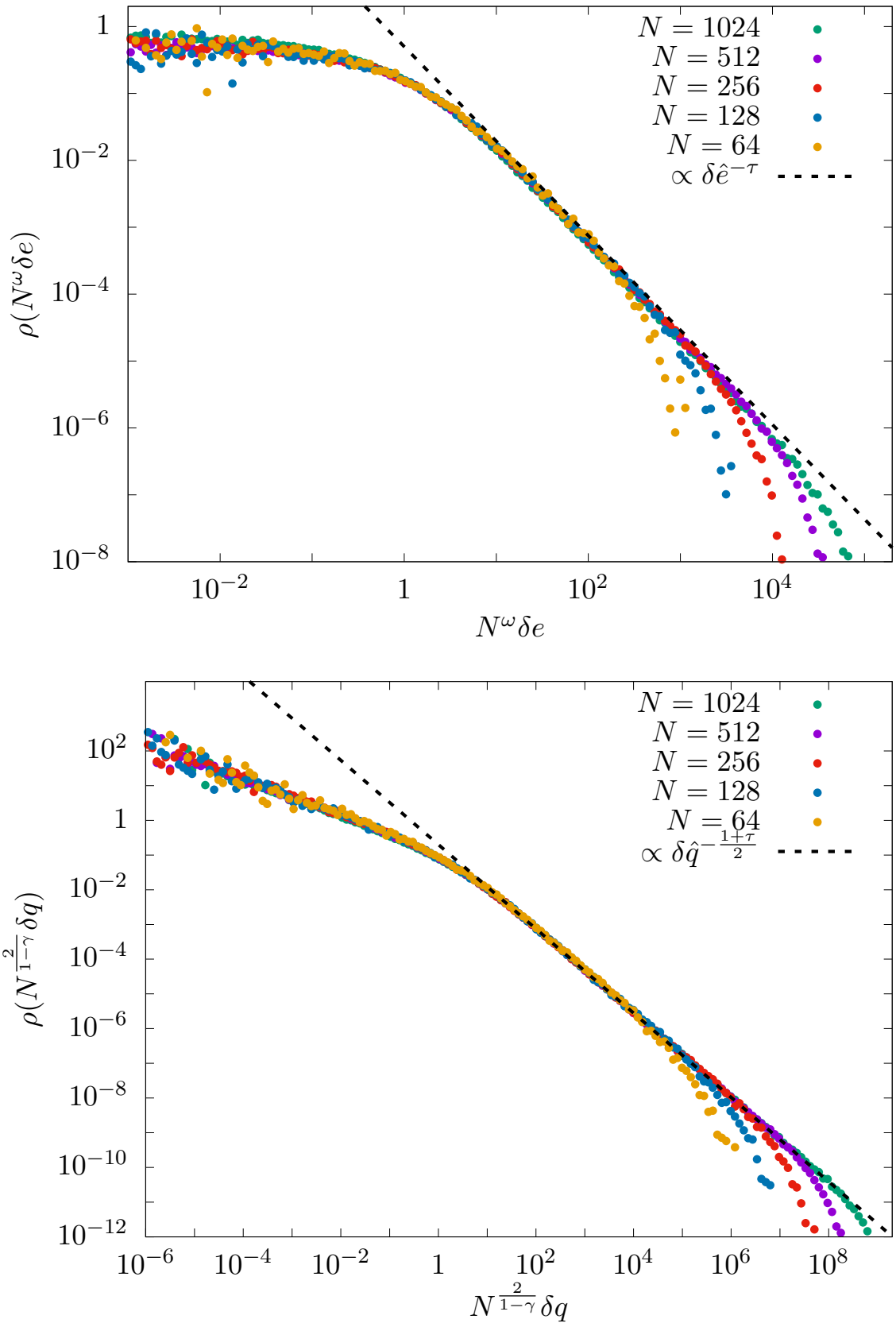

Figure 5.9: *Upper Panel.* Statistics of the scaled energy variations $\delta\hat{e} = N^{3/2+1/(1+\theta)}\delta e$. The dotted line is a fit to the form $\rho(\delta\hat{e}) \sim \delta\hat{e}^{-\tau}$. *Lower Panel.* Statistics of the scaled squared displacements $\hat{\delta q} = N^{2/(1-\gamma)}\delta q$. The dotted line is a fit to $\rho(\hat{\delta q}) \sim \hat{\delta q}^{-\frac{\tau+1}{2}}$.

As in the case of σ, a power law avalanche distribution with divergent first moment follows, and it is possible to see that the static avalanche exponent coincides with τ.

As far as the jumps in position $\mathbf{X}$ are concerned, we can see from Eq. (5.56) that for a typical displacement δX_i is of the order of the smallest non-zero gap h_{min}

$$\delta X_i \sim h_{min} \sim N^{-\frac{1}{1-\gamma}} \tag{5.65}$$

Therefore the squared displacement $|\delta \mathbf{X}|^2$ scales as

$$\delta q = \frac{1}{N}(\delta \mathbf{X})^2 \sim N^{-2/(1-\gamma)} = N^{-(1+2\beta)}. \tag{5.66}$$

Notice that the mean-squared displacement on the sphere corresponds to the overlap between successive minima, up to a factor 1: $\frac{1}{N}\mathbf{X}\cdot(\mathbf{X}+\delta\mathbf{X}) = 1-\frac{1}{N}\mathbf{X}\cdot\delta\mathbf{X} = 1-\frac{1}{N}|\delta\mathbf{X}|^2$. Also the distribution of displacements is a power law. The static avalanche exponent [153, 110] is in this case $\tau' = \frac{\tau+1}{2}$. In Fig. 5.9 we display the probability distributions of energy and displacement jumps, which confirm the above scaling, and shows that also in this case the dynamical avalanche exponents coincide with the static ones.

5.2.3 The critical behavior of the unjamming transition

Given the very fine control we have on the compression of the system, the algorithm is very well suited for studying the unjamming transition, that occurs when the pressure vanishes from positive values $p \to 0^+$.
From the study of unjamming in soft spheres with Hamiltonian $H = \sum_{i<j} |h_{ij}|^a \theta(-h_{ij})$, the features of this transition when the exponent a in the interaction potential is larger than unity are known [191, 246, 117]. The analysis can be extended to the perceptron along the line of [105] for the harmonic case. Using, as already done, the distance from the jamming point $\Delta\sigma = \sigma - \sigma_J$ as a control parameter, the pressure and the energy close to the transition behave as

$$\begin{aligned} p &\sim \Delta\sigma^{a-1} \\ e &\sim \Delta\sigma^{a} \end{aligned} \tag{5.67}$$

while the variation in the number of overlaps Δz with respect to the isostatic value $z = 1$, shows a square root singularity independently of a

$$\Delta z \sim \sqrt{\Delta\sigma}. \tag{5.68}$$

The Lagrange multiplier η, according to Eq. (5.12) is dominated by the pressure variation $\eta \approx \sigma_J\ p \sim \Delta\sigma^{a-1}$. The laws (5.67) are a consequence of the fact that, for $a > 1$, an increase of the margin $\Delta\sigma$ causes all the contacts to become overlaps with $|\delta h_c| \sim \Delta\sigma$, independently of a [246, 117]. Simple dimensional analysis gives then (5.67). In the compressed phase, the leading excitations are linear. Relation (5.68) expresses a condition of stability for the linear modes [246].

These relations should break down in the linear potential case $a = 1$, as it is manifest from the facts that (1) the pressure has to vanish for $\Delta\sigma \to 0$ and (2) all excitations are non-linear even away from jamming. The vanishing of the exponent relating p to $\Delta\sigma$ suggests that a logarithmic behavior could appear

$$\begin{aligned} p &\sim 1/\log(1/\Delta\sigma)^b \\ e &\sim \Delta\sigma/\log(1/\Delta\sigma)^b \end{aligned} \tag{5.69}$$

with b a positive exponent. Again $\eta \approx \sigma_J p \sim 1/\log(1/\Delta\sigma)^b$.

The behavior of the different quantities close to jamming should be accessible from the analysis of the exact mean-field equations of the replica method [108]. This analysis is rather simple for $\alpha < 2$, where replica symmetry holds. In that case, we have obtained in (3.143)-(3.133) that close to jamming the pressure, energy, and density of overlaps behave as

$$e \sim \frac{\Delta\sigma}{\sqrt{|\ln(\Delta\sigma)|}} \qquad p \sim \frac{1}{\sqrt{|\ln(\Delta\sigma)|}} \qquad n_o = \frac{O}{N} \sim \Delta\sigma \tag{5.70}$$

In Fig.5.10-Left Panel we plot these scalings for $\alpha = 1.5$ showing a good agreement. The predictions (5.70) could be questioned in the non-convex case. Notice that in the case $a > 1$, the replica symmetric analysis gives the correct scaling (5.67) of energy and pressure, while it predicts a linear behavior $\Delta z \sim \Delta\sigma$, rather than the square-root of the non-convex case.

In our case, if we look at the number of overlaps n_0 from numerical simulations in the non-convex case, we do not find either linear nor square root behavior. In Fig.5.11 we plot n_o *vs* $\Delta\sigma$ close to jamming for $\alpha = 4$ in double-log scale. We observe power law behavior $n_o \sim \Delta\sigma^\nu$, with an an exponent ν smaller than one but larger than $1/2$, that we estimate $\nu \simeq .83$, compatible with the value $\nu = 1/\beta$. The origin of $1/\beta$ can be traced to the behavior with N of δn_0 and $\delta\sigma$ in avalanches close to jamming. There, typical avalanches produce a small number of overlaps, therefore $\delta n_o \sim 1/N$. The statistics of jumps in σ, on the other hand, is likely to give $\langle\delta\sigma\rangle \sim N^{-\beta}$ untill jamming. If we suppose that the scaling $\delta n_o \sim 1/N$ remains valid for small but finite δn_o, we find

$$\boxed{n_o \sim \Delta\sigma^\nu \qquad \nu = \frac{1}{\beta} = \frac{2+2\theta}{3+\theta}} \tag{5.71}$$

The presence of the logarithms in the behavior of the pressure and energy can also be rationalized by qualitative scaling. The destabilizing jumps in pressure depend on the tail of the distribution of forces, which for the perceptron close to jamming has a Gaussian tail $p(f/p) \sim \exp(-A(f/p)^2)$, implying $\delta p \sim \frac{1}{\sqrt{\log N}}$. Supposing that this scaling holds untill to the very first events, we obtain, using (5.71), the relationship

$$p \sim \frac{1}{\sqrt{|\ln(\Delta\sigma)|}}, \tag{5.72}$$

and by dimensional reasons, $e \sim \frac{\Delta\sigma}{\sqrt{|\ln((\Delta\sigma)|}}$. We remark that these relations depend critically on the Gaussian tail of the distribution of the scaled forces at large argument. With a different tail this argument would give a different dependence: e.g. a stretched exponential, with stretching exponent $1/b$, would give rise to a log with a power $-b$ as in (5.69). It would be interesting to see if such a behavior could be produced in a physical system.

5.3 Extension of the algorithm to jammed linear spheres

The algorithm can be extended in a very natural manner for the compression of spheres with linear repulsive potential. Let us consider N spheres in d dimensions, with center

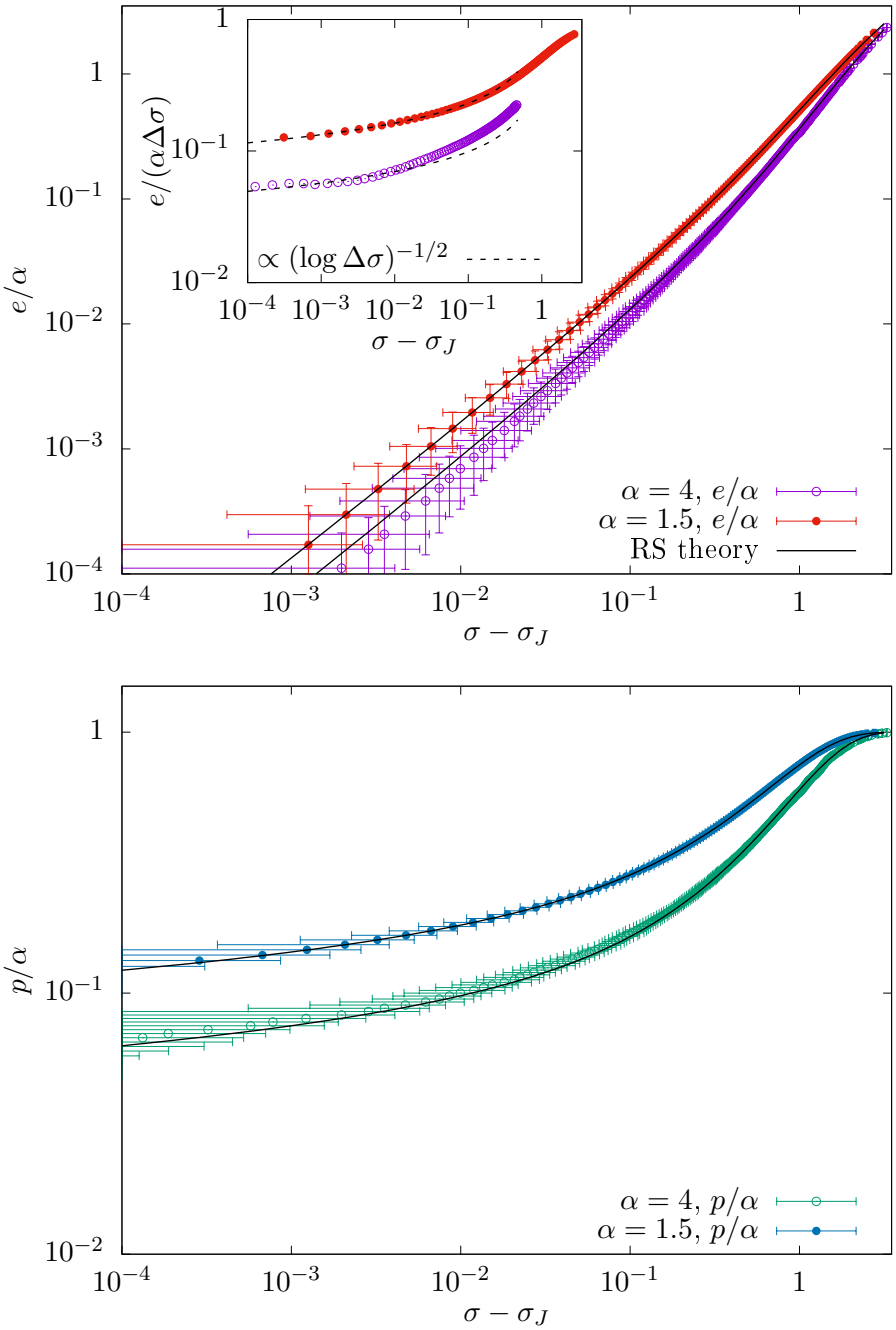

Figure 5.10: *Upper Panel.* The behavior of the scaled energy e/α as a function of the distance from jamming $\Delta\sigma = \sigma - \sigma_J$. For $\alpha = 1.5$, jamming is in the convex phase and we can use the replica symmetric theory to study the corresponding scaling behavior as in Eq. (5.70). For $\alpha = 4$, jamming is in the non-convex region and in principle the replica symmetric theory is not valid anymore. Anyway, we fit the numerical curves with the replica symmetric approximation and we see a good agreement, signaling the fact that for the energy the scaling behavior as a function of the distance from jamming is preserved. In the inset we plot the same quantities divided by $\sigma - \sigma_J$. This way we reveal the presence of logarithmic corrections to the linear scaling of the energy with respect to $\sigma - \sigma_J$. *Lower Panel.* The behavior of the scaled pressure p/α as a function of the distance from jamming $\Delta\sigma = \sigma - \sigma_J$. As for the energy, the replica symmetric theory gives a good prediction for the pressure also in the non-convex region. Data obtained with $N = 2048$ for $\alpha = 1.5$, $N = 512$ ($N = 1024$ in the inset) for $\alpha = 4$. Error bars are sample to sample fluctuations.

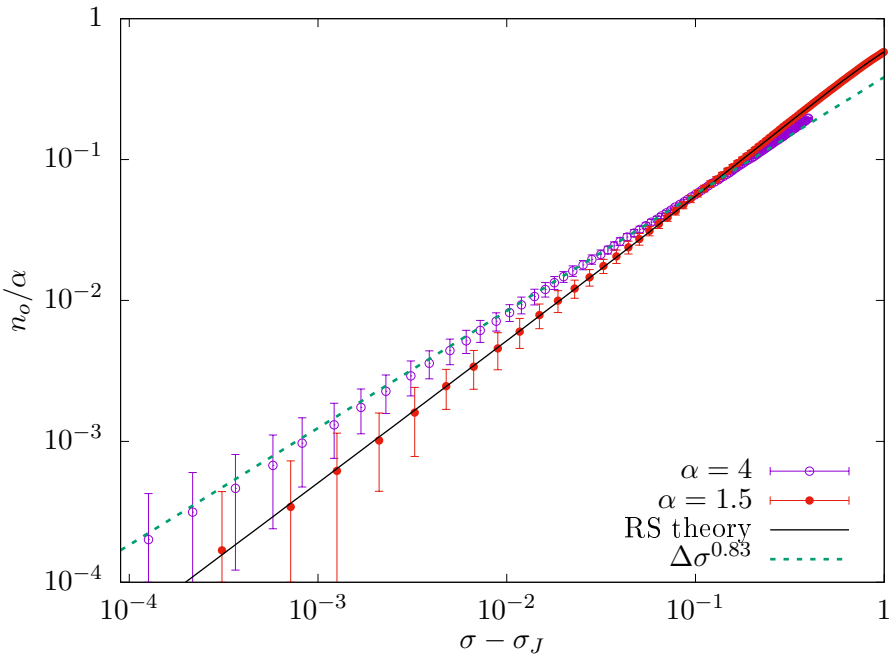

Figure 5.11: The scaled number of overlaps n_o/α as a function of the distance from jamming. In this case, the replica symmetric prediction clearly holds only in the convex region while the non-convex one shows the presence of a non-trivial power law behavior. The dotted line represent the prediction form the scaling analysis. Data has been produced with $N = 2048$ for $\alpha = 1.5$ and $N = 1024$ for $\alpha = 4$. Error bars are sample to sample fluctuations.

coordinates $\{\mathbf{x}_i\}_{i=1,\dots,N}$ and radii $R\sigma_i$, inside a cubic box of length L with periodic boundary conditions. The radii have been split in a component R, corresponding to the average radius, and a component σ_i, that can be distributed according to some polydispersity but with its mean being strictly equal to one: $\frac{1}{N}\sum_{i=1}^{N}\sigma_i = 1$. Keeping the box size L fixed, the average radius controls the packing fraction ϕ according to

$$\phi = \frac{\pi^{d/2}\sum_{i=1}^{N}\sigma_i^d}{\Gamma(1+\frac{d}{2})L^d}R^d = k_d\ R^d \tag{5.73}$$

with $\Gamma(x)$ the Euler gamma function and k_d constant. Using a Legendre transform, we change ensemble by introducing the pressure p that is the conjugate variable of the average radius R. Therefore, the Lagrangian (5.10) we wrote for the perceptron case, now reads

$$\mathscr{L}\left(\{\mathbf{X}_i\},\{f_{ij}\},R\right) = \sum_{(i,j)\in\mathcal{O}}\left(R\sigma_{ij} - |\,\mathbf{x}_i-\mathbf{x}_j\,|\right) + \sum_{(i,j)\in\mathcal{C}} f_{ij}\left(R\sigma_{ij} - |\,\mathbf{x}_i-\mathbf{x}_j\,|\right) - pR\sum_{i=1}^{N}\sigma_i \tag{5.74}$$

where $\sigma_{ij} = \sigma_i + \sigma_j$, the set $\mathcal{O}$ is the set of couples of overlapping spheres, i.e. $|\,\mathbf{x}_i-\mathbf{x}_j\,| - R\sigma_{ij} < 0$, the set $\mathcal{C}$ for those in contact, i.e. $|\,\mathbf{x}_i-\mathbf{x}_j\,| - R\sigma_{ij} \equiv 0$, and $f_{ij} \in (0,1)$ are the contact forces. Now the degrees of freedom (d.o.f.) are given by the coordinates of spheres' centers $\mathbf{x}_i$, that are Nd, and the average radius, that is one additional degree of freedom. Considering the d d.o.f. that are lost because of the periodic boundary conditions, perfect

isostaticity is obtained with a number of contacts $C = |\mathcal{C}|$ equal to $C = Nd - d + 1$. Once the sets $\mathcal{O}$ and $\mathcal{C}$ are known, the extrema of $\mathscr{L}$ satisfy the first-order condition

$$\begin{cases} \partial_{\mathbf{x}_i} \mathscr{L} & = - \sum\limits_{j \in \mathcal{O}(i)} \mathbf{n}_{ij} - \sum\limits_{j \in \mathcal{C}(i)} f_{ij}\, \mathbf{n}_{ij} = 0 \\ \partial_R \mathscr{L} & = \sum\limits_{(ij) \in \mathcal{O}} \sigma_{ij} + \sum\limits_{(ij) \in \mathcal{C}} f_{ij} \sigma_{ij} - p \sum\limits_{i=1}^{N} \sigma_i = 0 \end{cases} \tag{5.75}$$

$$\partial_{f_{ij}} \mathscr{L} = |\, \mathbf{x}_i - \mathbf{x}_j \,| - R\sigma_{ij} = 0, \qquad (ij) \in \mathcal{C} \tag{5.76}$$

where $\mathbf{n}_{ij} = \frac{\mathbf{x}_i - \mathbf{x}_j}{|\, \mathbf{x}_i - \mathbf{x}_j \,|}$, $\mathcal{O}(i)$ is the set of spheres overlapping with sphere i and $\mathcal{C}(i)$ is the set of spheres in contact with sphere i. The analogy with the equations of the perceptron (5.11) is quite strong. The equations (5.75) correspond to the force balance condition at a given pressure p, while (5.76) corresponds to the condition of having the pairs $(ij) \in \mathcal{C}$ in contact.
We can introduce the matrix $\underline{\underline{\mathrm{S}}}$ of dimension $(Nd+1) \times C$, where the first Nd rows have elements

$$S_{i\alpha,c} = -n_{ij}^{\alpha} \delta_{c,(ij)} \tag{5.77}$$

where $i = 1, ..., N$ indexes the sphere, $\alpha = 1, .., d$ indexes the dimensional component and c indexes the pairs of spheres in contact $c \in \{(ij) : h_{ij} = 0\}$. The last row of $\underline{\underline{\mathrm{S}}}$ is given by

$$S_{Nd+1,c} = \sigma_{ij} \delta_{c,(ij)} \tag{5.78}$$

Similarly, we introduce the $Nd + 1$ vector $\mathbf{v}$ whose first Nd components are

$$v_{i\alpha} = \sum_{j \in \mathcal{O}(i)} n_{ij}^{\alpha} \tag{5.79}$$

and the last one is

$$v_{Nd+1} = p \sum_{i=1}^{N} \sigma_i - \sum_{(ij) \in \mathcal{O}} \sigma_{ij} \tag{5.80}$$

Now, using the vector of contact forces $\mathbf{f} = \{f_{ij}\}_{(ij) \in \mathcal{C}}$, we can write the gradient of $\mathscr{L}$ in linear algebra form

$$\nabla \mathscr{L}\,(\mathbf{f}) = \begin{bmatrix} \partial_{x_i^{\alpha}} \mathscr{L} \\ \partial_R \mathscr{L} \end{bmatrix} = \underline{\underline{\mathrm{S}}}\, \mathbf{f} - \mathbf{v} \tag{5.81}$$

and the force balance condition $\nabla \mathscr{L} = 0$ gives a linear equation for the contact forces

$$\underline{\underline{\mathrm{S}}}^T\, \underline{\underline{\mathrm{S}}}\, \mathbf{f} = \underline{\underline{\mathrm{S}}}^T\, \mathbf{v} \tag{5.82}$$

Now we have all the elements to easily extend the compression algorithm for the spheres with linear cost-function

Step 0: jamming point configuration

The preliminary step is to produce a configuration at the jamming point. We do this by using the regularizing the Lagrangian for $h_{ij} \in [-\frac{\epsilon}{2}, \frac{\epsilon}{2}]$

$$\mathscr{L}_\epsilon\left(\{\mathbf{X}_i\}, R\right) = \sum_{(i,j)\in\mathcal{O}} \left(R\sigma_{ij} - |\,\mathbf{x}_i - \mathbf{x}_j\,|\right) + \frac{1}{2\epsilon}\sum_{(i,j)\in\mathcal{C}} \left(\frac{\epsilon}{2} + R\sigma_{ij} - |\,\mathbf{x}_i - \mathbf{x}_j\,|\right)^2 - pR\sum_{i=1}^{N}\sigma_i \tag{5.83}$$

where now $\mathcal{O} = \{(ij) : h_{ij} < -\frac{\epsilon}{2}\}$ and $\mathcal{C} = \{(ij) : -\frac{\epsilon}{2} < h_{ij} < \frac{\epsilon}{2}\}$. As we have already discussed for perceptron and spheres, we recover the original Lagrangian by $\lim_{\epsilon\to 0}\mathscr{L}_\epsilon = \mathscr{L}$ and the contact forces by $\lim_{\epsilon\to 0}\frac{\frac{\epsilon}{2}+R\sigma_{ij}-|\,\mathbf{x}_i-\mathbf{x}_j\,|}{\epsilon} = f_{ij} \in (0,1)$.
We can proceed by choosing a small value for the pressure, namely $p < p_J(N)$, with $p_J(N)$ the smallest pressure value in the jammed phase, and run a gradient-based minimizer over the $Nd+1$ variables $(\{\mathbf{X}_i\},\, R)$.
As for the perceptron, for $N \to \infty$ we get $p_J(N) \to 0$ logarithmically.

Compression step

Given an isostatic configuration, Eq. (5.82) gives the value of the contact forces $f_c = f_{ij}$ that must be contained in the interval $(0,1)$ to have a stable configuration. Increasing $p \to p + \delta p$, the contact forces have a variation $\delta f_c \propto \delta p$ and the configuration does not move until one of the them does not get to a boundary, $f_c + \delta f_c = 0$ or $f_c + \delta f_c = 1$. The corresponding contact gets destabilized and the system moves along the floppy mode defined by keeping the stable contacts in place. If more than one contact is unstable, we use the same prescription as for the perceptron

$$\nabla^*\mathscr{L} = \nabla\mathscr{L}\left(\mathbf{f}^*\right) \qquad \mathbf{f}^* = \underset{\mathbf{f}\in[0,1]^C}{argmin}|\nabla\mathscr{L}\left(\mathbf{f}\right)|^2 \tag{5.84}$$

that saturates the forces of unstable contacts to 0 or 1 and points along the softest/least descent direction in the manifold defined by the floppy modes.
The displacement of the configuration halts when a new contact is formed. By the way, the curvature of the spheres makes the condition of keeping the stable contacts in place $h_c = 0$ a non-linear one. Therefore, we need to adjust the direction of movement $\nabla^*\mathscr{L}\Big|_{\delta\mathbf{x}}$ according to $\delta\,\mathbf{x}_i$, δR. Therefore, the displacement $(\delta\,\mathbf{x}_i, \delta R)$ satisfies

$$(\delta\,\mathbf{x}_i, \delta R) = -t^*\nabla^*\mathscr{L}\Big|_{\delta\mathbf{x}} \tag{5.85}$$

with

$$t^* = \min_{(ij)}\{t_{(ij)} : t_{(ij)} > 0 \wedge |\,\mathbf{x}_i - \mathbf{x}_j + \delta\,\mathbf{x}_i - \delta\,\mathbf{x}_j\,| - \sigma_{ij}(R+dR) = 0,\ (ij)\notin\mathcal{C}\} \tag{5.86}$$

$$\nabla^*\mathscr{L}\Big|_{\delta\mathbf{x}} = \left(1 - \underline{\underline{\tilde{S}}}(\underline{\underline{\tilde{S}\tilde{S}}}^T)^{-1}\underline{\underline{\tilde{S}}}^T\right)\nabla^*\mathscr{L}\Big|_{\delta\mathbf{x}} \tag{5.87}$$

where the matrix $\underline{\underline{\tilde{S}}}$ is the same matrix as $\underline{\underline{S}}$ but with the perturbed entries $\tilde{S}_{i\alpha,\tilde{c}} = -\left(n^\alpha_{ij} + \delta n^\alpha_{ij}\right)\delta_{\tilde{c},(ij)}$ given by $\delta n^\alpha_{ij} = \frac{\delta\,\mathbf{x}_i - \delta\,\mathbf{x}_j}{|\,\mathbf{x}_i - \mathbf{x}_j\,|}$, and the index $\tilde{c}$ runs over the stable contacts only. In words, the projector $\left(1 - \underline{\underline{\tilde{S}}}(\underline{\underline{\tilde{S}\tilde{S}}}^T)^{-1}\underline{\underline{\tilde{S}}}^T\right)$ takes away the component of the

movement that would make the stable contacts develop a gap $O(|\delta \mathbf{x}|^2)$ if we simply follow $\nabla^* \mathscr{L}$.
For each step, the set (5.85),(5.86),(5.87) can be solved by iteration:

1 Start with $\nabla^* \mathscr{L}$ from (5.84).

2 Compute the corresponding t^* from (5.86) (eventually with a quadratic approximation of $|\mathbf{x}_i - \mathbf{x}_j + \delta \mathbf{x}_i - \delta \mathbf{x}_j|$).

3 Iterate (5.85),(5.86),(5.87) until convergence.

This procedure takes few iterations because it is made to get rid of terms $O(|\delta \mathbf{x}|^2)$ that would violate the condition of keeping stable contacts in place.

Remarks on the algorithm for the spheres

The compression algorithm for the spheres with linear repulsion has many similarities with the algorithms developed for the shear strain of hard spheres [71, 210, 79]. The main difference with them is the fact that a contact is destabilized also for getting its force $f_c = 1$ and not only for $f_c = 0$ as it is the case for hard-spheres. Moreover, in our case overlaps are allowed and we can move inside the jammed phase.
Another difference with the cited algorithms is the choice of following the least descent direction in the manifold of floppy modes: another common choice in the case of hard spheres under straining is following the floppy mode with largest traction, i.e. the one with a more negative $f_c < 0$.
As in the perceptron case, the step (5.84) is a constrained least-squares problem and can be computationally demanding for large matrices $\underline{\underline{S}}$.

5.4 Discussion

Using an athermal adiabatic compression algorithm, we have studied the statistics of plastic events in the critical jammed phase of the perceptron with linear cost-function. Consistently with the jamming universality class, the statistics and the scalings correspond to what is found for hard sphere packings under quasi-static strain [71, 210, 79]. This suggests that any local dynamics that destabilizes isostatic configurations and leads to other isostatic configurations has the same critical properties.
With this compression algorithm we have studied the unjamming transition and verified that the universal scalings holding for soft spheres at the jamming onset [191, 117] break down in the linear potential case. In particular, the number of overlaps, corresponding to the excess coordination number in softer potentials, does not scale as the square root of the distance from jamming but instead it has a different power law.
On the theoretical side, following [43] it would be interesting to count the number of solutions of the equilibrium equations for fixed control parameter α and p.
On the algorithmic side, it would be interesting to implement compression/decompression cycles and observe whether it is possible to anneal the system. It would give information about the energy barriers connecting different energy levels that may scale as N^t with $t < 1$, in analogy with what is found in the Sherrington-Kirkpatrick model where $t = 1/3$ [238, 139, 37].
An interesting point is the fact that the statistical properties of the avalanches created

by our compression algorithm are essentially indistinguishable from those obtained by a random local perturbation that brings isostatic minima to isostatic minima with similar statistical properties. This is a property of *stochastic stability*, a concept that is relevant for marginally stable disordered systems and has been extensively studied in spin-glasses [168, 2, 198, 72]. It states that random perturbations may move the system far away in the configuration space, but still to points having the same statistical properties as the starting ones. Its implication is that static and dynamical responses are controlled by the overlap distribution of the replica theory that can be extracted by a static computation [101, 100]. At zero temperature, it implies that static and dynamic avalanches share the same statistics, consistently with the correspondence between our simulations and the theory of Ref. [110]. A further analysis along this line is left for future work.

Chapter 6

Proliferation of non-linear excitations in the piecewise-linear perceptron

The content of this chapter is published in [215].

We have seen in chapter 3 and 4, Refs. [108, 107], that the jamming criticality does not belong exclusively to the jamming transition point. Using a repulsive linear potential, the criticality characterizes the entire jammed phase, both in the mean-field case (the perceptron) and in the case of finite dimensional soft spheres. In both models, at finite energy density local minima, the system *self-organizes* into marginally stable, critical, configurations characterized by non-linear excitations corresponding to the breaking and the formation of contacts. They are analogous to the ones characterizing the jamming transition, but richer in the sense that there are more mechanisms by which a contact can be broken or formed. Yet, the critical exponents controlling their density appear to be the same (within numerical precision) to the ones of the jamming point of hard spheres, suggesting that the underlying universality class could be broader than previously thought. The key feature that associates contacts to the linear potential in the jammed phase is the non-analyticity of the interaction potential. In this chapter we show what happens if we increase the number of non-analytic points. We study a piece-wise linear potential, with a ramp slope equal to 1 for gaps in the interval $(-H_0, 0)$ and a ramp slope equal to 2 for gaps in $(-\infty, -H_0)$. In this scenario, there are two kinds of "contacts" that the potential can sustain: gaps equal to 0 and gaps equal to $-H_0$. We show that a general notion of isostaticity holds also in this case, together with all the features of the jamming universality class. This result reinforces the idea that jamming criticality does not pertain only to the jamming point but it is rather related to three concomitant ingredients: the singular nature of the cost function, the non-convex nature of the problem and disorder.

6.1 The model

We define the usual perceptron model by an N dimensional vector $\mathbf{X}$, which lives on the N-dimensional sphere $|\mathbf{X}|^2 = N$, and $M = \alpha N$ N-dimensional random vectors (called patterns) $\boldsymbol{\xi}^\mu$ with $\mu = 1, \dots, M$. Every component of all these random vectors is a Gaussian random variable with zero mean and unit variance. Given the patterns and the state vector $\mathbf{X}$, the gap variables are defined as $h_\mu = \boldsymbol{\xi}^\mu \cdot \mathbf{X} / \sqrt{N} - \sigma$, where σ and α are control parameters of order one.

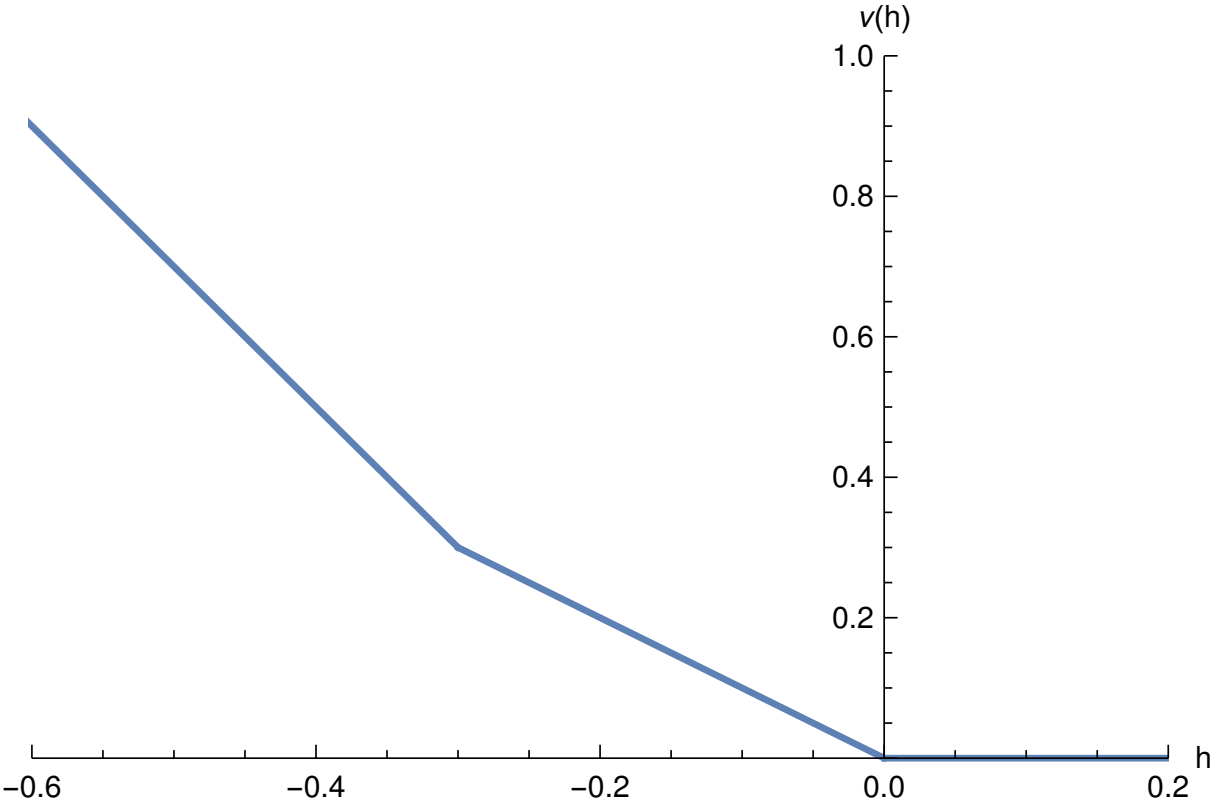

Figure 6.1: The piecewise linear cost function $\nu(h)$ defined in Eq. (6.2) where we set $H_0 = 0.3$.

The cost function to minimize for $\mathbf{X}$ is

$$H(\mathbf{X}) = \sum_{\mu=1}^{\alpha N} \nu(h_\mu) \tag{6.1}$$

In this chapter we consider the piecewise linear cost function defined as

$$\nu(h) = \begin{cases} -2h - H_0 & h < -H_0 \\ -h & h \in [-H_0, 0] \\ 0 & h > 0 \end{cases} \tag{6.2}$$

where H_0 is a positive constant of order one that is taken to be fixed. In Fig. 6.1 we sketch the form of the corresponding potential. The model admits a satisfiable (SAT) phase for α and σ small enough, where $h_\mu > 0$ for all $\mu = 1, \dots, M$, in the same way it happens in the perceptron of chapter 2. At fixed α, starting from the SAT phase and increasing σ there exists the jamming point (that may be algorithm-dependent) beyond which finding configurations where all gaps are positive becomes impossible. As always, the properties of the configurations at jamming do not depend on the cost function used in correspondence of the negative gaps, since up to jamming the gaps are still all positive. We are interested in going beyond the jamming point and entering the jammed phase. We want to characterize the properties of the minima found by minimizing the potential (6.1) by gradient-descent-like algorithms.
We have already studied in chapter 3[108] the phenomenology of the purely linear case, which corresponds to the present one by taking the limit $H_0 \to \infty$. In that case, the

jammed non-convex/glassy phase contains minima where the distribution of gap variables contains a Dirac delta peak at $h = 0$. The weight of the peak is equal to N which is the number of degrees of freedom in the problem. This implies that local minima have an isostatic number of gaps that are strictly equal to zero. Isostaticity is accompanied by power law divergences $\rho_h(h \to 0^{\pm}) \sim |h|^{-\gamma}$ in the distribution of small gaps. Moreover, the contact forces, i.e. the Lagrange multipliers needed to enforce that the corresponding gaps vanish, are distributed in the interval $(0, 1)$ with pseudo-gaps at the boundaries of their distribution, $\rho_f(f \to 0^+) \sim f^{\theta}$, $\rho_f(f \to 1^-) \sim (1 - f)^{\theta}$.
In the present case we expect a similar phenomenology. For the same arguments that contacts arises in the non-differentiable point $h \equiv 0$ of the purely linear potential, here we have the presence of two Dirac's delta in the gap distribution, one for $h = 0$ and the other one for $h = -H_0$. So, in this case, we have two species of contacts,

$$\mathcal{C}_0 = \{\mu : h_\mu \equiv 0\} \tag{6.3}$$

and

$$\mathcal{C}_{H_0} = \{\mu : h_\mu \equiv -H_0\} \tag{6.4}$$

associated with contact forces in $(0, 1)$ for the $\mathcal{C}_0$ and in $(1, 2)$ for $\mathcal{C}_{H_0}$. For convenience, let us define also the sets

$$\mathcal{O}_- = \{\mu : h_\mu < -H_0\} \tag{6.5}$$

and

$$\mathcal{O}_= = \{\mu : -H_0 < h_\mu < 0\} \tag{6.6}$$

Based on the phenomenology of the linear cost-function, we can write the Lagrangian

$$\begin{aligned} \mathcal{L}\left(\mathbf{X}, f_c, \tilde{f}_{\tilde{c}}, \mu\right) = &\sum_{\tilde{o} \in \mathcal{O}_-} (-2h_{\tilde{o}} - H_0) - \sum_{\tilde{c} \in \mathcal{C}_{H_0}} \tilde{f}_{\tilde{c}}(h + H_0) \\ &+ \sum_{o \in \mathcal{O}_=} (-h_o) - \sum_{c \in \mathcal{C}_0} f_c h \\ &+ \frac{\eta}{2}\left(|\,\mathbf{X}\,|^2 - N\right) \end{aligned} \tag{6.7}$$

Since we want to explore the jammed phase, we use the compression algorithm discussed in chapter 5 (Ref. [109]) by using the transformed Lagrangian

$$\mathscr{L}\left(\mathbf{X}, \sigma, f_c, \tilde{f}_{\tilde{c}}, \eta\right) = \mathcal{L} - p\sigma N \tag{6.8}$$

where now σ is a variable and the pressure p a control parameter.

6.1.1 Equilibrium conditions

Given the Lagrangian $\mathscr{L}$, a local minimum satisfies the variational equations with respect to $\mathbf{X}$ and σ, as well as w.r.t. the contact forces and η.

The constitutive equations for local minima are

$$\begin{cases} \eta\, X_i &= 2\sum_{\tilde{o} \in \mathcal{O}_-} \frac{\xi_i^{\tilde{o}}}{\sqrt{N}} + \sum_{o \in \mathcal{O}_=} \frac{\xi_i^{o}}{\sqrt{N}} + \sum_{c \in \mathcal{C}_0} f_c \frac{\xi_i^{c}}{\sqrt{N}} + \sum_{\tilde{c} \in \mathcal{C}_{H_0}} \tilde{f}_{\tilde{c}} \frac{\xi_i^{\tilde{c}}}{\sqrt{N}} \\ p &= \frac{2}{N}\sum_{\tilde{o} \in \mathcal{O}_-} 1 + \frac{1}{N}\sum_{o \in \mathcal{O}_=} 1 + \frac{1}{N}\sum_{c \in \mathcal{C}_0} f_c + \frac{1}{N}\sum_{\tilde{c} \in \mathcal{C}_{H_0}} \tilde{f}_{\tilde{c}} \end{cases} \tag{6.9}$$

$$\begin{cases} h_c & = 0 \qquad \forall c \in \mathcal{C}_0 \\ h_{\tilde{c}} & = -H_0 \qquad \forall \tilde{c} \in \mathcal{C}_{H_0} \\ |\,\mathbf{X}\,|^2 & = N \end{cases} \tag{6.10}$$

The equations (6.9) give a linear system for finding the contact forces in a minimum. Because of the slopes of the potential, they have to satisfy

$$\begin{aligned} f_c &\in (0,1) \qquad \forall c \in \mathcal{C}_0 \\ \tilde{f}_{\tilde{c}} &\in (1,2) \qquad \forall \tilde{c} \in \mathcal{C}_{H_0}\ . \end{aligned} \tag{6.11}$$

If a solution has contact forces that are outside the corresponding stability intervals, such solutions identify an unstable configuration.
To make the correspondence with the purely linear case clearer, we can redefine the contact forces $\tilde{f}_{\tilde{c}} \in (1,2)$ as $\tilde{f}_{\tilde{c}} = 1 + f_c$, with $f_c \in (0,1)$. So, the first equation of (6.9) can be rewritten as

$$\eta\, X_i = 2 \sum_{\tilde{o} \in \mathcal{O}_-} \frac{\xi_i^{\tilde{o}}}{\sqrt{N}} + \sum_{o \in \mathcal{O}_= \cup \mathcal{C}_{H_0}} \frac{\xi_i^{o}}{\sqrt{N}} + \sum_{c \in \mathcal{C}_0 \cup \mathcal{C}_{H_0}} f_c \frac{\xi_i^{c}}{\sqrt{N}} \tag{6.12}$$

where now we have again only one kind of contact forces $f_c \in (0,1)$.

We observe that, as it happens for the purely linear case [109], the Lagrangian $\mathcal{L}$ is effectively linear in all variables except for the term proportional to η. Therefore the convexity of the problem is self-determined and is fixed by the sign of η. If $\eta < 0$ we are in the non-convex phase with multiple minima and a glassy landscape, while if $\eta > 0$ we are in a convex phase with just one minimum.
Since we are interested in the glassy, critical phase, we use the compression algorithm in the regime $\alpha > 2$ so that the jamming happens in the non-convex phase and we enter the jammed phase in the glassy regime.

6.2 Numerical simulations

The compression algorithm of chapter 5 [109] can be used directly in this model with very small adaptations:

- using the form (6.12) for the equilibrium condition, the corresponding linear equation $\nabla \mathscr{L} = \underline{\underline{S}}\,\mathbf{f} + \mathbf{v}$ is the same as in the purely linear case up to an evident redefinition of the term $\mathbf{v}$; therefore, all kind of contacts get destabilized when the corresponding contact force f_c gets outside the interval $(0,1)$;
- when moving the configuration, we have to take into account not only the formation of a contact $h_{\tilde{\mu}} = 0$ but also the possibility of forming a contact $h_{\tilde{\mu}} = -H_0$: this simply enters in the definition of the step t^*. The configuration displacement remains $(\delta\,\mathbf{X}, \delta\sigma) = -t^* \nabla^* \mathscr{L}$ as discussed in section 5.1.4.

We fix $\alpha = 4$ and we study the compression along the phase diagram.
In Fig.6.2 we plot the behavior of the Lagrange multiplier η as a function of $\sigma - \sigma_J$ being σ_J the jamming point. It is clear that as soon as we enter the jammed phase, the landscape is strictly non-convex, since the Lagrange multiplier is negative. When

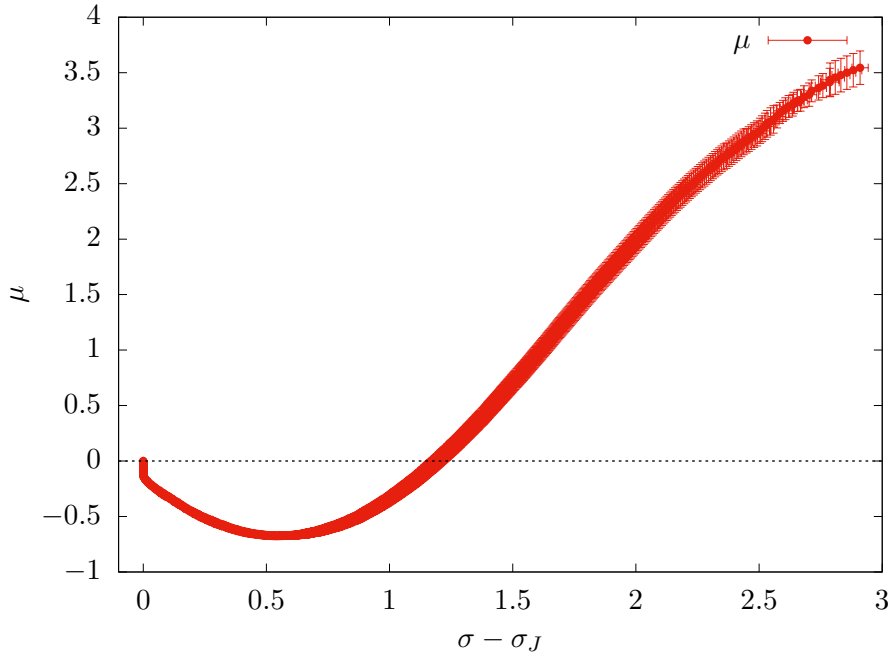

Figure 6.2: The Lagrange multiplier μ ($= \eta$) as a function of the distance from jamming. The jump observed at $\sigma = \sigma_J$ is due to finite size effects. Indeed in a finite system the configuration at jamming is stable for a finite amount of pressure before being destabilized and entering in the jammed phase [109]. The Lagrange multiplier is negative in the non-convex phase while it is positive when the landscape becomes convex. The figure has been produced simulating the model at $\alpha = 4$ and $N = 256$. The error bars represent sample to sample fluctuations.

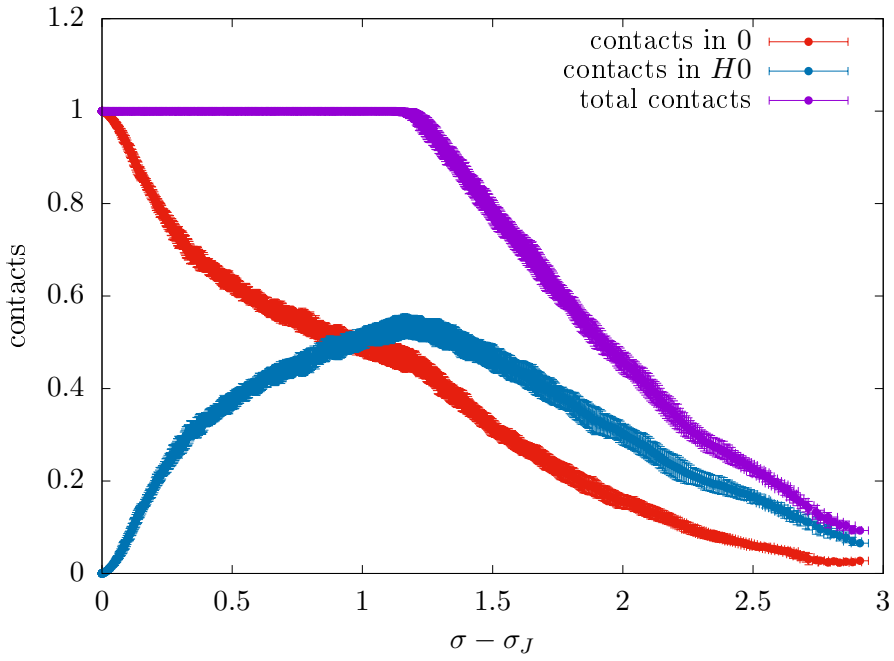

Figure 6.3: The number (normalized by N) of contacts in $h = 0$, meaning c_0, in $h = -H_0$, meaning c_{H_0} and their sum. We clearly see that in the whole interval in which the system is in the glassy/non-convex phase, the total number of gaps in the two non-analytic points of the cost functions, is isostatic. Isostaticity is lost when we enter the convex phase. Also in this case as for the purely linear cost function, we note that the sample to sample fluctuations away from isostaticity in the glassy phase are essentially absent. The figure has been produced simulating the model at $\alpha = 4$ and $N = 256$ and the error bars represent sample to sample fluctuations.

compressing the system further, it undergoes a topology trivialization transition towards a convex phase where the landscape is characterized by just one unique minimum and the Lagrange multiplier η becomes positive. We expect that this transition can also be found by analyzing the problem with the replica method and corresponds to the transition point between replica symmetry breaking and replica symmetry.

6.2.1 Contacts

Let us study now the number of contacts in the minima of the non-convex phase. In Fig. 6.3 we plot the cardinality of the sets $\mathcal{C}_0$ and $\mathcal{C}_{H_0}$ normalized over N. At the beginning of the compression protocol, the system contains N gaps in zero and therefore the system is isostatic with a number $|\mathcal{C}_0| = c_0 N = N$, as in the usual jamming. As soon as we enter the jammed phase, contacts in $h = -H_0$ start to appear, while those in $h = 0$ start to diminish. Remarkably, we find that if we define $|\mathcal{C}_{H_0}|/N = c_{H_0}$ we have that

$$c_0 + c_{H_0} = 1 \tag{6.13}$$

which implies that the system is isostatic only globally. The number of gaps in $h = 0$ or in $h = -H_0$ fluctuates but the total sum is equal to the number of degrees of freedom in the problem. It is very interesting to notice that the sample to sample fluctuations of c_0 and c_{H_0} seem to be normal yet completely anticorrelated in order to have Eq. (6.13)

satisfied even at finite N. The system self-organizes in such a way that only the sum of the number of gaps in zero and $-H_0$ is isostatic.

To understand this fact, we can use the smoothed version of the piece-wise linear potential, consisting in regularizing the non-differentiable points with an arc of parabola of curvature $\frac{1}{2\epsilon}$:

$$\nu_\epsilon(h) = \begin{cases} -2h - H_0 & h < -H_0 - \frac{\epsilon}{2} \\ -h + \frac{(h+H_0-\frac{\epsilon}{2})^2}{2\epsilon} & -H_0 - \frac{\epsilon}{2} < h < -H_0 + \frac{\epsilon}{2} \\ -h & -H_0 + \frac{\epsilon}{2} < h < -\frac{\epsilon}{2} \\ \frac{(h-\frac{\epsilon}{2})^2}{2\epsilon} & -\frac{\epsilon}{2} < h < \frac{\epsilon}{2} \\ 0 & h > \frac{\epsilon}{2} \end{cases} \tag{6.14}$$

As for the purely linear case [108], the smoothing removes the degeneracy of the contacts and allows for a real space description of the contact forces that appear as gaps contained within the smoothed regions. Since now the cost function $\mathcal{L}_\epsilon = \sum_\mu \nu_\epsilon(h_\mu) + \frac{\eta}{2}(|\,\mathbf{X}\,|^2 - N)$ admits a harmonic expansion, we can define a corresponding rescaled Hessian that takes a contribution from both the contacts in $h = 0$ as well as the ones in $h = -H_0$:

$$\mathcal{H}_{ij} = \epsilon \partial^2_{X_i X_j} \mathcal{L}_\epsilon = \sum_{c \in \mathcal{C}} \frac{\xi^c_i \xi^c_j}{N} + \epsilon\, \eta\, \delta_{ij} \tag{6.15}$$

where $\mathcal{C} = \mathcal{C}_0 \cup \mathcal{C}_{H_0}$. We notice that, neglecting correlations, $\mathcal{H}_{ij}$ is a Wishart random matrix shifted on the diagonal [106]. In the glassy phase where $\eta < 0$, we need to have that the Wishart part of the Hessian matrix is full-rank in order to have stable minima. Therefore we get the condition

$$|\mathcal{C}_0| + |\mathcal{C}_{H_0}| \geq N \tag{6.16}$$

If marginal stability holds, the bound is saturated and we get isostaticity [188]. This argument tells that the number of contacts in $h = 0$ and $h = -H_0$ can fluctuate but in a correlated way in order to satisfy Eq. (6.16).

6.2.2 Statistics of gaps and forces

We turn to the analysis of the force and gap distributions. The empirical distribution of gap variables is defined as

$$\rho(h) = \frac{1}{M} \sum_{\mu=1}^{M} \delta(h - h_\mu) \tag{6.17}$$

In Fig.6.4 we plot the histogram of $\rho(h)$ at $p = 4$ which corresponds to the point where $c_0 \sim c_{H_0}$. It is clear from this qualitative picture that the two Dirac delta functions in $h = 0, -H_0$ are surrounded by four power law divergences.

In order to characterize those divergences, in Fig.6.5 we plot the cumulative distribution function of the gaps, starting from $h = 0$ and $h = -H_0$. Within our numerical precision we observe that

$$\rho(h) \sim \begin{cases} A^+_0 h^{-\gamma} & h \to 0^+ \\ A^-_0 |h|^{-\gamma} & h \to 0^- \\ A^+_{H_0} (h + H_0)^{-\gamma} & h \sim -H^+_0 \\ A^-_{H_0} |h + H_0|^{-\gamma} & h \sim -H^-_0 \end{cases} \tag{6.18}$$

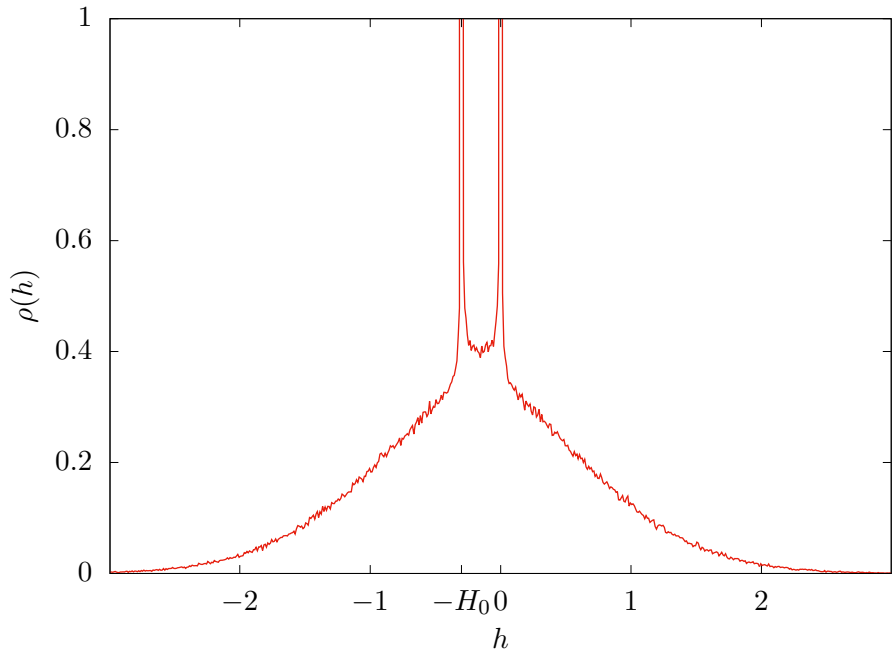

Figure 6.4: The empirical probability distribution function of the gap variables, obtained at pressure $p = 4$ and for $\alpha = 4$ and $N = 2048$.

where the exponent $\gamma \simeq 0.41\ldots$ coincide (within our numerical precision) with the one characterizing the distribution of positive gaps at the jamming transition point [63, 62] and the As are constants.

Finally we look at the contact forces. In Fig. 6.6 we plot the empirical distribution of contact forces both in $h = 0$ and in $h = -H_0$. We clearly see that there are four pseudogaps appearing close to the edges of the support of f_c.

In order to quantitatively analyze the behavior close to the four edges of the stability supports, we look at the cumulative distribution functions that we plot in Fig.6.7. We observe that, at the edges of the stability domains, the force distribution has four pseudogaps

$$\rho(f) \sim \begin{cases} B_0^+ f^\theta & f \to 0^+ \\ B_1^- (1-f)^\theta & f \to 1^- \\ B_1^+ (f-1)^\theta & f \to 1^+ \\ B_2^- (2-f)^\theta & f \to 2^- \end{cases} \tag{6.19}$$

where the Bs are constants of order one and the exponent $\theta = 0.42\ldots$ is compatible with the one controlling the small forces at the jamming transition point [63, 62].

6.3 Discussion

The results of the piece-wise linear potential show that all the discussion about marginal stability and self-organized criticality regarding the purely linear potential can be transferred verbatim to the general case of a potential whose first derivative has several discontinuities. The only novelty is the fact that different kinds of contacts can exist and consequently there is a proliferation of the possible excitations/relaxations of the system, consisting in breaking/forming all sorts of contacts. For example, it is possible to imagine

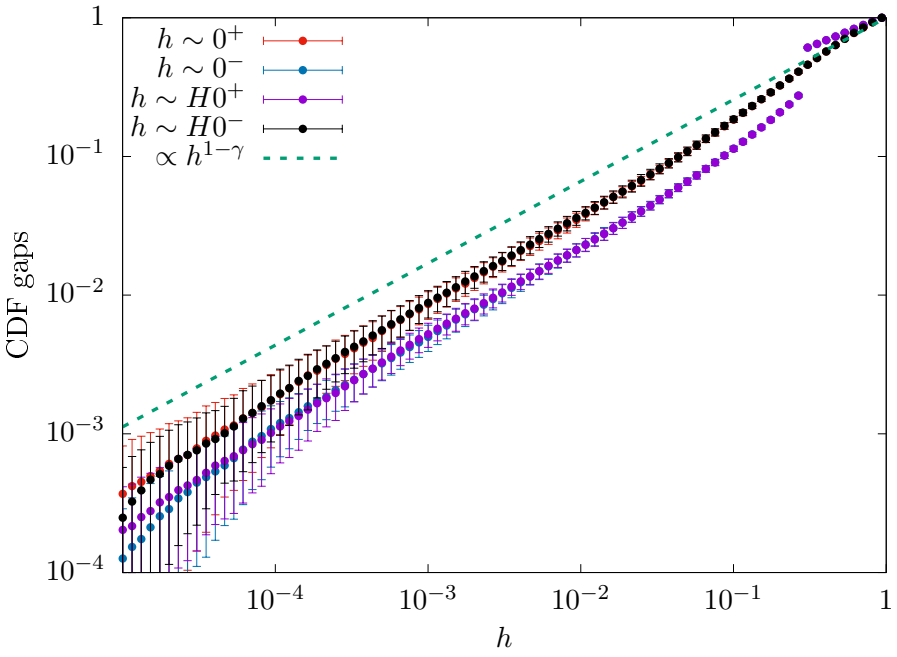

Figure 6.5: The cumulative distribution functions of the gaps on both sides of both Dirac delta peaks at $h = 0$ and $h = -H_0$.The plot has been produced looking at minima at $p = 4$ for $\alpha = 4$ and $N = 2048$. The error bars represent sample to sample fluctuations

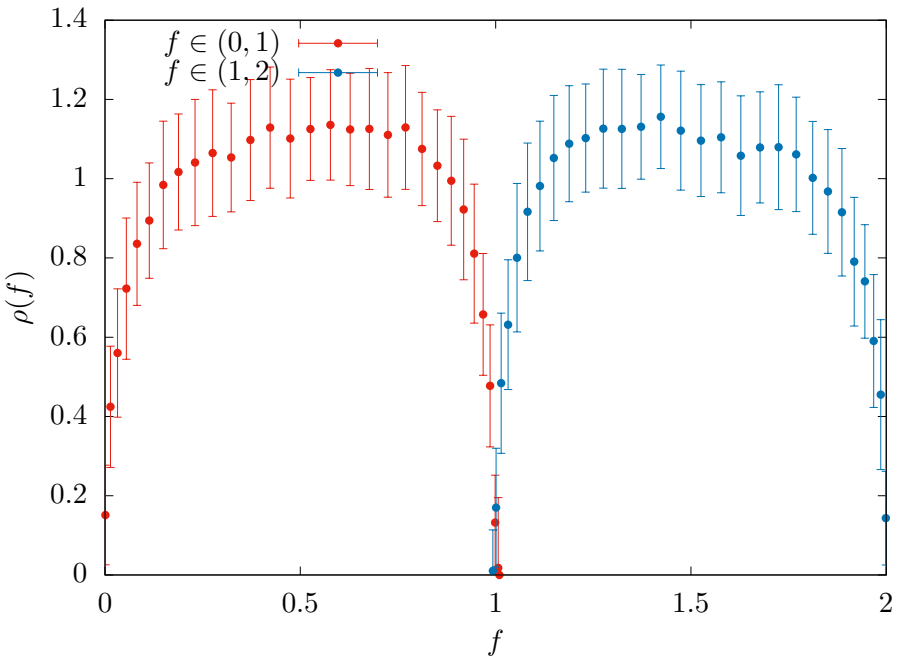

Figure 6.6: The empirical probability distribution function of the contact forces. In red we plot the ones corresponding to the gaps at $h = 0$ while in blue we plot the ones corresponding to the gaps at $h = -H_0$. The fact that the two pdfs appear rather similar is mainly due to the fact that we have measured such distributions at $p = 4$ where $c_0 \simeq c_{H_0}$.The plot has been produced looking at minima at $p = 4$ for $\alpha = 4$ and $N = 2048$. Error bars are obtained looking at sample to sample fluctuations.

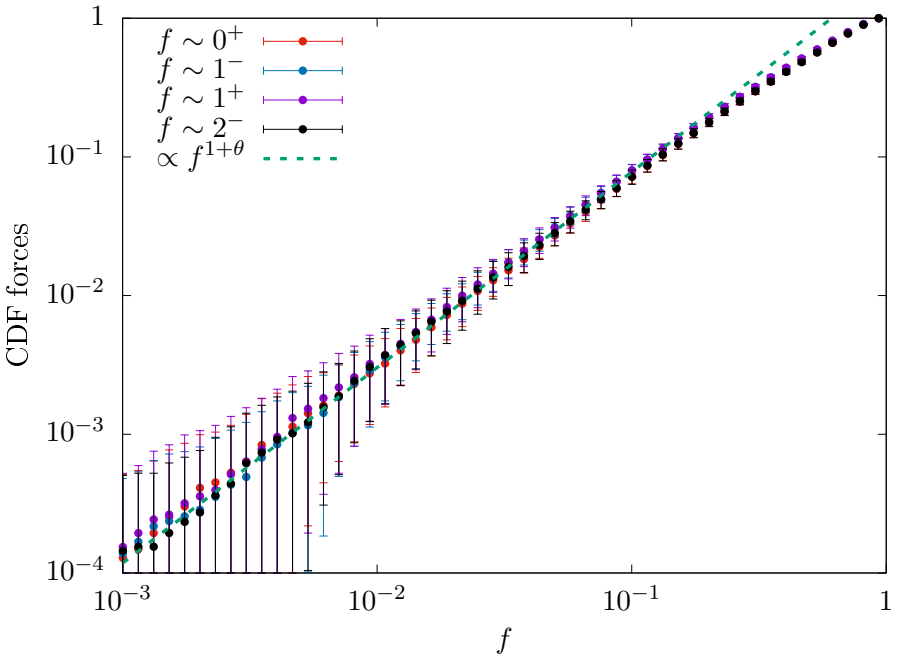

Figure 6.7: The cumulative distribution functions for the contact forces close to the edges of their stability supports. We see that the apparent prefactors look very similar and the dots are rather one onto the other, because we measured the forces at the rather symmetric point where the number of gaps in zero and in $-H_0$ is roughly the same. We do not expect such prefactors to be universal but to depend on the point of the phase diagram where local minima are probed. The plot has been produced looking at minima at $p = 4$ for $\alpha = 4$ and $N = 2048$ Error bars are obtained from sample to sample fluctuations.

a cost function of the form

$$H = \sum_{\mu} \nu(h_\mu) \qquad \nu(h) = \sum_{i=1}^{K} |h - H_i| \theta(-h + H_i) \tag{6.20}$$

that for each point H_i has a jump in the derivative. This model would have K species of "contacts" that, in the non-convex phase, would contribute to the global isostatic condition $\sum_{i=1}^{K} c_i = 1$.
Also in this case, perturbations of the local minima would trigger system-spanning avalanches and give rise to crackling noise.
In the same spirit of the purely linear potential [107], we expect this phenomenology to be found also for finite dimensional linear spheres.
The robustness of the observed critical behavior stems from the topological nature of the isostaticity condition. This is reflected in the fact that the number of contacts of a single kind, like c_0 and c_{H0} in Fig. 6.3, fluctuates normally, but their sum does not. This is analogous to the hyperuniformity of the contact network for linear spheres: the number of contacts of a single sphere can fluctuate, but on the large scale the sum of the number of contacts must be equal to the number of degrees of freedom.
From the theoretical point of view, the analysis of the piece-wise linear potential can be done using the replica formalism presented for the perceptron. In the critical phase, the scaling fullRSB theory should apply, giving a prediction of the observed critical exponents. The equality of the exponents appearing for every singular point of the potential is expected to be a consequence of the structure of the scaling solution discussed in section 3.3.3.

Chapter 7

Conclusions and perspectives

Although jamming has been extensively studied and characterized, it still provides interesting questions to be answered. In particular, its super-universality stems from the fact that simulations of packings of spheres have jamming critical behavior well described by mean-field theory (except for the local/finite-dimensional effects) [64]. In this thesis we have extended this universal behavior from a critical point to an entire critical phase by choosing a proper potential energy, i.e. a finite-range linear interaction.

- In chapter 3 we have studied a mean-field model, the perceptron, which we can analytically solve by the replica method. We have obtained the phase diagram, showing the existence of a convex, hypostatic phase described by the replica symmetric solution and a non-convex, isostatic, marginally stable phase, described by the full replica symmetry breaking solution.
  The convex phase is non-critical, reminiscent of the jamming point of ellipses and ellipsoids that is as well hypostatic and non-critical [83, 162]. On the other hand, the non-convex phase is critical, with the emergence of power laws whose critical exponents correspond to those characterizing the jamming point of spheres.
  We have validated the theory by numerical simulations, minimizing the energy of the model by gradient-descent-like algorithms. The different behavior of the two phases, with criticality emerging in the non-convex one, is fairly robust. In particular, the only stable configurations found by the algorithm in the non-convex phase are perfectly isostatic, accompanied by power-law divergences in the distribution of small positive and small negative gaps, as well as pseudo-gaps in the contact force distribution at the boundaries of its domain, i.e. $[0, 1]$. Therefore, if at the jamming transition there is one exponent for gaps and one for forces, in the critical phase there are two exponents for gaps and two for forces. Remarkably, they are equal in couples to the jamming ones. On this basis we say that the critical phase is an extended version of the jamming point.
  The replica theory in the non-convex phase is made of a system of partial differential equation that in principle can be solved numerically. Knowing that the critical phase is characterized by scaling behavior and knowing the form of the solution at the jamming point [200], we have inserted a scaling form in the equations: they provide a scaling theory giving a prediction of the critical exponents. It turns out that there is a mapping in the equations that ensures that the two exponents of the gap distribution have the same value, and the same holds for the force distribution. As a result, the scaling functions in our theory become equal to those of the jamming

solution, establishing the observed universality also on the theoretical level.

- In chapter 4, we have verified that the mean-field behavior is found also in finite dimensional systems: in this case soft spheres in two and three dimensions. We have done it by minimizing the energy of the model in the jammed phase, where energy and pressure are positive. This jammed phase is self-organized critical, isostatic and marginally stable, with the same critical exponents found in the mean-field model. Also real space quantity, like the suppression of fluctuations of the number of contacts at large distances [128, 129], behave in a jamming-like fashion. Therefore, we have extended arguments based on marginal stability at jamming [247] to this scenario, verifying the same kind of relationship between the critical exponents.
  We also have shown that quantities like energy, pressure and number of overlaps near the unjamming point have a behavior that is different from the one observed in other soft potentials.

- In chapter 5, we have characterized the microstructure of the energy landscape of the perceptron with linear potential by defining a compression algorithm. It consists in increasing the pressure until a single contact gets destabilized and following the gradient along the unstable modes. This creates avalanches and crackling noise, a signature of marginal stability [188]. We have characterized the avalanche size statistics, which is a power law with divergent mean, and the finite size scalings of different quantities that have non-trivial exponents. This has let us analyze in detail the unjamming transition, revealing a new scaling for the number of overlaps w.r.t. the distance from unjamming: we have found an exponent $\nu \simeq 0.83$ instead of $1/2$ generally observed in other soft potentials [191, 116]. These results are in agreement with the theoretical computation of Ref. [110] and the scalings found in shearing hard spheres [71, 79].

- In chapter 6, we have studied a variation of the purely linear potential, i.e. a piecewise linear one, where there are two discontinuities in the first derivative. We have used the same compression algorithm as the previous chapter, properly adapted, to study the jammed phase. The interest lies in the fact that two singularities in the potential transform in two kinds of possible contacts. In the non-convex phase of this model, while the number of a single kind of contacts can fluctuate, their sum verifies the isostatic condition. This reinforces the idea of isostaticity as a global condition on the system in order to achieve mechanical equilibrium. Remarkably, each kind of these contacts is accompanied by power law divergences of small gaps and pseudo-gaps for force distributions, giving a total of eight critical exponents. However, their values are found to be the same as the two known for gaps and forces at jamming. Also in this case, the exponents are related to the global isostaticity and marginal stability, controlling the excitation/relaxation mechanisms corresponding to breaking/forming all kinds of contacts.

The main result of this work sheds new light on the universality class of jamming. Its robustness with dimensionality is related to its strong geometrical nature, since the formation of an isostatic contact network can be seen as a topological condition.
In the models we have studied, ordered structures are frustrated by disorder or they are not accessible by local-searching algorithms, while the non-convex geometry makes every unconstrained degree of freedom unstable. As a result, the system finds a stable configuration only by constraining all the degrees of freedom, i.e. by becoming (at least) isostatic.

The virtue of the linear potential is to expose the underlying geometry of the problem, since it has no curvature that can contribute to create minima in the energy landscape other than the geometrically defined ones. To understand this point, it is useful to think of the function $|x|$, whose only minimum is in $x = 0$: it corresponds to the point where the function changes slope. The linear potential in high dimensions creates a similar picture: the only minima are those angular points surrounded by increasing energy ramps. For spheres interacting through $\nu(h_{ij}) = |h_{ij}|\theta(-h_{ij})$, where h_{ij} is the gap between two spheres, the points where the slope changes are those where $h_{ij} = 0$, that is when contacts are formed. Therefore the problem of finding a minimum can be recast as the problem of finding a stable contact network.
As we have shown with the piece-wise linear potential, increasing the number of non-differentiable points in the interaction creates the possibility for new kinds of "contacts" to appear: still isostaticity is the global condition for stability while power laws appear in corresponds of each singularity.
A natural question therefore is if there is some generic property of problems in high dimensions with disorder that gives rise to these special points characterized by highly universal properties.

We do not know if the critical phase we have studied is relevant for some experimental physical systems, since a linear interaction potential is quite uncommon. Nevertheless, it offers interesting perspectives in theory and in computer models.
In the case of spheres, we aim at characterizing their rheology and avalanches response [36, 205, 71, 110, 220]. Another interesting feature is inserting the temperature in the model and see if there exists a marginally stable phase at finite temperature: this would reveal the presence of a Gardner transition [30, 236].
On the mean-field side, we can modify the perceptron with more singular interaction potentials and see how the criticality behaves. It would be important to find the known scaling solution from a purely dynamical perspective, for example by using message passing algorithms [182, 3, 14].
Another interesting topic is connecting our findings to more general optimization problems. In fact, it is easy thinking of extensions of the perceptron model where a cost-function has to optimized over some continuous variables: choosing a linear cost-function could give rise to interesting behavior. We leave this subject for future explorations.

Appendices

Chapter A

Distribution of gaps and forces in the linear potential case

In this section we compute the distribution of gaps and forces for the linear potential case.
We do it for the general fullRSB case, clarifying the connection between the function $P(q_M, h)$ appearing in the theory (2.77) and the physical distributions.

The general formula for the gap distribution is:

$$g(h) = \frac{1}{\alpha}\frac{\mathrm{d}\,\mathrm{f}}{\mathrm{d}\,\nu(h)} = e^{-\beta\nu(h)} \int dz\ P(q_M, z) e^{-f(q_M,z)} \gamma_{1-q_M}(z-h) \tag{A.1}$$

where f is the free energy and $\nu(h)$ the arbitrary potential.
With the linear potential, using the asymptotic form of $f(q_M, z)$ for the zero temperature limit found in (3.99), we get

$$\begin{aligned} g(h) = & \\ &= \underbrace{e^{-\beta|h|\theta(-h)} \int_0^\infty dz P(q_M, z)\gamma_{1-q_M}(z-h)}_{A} + \\ &+ \underbrace{e^{-\beta|h|\theta(-h)} \int_{-\chi}^0 dz\ P(q_M, z) \exp\left[\frac{z^2}{2(1-q_M)}\right] \gamma_{1-q_M}(z-h)}_{B} + \\ &+ \underbrace{e^{-\beta|h|\theta(-h)} \int_{-\infty}^{-\chi} dz\ P(q_M, z) \exp\left[-\beta\left(z+\frac{\chi}{2}\right)\right] \gamma_{1-q_M}(z-h)}_{C} \\ &= A + B + C \end{aligned} \tag{A.2}$$

where we have divided our integral in 3 parts A, B, C.
We show that, in the limit $\beta \to \infty$ and $q_M \to 1$, the dominant term depends on the value of h.

- For $h > 0$:

$$A = \int_0^\infty dz P(q_M, z)\gamma_{1-q_M}(z-h) \underset{q_M\to 1}{=} P(1, h) \tag{A.3}$$

$$\begin{aligned} B &= \int_{-\chi}^{0} dz\ P(q_M,z)\exp\left[\frac{z^2}{2(1-q_M)}\right]\gamma_{1-q_M}(z-h) = \\ &= \int_{-\chi}^{0} dz\ P(q_M,z)\exp\left[-\frac{h^2-2hz}{2(1-q_M)}\right] < \\ &< \exp\left[-\frac{h^2}{2(1-q_M)}\right]\int_{-\chi}^{0} dz\ P(q_M,z) \underset{q_M\to 1}{=} O\left(e^{-\frac{h^2}{2(1-q_M)}}\right) << A \end{aligned} \tag{A.4}$$

$$\begin{aligned} C &= \int_{-\infty}^{-\chi} dz\ P(q_M,z)\exp\left[-\beta\left(z+\frac{\chi}{2}\right)\right]\gamma_{1-q_M}(z-h) = \\ &= \int_{-\infty}^{-\chi} dz\ P(q_M,z)\exp\left[-\frac{+2\chi z+\chi^2+h^2-2hz+z^2}{2(1-q_M)}\right] < \\ &< \exp\left[-\frac{h^2+2\chi h}{2(1-q_M)}\right]\int_{-\infty}^{-\chi} dz\ P(q_M,z) \underset{q_M\to 1}{=} O\left(e^{-\frac{h^2+2\chi h}{2(1-q_M)}}\right) << A \end{aligned} \tag{A.5}$$

So for $h>0$ it is the part A of the integral that dominates.

- For $h=0$:

$$A = \int_0^{\infty} dz P(q_M,z)\gamma_{1-q_M}(z) \underset{q_M\to 1}{=} P(1,0^+) \tag{A.6}$$

$$\begin{aligned} B &= \int_{-\chi}^{0} dz\ P(q_M,z)\exp\left[\frac{z^2}{2(1-q_M)}\right]\gamma_{1-q_M}(z) = \\ &= \int_{-\chi}^{0} dz\ P(q_M,z) \underset{q_M\to 1}{=} \int_{-\chi}^{0} dz\ P(1,z) \end{aligned} \tag{A.7}$$

$$\begin{aligned} C &= \int_{-\infty}^{-\chi} dz\ P(q_M,z)\exp\left[-\beta\left(z+\frac{\chi}{2}\right)\right]\gamma_{1-q_M}(z) = \\ &= \int_{-\infty}^{-\chi} dz\ P(q_M,z)\exp\left[-\frac{+2\chi z+\chi^2+z^2}{2(1-q_M)}\right] = \\ &= \int_{-\infty}^{-\chi} dz\ P(q_M,z)\gamma_{1-q_M}(z+\chi) \underset{q_M\to 1}{=} P(1,-\chi^-) \end{aligned} \tag{A.8}$$

We have found that for $h=0$ the gap distribution has not just a value but a weight given by the part B of the integral, i.e. $\int_{-\chi}^{0} dz\ P(1,z)$.

- For $h<0$:

$$\begin{aligned} A &= e^{-\beta|h|\theta(-h)}\int_0^{\infty} dz P(q_M,z)\gamma_{1-q_M}(z-h) < \\ &< \exp\left[-\frac{h^2-2\chi h}{2\,(1-q_M)}\right]\int_0^{\infty} dz P(q_M,z) \underset{q_M\to 1}{=} O\left(e^{-\frac{h^2-2\chi h}{2(1-q_M)}}\right) \end{aligned} \tag{A.9}$$

$$\begin{aligned} B &= e^{-\beta|h|\theta(-h)}\int_{-\chi}^{0} dz\ P(q_M,z)\exp\left[\frac{z^2}{2(1-q_M)}\right]\gamma_{1-q_M}(z-h) = \\ &= \int_{-\chi}^{0} dz\ P(q_M,z)\exp\left[-\frac{h^2-2hz-2\chi h}{2(1-q_M)}\right] < \\ &< \exp\left[-\frac{h^2-2\chi h}{2\,(1-q_M)}\right]\int_{-\chi}^{0} dz\ P(q_M,z) \underset{q_M\to 1}{=} O\left(e^{-\frac{h^2-2\chi h}{2(1-q_M)}}\right) \end{aligned} \tag{A.10}$$

$$
\begin{aligned}
C &= e^{-\beta|h|\theta(-h)} \int_{-\infty}^{-\chi} dz\ P(q_M, z) \exp\left[-\beta\left(z + \frac{\chi}{2}\right)\right] \gamma_{1-q_M}(z-h) = \\
&= \int_{-\infty}^{-\chi} dz\ P(q_M, z) \exp\left[-\frac{-2\chi h + 2\chi z + \chi^2 + h^2 - 2hz + z^2}{2(1-q_M)}\right] = \\
&= \int_{-\infty}^{-\chi} dz\ P(q_M, z) \exp\left[-\frac{(h-\chi-z)^2}{2(1-q_M)}\right] \underset{q_M \to 1}{=} P(1, h-\chi)
\end{aligned}
\tag{A.11}
$$

We have found that for $h < 0$ it is the part C that dominates the integral and the gap distribution corresponds to $P(1, h-\chi)$.

Summarizing, the gap distribution in the limit $T \to 0$ ($q_M \to 1$) reads

$$
\boxed{g(h) \underset{q_M \to 1}{=} \theta(h) P(1,h) + \ \delta(h) \int_{-\chi}^{0} dz P(1,z) + \theta(-h) P(1, h-\chi)}
\tag{A.12}
$$

The weight in the gap distribution associated to $\delta(h)$ gives the number of zero gaps (i.e. contacts) in the system. The integrand

$$
P(q_M, z) \qquad \text{for } -\chi < z < 0
\tag{A.13}
$$

is actually the distribution of contact forces $\tilde{f} = \frac{-z}{\chi}$, that are in fact inside the interval $(0, 1)$. So we have

$$
\rho(\tilde{f}) \propto P(q_M, -\chi\tilde{f}), \qquad \tilde{f} \in (0,1)
\tag{A.14}
$$

To see this is the case, it is possible to study the free energy of the smoothed Hamiltonian (3.14) and see that the distribution of $P(q_M, z)$ with $-\chi < z < 0$ corresponds to the distribution of the gaps in ϵ-window $(-\frac{\epsilon}{2}, \frac{\epsilon}{2})$, that converge in fact to the contact forces when $\epsilon \to 0$.
It is interesting to see that the peak of zero gaps and the distribution of their contact forces appear naturally in the thermodynamic calculation even if they were not specifically accounted for in the studied Hamiltonian.

Actually, equation (A.12) is not properly correct in the $full$RSB case: to get the right formula it is necessary to take the limit $q \to 1$ of the function $P(q, h)$ that solves the full-RSB partial differential equations (3.156). Moreover, χ has to be substituted by the corresponding quantity $\lim_{q\to 1} \hat{\lambda}(q) = \lim_{q \to 1} \beta\lambda(q)$, where the function $\lambda(q)$ is a generalization of χ defined in (3.157). The correct expression in the $full$RSB case is therefore

$$
g(h) \underset{q \to 1}{=} \theta(h) P(q,h) + \ \delta(h) \int_{-\hat{\lambda}(q)}^{0} dz P(q,z) + \theta(-h) P(q, h - \hat{\lambda}(q))
\tag{A.15}
$$

and similarly for contact forces

$$
\rho(\tilde{f}) \propto P(q, -\hat{\lambda}(q)\tilde{f})\Big|_{q\to 1}, \qquad \tilde{f} \in (0,1)
\tag{A.16}
$$

A.1 Replica symmetric gap and force distribution

In the case of the replica symmetric solution, we have

$$P(q_M, h) = \gamma_{q_M}(h + \sigma) \tag{A.17}$$

and so the gap distribution becomes

$$g(h) \underset{q_M \to 1}{=} \theta(h)\gamma(h+\sigma) + \ \delta(h) \int_{-\chi}^{0} dz \gamma(z+\sigma) + \theta(-h)\gamma(h+\sigma-\chi) \tag{A.18}$$

The associated contact force distribution reads

$$\rho(\tilde{f}) \propto \gamma\left(-\chi\tilde{f} + \sigma\right), \qquad \tilde{f} \in (0,1) \tag{A.19}$$

Chapter B

Computation of the spherical Lagrange multiplier η

We have study the partition function

$$Z = \int d\vec{X} \exp\left[-\beta\left(H[\vec{X}] + \frac{\mu}{2}\sum_j \left(X_j^2 - 1\right)\right)\right] \tag{B.1}$$

with the generic Hamiltonian

$$H[\vec{X}] = \sum_\mu \nu(h_\mu) \tag{B.2}$$

using replicas. The procedure is exactly the same as in section 2.3: we consider directly the general fullRSB case making the necessary modifications to the action (2.76).
Since X^2 is not constrained, now we have another parameter on diagonal of the overlap matrix, $Q_{a,a} = q_d$. The full RSB free energy of eq. (2.76) now reads:

$$\begin{aligned}
&s\left[q_d, q(x), \mu\right] = \\
&= \frac{1}{2}\left[\log\left(q_d - q_M\right) + \frac{q_M}{q_d - < q >} + \int_0^1 dx \frac{\dot{q}(x)}{\lambda(x)}\right] + \\
&+ \alpha\gamma_{q_m} * f(q,h)\Big|_{h=-\sigma} - \frac{\beta}{2}\mu(q_d - 1) + \\
&- \alpha\int dh P(q_M, h)\left[f(q_M, h) - \log\gamma_{q_d - q_M} * e^{-\beta\nu(h)}\right] + \\
&+ \alpha\int dh \int_{q_m}^{q_M} dq P(q,h)\left[\dot{f}(q,h) + \frac{1}{2}\left[f''(q,h) + x(q)f'(q,h)^2\right]\right]
\end{aligned} \tag{B.3}$$

where

$$\begin{aligned}
\lambda(x) &= q_d - xq(x) - \int_x^1 dy q(y) \\
\lambda(q) &= q_d - q_M - \int_q^{q_M} dp x(p)
\end{aligned} \tag{B.4}$$

The variational equations for $q(x)$, $f(q,h)$ and $P(q,h)$ are the same as already obtained in (2.73)-(2.77)-(2.78):

$$\dot{f}(q,h) = -\frac{1}{2}\left[f''(q,h) + x(q)f'(q,h)^2\right], \qquad q_m < q < q_M \tag{B.5}$$

$$\begin{cases} P(q_m,h) = \gamma_{q_m}(h+\sigma) \\ \dot{P}(q,h) = \frac{1}{2}\left[P''(q,h) - 2x(q)\left(P(q,h)f'(q,h)\right)'\right], \qquad q_m < q < q_M \end{cases} \tag{B.6}$$

$$\frac{q_m}{\lambda(q_m)^2} + \int_{q_m}^{q} dp \frac{1}{\lambda(p)^2} = \alpha \int dh P(q,h) f'(q,h)^2 \tag{B.7}$$

but with the different initial condition

$$f(q_M,h) = \log \gamma_{q_d - q_M} * e^{-\beta\nu(h)} \tag{B.8}$$

From equation (B.7) we also have the relationship

$$\frac{1}{\lambda(q)^2} = \alpha \int dh P(q,h) f''(q,h)^2 \tag{B.9}$$

Now we take the derivative w.r.t. q_d of the variational equation (B.3), that reads:

$$\frac{\beta\mu}{2} = \frac{1}{2}\left[\frac{1}{q_d - q_M} - \frac{q_m}{\lambda(q_m)^2} - \int_{q_m}^{q_M} dp \frac{1}{\lambda(p)^2}\right] + \alpha \int dh P(q_M,h) \frac{\partial}{\partial q_d} \log \gamma_{q_d - q_M} * e^{-\beta\nu(h)} \tag{B.10}$$

Using equations (B.5), (B.7) and posing $q_d = 1$, we can write

$$\beta\mu = \frac{1}{1-q_M} + \alpha \int P(q_M,h)\left[f''(q_M,h)\right] \tag{B.11}$$

B.1 Independence from q

The quantity μ might be a function of q. To show it is not the case, we write the right hand side of (B.11) in the general form depending on q and show that its derivative w.r.t. q is zero. We have

$$\beta\mu = \frac{1}{\lambda(q)} + \alpha \int dh P(q,h)\left[f''(q,h)\right] \tag{B.12}$$

We take the derivative w.r.t. q of the second term (we use a short hand notation omitting the integral $\int dh$):

$$\begin{aligned} &\dot{P}f'' + P\dot{f}'' = \dot{P}f'' + P''\dot{f} = \\ &= \left[\frac{P''}{2} - xP'f' - xPf''\right] f'' - \frac{P''}{2}\left[f'' + xf'^2\right] = \\ &= -xP'f'f'' - xPf''^2 + xP'f'f'' = \\ &= -xPf''^2 \end{aligned} \tag{B.13}$$

We take the derivative w.r.t. q of the first term:

$$\partial_q \frac{1}{\lambda(q)} = \frac{x(q)}{\lambda(q)^2} = \int dh x(q) P(q,h) f(q,h)''^2 \tag{B.14}$$

where we have used eq. (B.9).
Putting together B.14 and B.13 we have that

$$\frac{\partial}{\partial q}(\beta\mu) = 0 \tag{B.15}$$

B.1.1 RS case

In the RS case, $P(q_M, h) = \gamma_{q_M}(h)$ and the action reads

$$\begin{aligned} &s\left[q_d, q_M, \mu\right] = \\ &= \frac{1}{2}\left[\log(q_d - q_M) + \frac{q_M}{q_d - q_M}\right] + \alpha\gamma_{q_M} * f(q_M, h)\Big|_{h=-\sigma} - \frac{\beta\mu}{2}(q_d - 1) \end{aligned} \tag{B.16}$$

The derivative w.r.t. q_M gives the usual RS saddle point equation

$$\frac{q_M}{(q_d - q_M)^2} = \alpha\gamma_{q_M} * f'(q_M, h)^2\Big|_{h=-\sigma} \tag{B.17}$$

The derivative w.r.t. q_d gives

$$\beta\mu = \frac{1}{q_d - q_M} - \frac{q_M}{(q_d - q_M)^2} + \alpha\gamma_{q_M} * \left[f''(q_M, h) + f'(q_M, h)^2\right]\Big|_{h=-\sigma} \tag{B.18}$$

that, using (B.17), can be simplified into

$$\beta\mu = \frac{1}{q_d - q_M} + \alpha\gamma_{q_M} * \left[f''(q_M, h)\right]\Big|_{h=-\sigma} \tag{B.19}$$

We can now substitute $q_d = 1$ and study the limit $T \to 0$ by taking

$$q_M = 1 - \chi T \tag{B.20}$$

and the asymptotic form (3.101)

$$f''(q_M, h) = -\frac{1}{1 - q_M} \quad \text{for } -\chi < h < 0 \tag{B.21}$$

which gives

$$\mu = \frac{1}{\chi}\left[1 - \alpha\int_{-\chi}^{0}\gamma(h + \sigma)\right] \tag{B.22}$$

Chapter C

Nature of the Replica Symmetry Breaking in the linear perceptron

A way to study a replica symmetry breaking (RSB) transition is to take the general formula of the function $x(q)$ appearing in the RSB theory (2.83) and studying it when moving from the RSB phase to the RS one: exactly at the transition, we can plug into (2.83) the replica symmetric functions. This gives the so called *breaking point*, that is the point $m = x^*$ in which the profile of the order parameter, i.e. the function $q(x)$, changes from a flat one of the RS phase to an increasing one of the RSB phase. To have a consistent phase transition, the breaking point m must satisfy the condition $m < 1$, since the domain of $q(x)$ is $x \in [0, 1]$. If $m \geq 1$, it means that the deAlmeida-Touless (dAT) instability line gets divided into two transition lines: a "dynamical" one, with a 1RSB solution appearing discontinuously, and a true phase transition line, called "Kauzmann transition" or condensation. This discussion is outside the scope of this work and further information is found in references [105, 50, 146].
Our program is the following:

- we compute the breaking point m of $q(x)$ at the dAT instability line, showing we have a proper RS-RSB transition since $m \in (0, 1)$;

- we compute the derivative $\dot{q}(x)\Big|_{x=m}$, which gives the slope of the profile of $q(x)$ at the transition. We show that in our model $\dot{q}(m) > 0$, which implies a $full$RSB transition (see ref. [21] for a discussion of the slope of $q(x)$).

C.1 Breaking point

The general formula for the breaking point is given by (2.83) using the RS solution:

$$m = \frac{1 - q_M}{2} \frac{\int dh \gamma(h + \sigma) f'''(q_M, h)^2}{\int dh \gamma(h + \sigma) f''(q_M, h)^2 \left[1 + (1 - q_M) f''(q_M, h)\right]} \tag{C.1}$$

In the zero temperature limit, we can use the of $f(q_M, h)$ computed in (3.99):

$$\frac{d^2}{dh^2} f(h)\Big|_{q_M\to 1,\beta\to\infty} = \begin{cases} 0 & h >> \sqrt{1-q_M} \\ \frac{1}{1-q_M}\mathcal{F}''\left(\frac{h}{\sqrt{1-q_M}}\right) & h \sim O\left(\sqrt{1-q_M}\right) \\ -\frac{1}{1-q_M} & -\chi < h < 0 \\ \frac{1}{1-q_M}\mathcal{F}\left(-\frac{h+\chi}{\sqrt{1-q_M}}\right) & h+\chi \sim O\left(\sqrt{1-q_M}\right) \\ 0 & h << -\chi - \sqrt{1-q_M} \end{cases} \tag{C.2}$$

$$\frac{d^3}{dh^3} f(h)\Big|_{q_M\to 1,\beta\to\infty} = \begin{cases} 0 & h >> \sqrt{1-q_M} \\ \frac{1}{(1-q_M)^{\frac{3}{2}}}\mathcal{F}'''\left(\frac{h}{\sqrt{1-q_M}}\right) & h \sim O\left(\sqrt{1-q_M}\right) \\ 0 & -\chi < h < 0 \\ -\frac{1}{(1-q_M)^{\frac{3}{2}}}\mathcal{F}\left(-\frac{h+\chi}{\sqrt{1-q_M}}\right) & h+\chi \sim O\left(\sqrt{1-q_M}\right) \\ 0 & h << -\chi - \sqrt{1-q_M} \end{cases} \tag{C.3}$$

Therefore:

- the numerator:

$$\begin{aligned} &\int dh\gamma(h+\sigma) f'''(q_M,h)^2 = \\ &\frac{\sqrt{1-q_M}}{(1-q_M)^3}\gamma(\sigma)\int dx\mathcal{F}'''(x)^2 + \frac{\sqrt{1-q_M}}{(1-q_M)^3}\gamma(\sigma-\chi)\int dx\mathcal{F}'''(x)^2 = \\ &= \frac{\gamma(\sigma)+\gamma(-\chi+\sigma)}{(1-q_M)^{\frac{5}{2}}}\int dx\mathcal{F}'''(x)^2 \end{aligned} \tag{C.4}$$

- the denominator:

$$\begin{aligned} &\int dh\gamma(h+\sigma) f''(q_M,h)^2\left[1+(1-q_M)f''(q_M,h)\right] = \\ &= \int_{-\chi}^{0} dh\gamma(h+\sigma)\frac{1}{(1-q_M)^2}\left[1-1\right] + \\ &+ \gamma(\sigma)\frac{\sqrt{1-q_M}}{(1-q_M)^2}\int dx\mathcal{F}''(x)^2\left[1+\mathcal{F}''(x)\right] + \\ &+ \gamma(-\chi+\sigma)\frac{\sqrt{1-q_M}}{(1-q_M)^2}\int dx\mathcal{F}''(x)^2\left[1+\mathcal{F}''(x)\right] = \\ &= \frac{\gamma(\sigma)+\gamma(-\chi+\sigma)}{(1-q_M)^{\frac{3}{2}}}\int dx\mathcal{F}''(x)^2\left[1+\mathcal{F}''(x)\right] \end{aligned} \tag{C.5}$$

Putting together, the breaking point reads:

$$m = \frac{1-q_M}{2}\frac{\frac{\gamma(\sigma)+\gamma(-\chi+\sigma)}{(1-q_M)^{\frac{5}{2}}}\int dx\mathcal{F}'''(x)^2}{\frac{\gamma(\sigma)+\gamma(-\chi+\sigma)}{(1-q_M)^{\frac{3}{2}}}\int dx\mathcal{F}''(x)^2\left[1+\mathcal{F}''(x)\right]} = \frac{1}{2}\frac{\int dx\mathcal{F}'''(x)^2}{\int dx\mathcal{F}''(x)^2\left[1+\mathcal{F}''(x)\right]} \tag{C.6}$$

We have thus obtained that the braking point m on the dAT-line, for $T \to 0$, tends to a constant independent of the point of the phase diagram:

$$m = \frac{\int dx\mathcal{F}'''(x)^2}{2\int dx\mathcal{F}''(x)^2\left[1+\mathcal{F}''(x)\right]} \simeq 0.125 \tag{C.7}$$

We have $m \in (0,1)$, therefore at the dAT instability line there is a properly defined RS-RSB transition.

C.2 Slope of the function $q(x)$

The formula for the slope $\dot{q}(x)$ is obtained by deriving eq. (2.83) with respect to x:

$$\dot{q}(x) = \left[\frac{\alpha}{2}\int dh P(x,h)A(x,h) - \frac{3x^2}{\lambda(x)^4}\right]^{-1}\left(\frac{1}{\lambda(x)^3} + \alpha\int dh P(x,h) f(x,h)'^3\right) \tag{C.8}$$

with

$$A(x,h) = f''''(x,h)^2 - 12x f''(x,h) f'''(x,h)^2 + 6x^2 f''(x,h)^4 \tag{C.9}$$

We need to evaluate this expression for $x = m$ using the replica symmetric solution. Therefore we can substitute:

$$\begin{aligned} P(x,h) &= \gamma(h+\sigma) \\ \lambda(x) &= 1 - q_M \\ f(x,h) &= f(q_M,h) \\ x &= m \end{aligned} \tag{C.10}$$

Looking at the form of $f(q_M,h)$ for $T \to 0$ in eq. (3.99), all the derivatives higher than the second order get a contribution only from the scaling part $\mathcal{F}(x)$. The numerator at leading order:

$$\frac{1}{(1-q_M)^3}\left(1 - \alpha\int_{-\chi}^{0} dh\gamma(h+\sigma)\right) = 0 \tag{C.11}$$

because of the isostaticity condition (3.151) on the dAT line.
At the next-to-leading order:

$$\alpha\frac{\gamma(\sigma)+\gamma(\sigma-\chi)}{(1-q_M)^{\frac{5}{2}}}\int dx\mathcal{F}''(x)^3 \tag{C.12}$$

For the denominator, we have:

$$\begin{aligned} &\frac{\alpha}{2}\frac{\gamma(\sigma)+\gamma(\sigma-\chi)}{(1-q_M)^{\frac{7}{2}}}\int dx\left[\mathcal{F}''''(x)^2 - 12m\mathcal{F}''(x)\mathcal{F}'''(x)^2 + 6m^2\mathcal{F}''(x)^4\right] + \\ &+ \frac{\alpha}{2}\frac{6m^2}{(1-q_M)^4}\int_{-\chi}^{0} dh\gamma(h+\sigma) + \\ &- \frac{3m^2}{(1-q_M)^4} \end{aligned} \tag{C.13}$$

We see that the terms $\frac{1}{(1-q_M)^4}$ cancel out because of the isostaticity condition. Putting everything together, we get:

$$\begin{aligned} \dot{q}(x)\Big|_{x=m} &= \frac{\int dx\mathcal{F}''(x)^3}{\int dx\left[\mathcal{F}''''(x)^2 - 12m\mathcal{F}''(x)\mathcal{F}'''(x)^2 + 6m^2\mathcal{F}''(x)^4\right]}\frac{1-q_M}{2} = \\ &= k\chi T > 0 \end{aligned} \tag{C.14}$$

where k is a positive number. Therefore we have a positive slope, vanishing in T, of the $q(x)$ at the dAT instability line: this tells that the transition is to a $full$RSB phase.

Bibliography

[1] Elisabeth Agoritsas. "Mean-field dynamics of infinite-dimensional particle systems: global shear versus random local forcing". In: *arXiv preprint arXiv:2009.08944* (2020).

[2] Michael Aizenman and Pierluigi Contucci. "On the stability of the quenched state in mean-field spin-glass models". In: *Journal of statistical physics* 92.5-6 (1998), pp. 765–783.

[3] Ahmed El Alaoui, Andrea Montanari, and Mark Sellke. "Optimization of mean-field spin glasses". In: *arXiv preprint arXiv:2001.00904* (2020).

[4] Jairo RL de Almeida and David J Thouless. "Stability of the Sherrington-Kirkpatrick solution of a spin glass model". In: *Journal of Physics A: Mathematical and General* 11.5 (1978), p. 983.

[5] Ada Altieri. "Higher-order corrections to the effective potential close to the jamming transition in the perceptron model". In: *Physical Review E* 97.1 (2018), p. 012103.

[6] Ada Altieri. "The Jamming Transition". In: *Jamming and Glass Transitions*. Springer, 2019, pp. 45–64.

[7] Ada Altieri, Silvio Franz, and Giorgio Parisi. "The jamming transition in high dimension: an analytical study of the TAP equations and the effective thermodynamic potential". In: *Journal of Statistical Mechanics: Theory and Experiment* 2016.9 (2016), p. 093301.

[8] P W Anderson, BI Halperin, and C M Varma. "Anomalous low-temperature thermal properties of glasses and spin glasses". In: *Philosophical Magazine* 25.1 (1972), pp. 1–9.

[9] P. W. Anderson. "Through the Glass Lightly". In: *Science* 267.5204 (1995), pp. 1615–1616. ISSN: 0036-8075. DOI: 10.1126/science.267.5204.1615-e. eprint: https://science.sciencemag.org/content/267/5204/1615.6.full.pdf. URL: https://science.sciencemag.org/content/267/5204/1615.6.

[10] Maria Chiara Angelini and Giulio Biroli. "Spin Glass in a Field: A New Zero-Temperature Fixed Point in Finite Dimensions". In: *Phys. Rev. Lett.* 114 (9 Mar. 2015), p. 095701. DOI: 10.1103/PhysRevLett.114.095701. URL: https://link.aps.org/doi/10.1103/PhysRevLett.114.095701.

[11] C Austen Angell. "Perspective on the glass transition". In: *Journal of Physics and Chemistry of Solids* 49.8 (1988), pp. 863–871.

[12] C Austin Angell, Kia L Ngai, Greg B McKenna, Paul F McMillan, and Steve W Martin. "Relaxation in glassforming liquids and amorphous solids". In: *Journal of applied physics* 88.6 (2000), pp. 3113–3157.

[13] C. A. Angell. "Formation of Glasses from Liquids and Biopolymers". In: *Science* 267.5206 (1995), pp. 1924–1935. ISSN: 0036-8075. DOI: 10.1126/science.267.5206.1924. eprint: https://science.sciencemag.org/content/267/5206/1924.full.pdf. URL: https://science.sciencemag.org/content/267/5206/1924.

[14] Fabrizio Antenucci, Florent Krzakala, Pierfrancesco Urbani, and Lenka Zdeborová. "Approximate survey propagation for statistical inference". In: *Journal of Statistical Mechanics: Theory and Experiment* 2019.2 (2019), p. 023401.

[15] Francesco Arceri and Eric I. Corwin. "Vibrational Properties of Hard and Soft Spheres Are Unified at Jamming". In: *Phys. Rev. Lett.* 124 (23 June 2020), p. 238002. DOI: 10.1103/PhysRevLett.124.238002. URL: https://link.aps.org/doi/10.1103/PhysRevLett.124.238002.

[16] Neil W Ashcroft, N David Mermin, et al. *Solid state physics [by] Neil W. Ashcroft [and] N. David Mermin.* 1976.

[17] Per Bak, Chao Tang, and Kurt Wiesenfeld. "Self-organized criticality". In: *Physical review A* 38.1 (1988), p. 364.

[18] Alain Barrat, Silvio Franz, and Giorgio Parisi. "Temperature evolution and bifurcations of metastable states in mean-field spin glasses, with connections with structural glasses". In: *Journal of Physics A: Mathematical and General* 30.16 (1997), pp. 5593–5612. URL: http://stacks.iop.org/0305-4470/30/5593.

[19] G.M. Bartenev. *The Structure and Mechanical Properties of Inorganic Glasses.* Wolters-Noordhoff, 1970. ISBN: 9789001054502. URL: https://books.google.fr/books?id=T2h8AAAAIAAJ.

[20] H. Bässler. "Viscous flow in supercooled liquids analyzed in terms of transport theory for random media with energetic disorder". In: *Phys. Rev. Lett.* 58 (8 Feb. 1987), pp. 767–770. DOI: 10.1103/PhysRevLett.58.767. URL: https://link.aps.org/doi/10.1103/PhysRevLett.58.767.

[21] R Baviera and M A Virasoro. "A method that reveals the multi-level ultrametric tree hidden in p -spin-glass-like systems". In: *Journal of Statistical Mechanics: Theory and Experiment* 2015.12 (Dec. 2015), P12007. DOI: 10.1088/1742-5468/2015/12/p12007. URL: https://doi.org/10.1088%2F1742-5468%2F2015%2F12%2Fp12007.

[22] Fernanda PC Benetti, Giorgio Parisi, Francesca Pietracaprina, and Gabriele Sicuro. "Mean-field model for the density of states of jammed soft spheres". In: *Phys. Rev. E* 97.6 (2018), p. 062157. DOI: 10.1103/PhysRevE.97.062157.

[23] Ulf Bengtzelius, W Gotze, and A Sjolander. "Dynamics of supercooled liquids and the glass transition". In: *Journal of Physics C: solid state Physics* 17.33 (1984), p. 5915.

[24] L. Berthier, G. Biroli, J-P Bouchaud, L. Cipelletti, and W. van Saarloos. *Dynamical Heterogeneities and Glasses.* Oxford University Press, 2011.

[25] L. Berthier, G. Biroli, J.P. Bouchaud, L. Cipelletti, D. El Masri, D. L'Hôte, F. Ladieu, and M. Pierno. "Direct experimental evidence of a growing length scale accompanying the glass transition". In: *Science* 310.5755 (2005), pp. 1797–1800.

[26] Ludovic Berthier. "Dynamic heterogeneity in amorphous materials". In: *arXiv preprint arXiv:1106.1739* (2011).

[27] Ludovic Berthier and Giulio Biroli. "Theoretical perspective on the glass transition and amorphous materials". In: *Rev. Mod. Phys.* 83 (2 June 2011), pp. 587–645. DOI: 10.1103/RevModPhys.83.587. URL: http://link.aps.org/doi/10.1103/RevModPhys.83.587.

[28] Ludovic Berthier, Giulio Biroli, Jean-Philippe Bouchaud, Luca Cipelletti, and Wim van Saarloos. *Dynamical heterogeneities in glasses, colloids, and granular media*. Vol. 150. OUP Oxford, 2011.

[29] Ludovic Berthier, Giulio Biroli, Patrick Charbonneau, Eric I Corwin, Silvio Franz, and Francesco Zamponi. "Gardner physics in amorphous solids and beyond". In: *The Journal of chemical physics* 151.1 (2019), p. 010901.

[30] Ludovic Berthier, Patrick Charbonneau, Yuliang Jin, Giorgio Parisi, Beatriz Seoane, and Francesco Zamponi. "Growing timescales and lengthscales characterizing vibrations of amorphous solids". In: *Proc. Natl. Acad. Sci. U.S.A.* 113.30 (2016), pp. 8397–8401. DOI: 10.1073/pnas.1607730113.

[31] Ludovic Berthier and Thomas A. Witten. "Glass transition of dense fluids of hard and compressible spheres". In: *Phys. Rev. E* 80.2 (Aug. 2009), p. 021502. DOI: 10.1103/PhysRevE.80.021502.

[32] Kurt Binder and Walter Kob. *Glassy materials and disordered solids: An introduction to their statistical mechanics*. World scientific, 2011.

[33] G. Biroli and J.P. Bouchaud. "The Random First-Order Transition Theory of Glasses: a critical assessment". In: *Structural Glasses and Supercooled Liquids: Theory, Experiment and Applications*. Ed. by P.G.Wolynes and V.Lubchenko. Wiley & Sons, 2012. eprint: {\ttarXiv:0912.2542}.

[34] Giulio Biroli and J-P Bouchaud. "Diverging length scale and upper critical dimension in the Mode-Coupling Theory of the glass transition". In: *EPL (Europhysics Letters)* 67.1 (2004), p. 21.

[35] Giulio Biroli, Jean-Philippe Bouchaud, and Gilles Tarjus. "Are defect models consistent with the entropy and specific heat of glass formers?" In: *The Journal of chemical physics* 123.4 (2005), p. 044510.

[36] Giulio Biroli and Pierfrancesco Urbani. "Breakdown of elasticity in amorphous solids". In: *Nature physics* 12.12 (2016), pp. 1130–1133. DOI: https://doi.org/10.1038/nphys3845.

[37] Elmar Bittner and Wolfhard Janke. "Free-energy barriers in the Sherrington-Kirkpatrick model". In: *EPL (Europhysics Letters)* 74.2 (2006), p. 195.

[38] Erik Bitzek, Pekka Koskinen, Franz Gähler, Michael Moseler, and Peter Gumbsch. "Structural relaxation made simple". In: *Phys. Rev. Lett.* 97.17 (2006), p. 170201. DOI: 10.1103/PhysRevLett.97.170201.

[39] André Blandin, Marc Gabay, and Thomas Garel. "On the mean-field theory of spin glasses". In: *Journal of Physics C: Solid State Physics* 13.3 (1980), p. 403.

[40] Lin Bo, Romain Mari, Chaoming Song, and Hernan A. Makse. "Cavity method for force transmission in jammed disordered packings of hard particles". In: *Soft Matter* (2014). ISSN: 1744-683X. DOI: 10.1039/c4sm00667d. URL: file:///Users/pc61/Documents/Recherche.Articles/SoftMatter/Bo2014.pdf.

[41] M Bouten and B Derrida. "Replica symmetry instability in perceptron models". In: *Journal of Physics A: Mathematical, Nuclear and General* 27.17 (1994), pp. 6021–6025.

[42] G. Brambilla, D. El Masri, M. Pierno, L. Berthier, L. Cipelletti, G. Petekidis, and A. B. Schofield. "Probing the Equilibrium Dynamics of Colloidal Hard Spheres above the Mode-Coupling Glass Transition". In: *Physical Review Letters* 102.8, 085703 (2009), p. 085703. DOI: 10.1103/PhysRevLett.102.085703. URL: http://link.aps.org/abstract/PRL/v102/e085703.

[43] AJ Bray and MA Moore. "Metastable states in spin glasses". In: *Journal of Physics C: Solid State Physics* 13.19 (1980), p. L469.

[44] C. Brito and M. Wyart. "Geometric interpretation of previtrification in hard sphere liquids". In: *The Journal of Chemical Physics* 131.2 (2009), p. 024504.

[45] C. Brito and M. Wyart. "On the rigidity of a hard-sphere glass near random close packing". In: *Europhysics Letters (EPL)* 76.1 (2006), pp. 149–155. URL: http://stacks.iop.org/0295-5075/76/149.

[46] U. Buchenau, N. Nücker, and A. J. Dianoux. "Neutron Scattering Study of the Low-Frequency Vibrations in Vitreous Silica". In: *Phys. Rev. Lett.* 53 (24 Dec. 1984), pp. 2316–2319. DOI: 10.1103/PhysRevLett.53.2316. URL: https://link.aps.org/doi/10.1103/PhysRevLett.53.2316.

[47] U. Buchenau, M. Prager, N. Nücker, A. J. Dianoux, N. Ahmad, and W. A. Phillips. "Low-frequency modes in vitreous silica". In: *Phys. Rev. B* 34 (8 Oct. 1986), pp. 5665–5673. DOI: 10.1103/PhysRevB.34.5665. URL: https://link.aps.org/doi/10.1103/PhysRevB.34.5665.

[48] Richard H Byrd, Peihuang Lu, Jorge Nocedal, and Ciyou Zhu. "A limited memory algorithm for bound constrained optimization". In: *SIAM Journal on Scientific Computing* 16.5 (1995), pp. 1190–1208. DOI: https://doi.org/10.1145/279232.279236.

[49] Miguel Cardenas, Silvio Franz, and Giorgio Parisi. "Glass transition and effective potential in the hypernetted chain approximation". In: *Journal of Physics A: Mathematical and General* 31.9 (1998), pp. L163–L169. URL: http://stacks.iop.org/0305-4470/31/L163.

[50] Tommaso Castellani and Andrea Cavagna. "Spin glass theory for pedestrians". In: *Journal of Statistical Mechanics: Theory and Experiment* 2005 (2005), P05012.

[51] A. Cavagna. "Supercooled liquids for pedestrians". In: *Physics Reports* 476.4-6 (2009), pp. 51–124.

[52] David Chandler and Juan P Garrahan. "Dynamics on the way to forming glass: Bubbles in space-time". In: *Annual review of physical chemistry* 61 (2010), pp. 191–217.

[53] Kenneth Chang. "The nature of glass remains anything but clear". In: *New York Times* 29 (2008).

[54] P. Charbonneau, A. Ikeda, J. A. van Meel, and K. Miyazaki. "Numerical and theoretical study of a monodisperse hard-sphere glass former". In: *Phys. Rev. E* 81 (4 Apr. 2010), p. 040501.

[55] P. Charbonneau, A. Ikeda, G. Parisi, and F. Zamponi. "Dimensional study of the caging order parameter at the glass transition". In: *Proceedings of the National Academy of Sciences* 109.35 (2012), pp. 13939–13943.

[56] Patrick Charbonneau, Eric I Corwin, Giorgio Parisi, Alexis Poncet, and Francesco Zamponi. "Universal non-Debye scaling in the density of states of amorphous solids". In: *arXiv preprint arXiv:1512.09100* (2015).

[57] Patrick Charbonneau, Eric I. Corwin, Giorgio Parisi, and Francesco Zamponi. "Jamming Criticality Revealed by Removing Localized Buckling Excitations". In: *Phys. Rev. Lett.* 114 (12 2015), p. 125504. DOI: 10.1103/PhysRevLett.114.125504.

[58] Patrick Charbonneau, Eric I. Corwin, Giorgio Parisi, and Francesco Zamponi. "Universal Microstructure and Mechanical Stability of Jammed Packings". In: *Phys. Rev. Lett.* 109 (20 2012), p. 205501. DOI: 10.1103/PhysRevLett.109.205501.

[59] Patrick Charbonneau, Yi Hu, Archishman Raju, James P. Sethna, and Sho Yaida. "Morphology of renormalization-group flow for the de Almeida–Thouless–Gardner universality class". In: *Phys. Rev. E* 99 (2 Feb. 2019), p. 022132. DOI: 10.1103/PhysRevE.99.022132. URL: https://link.aps.org/doi/10.1103/PhysRevE.99.022132.

[60] Patrick Charbonneau, Atsushi Ikeda, Giorgio Parisi, and Francesco Zamponi. "Glass Transition and Random Close Packing above Three Dimensions". In: *Phys. Rev. Lett.* 107 (18 Oct. 2011), p. 185702.

[61] Patrick Charbonneau, Yuliang Jin, Giorgio Parisi, Corrado Rainone, Beatriz Seoane, and Francesco Zamponi. "Numerical detection of the Gardner transition in a mean-field glass former". In: *Physical Review E* 92.1 (2015), p. 012316.

[62] Patrick Charbonneau, Jorge Kurchan, Giorgio Parisi, Pierfrancesco Urbani, and Francesco Zamponi. "Exact theory of dense amorphous hard spheres in high dimension. III. The full replica symmetry breaking solution". In: *JSTAT* 2014.10 (2014), P10009. DOI: https://doi.org/10.1088/1742-5468/2014/10/P10009.

[63] Patrick Charbonneau, Jorge Kurchan, Giorgio Parisi, Pierfrancesco Urbani, and Francesco Zamponi. "Fractal free energies in structural glasses". In: *Nat. Commun.* 5 (2014), p. 3725. DOI: 10.1038/ncomms4725.

[64] Patrick Charbonneau, Jorge Kurchan, Giorgio Parisi, Pierfrancesco Urbani, and Francesco Zamponi. "Glass and jamming transitions: From exact results to finite-dimensional descriptions". In: *Annu. Rev. Condens. Matter Phys.* 8 (2017), pp. 265–288. DOI: 10.1146/annurev-conmatphys-031016-025334.

[65] Patrick Charbonneau and Sho Yaida. "Nontrivial Critical Fixed Point for Replica-Symmetry-Breaking Transitions". In: *Phys. Rev. Lett.* 118 (21 May 2017), p. 215701. DOI: 10.1103/PhysRevLett.118.215701. URL: https://link.aps.org/doi/10.1103/PhysRevLett.118.215701.

[66] Pinaki Chaudhuri, Ludovic Berthier, and Srikanth Sastry. "Jamming Transitions in Amorphous Packings of Frictionless Spheres Occur over a Continuous Range of Volume Fractions". In: *Phys. Rev. Lett.* 104.16 (2010), p. 165701.

[67] Ke Chen, Wouter G. Ellenbroek, Zexin Zhang, Daniel T. N. Chen, Peter J. Yunker, Silke Henkes, Carolina Brito, Olivier Dauchot, Wim van Saarloos, Andrea J. Liu, and A. G. Yodh. "Low-Frequency Vibrations of Soft Colloidal Glasses". In: *Phys. Rev. Lett.* 105 (2 July 2010), p. 025501. DOI: 10.1103/PhysRevLett.105.025501. URL: https://link.aps.org/doi/10.1103/PhysRevLett.105.025501.

[68] Richard Christensen. *Theory of viscoelasticity: an introduction*. Elsevier, 2012.

[69] Luca Cipelletti and Eric R Weeks. "Glassy dynamics and dynamical heterogeneity in colloids". In: *Dynamical heterogeneities in glasses, colloids, and granular media* 150 (2011), p. 110.

[70] Henry Cohn, Abhinav Kumar, Stephen D. Miller, Danylo Radchenko, and Maryna Viazovska. "The sphere packing problem in dimension 24". In: *cond-mat* (2016), p. 1603.06518. URL: file:///Users/pc61/Documents/Recherche.Articles/cond-mat/160306518v1.pdf.

[71] Gaël Combe and Jean-Noël Roux. "Strain versus stress in a model granular material: a Devils staircase". In: *Physical Review Letters* 85.17 (2000), p. 3628. DOI: 10.1103/PhysRevLett.85.3628.

[72] Pierluigi Contucci and Cristian Giardina. "Spin-glass stochastic stability: a rigorous proof". In: *Annales Henri Poincare*. Vol. 6. 5. Springer. 2005, pp. 915–923.

[73] John Horton Conway and Neil James Alexander Sloane. *Sphere packings, lattices and groups*. Vol. 290. Springer Science & Business Media, 2013.

[74] A Crisanti and F Ritort. "Potential energy landscape of finite-size mean-field models for glasses". In: *EPL (Europhysics Letters)* 51.2 (2000), p. 147.

[75] Leticia F Cugliandolo. "Dynamics of glassy systems". In: *Slow Relaxations and nonequilibrium dynamics in condensed matter*. Springer, 2003. eprint: {\ttarXiv:cond-mat/0210312}.

[76] Leticia F. Cugliandolo and Jorge Kurchan. "Analytical solution of the off-equilibrium dynamics of a long-range spin-glass model". In: *Phys. Rev. Lett.* 71.1 (1993), pp. 173–176.

[77] C De Dominicis and I Kondor. "Eigenvalues of the stability matrix for Parisi solution of the long-range spin-glass". In: *Physical Review B* 27 (1983), pp. 606–608.

[78] P.G. Debenedetti. *Metastable liquids: concepts and principles*. Princeton Univ Press, 1996.

[79] E DeGiuli, G Düring, E Lerner, and M Wyart. "Unified theory of inertial granular flows and non-Brownian suspensions". In: *Physical Review E* 91.6 (2015), p. 062206.

[80] Eric DeGiuli, Adrien Laversanne-Finot, Gustavo Düring, Edan Lerner, and Matthieu Wyart. "Effects of coordination and pressure on sound attenuation, boson peak and elasticity in amorphous solids". In: *Soft Matter* 10.30 (2014), pp. 5628–5644.

[81] Eric DeGiuli, Edan Lerner, Carolina Brito, and Matthieu Wyart. "Force distribution affects vibrational properties in hard-sphere glasses". In: *Proceedings of the National Academy of Sciences* 111.48 (2014), pp. 17054–17059.

[82] C. Donati, S. Franz, S.C. Glotzer, and G. Parisi. "Theory of non-linear susceptibility and correlation length in glasses and liquids". In: *Journal of non-crystalline solids* 307 (2002), pp. 215–224.

[83] Aleksandar Donev, Robert Connelly, Frank H. Stillinger, and Salvatore Torquato. "Underconstrained jammed packings of nonspherical hard particles: Ellipses and ellipsoids". In: *Physical Review E (Statistical, Nonlinear, and Soft Matter Physics)* 75.5, 051304 (2007), p. 051304. DOI: 10.1103/PhysRevE.75.051304. URL: http://link.aps.org/abstract/PRE/v75/e051304.

[84] E Donth. *The glass transition: relaxation dynamics in liquids and disordered materials*. Vol. 48. Springer Science & Business Media, 2013.

[85] Douglas J Durian. "Foam mechanics at the bubble scale". In: *Phys. Rev. Lett.* 75.26 (1995), p. 4780. DOI: 10.1103/PhysRevLett.75.4780.

[86] Jeppe C Dyre. "Colloquium: The glass transition and elastic models of glass-forming liquids". In: *Reviews of modern physics* 78.3 (2006), p. 953.

[87] J. D. Eaves and D. R. Reichman. "Spatial Dimension and the Dynamics of Supercooled Liquids". In: *Proc. Nat. Acad. Sci. U.S.A.* 106 (2009), p. 15171. URL: file:///Users/pc61/Documents/Recherche.Articles/PNAS/Eaves2009.pdf.

[88] Mark D Ediger. "Spatially heterogeneous dynamics in supercooled liquids". In: *Annual review of physical chemistry* 51.1 (2000), pp. 99–128.

[89] Wouter G Ellenbroek, Zorana Zeravcic, Wim van Saarloos, and Martin van Hecke. "Non-affine response: Jammed packings vs. spring networks". In: *EPL (Europhysics Letters)* 87.3 (2009), p. 34004.

[90] Wouter G. Ellenbroek, Martin van Hecke, and Wim van Saarloos. "Jammed frictionless disks: Connecting local and global response". In: *Phys. Rev. E* 80 (6 Dec. 2009), p. 061307. DOI: 10.1103/PhysRevE.80.061307. URL: https://link.aps.org/doi/10.1103/PhysRevE.80.061307.

[91] Wouter G. Ellenbroek, Ellák Somfai, Martin van Hecke, and Wim van Saarloos. "Critical Scaling in Linear Response of Frictionless Granular Packings near Jamming". In: *Phys. Rev. Lett.* 97 (25 Dec. 2006), p. 258001. DOI: 10.1103/PhysRevLett.97.258001. URL: https://link.aps.org/doi/10.1103/PhysRevLett.97.258001.

[92] Yael S. Elmatad, Robert L. Jack, David Chandler, and Juan P. Garrahan. "Finite-temperature critical point of a glass transition". In: *Proceedings of the National Academy of Sciences* 107.29 (2010), pp. 12793–12798. ISSN: 0027-8424. DOI: 10.1073/pnas.1006306107. eprint: https://www.pnas.org/content/107/29/12793.full.pdf. URL: https://www.pnas.org/content/107/29/12793.

[93] Daniel S Fisher. "Collective transport in random media: from superconductors to earthquakes". In: *Physics reports* 301.1-3 (1998), pp. 113–150.

[94] S Franz and A Montanari. "Analytic determination of dynamical and mosaic length scales in a Kac glass model". In: *Journal of Physics A: Mathematical and Theoretical* 40.11 (2007), F251. URL: http://stacks.iop.org/1751-8121/40/i=11/a=F01.

[95] S. Franz and G. Parisi. "Recipes for Metastable States in Spin Glasses". In: *Journal de Physique I* 5.11 (1995), pp. 1401–1415.

[96] S. Franz, G. Parisi, F. Ricci-Tersenghi, and T. Rizzo. "Field theory of fluctuations in glasses". In: *The European Physical Journal E: Soft Matter and Biological Physics* 34.9 (2011), pp. 1–17.

[97] Silvio Franz, Claudio Donati, Giorgio Parisi, and Sharon C Glotzer. "On dynamical correlations in supercooled liquids". In: *Philosophical Magazine B* 79.11-12 (1999), pp. 1827–1831.

[98] Silvio Franz, Hugo Jacquin, Giorgio Parisi, Pierfrancesco Urbani, and Francesco Zamponi. "Quantitative field theory of the glass transition". In: *Proceedings of the National Academy of Sciences* 109.46 (2012), pp. 18725–18730.

[99] Silvio Franz, Hugo Jacquin, Giorgio Parisi, Pierfrancesco Urbani, and Francesco Zamponi. "Static replica approach to critical correlations in glassy systems". In: *The Journal of chemical physics* 138.12 (2013), 12A540.

[100] Silvio Franz, Marc Mezard, Giorgio Parisi, and Luca Peliti. "The response of glassy systems to random perturbations: A bridge between equilibrium and off-equilibrium". In: *Journal of statistical physics* 97.3-4 (1999), pp. 459–488.

[101] Silvio Franz, Marc Mézard, Giorgio Parisi, and Luca Peliti. "Measuring equilibrium properties in aging systems". In: *Physical Review Letters* 81.9 (1998), p. 1758.

[102] Silvio Franz and Giorgio Parisi. "On non-linear susceptibility in supercooled liquids". In: *Journal of Physics: Condensed Matter* 12.29 (2000), p. 6335.

[103] Silvio Franz and Giorgio Parisi. "Phase Diagram of Coupled Glassy Systems: A Mean-Field Study". In: *Phys. Rev. Lett.* 79.13 (Sept. 1997), pp. 2486–2489. DOI: 10.1103/PhysRevLett.79.2486.

[104] Silvio Franz and Giorgio Parisi. "The simplest model of jamming". In: *Journal of Physics A: Mathematical and Theoretical* 49.14 (2016), p. 145001. DOI: https://doi.org/10.1088/1751-8113/49/14/145001.

[105] Silvio Franz, Giorgio Parisi, Maxim Sevelev, Pierfrancesco Urbani, and Francesco Zamponi. "Universality of the SAT-UNSAT (jamming) threshold in non-convex continuous constraint satisfaction problems". In: *SciPost Physics* 2.3 (2017), p. 019. DOI: 10.21468/SciPostPhys.2.3.019.

[106] Silvio Franz, Giorgio Parisi, Pierfrancesco Urbani, and Francesco Zamponi. "Universal spectrum of normal modes in low-temperature glasses". In: *Proc. Natl. Acad. Sci. U.S.A.* 112.47 (2015), pp. 14539–14544. DOI: https://doi.org/10.1073/pnas.1511134112.

[107] Silvio Franz, Antonio Sclocchi, and Pierfrancesco Urbani. "Critical energy landscape of linear soft spheres". In: *SciPost Phys.* 9 (1 2020), p. 12. DOI: 10.21468/SciPostPhys.9.1.012. URL: https://scipost.org/10.21468/SciPostPhys.9.1.012.

[108] Silvio Franz, Antonio Sclocchi, and Pierfrancesco Urbani. "Critical Jammed Phase of the Linear Perceptron". In: *Phys. Rev. Lett.* 123.11 (2019), p. 115702. DOI: 10.1103/PhysRevLett.123.115702.

[109] Silvio Franz, Antonio Sclocchi, and Pierfrancesco Urbani. "Surfing on minima of isostatic landscapes: avalanches and unjamming transition". In: *Journal of Statistical Mechanics: Theory and Experiment* 2021.2 (Feb. 2021), p. 023208. DOI: 10.1088/1742-5468/abdc16. URL: https://doi.org/10.1088/1742-5468/abdc16.

[110] Silvio Franz and Stefano Spigler. "Mean-field avalanches in jammed spheres". In: *Phys. Rev. E* 95.2 (2017), p. 022139. DOI: 10.1103/PhysRevE.95.022139.

[111] E Gardner and B Derrida. "Optimal storage properties of neural network models". In: *Journal of Physics A: Mathematical and general* 21.1 (1988), p. 271.

[112] E. Gardner. "Spin Glasses with p-Spin Interactions". In: *Nuclear Physics B* 257 (1985), pp. 747–765.

[113] Elizabeth Gardner. "The space of interactions in neural network models". In: *Journal of physics A: Mathematical and general* 21.1 (1988), p. 257.

[114] J.P. Garrahan, P. Sollich, and C. Toninelli. "Kinetically constrained models". In: *Dynamical Heterogeneities and Glasses*. Ed. by L. Berthier, G. Biroli, J-P Bouchaud, L. Cipelletti, and W. van Saarloos. Oxford University Press, 2011. eprint: {\ttarXiv:1009.6113}.

[115] Juan P Garrahan and David Chandler. "Coarse-grained microscopic model of glass formers". In: *Proceedings of the National Academy of Sciences* 100.17 (2003), pp. 9710–9714.

[116] Carl P Goodrich, Andrea J Liu, and Sidney R Nagel. "Finite-size scaling at the jamming transition". In: *Physical review letters* 109.9 (2012), p. 095704.

[117] Carl P Goodrich, Andrea J Liu, and James P Sethna. "Scaling ansatz for the jamming transition". In: *Proc. Natl. Acad. Sci. U.S.A.* 113.35 (2016), pp. 9745–9750. DOI: https://doi.org/10.1073/pnas.1601858113.

[118] W Götze. *Liquids, freezing and the glass transition*. 1991.

[119] Wolfgang Götze. *Complex Dynamics of Glass-Forming Liquids: A Mode-Coupling Theory: A Mode-Coupling Theory*. Vol. 143. OUP Oxford, 2008.

[120] Tomás S Grigera, Victor Martin-Mayor, Giorgio Parisi, and Paolo Verrocchio. "Phonon interpretation of the 'boson peak' in supercooled liquids". In: *Nature* 422.6929 (2003), pp. 289–292.

[121] DJ Gross, I Kanter, and Haim Sompolinsky. "Mean-field theory of the Potts glass". In: *Physical review letters* 55.3 (1985), p. 304.

[122] Francesco Guerra and Fabio Lucio Toninelli. "The thermodynamic limit in mean field spin glass models". In: *Communications in Mathematical Physics* 230.1 (2002), pp. 71–79.

[123] Iwan Gutzow and Jürn Schmelzer. *The vitreous state*. Springer, 1995.

[124] G Györgyi and P Reimann. "Beyond storage capacity in a single model neuron: Continuous replica symmetry breaking". In: *Journal of Statistical Physics* 101.1-2 (2000), pp. 679–702.

[125] Géza Györgyi. "Techniques of replica symmetry breaking and the storage problem of the McCulloch–Pitts neuron". In: *Phys. Rep.* 342.4-5 (2001), pp. 263–392. DOI: https://doi.org/10.1016/S0370-1573(00)00073-9.

[126] DA Head, AV Tkachenko, and TA Witten. "Robust propagation direction of stresses in a minimal granular packing". In: *The European Physical Journal E* 6.1 (2001), pp. 99–105.

[127] Tina Hecksher, Albena I Nielsen, Niels Boye Olsen, and Jeppe C Dyre. "Little evidence for dynamic divergences in ultraviscous molecular liquids". In: *Nature Physics* 4.9 (2008), pp. 737–741.

[128] Daniel Hexner, Andrea J Liu, and Sidney R Nagel. "Two diverging length scales in the structure of jammed packings". In: *Phys. Rev. Lett.* 121.11 (2018), p. 115501. DOI: 10.1103/PhysRevLett.121.115501.

[129] Daniel Hexner, Pierfrancesco Urbani, and Francesco Zamponi. "Can a Large Packing be Assembled from Smaller Ones?" In: *Phys. Rev. Lett.* 123 (6 2019), p. 068003. DOI: 10.1103/PhysRevLett.123.068003.

[130] J. P. Bouchaud and G. Biroli. "On the Adam-Gibbs-Kirkpatrick-Thirumalai-Wolynes scenario for the viscosity increase in glasses". In: *J. Chem. Phys.* 121 (2004), p. 7347.

[131] Liesbeth M. C. Janssen. "Mode-Coupling Theory of the Glass Transition: A Primer". In: *Frontiers in Physics* 6 (2018), p. 97. ISSN: 2296-424X. DOI: 10.3389/fphy.2018.00097. URL: https://www.frontiersin.org/article/10.3389/fphy.2018.00097.

[132] Liesbeth MC Janssen, Peter Mayer, and David R Reichman. "Generalized mode-coupling theory of the glass transition: schematic results at finite and infinite order". In: *Journal of Statistical Mechanics: Theory and Experiment* 2016.5 (2016), p. 054049.

[133] Liesbeth MC Janssen, Peter Mayer, and David R Reichman. "Relaxation patterns in supercooled liquids from generalized mode-coupling theory". In: *Physical Review E* 90.5 (2014), p. 052306.

[134] Yuliang Jin, Pierfrancesco Urbani, Francesco Zamponi, and Hajime Yoshino. "A stability-reversibility map unifies elasticity, plasticity, yielding, and jamming in hard sphere glasses". In: *Science advances* 4.12 (2018), eaat6387.

[135] Yuliang Jin and Hajime Yoshino. *A jamming plane of sphere packings*. 2020. arXiv: 2003.10814 [cond-mat.soft].

[136] W. Kauzmann. "The glassy state and the behaviour of liquids at low temperature". In: *Chem Rev* 43 (1948), pp. 219–256.

[137] Willem K Kegel and Alfons van Blaaderen. "Direct observation of dynamical heterogeneities in colloidal hard-sphere suspensions". In: *Science* 287.5451 (2000), pp. 290–293.

[138] Jacek Kierzenka and Lawrence F. Shampine. "A BVP Solver Based on Residual Control and the Maltab PSE". In: *ACM Trans. Math. Softw.* 27.3 (Sept. 2001), pp. 299–316. ISSN: 0098-3500. DOI: 10.1145/502800.502801. URL: https://doi.org/10.1145/502800.502801.

[139] Harald Kinzelbach and Heinz Horner. "Dynamics of the finite SK spin-glass". In: *Zeitschrift für Physik B Condensed Matter* 84.1 (1991), pp. 95–114.

[140] Scott Kirkpatrick and David Sherrington. "Infinite-ranged models of spin-glasses". In: *Physical Review B* 17.11 (1978), p. 4384.

[141] T. R. Kirkpatrick, D. Thirumalai, and P. G. Wolynes. "Scaling concepts for the dynamics of viscous liquids near an ideal glassy state". In: *Phys. Rev. A* 40.2 (July 1989), pp. 1045–1054. DOI: 10.1103/PhysRevA.40.1045.

[142] T. R. Kirkpatrick and P. G. Wolynes. "Connections between some kinetic and equilibrium theories of the glass transition". In: *Phys. Rev. A* 35.7 (Apr. 1987), pp. 3072–3080. DOI: 10.1103/PhysRevA.35.3072.

[143] T. R. Kirkpatrick and P. G. Wolynes. "Stable and metastable states in mean-field Potts and structural glasses". In: *Phys. Rev. B* 36.16 (Dec. 1987), pp. 8552–8564. DOI: 10.1103/PhysRevB.36.8552.

[144] Steven A Kivelson and Gilles Tarjus. "In search of a theory of supercooled liquids". In: *Nature materials* 7.11 (2008), pp. 831–833.

[145] Walter Kob. "Course 5: supercooled liquids, the glass transition, and computer simulations". In: *Slow Relaxations and nonequilibrium dynamics in condensed matter*. Springer, 2003, pp. 199–269.

[146] F. Krzakala, A. Montanari, F. Ricci-Tersenghi, G. Semerjian, and L. Zdeborova. "Gibbs states and the set of solutions of random constraint satisfaction problems". In: *Proceedings of the National Academy of Sciences* 104.25 (2007), p. 10318.

[147] Nishant Kumar and Stefan Luding. "Memory of jamming–multiscale models for soft and granular matter". In: *Granular Matter* 18.3 (2016), p. 58.

[148] Jorge Kurchan, Giorgio Parisi, Pierfrancesco Urbani, and Francesco Zamponi. "Exact Theory of Dense Amorphous Hard Spheres in High Dimension. II. The High Density Regime and the Gardner Transition". In: *J. Phys. Chem. B* 117 (2013), pp. 12979–12994. DOI: https://doi.org/10.1021/jp402235d.

[149] Jorge Kurchan, Giorgio Parisi, and Francesco Zamponi. "Exact theory of dense amorphous hard spheres in high dimension. I. The free energy". In: *JSTAT* 2012.10 (2012), P10012.

[150] James S Langer. "Theories of glass formation and the glass transition". In: *Reports on Progress in Physics* 77.4 (2014), p. 042501.

[151] WT Laughlin and Donald R Uhlmann. "Viscous flow in simple organic liquids". In: *The Journal of Physical Chemistry* 76.16 (1972), pp. 2317–2325.

[152] Charles L Lawson and Richard J Hanson. *Solving least squares problems*. SIAM, 1995.

[153] Pierre Le Doussal, Markus Müller, and Kay Jörg Wiese. "Avalanches in mean-field models and the Barkhausen noise in spin-glasses". In: *EPL (Europhysics Letters)* 91.5 (2010), p. 57004.

[154] Edan Lerner, Gustavo During, and Matthieu Wyart. "Low-energy non-linear excitations in sphere packings". In: *Soft Matter* 9 (34 2013), pp. 8252–8263. DOI: 10.1039/C3SM50515D.

[155] L. Leuzzi and T.M. Nieuwenhuizen. *Thermodynamics of the glassy state*. Taylor & Francis, 2007.

[156] Luca Leuzzi and Th M Nieuwenhuizen. *Thermodynamics of the glassy state*. CRC Press, 2007.

[157] Qinyi Liao and Ludovic Berthier. "Hierarchical Landscape of Hard Disk Glasses". In: *Phys. Rev. X* 9 (1 Mar. 2019), p. 011049. DOI: 10.1103/PhysRevX.9.011049. URL: https://link.aps.org/doi/10.1103/PhysRevX.9.011049.

[158] Andrea J Liu and Sidney R Nagel. "The jamming transition and the marginally jammed solid". In: *Annu. Rev. Condens. Matter Phys.* 1.1 (2010), pp. 347–369. DOI: 10.1146/annurev-conmatphys-070909-104045.

[159] Andrea J. Liu and Sidney R. Nagel. "Jamming is not just cool any more". In: *Nature* 396.6706 (1998), pp. 21–22. DOI: https://doi.org/10.1038/23819.

[160] Andrea J. Liu, Sidney R. Nagel, Wim Van Saarloos, and Matthieu Wyart. "The jamming scenario – an introduction and outlook". In: *Dynamical Heterogeneities and Glasses*. Ed. by L. Berthier, G. Biroli, J-P Bouchaud, L. Cipelletti, and W. van Saarloos. Oxford University Press, 2011. DOI: 10.1093/acprof:oso/9780199691470.003.0009.

[161] Vassiliy Lubchenko and Peter G. Wolynes. "Theory of Structural Glasses and Supercooled Liquids". In: *Annual Review of Physical Chemistry* 58.1 (2007), pp. 235–266. DOI: 10.1146/annurev.physchem.58.032806.104653. eprint: {\ttarXiv.org:cond-mat/0607349}.

[162] Mitch Mailman, Carl F Schreck, Corey S O'Hern, and Bulbul Chakraborty. "Jamming in systems composed of frictionless ellipse-shaped particles". In: *Physical review letters* 102.25 (2009), p. 255501.

[163] Thibaud Maimbourg, Jorge Kurchan, and Francesco Zamponi. "Solution of the Dynamics of Liquids in the Large-Dimensional Limit". In: *Phys. Rev. Lett.* 116.1 (2016), p. 015902. URL: file:///Users/pc61/Documents/Recherche.Articles/PRL/Maimbourg2016.pdf.

[164] P Majer, A Engel, and A Zippelius. "Perceptrons above saturation". In: *J. Phys. A* 26.24 (1993), p. 7405. DOI: https://doi.org/10.1088/0305-4470/26/24/015.

[165] T. S. Majmudar, M. Sperl, S. Luding, and R. P. Behringer. "Jamming Transition in Granular Systems". In: *Physical Review Letters* 98.5, 058001 (2007), p. 058001. DOI: 10.1103/PhysRevLett.98.058001. URL: http://link.aps.org/abstract/PRL/v98/e058001.

[166] M. L. Manning and A. J. Liu. "A random matrix definition of the boson peak". In: *EPL (Europhysics Letters)* 109.3 (Feb. 2015), p. 36002. DOI: 10.1209/0295-5075/109/36002. URL: https://doi.org/10.1209%2F0295-5075%2F109%2F36002.

[167] M. L. Manning and A. J. Liu. "Vibrational Modes Identify Soft Spots in a Sheared Disordered Packing". In: *Phys. Rev. Lett.* 107 (10 Aug. 2011), p. 108302. DOI: 10.1103/PhysRevLett.107.108302. URL: https://link.aps.org/doi/10.1103/PhysRevLett.107.108302.

[168] Marc Mézard, Giorgio Parisi, and Miguel A. Virasoro. *Spin glass theory and beyond*. Singapore: World Scientific, 1987.

[169] Vladimir Alexandrovich Marchenko and Leonid Andreevich Pastur. "Distribution of eigenvalues for some sets of random matrices". In: *Matematicheskii Sbornik* 114.4 (1967), pp. 507–536.

[170] Romain Mari, Florent Krzakala, and Jorge Kurchan. "Jamming versus Glass Transitions". In: *Phys. Rev. Lett.* 103.2 (July 2009), p. 025701. DOI: 10.1103/PhysRevLett.103.025701.

[171] C. Masciovecchio, G. Ruocco, F. Sette, M. Krisch, R. Verbeni, U. Bergmann, and M. Soltwisch. "Observation of Large Momentum Phononlike Modes in Glasses". In: *Phys. Rev. Lett.* 76 (18 Apr. 1996), pp. 3356–3359. DOI: 10.1103/PhysRevLett.76.3356. URL: https://link.aps.org/doi/10.1103/PhysRevLett.76.3356.

[172] J Clerk Maxwell. "L. on the calculation of the equilibrium and stiffness of frames". In: *The London, Edinburgh, and Dublin Philosophical Magazine and Journal of Science* 27.182 (1864), pp. 294–299.

[173] James Clerk Maxwell. "IV. On the dynamical theory of gases". In: *Philosophical Transactions of the Royal Society of London* 157 (1867), pp. 49–88. DOI: 10.1098/rstl.1867.0004. URL: https://royalsocietypublishing.org/doi/abs/10.1098/rstl.1867.0004.

[174] Peter Mayer, Kunimasa Miyazaki, and David R Reichman. "Cooperativity beyond caging: Generalized mode-coupling theory". In: *Physical review letters* 97.9 (2006), p. 095702.

[175] Warren S McCulloch and Walter Pitts. "A logical calculus of the ideas immanent in nervous activity". In: *The bulletin of mathematical biophysics* 5.4 (1943), pp. 115–133.

[176] J. A. van Meel, B. Charbonneau, A. Fortini, and P. Charbonneau. "Hard-sphere crystallization gets rarer with increasing dimension". In: *Phys. Rev. E* 80.6 (2009), p. 061110. URL: file:///Users/pc61/Documents/Recherche.Articles/PRE/vanMeel2009b.pdf.

[177] J. A. van Meel, B. Charbonneau, A. Fortini, and P. Charbonneau. "Hard-sphere crystallization gets rarer with increasing dimension". In: *Phys. Rev. E* 80.6 (2009), p. 061110.

[178] J. A. van Meel, D. Frenkel, and P. Charbonneau. "Geometrical frustration: A study of four-dimensional hard spheres". In: *Physical Review E (Statistical, Nonlinear, and Soft Matter Physics)* 79.3, 030201 (2009), p. 030201. DOI: 10.1103/PhysRevE.79.030201. URL: http://link.aps.org/abstract/PRE/v79/e030201.

[179] Marc Mézard and Giorgio Parisi. "Replica field theory for random manifolds". In: *Journal de Physique I* 1.6 (1991), pp. 809–836.

[180] Marc Mézard, Giorgio Parisi, and Miguel-Angel Virasoro. "Spin glass theory and beyond." In: (1990).

[181] Marvin Minsky and Seymour Papert. "Perceptrons: An essay in computational geometry". In: *MIT Press.* (1969).

[182] Andrea Montanari. "Optimization of the Sherrington-Kirkpatrick hamiltonian". In: *2019 IEEE 60th Annual Symposium on Foundations of Computer Science (FOCS).* IEEE. 2019, pp. 1417–1433.

[183] Andrea Montanari and Guilhem Semerjian. "Rigorous inequalities between length and time scales in glassy systems". In: *Journal of statistical physics* 125.1 (2006), p. 23.

[184] M. A. Moore and Barbara Drossel. "p-Spin Model in Finite Dimensions and Its Relation to Structural Glasses". In: *Phys. Rev. Lett.* 89 (21 Nov. 2002), p. 217202. DOI: 10.1103/PhysRevLett.89.217202. URL: https://link.aps.org/doi/10.1103/PhysRevLett.89.217202.

[185] José Luis Morales and Jorge Nocedal. "Remark on "Algorithm 778: L-BFGS-B: Fortran subroutines for large-scale bound constrained optimization"". In: *ACM Transactions on Mathematical Software (TOMS)* 38.1 (2011), pp. 1–4.

[186] Cristian F. Moukarzel. "Isostatic Phase Transition and Instability in Stiff Granular Materials". In: *Phys. Rev. Lett.* 81 (8 Aug. 1998), pp. 1634–1637.

[187] Markus Mueller and LB Ioffe. "Glass transition and the Coulomb gap in electron glasses". In: *Physical review letters* 93.25 (2004), p. 256403.

[188] Markus Mueller and Matthieu Wyart. "Marginal Stability in Structural, Spin, and Electron Glasses". In: *Ann. Rev. Cond. Matt. Phys.* 6.1 (2015), null. DOI: doi:10.1146/annurev-conmatphys-031214-014614. URL: file:///Users/pc61/Documents/Recherche.Articles/AnnuRevCondMat/Mueller2015.pdf.

[189] Tsuneyoshi Nakayama. "Boson peak and terahertz frequency dynamics of vitreous silica". In: *Reports on Progress in Physics* 65.8 (2002), p. 1195.

[190] Corey S. O'Hern, Stephen A. Langer, Andrea J. Liu, and Sidney R. Nagel. "Random Packings of Frictionless Particles". In: *Phys. Rev. Lett.* 88.7 (2002), p. 075507. DOI: 10.1103/PhysRevLett.88.075507.

[191] Corey S. O'Hern, Leonardo E. Silbert, Andrea J. Liu, and Sidney R. Nagel. "Jamming at zero temperature and zero applied stress: The epitome of disorder". In: *Phys. Rev. E* 68.1 (2003), p. 011306. DOI: 10.1103/PhysRevE.68.011306.

[192] Michio Otsuki and Hisao Hayakawa. "Critical scaling of a jammed system after a quench of temperature". In: *Physical Review E* 86.3 (2012), p. 031505.

[193] Dmitry Panchenko. "The Parisi ultrametricity conjecture". In: *Annals of Mathematics* (2013), pp. 383–393.

[194] Dmitry Panchenko. *The Sherrington-Kirkpatrick model*. Springer Science & Business Media, 2013.

[195] G Parisi and G Toulouse. "A Simple hypothesis for the spin glass phase of the infinite-ranged SK model". In: *Journal de Physique Lettres* 41.15 (1980), pp. 361–364.

[196] G. Parisi and T. Rizzo. "On Critical Dynamics in Disordered Systems". In: *arXiv:1205.3360* (2012).

[197] Giorgio Parisi. "Soft modes in jammed hard spheres (i): Mean field theory of the isostatic transition". In: *arXiv preprint* (2014). DOI: arXiv:1401.4413.

[198] Giorgio Parisi. "Stochastic stability". In: *AIP Conference Proceedings*. Vol. 553. 1. American Institute of Physics. 2001, pp. 73–79.

[199] Giorgio Parisi. "The order parameter for spin glasses: a function on the interval 0-1". In: *Journal of Physics A: Mathematical and General* 13.3 (1980), p. 1101.

[200] Giorgio Parisi, Pierfrancesco Urbani, and Francesco Zamponi. *Theory of Simple Glasses: Exact Solutions in Infinite Dimensions*. Cambridge University Press, 2020. DOI: 10.1017/9781108120494.

[201] Giorgio Parisi and Francesco Zamponi. "Amorphous packings of hard spheres for large space dimension". In: *Journal of Statistical Mechanics: Theory and Experiment* 2006.03 (2006), P03017. URL: http://stacks.iop.org/1742-5468/2006/P03017.

[202] Giorgio Parisi and Francesco Zamponi. "Mean-field theory of hard sphere glasses and jamming". In: *Rev. Mod. Phys.* 82.1 (Mar. 2010), pp. 789–845. DOI: 10.1103/RevModPhys.82.789.

[203] William Andrew Phillips and AC Anderson. *Amorphous solids: low-temperature properties*. Vol. 24. Springer, 1981.

[204] Corrado Rainone and Pierfrancesco Urbani. "Following the evolution of glassy states under external perturbations: The full replica symmetry breaking solution". In: *Journal of Statistical Mechanics: Theory and Experiment* 2016.5 (2016), p. 053302.

[205] Corrado Rainone, Pierfrancesco Urbani, Hajime Yoshino, and Francesco Zamponi. "Following the Evolution of Hard Sphere Glasses in Infinite Dimensions under External Perturbations: Compression and Shear Strain". In: *Phys. Rev. Lett.* 114.1 (2015), p. 015701. DOI: 10.1103/PhysRevLett.114.015701.

[206] Harold N Ritland. "Density phenomena in the transformation range of a borosilicate crown glass". In: *Journal of the American Ceramic Society* 37.8 (1954), pp. 370–377.

[207] F. Ritort and P. Sollich. "Glassy dynamics of kinetically constrained models". In: *Advances in Physics* 52.4 (2003), pp. 219–342.

[208] F. Rosenblatt. *Principles of Neurodynamics: Perceptrons and the Theory of Brain Mechanisms*. Cornell Aeronautical Laboratory. Report no. VG-1196-G-8. Spartan Books, 1962. URL: https://books.google.it/books?id=7FhRAAAAMAAJ.

[209] Jean-Noël Roux. "Geometric origin of mechanical properties of granular materials". In: *Phys. Rev. E* 61 (6 June 2000), pp. 6802–6836.

[210] Jean-Noël Roux and Gaël Combe. "Quasistatic rheology and the origins of strain". In: *Comptes Rendus Physique* 3.2 (2002), pp. 131–140.

[211] C. Patrick Royall and Stephen R. Williams. "The role of local structure in dynamical arrest". In: *Physics Reports* 560 (2015). The role of local structure in dynamical arrest, pp. 1–75. ISSN: 0370-1573. DOI: https://doi.org/10.1016/j.physrep.2014.11.004. URL: http://www.sciencedirect.com/science/article/pii/S0370157314004062.

[212] S. Alexander. "Amorphous solids: their structure, lattice dynamics and elasticity". In: *Phys. Rep.* 296 (1998), p. 65.

[213] Rolf Schilling. "Theories of the structural glass transition". In: *Collective Dynamics of Nonlinear and Disordered Systems*. Springer, 2005, pp. 171–202.

[214] Carl F Schreck, Mitch Mailman, Bulbul Chakraborty, and Corey S O'Hern. "Constraints and vibrations in static packings of ellipsoidal particles". In: *Physical Review E* 85.6 (2012), p. 061305.

[215] Antonio Sclocchi and Pierfrancesco Urbani. "Proliferation of non-linear excitations in the piecewise-linear perceptron". In: *SciPost Phys.* 10 (1 2021), p. 13. DOI: 10.21468/SciPostPhys.10.1.013. URL: https://scipost.org/10.21468/SciPostPhys.10.1.013.

[216] Shiladitya Sengupta, Smarajit Karmakar, Chandan Dasgupta, and Srikanth Sastry. "Breakdown of the Stokes-Einstein relation in two, three, and four dimensions". In: *J. Chem. Phys.* 138.12 (2013), 12A548–14. URL: file:///Users/pc61/Documents/Recherche.Articles/JChemPhys/Sengupta2013.pdf.

[217] Beatriz Seoane and Francesco Zamponi. "Spin-glass-like aging in colloidal and granular glasses". In: *Soft Matter* 14.25 (2018), pp. 5222–5234.

[218] James P Sethna, Karin A Dahmen, and Christopher R Myers. "Crackling noise". In: *Nature* 410.6825 (2001), pp. 242–250.

[219] LF Shampine, PH Muir, and H Xu. "A user-friendly Fortran BVP solver". In: *J. Numer. Anal. Ind. Appl. Math* 1.2 (2006), pp. 201–217.

[220] Baoshuang Shang, Pengfei Guan, and Jean-Louis Barrat. "Elastic avalanches reveal marginal behavior in amorphous solids". In: *Proceedings of the National Academy of Sciences* 117.1 (2020), pp. 86–92.

[221] Zane Shi, Pablo G Debenedetti, and Frank H Stillinger. "Relaxation processes in liquids: Variations on a theme by Stokes and Einstein". In: *The Journal of chemical physics* 138.12 (2013), 12A526.

[222] L.E. Silbert, A.J. Liu, and S.R. Nagel. "Vibrations and Diverging Length Scales Near the Unjamming Transition". In: *Physical Review Letters* 95.9 (2005), p. 098301.

[223] Leonardo E. Silbert, Andrea J. Liu, and Sidney R. Nagel. "Normal modes in model jammed systems in three dimensions". In: *Phys. Rev. E* 79 (2 Feb. 2009), p. 021308. DOI: 10.1103/PhysRevE.79.021308. URL: https://link.aps.org/doi/10.1103/PhysRevE.79.021308.

[224] Monica Skoge, Aleksandar Donev, Frank H. Stillinger, and Salvatore Torquato. "Packing hyperspheres in high-dimensional Euclidean spaces". In: *Physical Review E (Statistical, Nonlinear, and Soft Matter Physics)* 74.4, 041127 (2006), p. 041127. DOI: 10.1103/PhysRevE.74.041127. URL: http://link.aps.org/abstract/PRE/v74/e041127.

[225] H-J Sommers and Werner Dupont. "Distribution of frozen fields in the mean-field theory of spin glasses". In: *Journal of Physics C: Solid State Physics* 17.32 (1984), p. 5785.

[226] Grzegorz Szamel. "Colloidal glass transition: Beyond mode-coupling theory". In: *Physical review letters* 90.22 (2003), p. 228301.

[227] M. Talagrand. *Spin glasses: a challenge for mathematicians: cavity and mean field models*. Springer, 2003.

[228] G Tarjus and D Kivelson. *Jamming and Rheology: Constrained Dynamics on Microscopic and Macroscopic Scales*. 2001.

[229] Gilles Tarjus. "An overview of the theories of the glass transition". In: *Dynamical Heterogeneities in Glasses, Colloids, and Granular Media* 150 (2011), p. 39.

[230] Gilles Tarjus and Daniel Kivelson. "Breakdown of the Stokes–Einstein relation in supercooled liquids". In: *The Journal of chemical physics* 103.8 (1995), pp. 3071–3073.

[231] DJ Thouless, JRL De Almeida, and JM Kosterlitz. "Stability and susceptibility in Parisi's solution of a spin glass model". In: *Journal of Physics C: Solid State Physics* 13.17 (1980), p. 3271.

[232] Alexei V Tkachenko and Thomas A Witten. "Stress in frictionless granular material: Adaptive network simulations". In: *Physical Review E* 62.2 (2000), p. 2510.

[233] S. Torquato and F. H. Stillinger. "Jammed hard-particle packings: From Kepler to Bernal and beyond". In: *Rev. Mod. Phys.* 82.3 (Sept. 2010), pp. 2633–2672. DOI: 10.1103/RevModPhys.82.2633.

[234] Pierfrancesco Urbani. *Statistical Physics of glassy systems: tools and applications.* 2018.

[235] Pierfrancesco Urbani and Giulio Biroli. "Gardner transition in finite dimensions". In: *Phys. Rev. B* 91 (10 Mar. 2015), p. 100202. DOI: 10.1103/PhysRevB.91.100202. URL: https://link.aps.org/doi/10.1103/PhysRevB.91.100202.

[236] Pierfrancesco Urbani and Giulio Biroli. "Gardner transition in finite dimensions". In: *Physical Review B* 91.10 (2015), p. 100202.

[237] J Vannimenus, G Toulouse, and G Parisi. "Study of a simple hypothesis for the mean-field theory of spin-glasses". In: *Journal de Physique* 42.4 (1981), pp. 565–571.

[238] D Vertechi and MA Virasoro. "Energy barriers in SK spin-glass model". In: *Journal de Physique* 50.17 (1989), pp. 2325–2332.

[239] Maryna Viazovska. "The sphere packing problem in dimension 8". In: *cond-mat* (2016), p. 1603.04246. URL: file:///Users/pc61/Documents/Recherche.Articles/cond-mat/160304246v1.pdf.

[240] Pauli Virtanen, Ralf Gommers, Travis E. Oliphant, Matt Haberland, Tyler Reddy, David Cournapeau, Evgeni Burovski, Pearu Peterson, Warren Weckesser, Jonathan Bright, Stéfan J. van der Walt, Matthew Brett, Joshua Wilson, K. Jarrod Millman, Nikolay Mayorov, Andrew R. J. Nelson, Eric Jones, Robert Kern, Eric Larson, C J Carey, İlhan Polat, Yu Feng, Eric W. Moore, Jake VanderPlas, Denis Laxalde, Josef Perktold, Robert Cimrman, Ian Henriksen, E. A. Quintero, Charles R. Harris, Anne M. Archibald, Antônio H. Ribeiro, Fabian Pedregosa, Paul van Mulbregt, and SciPy 1.0 Contributors. "SciPy 1.0: Fundamental Algorithms for Scientific Computing in Python". In: *Nature Methods* 17 (2020), pp. 261–272. DOI: 10.1038/s41592-019-0686-2.

[241] Vincenzo Vitelli, Ning Xu, Matthieu Wyart, Andrea J. Liu, and Sidney R. Nagel. "Heat transport in model jammed solids". In: *Phys. Rev. E* 81 (2 Feb. 2010), p. 021301. DOI: 10.1103/PhysRevE.81.021301. URL: https://link.aps.org/doi/10.1103/PhysRevE.81.021301.

[242] Eric R Weeks, John C Crocker, Andrew C Levitt, Andrew Schofield, and David A Weitz. "Three-dimensional direct imaging of structural relaxation near the colloidal glass transition". In: *Science* 287.5453 (2000), pp. 627–631.

[243] Asaph Widmer-Cooper, Heidi Perry, Peter Harrowell, and David R Reichman. "Irreversible reorganization in a supercooled liquid originates from localized soft modes". In: *Nature Physics* 4.9 (2008), pp. 711–715.

[244] John Wishart. "The generalised product moment distribution in samples from a normal multivariate population". In: *Biometrika* (1928), pp. 32–52.

[245] M. Wyart. "Scaling of phononic transport with connectivity in amorphous solids". In: *EPL (Europhysics Letters)* 89 (2010), p. 64001.

[246] M. Wyart, L.E. Silbert, S.R. Nagel, and T.A. Witten. "Effects of compression on the vibrational modes of marginally jammed solids". In: *Physical Review E* 72.5 (2005), p. 051306.

[247] Matthieu Wyart. "Marginal Stability Constrains Force and Pair Distributions at Random Close Packing". In: *Phys. Rev. Lett.* 109 (12 2012), p. 125502. DOI: 10.1103/PhysRevLett.109.125502.

[248] Matthieu Wyart, Sidney R Nagel, and Thomas A Witten. "Geometric origin of excess low-frequency vibrational modes in weakly connected amorphous solids". In: *EPL* 72.3 (2005), p. 486.

[249] Matthieu Wyart, Sidney R Nagel, and Thomas A Witten. "Geometric origin of excess low-frequency vibrational modes in weakly connected amorphous solids". In: *EPL (Europhysics Letters)* 72.3 (2005), p. 486. DOI: https://doi.org/10.1209/epl/i2005-10245-5.

[250] Wyart, M. "On the rigidity of amorphous solids". In: *Ann. Phys. Fr.* 30.3 (2005), pp. 1–96. DOI: 10.1051/anphys:2006003. URL: https://doi.org/10.1051/anphys:2006003.

[251] X. Xia and P. G. Wolynes. "Fragilities of liquids predicted from the random first order transition theory of glasses". In: *Proc. Nat. Acad. Sci.* 97 (2001), pp. 2990–2994.

[252] Xiaoyu Xia and Peter G. Wolynes. "Microscopic Theory of Heterogeneity and Nonexponential Relaxations in Supercooled Liquids". In: *Phys. Rev. Lett.* 86.24 (June 2001), pp. 5526–5529. DOI: 10.1103/PhysRevLett.86.5526.

[253] N. Xu, V. Vitelli, A. J. Liu, and S. R. Nagel. "Anharmonic and quasi-localized vibrations in jammed solids, Modes for mechanical failure". In: *Europhys. Lett.* 90.5 (2010), p. 56001.

[254] Ning Xu, Matthieu Wyart, Andrea J. Liu, and Sidney R. Nagel. "Excess Vibrational Modes and the Boson Peak in Model Glasses". In: *Phys. Rev. Lett.* 98 (17 Apr. 2007), p. 175502. DOI: 10.1103/PhysRevLett.98.175502. URL: https://link.aps.org/doi/10.1103/PhysRevLett.98.175502.

[255] Le Yan, Eric DeGiuli, and Matthieu Wyart. "On variational arguments for vibrational modes near jamming". In: *EPL* 114.2 (2016), p. 26003. DOI: https://doi.org/10.1209/0295-5075/114/26003.

[256] Joonhyun Yeo and M. A. Moore. "Origin of the growing length scale in M-p-spin glass models". In: *Phys. Rev. E* 86 (5 Nov. 2012), p. 052501. DOI: 10.1103/PhysRevE.86.052501. URL: https://link.aps.org/doi/10.1103/PhysRevE.86.052501.

[257] Zorana Zeravcic, Wim van Saarloos, and David R. Nelson. "Localization behavior of vibrational modes in granular packings". In: *EPL (Europhysics Letters)* 83.4 (2008), 44001 (6pp). URL: http://stacks.iop.org/0295-5075/83/44001.

[258] Kai Zhang, W. Wendell Smith, Minglei Wang, Yanhui Liu, Jan Schroers, Mark D. Shattuck, and Corey S. O'Hern. "Connection between the packing efficiency of binary hard spheres and the glass-forming ability of bulk metallic glasses". In: *Phys. Rev. E* 90.3 (2014), p. 032311. URL: file:///Users/pc61/Documents/Recherche.Articles/PRE/Zhang2014b.pdf.

[259] Cang Zhao, Kaiwen Tian, and Ning Xu. "New jamming scenario: From marginal jamming to deep jamming". In: *Physical review letters* 106.12 (2011), p. 125503.

[260] Ciyou Zhu, Richard H Byrd, Peihuang Lu, and Jorge Nocedal. "Algorithm 778: L-BFGS-B: Fortran subroutines for large-scale bound-constrained optimization". In: *ACM Transactions on Mathematical Software (TOMS)* 23.4 (1997), pp. 550–560.

université PARIS-SACLAY

ÉCOLE DOCTORALE
Physique en île-de-France (EDPIF)

Titre: Une nouvelle phase critique pour les modèles brouillés : le brouillage ("jamming") est encore plus cool qu'avant

Mots clés: Jamming, brouillage, criticité auto-organisée, stabilité marginale, avalanches, systèmes désordonnés, verres

Résumé Au cours des vingt dernières années, un courant de recherche important a caractérisé la transition de brouillage, un point critique à température zéro des systèmes ayant des interactions répulsives à courte portée. Plusieurs de ses propriétés sont indépendantes de la dimension spatiale, avec des prédictions de champ moyen étant valables même pour les systèmes bidimensionnels. Dans cette thèse, nous montrons l'existence de ce comportement critique du point de brouillage ("jamming") dans toute une phase brouillée ("jammed"). Ce comportement est observé en étudiant le potentiel de répulsion linéaire dans les sphères molles et le modèle de champ moyen correspondant, c'est-à-dire le perceptron. Nous montrons que le point non différentiable du potentiel d'interaction produit un réseau de contact de sphères tangentes à chaque densité surcomprimée, même loin de la transition de jamming. Les réseaux de contact caractérisant les minima du système sont isostatiques, critiquement auto-organisés et marginalement stables. Dans la première partie, nous utilisons la théorie du champ moyen pour le cas du perceptron et nous la validons par des simulations numériques. Ensuite, nous utilisons des simulations numériques pour étudier le cas des sphères molles en deux et trois dimensions. Dans les deux cas, nous caractérisons la phase marginalement stable et nous montrons que les exposants critiques correspondent à ceux connus pour la transition de jamming. De plus, nous définissons un protocole de compression et nous étudions numériquement les propriétés statistiques des avalanches dans la phase critique du perceptron. Nos résultats sont en accord parfait avec la théorie sous-jacente. Ce travail montre l'existence d'une phase critique dans les dimensions finies dont la classe d'universalité correspond au jamming des sphères. Cela ouvre de nouvelles perspectives pour l'étude des verres marginalement stables et des paysages énergétiques qui leur sont associés.

Title: A new critical phase in jammed models: jamming is even cooler than before

Keywords: Jamming, self-organized criticality, marginal stability, avalanches, disordered systems, glasses

Abstract Over the last two decades, an intensive stream of research has characterized the jamming transition, a zero-temperature critical point of systems with short-range repulsive interactions. Many of its properties are independent of spatial dimensionality, with mean-field scalings being valid even for two-dimensional systems. In this thesis, we show the existence of this critical behaviour not only at the jamming point, but also in an entire jammed phase. This is observed by studying the linear repulsive interaction potential for soft spheres and in its correspondent mean-field model, i.e. the perceptron. We show that the non-differentiable point in the interaction potential produces a contact network of tangent spheres at every overcompressed density, even far away from the jamming transition. The contact networks characterizing the minima of the system are isostatic, critically self-organized and marginally stable. First, we solve the mean-field theory for the perceptron case and we validate it through numerical simulations. Furthermore, we use numerical simulations to study the soft spheres case in two and three dimensions. In both cases, we characterize the marginally stable phase and we show that the critical exponents correspond to those known for the jamming transition. Moreover, we define a compression protocol and we study numerically the avalanche statistics in the critical phase of the perceptron. Our findings are strongly consistent with the underlying theory. This work shows the existence of a critical phase in finite dimensions whose universality class corresponds to the jamming of spheres. This opens new perspectives to study marginally stable glasses and their related energy landscapes.

Université Paris-Saclay
Espace Technologique / Immeuble Discovery
Route de l'Orme aux Merisiers RD 128 / 91190 Saint-Aubin, France